Design and syntheses of some heterocyclic liquid crystals and organogelators

A Dissertation submitted in Partial Fulfillment of the

Requirements for the Degree

of

Doctor of Philosophy

at

IIT Guwahati

by

Subrata Nath

Department of Chemistry
Indian Institute of Technology Guwahati
Guwahati-781039, Assam
India

August 2017

BE AN ARTISAN OF KNOWLEDGE
Discern and know things
with all their constituents
and make,
till with skillful adjustment
In practical progressive performance
with every inquisitive urge
and be an artisan of knowledge,
Science is there.

(Message, Vol 8, Sri Sri Thakur)

"Bande Purushottamam"

Dedicated at the holy feet of my Beloved Guru Sri Sri Thakur Anukulchandra and guiding star of my life Pujaniya Babaida.

DECLARATION

I do hereby declare that the research work embodied in this thesis entitled "***Design and syntheses of some heterocyclic liquid crystals and organogelators***" has been carried out by me under the supervision of **Dr. A. S. Achalkumar** in the Department of Chemistry, Indian Institute of Technology Guwahati, Assam– 781039, India.

In keeping with the general practice of reporting scientific observations, due acknowledgements have been made wherever the work described is based on the findings of other investigators.

IIT Guwahati Subrata Nath

August, 2017

Dr. A. S. Achalkumar
Associate Professor
Department of Chemistry
Indian Institute of Technology Guwahati
Guwahati – 781039, Assam, India
Phone: +91-361-258-2329
Fax: +91-361-258-2349
E-mail: achalkumar@iitg.ernet.in
achalkumar78@gmail.com

CERTIFICATE

This is to certify that the research work presented in this thesis entitled "***Design and syntheses of some heterocyclic liquid crystals and organogelators***" is an authentic record of the results obtained from the research work carried out by **Mr. Subrata Nath (Roll No. 126122036)** under my supervision in the Department of Chemistry, Indian Institute of Technology Guwahati, India. This work is original and has not been submitted elsewhere for a degree or award.

IIT Guwahati
August, 2017

Dr. A. S. Achalkumar
(Thesis Supervisor)

ACKNOWLEDGEMENTS

The journey towards the completion of my thesis with the outcome of the years of experience, ideas generated in the form of knowledge, was full of hurdles paved way to the fruitful success. Over five years of my research career I have been supported and assisted by a large number of people, in regards to whom I want to convey my words for heartfelt thanks for their kindness, grace, attention, encouragement and support.

At the very onset, with a deepest sense of gratitude, I wish to express my sincere thanks to my supervisor, Dr. Ammathnadu S. Achalkumar for his proficient guidance, inspiration, creative and scientific ideas which helped me to explore the domain of my work assembled in this thesis. He has given me an extraordinary amount of freedom to be creative and to work on the problems that have interested me. I have spent countless hours discussing research and ideas in science with him. Without his patience and guidance, I would not have finished this work. Of course, wherever I was standing in the shadow of fear of travel, he helped me to achieve the target by his constant encouragement with his true scientific spirit. It was one of the best choices I have ever made to choose him as my supervisor. He is the only person who used to make me feel the sayings, "If you rest, you will rust". He has motivated me always to do good research and to develop an interest for organic chemistry and its application in material Science. His '*Guru Gyans*' will definitely help me a lot to shape up my future life.

Besides my supervisor, I would also like to express my deepest sense of gratitude and heartfelt thanks to my doctoral committee members, Dr.Lal Mohan Kundu, Dr. Subhas Chandra Pan and Dr. Bosanta R Boruah for their periodic evaluation of my work, valuable suggestions, constant support and encouragement. I would like to thank all of the professors at Gauhati University who taught me the M. Sc. courses. Their genuine concern in the teachings in the field of chemistry is evident in the synthesis of my liquid crystal molecules. I am greatly indebted to them. I would like to express my sincere thanks to Dr. Chandan Mukherjee for providing me his electrochemical work station for the analysis. I would like to acknowledge Joydip De, and Dr. Santanu Kumar Pal, Associate Professor, IISER Mohali, for helping me with X-ray Diffraction analysis and rheological studies. Of course nothing would function properly without our gifted scientific officer, Dr. Babulal Das and other non-teaching staffs, of Department of Chemistry, IITG. I acknowledge them gratefully. I would like to acknowledge Central Instruments Facility, IIT Guwahati for providing me the analytical facilities required during my research work.

I wish to express my sincere gratitude to Indian Institute of Technology Guwahati for nurturing our research career and for all the facilities and financial support that were made available to me.

Alongside I have been fortunate to have wonderful lab members and of course no words can ever be adequate to express my heartiest thanks to my closest friend, lab mate cum mentor Dr. Suraj Kumar Pathak who motivated me to join IITG for my PhD and have been constantly guiding and supporting me in my research life to personal life. He spent many sleepless nights to support and to solve my personal problems and also long hours for planning and working in the lab and everything which we faced in the long run. He was standing just like a pillar throughout my PhD work and helped selflessly in the completion of my thesis work. We faced together all the problems in our newly born lab to make it a well-established one in reality in the initial days. I realize again that when something is done however small it is, it is not done alone. I express my deep sense of gratitude to all my lab members (present and past) Ms. Pratika Basumatary, Mr. Ravindra Kumar Gupta, Mr. Balaram Pradhan, Mr. Vinod Kumar Vishwakarma, Dr. Nirmalangshu Chakraborthy, Dr. Sachin Kumar Singh, Dr. Srikant Turlapati, Dr. Hidayath Ulla, Dr. Hemant Kumar Singh and Dr. Hemanta Kalita for their imperishable help, scientific conversations and also maintaining a pleasant working environment throughout my PhD tenure.

I am grateful to Prof. Lingraj Sahoo (Dept. of BSBE, IITG) and Prof. Bhaben Tanti (Dept. of Botany, Gauhati University) for their help and for sharing their valuable ideas and suggestions over the last few years.

Finally, my PhD would not have been completed without the eternal love, care, bless, support, patience, non-refundable sacrifices and encouragement of my parents Mr. Sunil Chandra Nath and Mrs. Anju Nath and my two wonderful sisters Mrs. Suparna Nath and Miss Sumi Nath. They encouraged me to pay attention to the world around me and to wonder why and how things work. My deep sense of gratitude to my other relatives and my childhood friends specially Bapan and Tinkuda for being with me all the time starting from the beginning of my educational career and for their help and taking care of my aging parents in my absence.

Of course everything will go invalid if I forget the blessings of Almighty without whom nothing will function and I pray Him for his blessings.

Subrata

Some of the findings of this thesis have been communicated / published in international journals as given below.

1. Contrasting effects of heterocycle substitution and branched tails in the arms of star-shaped molecules. Suraj Kumar Pathak, **Subrata Nath**, Joydip De, Santanu Kumar Pal and A. S. Achalkumar, *New J. Chem.*, 2017, **41**, 4680-4688.
2. Effect of regioisomerism on the mesomorphic and photophysical behavior of oxadiazole-based tris(N-salicylideneaniline)s: Synthesis and characterization. Suraj Kumar Pathak[#], **Subrata Nath**[#], Joydip De, Santanu Kumar Pal and A. S. Achalkumar, *New J. of Chem*, DOI: 10.1039/C7NJ01766A.
3. Star-shaped π-gelators based on oxadiazole and thiadiazoles: a structure-property correlation. **Subrata Nath**, Suraj Kumar Pathak, Joydip De, Santanu Kumar Pal and A. S. Achalkumar, *Molecular system design and engineering*, DOI: 10.1039/C7ME00040E.
4. Tetrazole based supergelator as a sensitive and selective sensor for picric acid, with a fluorescence switching response. **Subrata Nath**, Suraj Kumar Pathak, Balaram Pradhan, K. Anki Reddy, G. Krishnamoorthy, A. S. Achalkumar (Communicated).

Articles on results not included in this thesis

1. Columnar self-assembly of star-shaped luminescent oxadiazole and thiadiazole derivatives. S. K. Pathak, R. K. Gupta, **S. Nath**, D. S. Shankar Rao, S. K. Prasad and A. S. Achalkumar, *J. Mater. Chem. C*. 2015, **3**, 2940-2952.
2. Effect of regioisomerism on the self-assembly and photophysical behavior of 1,3,4-thiadiazole based polycatenars. S. K. Pathak, **S. Nath**, R. K. Gupta, D. S. Shankar Rao, S. K. Prasad and A. S. Achalkumar, *J. Mater. Chem. C*. 2015, **3**, 8166-8182. (Hot article)

3. Tuning the self-assembly and photophysical properties of bi-1,3,4-Thiadiazole derivatives through electron donor-acceptor interactions and their application in OLEDs. Abhay Kumar Yadav,[#] Balaram Pradhan,[#] Hidayath Ulla,[#] **Subrata Nath**, Joydip De, Santanu Kumar Pal, M. N. Satyanarayan, A. S. Achalkumar, *J. Mater. Chem. C* (DOI 10.1039/C7TC01420A).

List of Conferences/symposiums

- Presented a poster at National conference on Liquid Crystals (NCLC-22) held at DIT University, Dehradun, 21-23 Dec. 2015.
- Presented a poster at RESEARCH CONCLAVE'16 held at IIT Guwahati 2016.
- Presented a poster at REFLUX'16 held at IIT Guwahati, 25-27 March, 2016.
- Presented a poster at FICS-2016 held at IIT Guwahati, 08-10 December, 2016.
- Presented a poster at 20th CRSI National Synposium in Chemistry held at Gauhati University, 03-05 February, 2017.
- Presented a poster at RESEARCH CONCLAVE'17 held at IIT Guwahati 16-19 March, 2017.

CONTENTS

Chapter IV

Oxadiazole / thiadiazole based stars and polycatenars

Chapter V

Tetrazole based supergelator as a sensitive and selective sensor for picric acid

List of abbreviations used in the text

anhyd	anhydrous
brd	broad doublet
brs	broad singlet
Cr	crystal
d	doublet
dd	doublet of a doublet
DMF	*N, N'*-dimethylformamide
DMSO	dimethyl sulphoxide
DSC	differential scanning calorimetry
equiv	equivalents
Et	ethyl
Et_2O	diethylether
Et_3N	triethylamine
EtOAc	ethyl acetate
Fig	figure
g	gram
h	hour
Hz	hertz
I	isotropic
ITO	indium-tin oxide
IR	infrared
j	joules
J	coupling constant
LC	liquid crystal
m	multiplet

MHz	megahertz
min	minutes
mmol	milli mole(s)
mp	melting point
NMR	nuclear magnetic resonance
N	nematic
N*	chiral nematic
p	para
POM	polarizing optical microscopy
ppm	parts per million
q	quartet
R_f	retention factor
rt	room temperature
s	singlet
t	triplet
THF	tetrahydrofuran
TMS	tetramethyl silane
TLC	thin layer chromatography
UV	ultra violet
XRD	X-ray diffraction

GENERAL REMARKS

All commercially obtained chemicals were used as received. As required the solvents were dried as per the standard protocols. Silica gel or neutral alumina used as stationery phase for column chromatography. Aluminium sheets coated with silica gel were used for thin layer chromatography (TLC) to monitor the reactions and column purifications. Infrared spectra were measured on a Perkin Elmer IR spectrometer at room temperature by preparing the KBr pellet. ^{1}H and ^{13}C NMR spectra were recorded using Varian Mercury 400 MHz or Bruker 600 MHz NMR spectrometer. Mass spectrometry was carried out using MALDI-TOF mass spectrometer (Bruker Autoflex Speed MALDI TOF/TOF Mass spectrometer) or High Resolution Mass Spectrometer. Polarizing optical microscope (POM) (Nikon Eclipse LV100POL) in conjunction with a controllable hot stage (Mettler Toledo FP90) was used for the characterization of mesogens. The phase transitions, associated enthalpy changes were obtained by differential scanning calorimeter (DSC) (Mettler Toledo DSC1). X-ray diffraction (XRD) studies were carried out using image plate and a detector. This setup had CuKα (λ =0.15418 nm) radiation from a source (GeniX3D, Xenocs) operating at 50 kV and 0.6 mA in conjunction with a multilayer mirror was used to irradiate the sample. Glass capillaries containing the sample were used for the measurements. Thermogravimetric analysis (TGA) was accomplished with a thermogravimetric analyzer (Mettler Toledo, model TG/SDTA 851 e). Perkin-Elmer Lambda 750, UV/VIS/NIR spectrometer was used to obtain UV-Vis spectra, while Fluoromax-4 fluorescence spectrophotometer was used to obtain emission spectra in solution state and solid thin film state. Steady State anisotropy experiment was performed on Horiba Scientific Fluoromax spectrofluorometer 4. Time resolved lifetime measurements were done on time correlated single photon counter from Horiba Jobin Yvon. Cyclic Voltammetry (CV) studies were carried out using a Versa Stat 3 (Princeton Applied Research) instrument. Atomic Force microscopy (AFM) images were obtained for the spin-coated films using Agilent 5500-STM instrument. SEM images were obtained on a JEOL 7600F FESEM instrument. TEM images were obtained on a JEM-2100 Transmission Electron Microscope. Rheological data is obtained using Rheometer MCR-302 Anton Paar.

PREFACE

Liquid crystals (LCs) are unique functional soft materials combining both order and mobility on molecular, supramolecular and macroscopic levels. The shape anisotropic molecules which exhibit this unique behavior are also known as mesogens. They can be organic (forming thermotropic and lyotropic phases), inorganic (metal oxides forming lyotropic phases) or organometallic (metallomesogens) in nature. Liquid crystals have found many applications in material science as well as life science. Important applications of thermotropic LCs are electro-optic displays, temperature sensors and selective reflecting pigments. Lyotropic systems form an important constituent of living systems (eg. DNA, biomembranes *etc*.). Apart from that they are used in cleaning process, cosmetic industries, and templates for the preparation of mesoporous materials and also serve as model systems for biomembranes.

Conventionally, the anisometric molecules employed to stabilize thermotropic LC phases are either rod-like (calamitic) or disc-like (discotic). Calamitics form the backbone of the well-established flat panel display industry. Discotic LCs also have made notable progress in recent years, both from scientific and application viewpoints and slowly they are finding a foothold in the main stream of organic molecular electronics. It is also known that LC behavior is realizable with molecules differing in their shape-anisotropy from conventional ones. The general feature of majority of such materials is the molecular structural contrast within a molecule *i.e.*, these molecules are made up of chemically different molecular parts that are incompatible with each other. Some of the important examples of nonconventional systems are oligomers, polycatenars, bent-core molecules, polyhydroxy amphiphiles, octahedral complexes, star shaped molecules, rod-coil molecules and dendrimers. In the case of nonconventional LCs, the main driving force for the self-assembly of these molecules to form liquid-crystalline (LC) phases is based on the nanoseggregation of chemically or physically different building blocks and the tendency to efficiently fill the space in condensed state.

Polycatenars and star-shaped molecules, in particular display a remarkable mesophase behavior. Compared to the synthetic difficulty associated with discotics, this molecular design is advantageous due to the inherent synthetic flexibility. Thus, new types of polycatenar and star-shaped molecules have been designed, synthesized and characterized. All the synthesized materials have been characterized by the requisite characterization techniques for their structural identity and thermal behavior.

Organogels comprise a three-dimensional network of entangled supramolecular fibers that is formed by the self-assembly of a low-molecular-weight gelator, entrapping a large volume of the solvent. The driving force for such assembly is mainly nanophase segregation between the incompatible molecular subunits in addition to other secondary interactions like H-bonding, π-π interactions, ionic, hydrophilic or hydrophobic interactions. With a careful molecular design one can predict the outcome of the self-assembly of such shape anisotropic molecules. Gelators are another class of molecules with specific structural features, which immobilize a large amount of solvents when they self-assemble. They may gelate organic or aqueous solvents. The self-assembly of such molecules to form gels is assisted by weak forces like H-bonding, π-π interactions, hydrophobic–hydrophilic or van der Waals interactions. Gelation brings about drastic changes in the electronic and optical properties. The 1D self-assembly of the molecules in the form of fibers has great potential in the areas of optoelectronics, controlled drug release, energy transfer, sensing, and security. The incorporation of functionalities such as amide, hydroxyl, acid, large aromatic units, and steroid moieties often known to support gelation and in a few cases less than 1 wt % of a molecule is sufficient to gelate a large volume of solvents. Such compounds are known as supergelators.

Development of new approaches for the detection methods and design of novel materials that are involved in ultra-low level detection is a very challenging area of chemical sensors. In recent years, chemical sensors with high sensitivity for the detection of compounds such as trinitrotoluene (TNT), 2,4-dinitrotoluene (DNT), 1,3,5-trinitroperhydro-1,3,5-triazine (RDX) and picric acid (PA), the principal ingredients of explosives, have attracted much attention for wide applications in public security,

pollution problems for humans and ecosystems. Various analytical methods have been developed for sensitive detection of nitroaromatic compounds. Among the physical methods, photoluminescence based chemosensors that exploit sensitive fluorescence quenching by nitroaromatic derivatives have been investigated extensively for both vapor and solution phases at low concentrations with high sensitivity and selectivity.

The results of these studies are embodied in the present doctoral thesis, which comprises five chapters, as given below. Throughout the thesis, the potential of the synthesized non-conventional liquid crystals for practical applications has been discussed intensively. The last chapter is mainly focused on gelation and sensing studies.

Chapter 1 This is an introductory chapter to LCs in general describing their classification and their important significance in material science. The chapter focuses in greater detail on the physical properties of nonconventional liquid crystals. Beginning with an overview of thermotropic LCs and their brief history, this chapter mainly focuses the major classes of columnar mesophases formed by non-conventional LCs, relevant mesomorphic and physical properties and finally, some applications and perspectives in material science and molecular electronics. Lastly a brief introduction on organic gelators along with their practical application as sensor has been described.

Chapter 2 Star-shaped tris(*N*-salicylideneaniline)s (TSANs) containing 1,3,4-oxadiazole based and 1,3,4-thiadiazole based arms have been synthesized and characterized. The introduction of branched tails at periphery had different effects on these tris(*N*-salicylideneaniline)s, which were dependent on the type of the heterocycle. TSANs with 1,3,4-oxadiazole arms with branched tails exhibited a room temperature columnar rectangular phase in comparison to the high temperature columnar hexagonal phase exhibited by hexadecyloxy chain analogue. In the case of thiadiazole based TSANs, the compound with hexadecyloxy chains exhibited columnar rectangular phase of wide range including room temperature, while the branched chain analogue turned to be a liquid. Thus in the case of star-shaped molecules, the type of the peripheral tails not only affects

the transition temperature, but also affects the type of self-assembly, which is in contrary to conventional discotic liquid crystals. Introduction of substituted 1,3,4-thiadiazole rings helps in the reduction of melting point and enhances the mesophase width. Presence of the bulky branched tails at the periphery enhances the intermolecular interaction between the cores of 1,3,4-oxadiazole based TSANs, thus leading to the stabilization of columnar rectangular phase. 1,3,4-Thiadiazole based TSANs exhibit columnar rectangular phase even with the straight peripheral chains, because of the attractive intermolecular interactions of the thiadiazole ring.

Chapter 3 Two new regioisomeric star-shaped tris(*N*-salicylideneaniline)s are synthesized and characterized. The arms of these star-shaped mesogens differ from each other with respect to the substitution on the 3,5-positions of the central 1,2,4-oxadiazole moieties. The unsymmetrical nature of substitution leads to a change in the distribution of electron density, which will have an effect on the type of the columnar self-assembly. One of these molecules stabilize columnar hexagonal phase, while the other one stabilize columnar rectangular phase. Columnar rectangular phase, which require enhanced intermolecular interactions are observed in the case of star-shaped molecule, where the trialkoxy phenyl group is connected at the 5-position of the heterocycle, whereas columnar hexagonal phase was observed in the case of star-shaped molecule, where the trialkoxy phenyl group is connected at the 3-position of the heterocycle. These compounds showed reduced melting point, clearing point and enhanced mesophase range with respect to the symmetric counterpart (1,3,4-oxadiazole derivative) reported earlier. All the molecules exhibited green light emission in solution, with good quantum yield. The emission of 1,2,4-oxadiazole derivatives was much red-shifted in comparison to 1,3,4-oxadiazole derivatives. This study emphasizes how a minor change in the molecular structure brings about a beneficial change in the self-assembly characteristics of star-shaped molecules.

Chapter 4 Several new star-shaped and tetracatenar derivatives based on 1,3,4-oxadiazole and thiadiazole derivatives were synthesized. The self-assembly of these

molecules were studied in bulk and in presence of hydrocarbon solvents. The peripheral substitution of alkyl tails was at 3 and 5 positions of the peripheral benzene rings. It is interesting to note that the self-assembly and photophysical properties of these molecules is extremely sensitive to the type of the heteroatom present in the molecule and the pattern of peripheral substitution. Only the star-shaped molecule with substituted oxadiazole arms was liquid crystalline, while tetracatenars were crystalline. This star-shaped oxadiazole derivative exhibited columnar hexagonal phase. This compound was also able to gelate in long chain hydrocarbon solvents at a concentration less than 1 weight percent; qualifying it as a supergelator. The gelation is mainly supported by attractive π-π interactions. This phenomenon is very rare, in comparison to earlier reports where the supergelation is supported by H-bonding interactions. This compound also exhibited aggregation-induced emission (AIE) with a several fold increase in luminescence intensity upon gelation. The corresponding regioisomeric oxadiazole and thiadiazole star-shaped molecules, with peripheral chains substituted at 3 and 4 positions were liquid crystalline and stabilized gelation as well. This shows that in addition to π-π interactions, nanoseggregation of incompatible molecular subunits like flexible tails also play a major role in stabilizing the organogelation and liquid crystalline self-assembly. The extensive microscopic studies of the xerogels showed the entangled network of fibers of several micrometer lengths confirming the long range self-assembly of these molecules. DFT calculations and electrochemical studies were also carried out to understand the effect of peripheral substitution on the HOMO-LUMO levels and the band gaps.

Chapter 5 A low molecular weight organogelator containing 3,5-substituted 1,3,4-oxadiazole and tetrazole units was synthesized and characterized. This compound was only soluble in DMSO and forms a stable gel. The solution and gel exhibit a blue light emission. The gel was characterized by atomic force emission microscopy, field-emission scanning electron microscopy, ^{1}H NMR and fluorescence measurements. The gel to solution interconversion was reversible for many cycles of heating and cooling. The compound in solution exhibited a high selectivity for the detection of common explosive

and water pollutant picric acid. Fluorometric titration studies with nitro explosive compounds revealed that emission of the compound was red shifted in response to the addition of picric acid, and exhibited a shifting of fluorescence from blue to green. Theoretical and experimental studies revealed that the sensing property is not due to ground state electron transfer; rather it is due to the formation of protonated complex with the picrate anion. The shifting of emission in response to picric acid in the visual region is ideal for the naked eye detection of the explosives and therefore it is promising in comparison to the detection methods based on fluorescence quenching.

Chapter I

Introduction to liquid crystals and organogelators

1.1. The liquid crystal state

Liquid crystal (LC) is a state of matter (which is also known as fourth state of matter), that has properties between those of conventional liquids and crystalline solids.[1] For instance, a LC may flow like a liquid, but its molecules may be oriented in a crystal-like way. Liquid crystals have a small degree of order among the molecules (mesogens) that form LC phase along with the fluidic nature. In highly structured solid phase, the constituent molecules have no chance to move and reorient themselves with respect to one another and point their axes in one direction. Thus in crystals, molecules usually possess both orientation and three dimensional positional orders. However if the same solid melts to a isotropic liquid state, the molecules tumble in all possible directions, which results in the loss of positional and orientational order. On the other hand LC phases possess either positional or orientational order (tendency of the molecules to point along a common direction called the director ***n***) due to anisotropic weak intermolecular interactions between the mesogens. Thus they possess a less degree of organization than the crystalline solids, but having more degree of organization than liquids. In other words, solids usually have both positional and orientational order which implies that center of mass of molecules at specific location and molecular axes point at certain directions. In case of liquid, there is no specific location for center of mass of molecules as it varies, since molecules diffuse in all direction. Therefore physical properties not dependent on direction and hence this state called isotropic state. Overall, mesogens are anisotropic ordered fluids and sometimes described as "positionally disordered crystals" or "orientationally ordered liquids".[1] The molecular mobility and the propensity to self-organize promotes self-healing processes after the material is perturbed by external forces. These properties make such compounds fascinating and extremely appealing for applications in materials sciences and biology.[2c-d]

It is generally believed that an Austrian botanist, Friedrich Reinitzer first observed this "double melting" behavior when he was studying cholesteryl benzoate in 1888. He discovered this strange property that exhibited a mesophase between solid state and liquid state. At a temperature of 145 ^{o}C, it melted, becoming cloudy white and viscous. At a temperature of 179 ^{o}C, it became isotropic and clear. In beginning, Reinitzer attributed this phenomenon to the presence of impurities in the material, but he observed same behavior after further purification. On March 14, 1889, he wrote a letter to Otto Lehmann, Professor of Physics at the Technical

University Karlsruhe of Germany, mentioning him about the two melting points. Lehmann studied the material and discovered that the liquid at the mesophase exhibited a double refraction effect, the characteristic of a crystal. He named it "fliessende krystalle" (flowing crystals) and hence the name "liquid crystal" was born sharing the imperative properties of both solid and liquid.[2e]

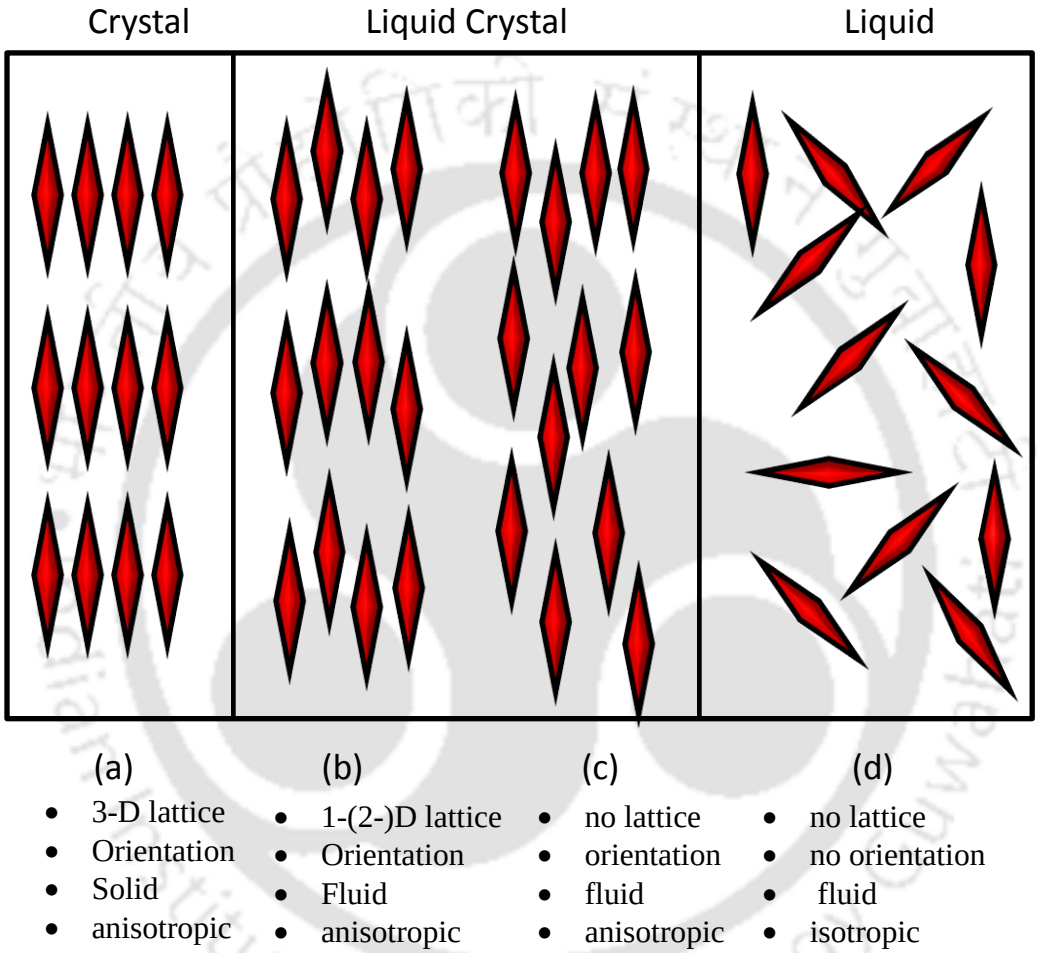

Figure 1.1. Basic structural difference among crystalline solid, liquid crystal and isotropic liquid.

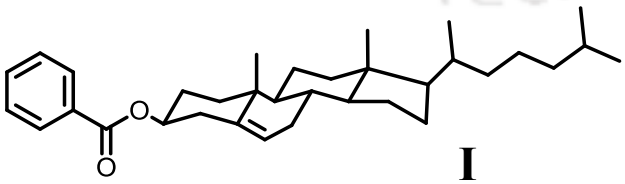

I

Cr 146^{o}C N* 178 ^{o}C I

Figure 1.2. Structure of cholesteryl benzoate

It was originally thought that mesomorphism could only be generated by molecules of rod like structure. In 1977, Chandrasekhar *et.al* discovered that not only rod-like *i.e.* calamitic molecules, but also compounds with disc-like molecular shape can also form mesophases.[5] Currently, more than 3000 discotic LCs are known in the literature. In 1986, LCs formed by board-like (lath-like) shape were reported.[6] Depending on the relative size of the main axes; these molecules can be derived from rod-like or disc-like molecules. Banana-shaped molecules are the latest addition to the LC family since 1996.[11] Typically, their molecular structure can be regarded as being composed of three units; an angular central unit, two linear rigid cores and terminal chains. The discovery of ferroelectricity in non-chiral banana shaped molecules has led to a very intense research activity, which led to the synthesis of several hundred bent shaped compounds so far. These molecules provide access to mesophases with polar order and supramolecular chirality. These and many other non-conventional structures exhibit interesting mesophase morphologies. Among them, one attracting class having particular attention is the oligomeric liquid crystals [OLCs][9] which are composed of more than two similar or different mesogenic moieties connected together via flexible spacers. The overall shape of an oligomesogen may vary from linear to star shaped, depending on the molecular topology, *i.e.,* the manner in which the mesogenic fragments are connected to each other or one another. Similarly many nonconventional molecular designs were incorporated to stabilize liquid crystallinity, which will be discussed in following sections.

1.2. Classification of liquid crystals

Liquid Crystals can be classified as shown in the Figure 1.3. Broadly they can be classified into Lyotropic[7] LCs, whose mesophase formation is concentration and solvent dependent and Thermotropic[7a] LCs, whose mesophase formation is temperature (T) dependent. Some molecules that exhibit LC phases under the influence of both heat and solvent; have been referred to as amphotropic LCs.[7c] Lyotropic LC phases are frequently encountered in everyday life, and most importantly, life itself is critically based on such ordered fluids. In 1850, a birefringent texture was observed by optical polarizing microscopy when myelin (from the sleeve that protects nerve cells) was mixed with water. Accordingly, lyotropic LCs were actually discovered before their thermotropic analogues but their significance was overlooked. Despite the significance of lyotropic LCs, thermotropic LCs have claimed a relatively greater attention,

firstly because they are simple to realize and easy to handle, and secondly they serve as important medium in fabricating low-power display devices.

The classification of mesophases is a complicated task as over the last few decades varieties of mesophases have been discovered or synthesized through conventional, nonconventional or via new molecular architecture. There are different ways to classify these mesophases, in terms of shape (calamitic, discotic and banana shaped mesogens *etc*.), molecular size (as low- and high molecular weight) and with respect to the type of mesophase formed (nematic, cholesteric, smectic, columnar *etc*.). The present work is mostly concentrated on thermotropic LCs and therefore the discussion is restricted to this topic only.

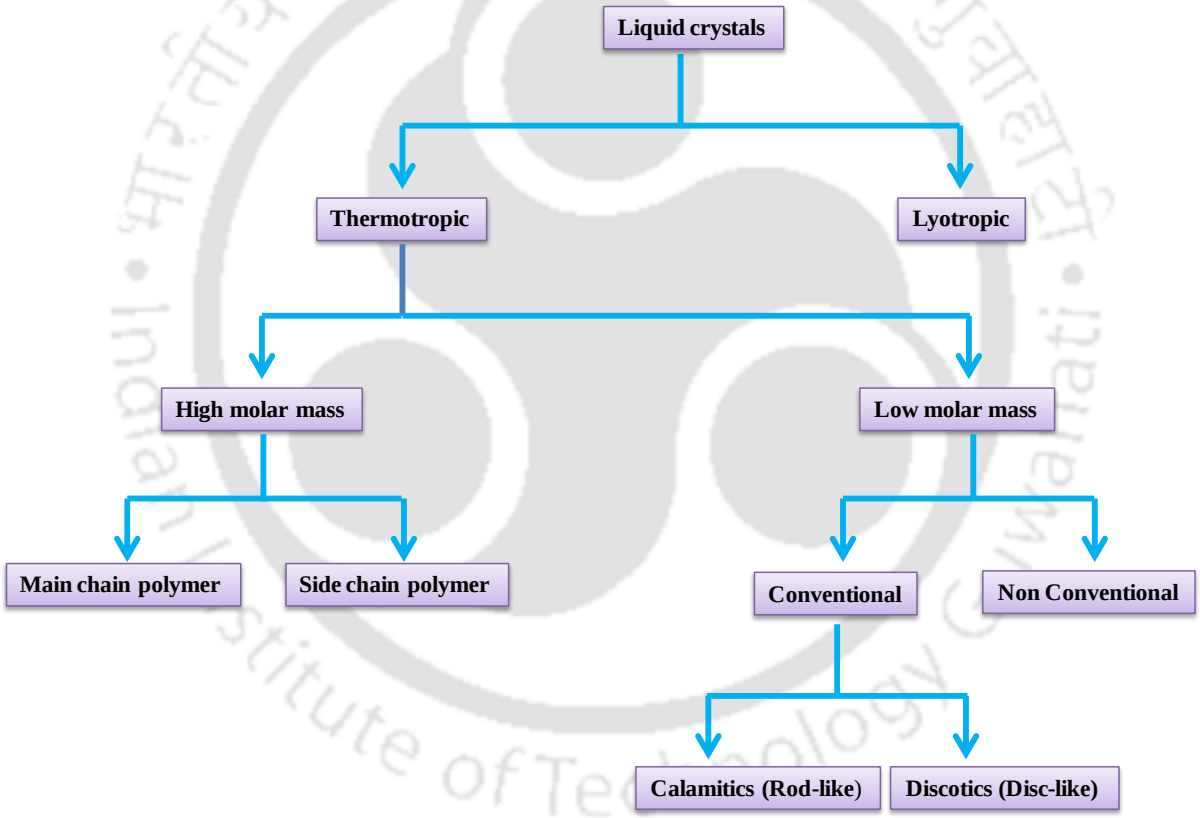

Figure 1.3. Schematic representation of general classification of liquid crystals.

1.3. Thermotropic liquid crystals

Most of the crystals on heating transform into the isotropic liquid phase by simultaneous loss of the long range positional and orientational orders. If the molecules possess certain amount

of shape anisotropy, then the disappearance in one, two or three dimensions of long-range translational periodicity in the crystals may precede the collapse of the long range orientational order. Such compounds may show a series of mesomorphic transitions into fluid states that exhibit varying degrees of the structural symmetries. The temperature at which the crystal transforms into mesophase is called melting point while that from the mesophase to isotropic state is called clearing point. Thermodynamically stable mesophases which appear both on heating and cooling are termed as enantiotropic, while the thermotropic mesophases that appear only on cooling are monotropic. Thermotropic LCs can be either high molar mass (polymeric) or low molar mass. Low molar mass thermotropic LCs can be classified further into conventional and non-conventional LCs.[8]

1.4. Conventional liquid crystals

Conventionally, rod-like and disc-shaped mesogens exhibit thermotropic mesomorphism; they are popularly known as calamitics and discotics respectively. For many years it was believed that the molecule has to be long or rod-shaped molecule (Fig. 1.4a) such as 4-methoxybenzylidene-4'-*n*-butylaniline, MBBA (**II**)[9] could be mesogenic. However, in 1977 Chandrasekhar *et.al.* demonstrated that disk-like molecules (Fig. 1.4b) such as benzene-1,2,3,4,5,6-hexayl hexaoctanoate (**III**) display mesomorphism.[5a]

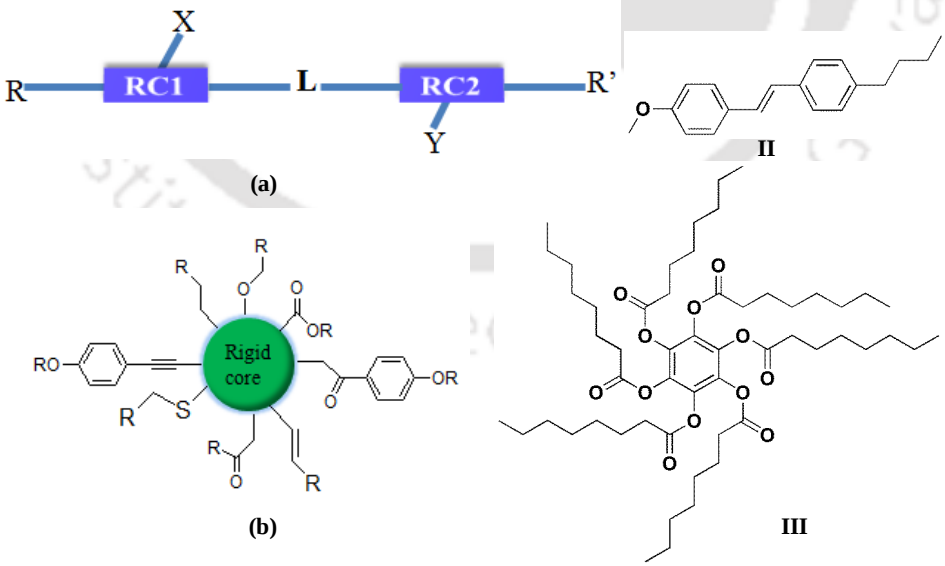

Figure 1.4. General templates for the rod-like (a) and disk-shaped (b) mesogens and their respective representative examples **II** and **III**

RC1 and RC2 are the rigid cores that are often aromatic in nature (*e.g.*, 1, 4-phenyl, 2, 5-pyrimidinyl, 2, 6-naphthyl *etc.*) but can also be alicyclic (*e.g.*, trans-4-cyclohexyl, cholesteryl *etc.*). In many examples these two cores are connected via a covalent bond and in some cases they are connected by linking unit L (*e.g.*,-COO-, -CH_2-CH_2, -CH=N-, -N=N- *etc.*). The terminal substituents R and R' are usually either alkyl or alkoxy chains. In many cases one of the terminal units is a polar substituent (e. g., CN, F, NCO, NCS, NO_2, *etc*). In some special cases the lateral units X and Y (*e.g.*, F, Cl, CN, CH_3 *etc.*) are incorporated in the main molecular structure. Rod-like or calamitic molecules have an elongated shape *i.e.* the molecular length (l) is notably greater than the molecular breadth (h) as depicted in Fig. 1.5.

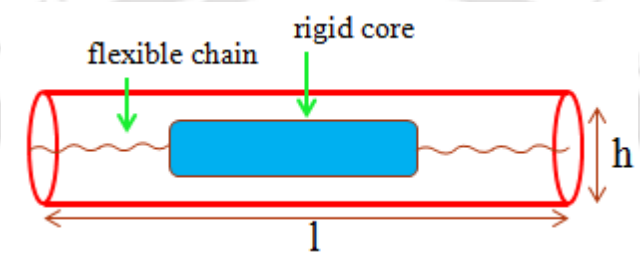

Figure 1.5. Representation of Calamitic LCs where l > > h

Discotic LCs are composed of a rigid core which is surrounded by three or more flexible aliphatic chains. Any type of change in the rigid core and peripheral flexible chains controls their self-assembly in bulk as well as in solution. These materials frequently have two, three, four or six-fold rotational symmetry. However, there are many exceptions and materials with low symmetry, a non-planar, non-aromatic core having shorter number of chains are also documented to display discotic mesophase. The mesomorphism is the result of the microsegregation of the two constituents: the face on interactions between the conjugated rigid cores promote the crystalline character while the liquid character originates from the melting of the saturated peripheral alkyl chains in the mesophase. Contrary to crystalline materials, discotic LCs have capacity of repairing structural defects because of the fact that, molecules in this phase organize spontaneously under the form of one-dimensional columns, which can be oriented easily and possess self-healing properties. The search for such mesophase is mostly regulated by delicate changes in the number, size and nature of the lateral chains in addition to the central core. A general template for discotic mesogens is shown in Figure 1.4b. Most of the disc-shaped molecules display only one type of mesophase but few examples are known to exhibit

polymorphism. Mesophases formed by discotic molecules are primarily classified as: nematic phases, columnar phases, lamellar phases.[5]Most common phase in discotics is columnar phase followed by nematic phase whereas the other phases are rarely observed. The nematic phases of disk-like molecules can be subdivided into four types: (i) discotic nematic (N_D), (ii) chiral nematic (N_D*), (iii) columnar nematic (N_{Col}), and (iv) nematic lateral (N_L). The structure of these nematic phases is shown in Fig. 1.6. Discotic nematic (N_D) phase is the least ordered, least viscous, and more symmetric mesophase among the other nematic phases.[5b] In a discotic nematic mesophase, the discotic molecules possess full translational and rotational freedom around their short molecular axis (disk normal) but on an average, the short molecular axes are oriented in a preferred direction called the director ***n***. In other words, the short molecular axes of the molecules orient more or less parallel to each other, while their centers of mass are isotropically distributed in the nematic phase. N_D has the same symmetry as that of calamitic nematic phase but both are not miscible with one another and hence phase separation occurs owing to the fundamental structural differences. Like chiral calamitic or cholesteric phase chiral discotic nematic phase N_D* also exists.[5c] The mesophase occurs in mixtures of discotic nematic and mesomorphic or non-mesomorphic chiral dopants as well as in pure chiral discotic molecules.[5d] The helical structure of the chiral discotic nematic phase is shown in Figure 1.6b. The columnar nematic phase (N_{Col}) is characterized by a columnar stacking of the molecules. However these columns do not form any 2D lattice structures.[5e-i] They display a positional short-range order and an orientational long-range order. The columns behave like supramolecular rods and can be regarded as building blocks of the N_{Col} phase instead of single molecules. Recently, another nematic phase has been reported, where the disk-shaped molecules aggregate into large superstructure, and these supramolecular aggregates show a nematic arrangement.

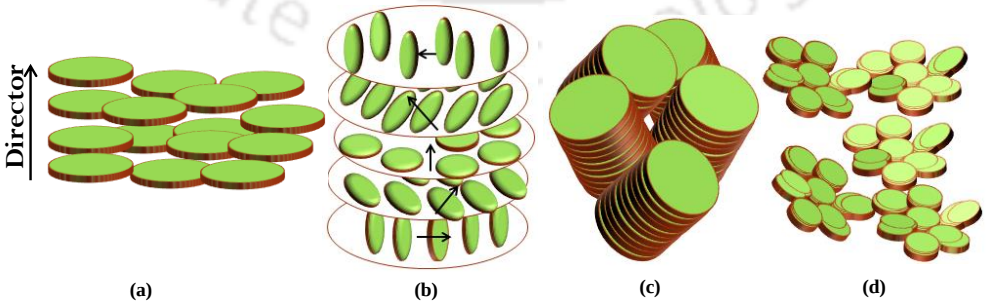

Figure 1.6. Structure of various nematic phases exhibited by discotic mesogens: (a) discotic nematic, (b) chiral nematic, (c) columnar nematic, and (d) nematic lateral.

The phase is referred to as the nematic lateral phase (N_L) due to the strong lateral interactions. [5j-l] Since this thesis deals with non-conventional LCs, our discussion on conventional LCs is restricted to this topic only.

1.5. Non-conventional liquid crystals

One can get materials of interesting properties by combining more than one contrasting or different functionalities within a molecule. The structure and property of these materials deviate from ordinary or conventional LCs. These types of liquid crystals are called non-conventional liquid crystals[8] which have become very popular in recent years, lack shape-anisotropy of the core unit. A lot of combinations are possible *e.g.* thermotropic/lyotropic, hydrophilic/hydrophobic, non-polar/polar, hydrocarbon/fluorocarbon, rigid/flexible, disc/rod, electron donor/electron acceptor, mesogenic/dimeric, mesogenic/oligomeric, mesogenic/polymeric *etc*. Non-conventional mesogens bridge the gap between entirely different chemical or physical properties. It is well known that anisotropic molecular shape and space filling play vital role in self-assembly of mesogens. However, nanoscale segregation of incompatible molecular parts *i.e.* micro segregation has also been realized to play an important role in mesogenic self-assembly, resulting in to new mesophase morphologies. On account of their astonishing self-assembly into complex soft materials, non-conventional liquid crystals are of massive interest at present. The general feature of majority of such materials is the molecular structural contrast within a molecule *i.e.*, these molecules are made up of chemically different molecular parts that are incompatible with each other. Some of the important examples of non conventional systems (see Fig. 1.7) are oligomers (**IV**)[9], Polycatenars (**V**)[10], bent-core molecules (**VI**) [11], polyhydroxy amphiphiles (**VII**)[12], octahedral complexes (**VIII**)[13], star shaped molecules (**IX**)[14], rod-coil molecules[15] (**X**) and dendrimers (**XI**)[16-17].

1.6. Bent-core mesogens

Though conventional thermotropic liquid crystals (LCs) are commonly made up of calamitic and disk-like molecules, Banana shaped mesogens are made of unconventional molecular architectures with a bend in the middle of the mesogenic part.[11] Niori *et al.*[11a] first reported the phenomenon of ferroelectricity in a smectic liquid crystalline phase which was

created from achiral banana-shaped molecules. Since then, several other research groups have reported banana-shaped molecules that exhibited ferroelectric properties in the mesophase.[11n] The ferroelectricity is attributed to the polar packing of molecules with C_{2v} symmetry where the molecules are packed in the same direction. Banana-shaped mesogens are also called as bent

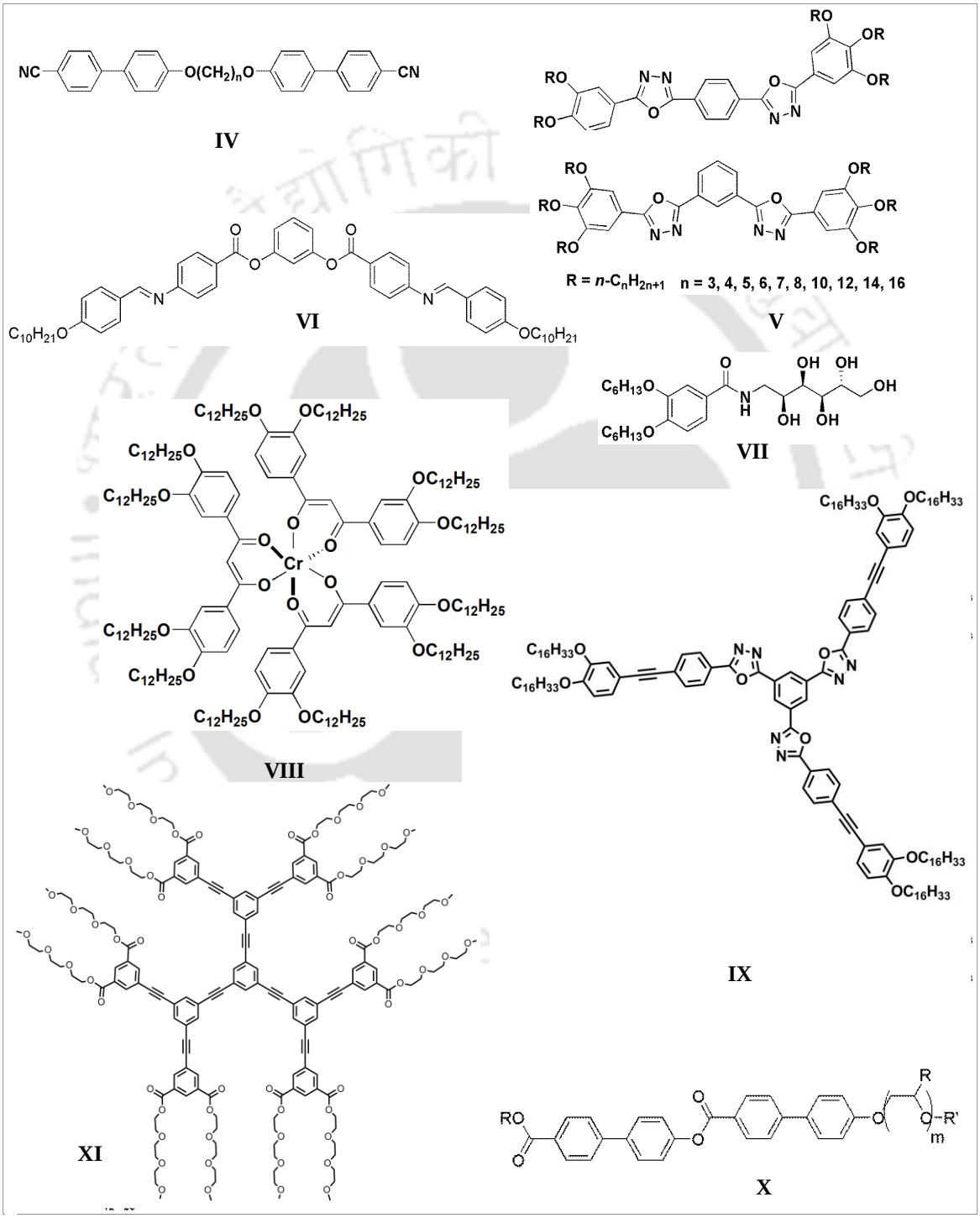

Figure 1.7. Molecular structures of different types of non-conventional LCs

core liquid crystals. Generally, these compounds are composed of a bent central aromatic part (*i.e.* a 1,3-disubstituted benzene) and two flexible tails. The curve in the middle of rigid core of the banana shaped compounds causes a reduction of the rotational disorder of the molecules about their long axes. The reduced symmetry of the rigid segments of such molecules leads to a directed packing of the molecules within layers. The main outcome of the directed packing of such molecules is the occurrence of a polar order parallel to the smectic layers. In order to escape from a macroscopic polarization, the layer structures are modified, and this leads to new mesophase morphologies. Bent core molecules are the first examples which have experimentally shown that antiferroelectric switching with large spontaneous polarization is indeed possible in a liquid crystal phase composed of non-chiral materials. Various new applications of these materials include nonlinear optics, flexoelectricity, photoconductivity, molecular electronics and the design of biaxial nematic phase. Figure 1.8 shows a general template of banana shaped liquid crystal molecules.

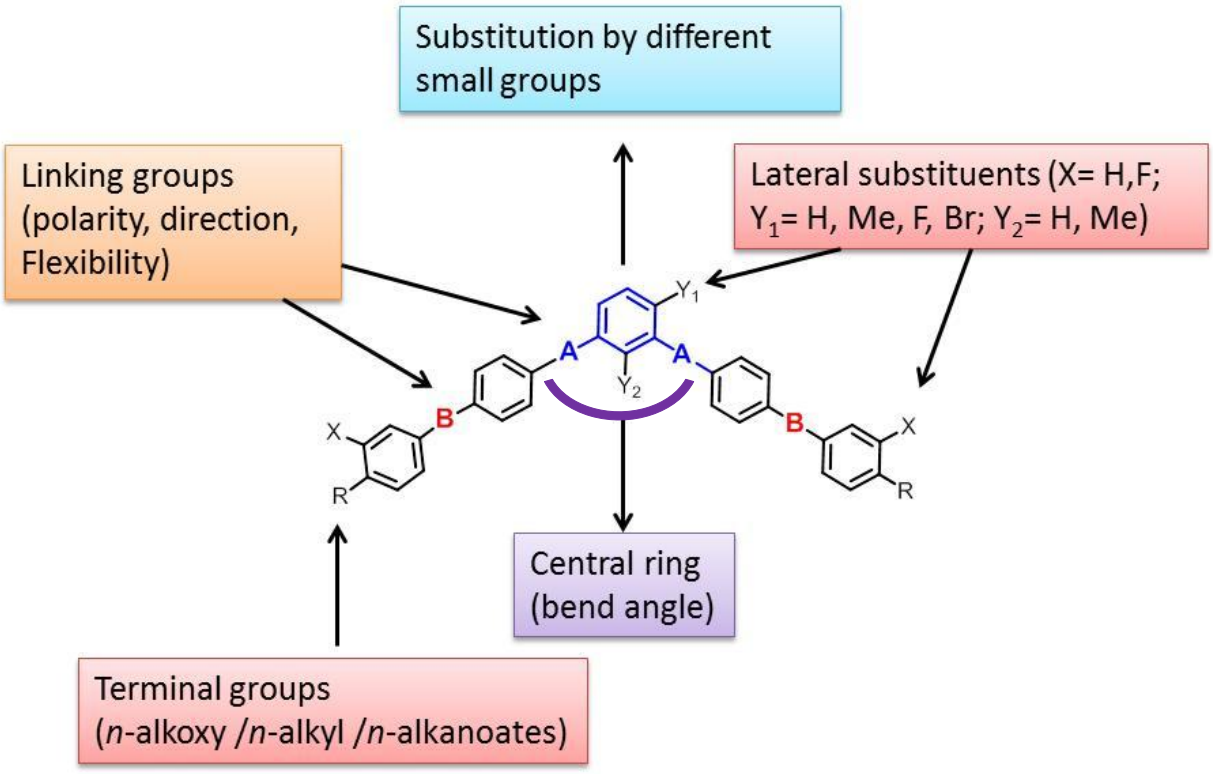

Figure 1.8. General template for banana liquid crystals. [11]

1.7. Oligomers

Oligomeric liquid crystals (OLCs) are supramolecular liquid crystals formed by the linking of two or more mesogenic (functional) segments by flexible spacers. Again the individual mesogenic units can be connected axially, laterally or radially. Among them, the linear oligomeric liquid crystals (LOLCs) having the individual mesogenic segments axially connected through paraffinic spacers[9c] are getting increasing attention. The reasons are obvious: firstly, it is a practical approach towards the attainment of multifunctional material with increased order and processability.[9i-l] Secondly, these macromolecules can exhibit the properties related to polymers, while retaining the fluidity and viscosity of low molar mass LCs. Thirdly, if the molecule is monodisperse it will lead to well defined properties unlike in polymers. Apart from these benefits, they will provide a platform to understand the supramolecular chemistry involved in the self-assembly of shape anisotropic macromolecules and this knowledge is of great importance in material sciences. A linear addition of one more mesogenic unit to a dimer through an alkylene spacer results in the next higher LOLC namely, trimer. Further addition of mesogenic segments results in tetramer, pentamer or hexamers and so on. Depending on the similarity of the molecular structure of the individual mesogenic units, these LOLCs can be classified as (i) symmetrical LOLCs- all the mesogenic units are identical, (ii) partially identical or C_2 symmetric LOLCs – some of the mesogenic units are identical and (iii) unsymmetrical

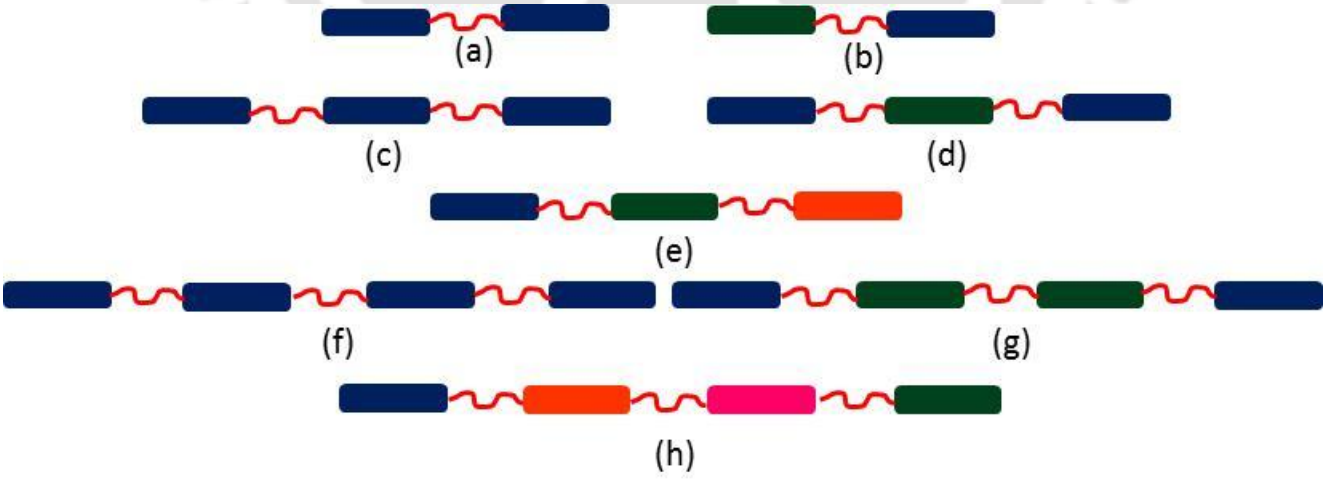

Figure 1.9. Schematic representation of various LOLCs: (a) symmetrical dimer, (b) unsymmetrical dimer, (c) symmetrical trimer, (d) C_2 symmetric or partially identical trimer, (e) unsymmetrical trimer, (f) symmetrical tetramer, (g) unsymmetrical tetramer. (Rectangular blocks in general represent the mesogenic segments)

LOLCs – none of the mesogenic units are identical (Fig. 1.9). The mesogenic units can be either rod like or disc like or any unconventional shape like bent systems.

1.8. Star-shaped mesogens (Hekates)

Non-conventional liquid crystals lack shape anisotropy in the core unit, but their lack of shape anisotropy to exhibit mesophases is compensated by the nanophase segregation of chemically or physically different molecular subunits and their tendency of efficient space filling. The simplest multiarm mesogens that do not fall in the category of rod shaped mesogens, dimers or bananas are molecules with three arms symmetrically linked with core units, which possess C_3 symmetry where all arms are identical are frequently known as star-shaped mesogens or hekates[14e, 22] as shown in Fig. 1.10.

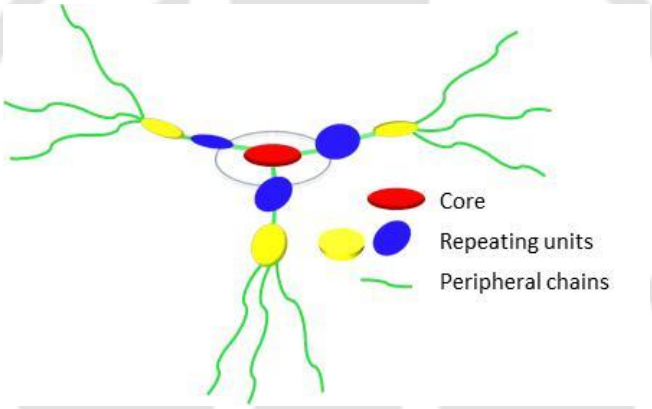

Figure 1.10. General structure of star shaped mesogens with three arms.

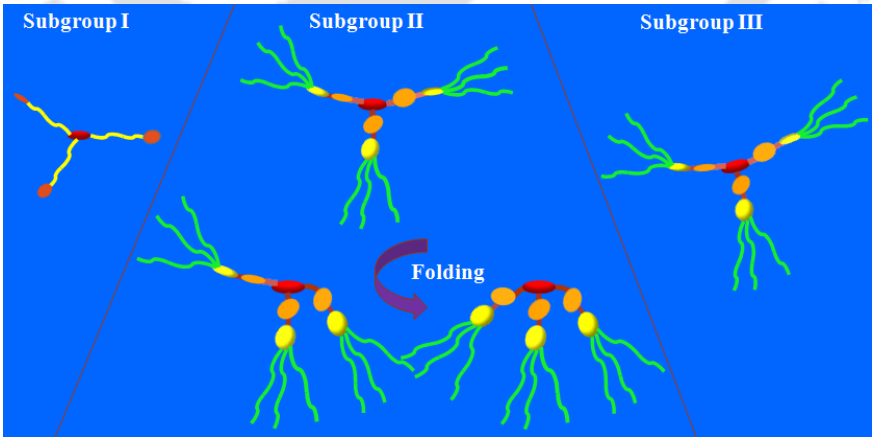

Figure 1.11. Classification of star-shaped three- arm mesogens.

The star mesogens can be divided into three subgroups; stars with three promesogens and mesogens linked to the central core with flexible spacers (subgroup I)[14e, 23] star with semiflexible scaffold (subgroup II)[14, 24]. Shape persistent star shaped mesogens are obtained on connecting the

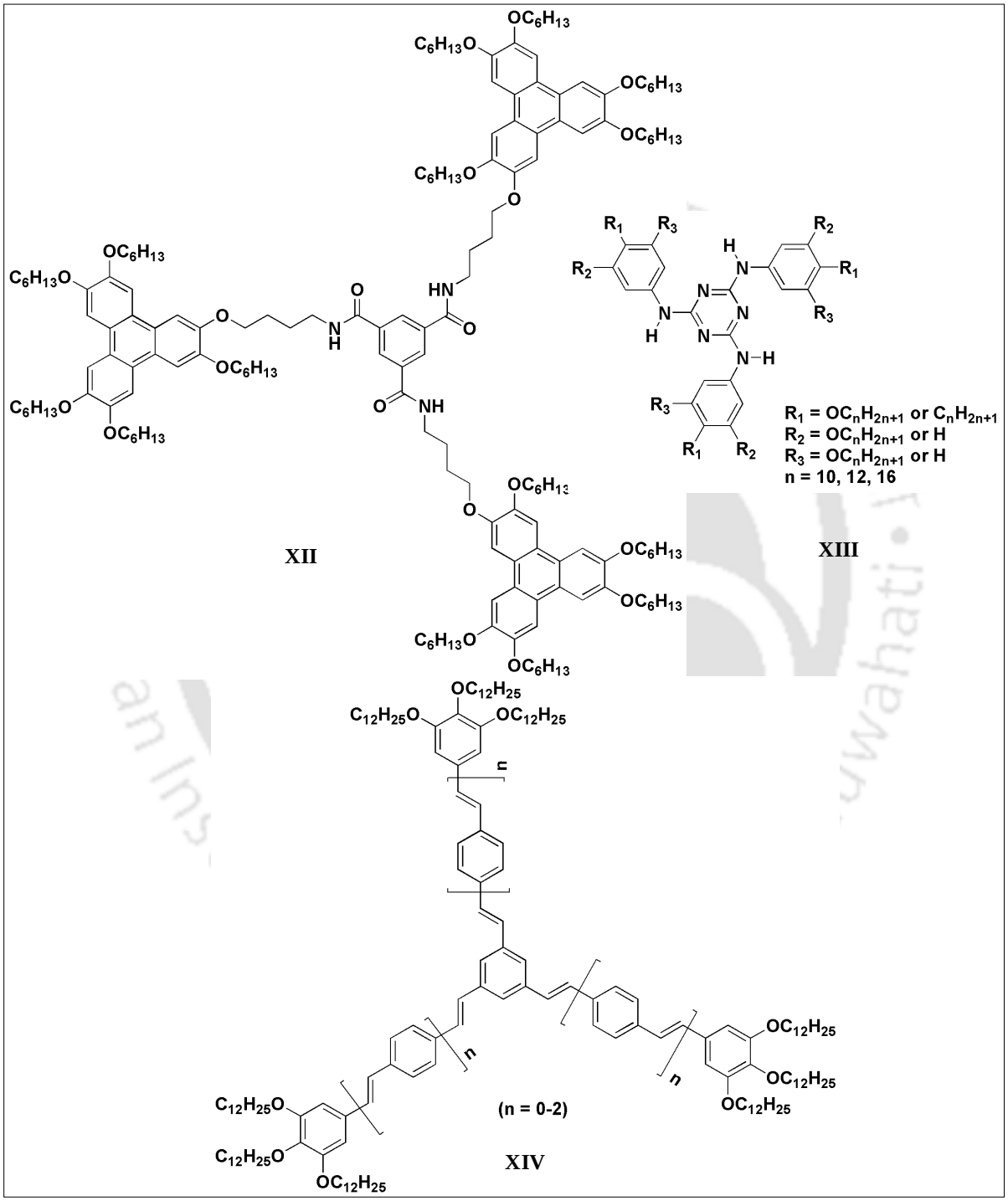

Figure 1.12. Flexible hekates (subgroup I)(**XII**); Semiflexible hekates (subgroup II)(**XIII**); and shape persistent hekates (subgroup III)(**XIV**).

three rigid arms to central core through linkers (subgroup III)[14, 25] as shown in Fig. 1.11 and 1.12. Inherent synthetic flexibility made these molecules advantageous over discotic molecules associated with synthetic difficulties. Thus the Col phases can be incorporated with other functional properties like hole or electron transport, nonlinear optical activity or fluorescence. Apart from this aspect, star shaped molecules are capable of exhibiting a rich variety of mesophases like nematic, columnar, cubic or soft crystal phases, because of their peculiar structure and tunable molecular design. The presence of the voids between the arms of the molecular structure helps to avoid the crystallization of mesophases and promote the glassy state. Columnar phases with glassy nature are important as they allow the movement of charge carriers through them with the simultaneous restriction of ionic impurities.[16] There is large void between the individual arms that has to be filled in condensed phases. Thus, a priori, one would not expect these molecules to form mesophases based on nanosegregation, since space-filling would likely lead to mixing of core and periphery of the stars, especially in the subgroup of shape-persistent molecules (Subgroup III). The void is used advantageously by incorporating larger chromophores in the arm scaffold by covalent bonds or guest molecules by supramolecular interactions. Complementary hydrogen-bond donors and acceptors can interact to give planar

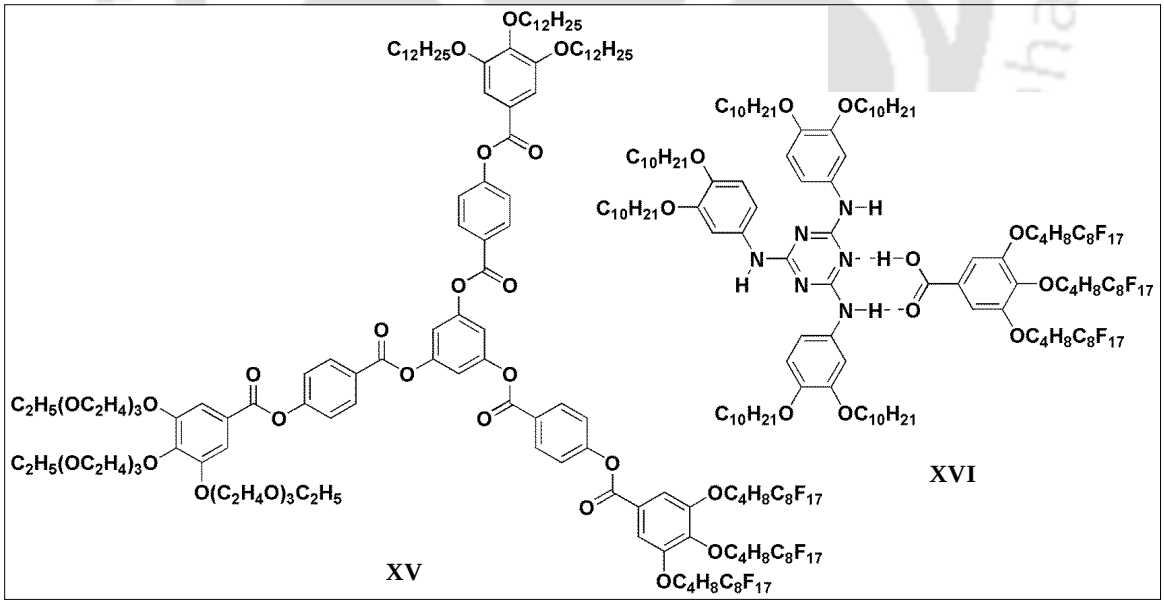

Figure 1.13. Janus-type hekates with incompatible peripheral chains (**XV**); Janus-type hekate forming a 1:1 host-guest complex with semi-perfluorinated chains (**XVI**).

disc-shaped aggregates due to the available void between the arms of the three-armed structure. Hekates afforded Janus-type complexes (Figure 1.13) that self-assemble in complex columnar hexagonal structures.[26]

1.9. Polycatenars

Polycatenar mesogens or phasmids are regarded as the connecting link between conventional rod like (calamitics) and disc like (discotics) mesogens as they possess the structural features and exhibit rich mesomorphic behavior common to both class of conventional LCs as shown in Fig. 1.14.[27] With regard to the stabilization of Col phase, this class of molecules are advantageous due to their lower melting/clearing point which helps in the alignment and the inherent synthetic flexibility to incorporate various functionalities, in comparison to discotics.

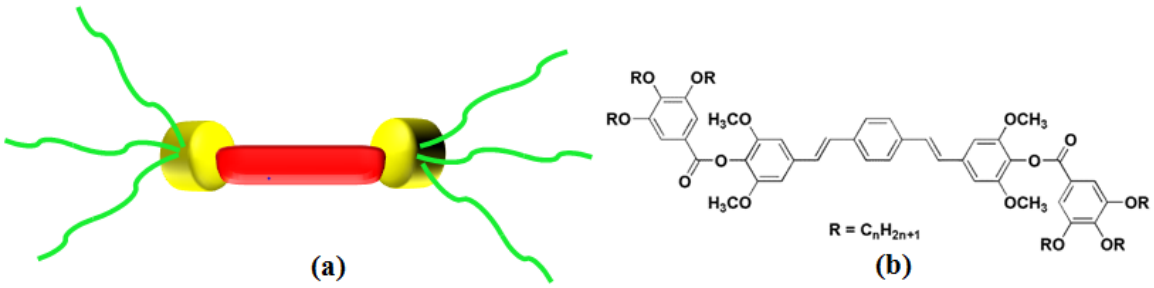

Figure 1.14. General structure of polycatenar mesogens (a) hexacatenar compound reported by Gin *et.al.* (b).

These molecules self-assemble into different LC phases due to the nanosegregation of aromatic units and flexible chains. Since polycatenars share the structural features of both calamitic and discotic LCs, they exhibit various LC phases like nematic, smectic (lamellar), cubic, and columnar phases, depending on the number of peripheral tails. Recently it was reported that some polycatenars based on an indigoid system (**XVIII**) even exhibited mesophases similar to bent core LC phases.[28] Incorporation of an extended π-conjugated aromatic system in the polycatenar molecular structure is very important from the viewpoint of charge carrier and luminescence properties.[29] Gin *et. al* reported a polycatenar system (**XVII**) with photophysical functions.[30] Yelamaggad *et. al.* incorporated hydrogen-bonding oligopeptides (**XIX**) in the polycatenar structure, which stabilized a Columnar phase.[31] Prasad *et.al* introduced a photoisomerizable azobenzene unit (**XX**) in the polycatenar structure.[32a] There are many reports

on luminescent polycatenar LCs.[29d-i]

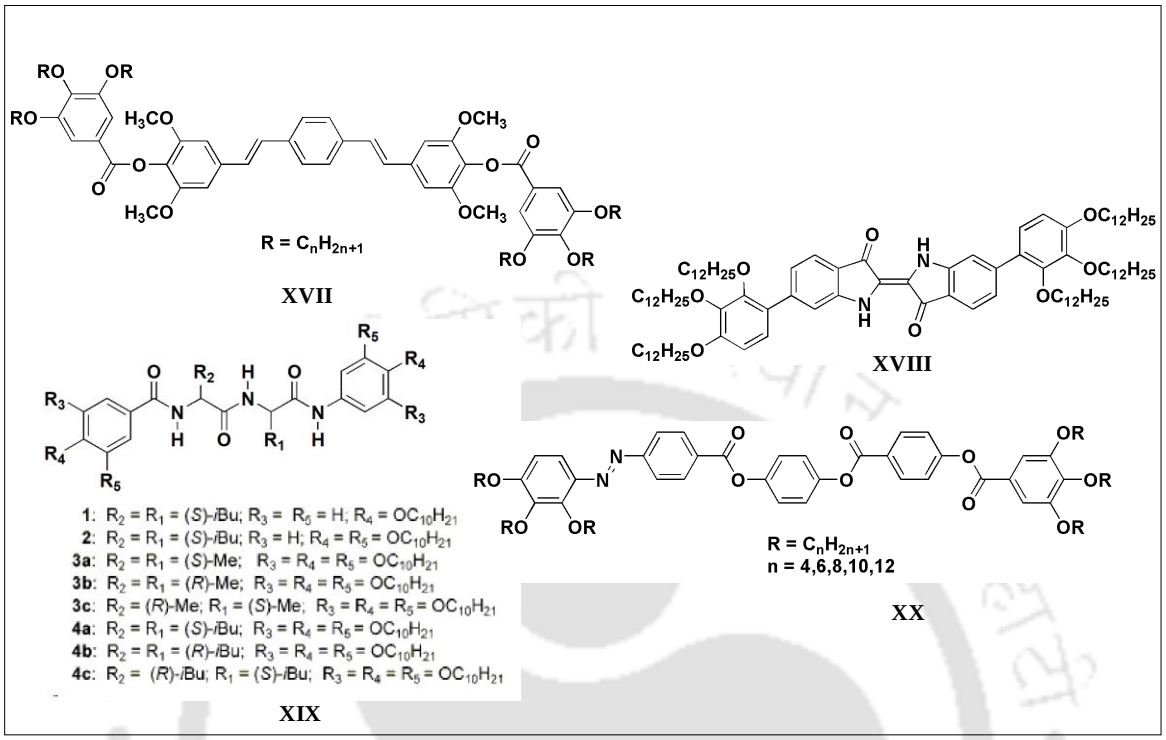

Figure 1.15. Molecular structures of different types of polycatenar mesogens.

1.10. Mesophase morphologies of thermotropic liquid crystals

Depending on the chemical structure and the shape of the constituent molecules and external parameters such as temperature and pressure, a rich variety of LC phases have been observed. In this section, columnar mesomorphism exhibited by conventional and non-conventional molecules are discussed.

1.11. Columnar phases of conventional and non-conventional liquid crystals: phase types and structures

Depending on the degree of order in the molecular stacking, orientation of the molecules along the columnar axis, the dynamics of the molecules within the columns and the two-dimensional lattice symmetry of the columnar packing, the columnar mesophases may be classified in various classes *eg.* Columnar hexagonal mesophase (Col_h), Columnar rectangular mesophase (Col_r), Columnar oblique phase (Col_{ob}), Columnar plastic phase (Col_p), Columnar

square (tetragonal) phase (Col_{tet}), Columnar helical (H) phase, (vii) Columnar lamellar phase (Col_L).

(i) Columnar hexagonal mesophase (Col_h)

Columnar hexagonal mesophase is characterized by a hexagonal packing of the molecular columns as shown in table1. Hexagonal mesophases are often denoted as Col_{ho} or Col_{hd} where "h" stands for hexagonal and "o" and "d" for ordered or disordered stacking of the molecules. In both cases, fluidity exists; only the correlation lengths are different and, therefore, it is recommended to discontinue o and d subscripts. The recommended abbreviation for columnar hexagonal phase is "Col_h." The planar space group of a hexagonal columnar mesophase is *p*6*mm*. The x-ray scattering profiles in the small-angle region, the columnar hexagonal phase generally exhibits four peaks whose spacings are in the ratio $1:1/\sqrt{3}:1/\sqrt{4}:1/\sqrt{7}$ along with two broad peaks in the wide-angle region. However, geometric considerations suggest that the Col_h phase can, in principle, display more reflections in the small-angle region. Out of the two wide-angle reflections, one corresponds to the liquid-like packing of flexible alkyl chains and the other one, which is relatively narrow, corresponds to the intracolumnar stacking of discotic cores.[36]

(ii) Columnar rectangular mesophase (Col_r)

Here the columns are arranged in a rectangular pattern as shown in table 1 and is denoted by Col_r. The two dimensional space group of rectangular columnar phase are *p2mm, c2mm, p2gg* and *p2mg* depends on the direction of the principle symmetry axis, which is the direction of columns. The molecules are elliptically placed in the plane which results in the deviation of symmetry of Col_r from a proper hexagonal arrangement. For that reason, strong core-core interactions are needed in the stabilization of the columnar rectangular phase because the cores of one column must be tilted with respect to cores of neighbouring columns. Therefore with increasing of side-chain length, cross over from columnar rectangular to columnar hexagonal has been observed.[18]

(iii) Columnar oblique phase (Col_{ob})

In a columnar oblique (Col_{ob}) mesophase, the arrangement of the columns, in which the tilted columns are represented by elliptic cross sections as shown in Table 1. The symmetry of this 2D lattice corresponds to the space group *p*1. Examples of columnar oblique mesophases are rare because of strong core–core interactions.[19b-d] Since *p*1 is a primitive planar space group, there are no reflection conditions like columnar hexagonal and rectangular phases and therefore all peaks are allowed. Hence, the assignment of the oblique mesophase by x-ray diffraction study is not so straightforward. Fan-shaped textures and spiral textures are characteristic for Col_{ob} phase.[19]

(iv) Columnar plastic phase (Col_p)

Columnar plastic phase, denoted as Col_p, is characterized by 3D crystal-like order of the center of mass of the molecules, but the columns are arranged in a 2D hexagonal lattice, while the disks within the columns are able to rotate about the column axis (Table 1). In the case of Col_h phase, structural disorders such as nonparallel arrangement of the disks, longitudinal and lateral displacements, and rotation around the columnar axis occur, while the motional freedom of disks in the Col_p phase is restricted. The x-ray diffraction pattern of Col_p phase exhibits low-angle reflections that can be indexed to form a 2D hexagonal lattice. In addition, the profile for the plastic phase has reflections having mixed indices. The presence of the diffuse peak in the wide angle which is due to the alkyl chains differentiates this phase from a truly crystalline phase. The wide angle core–core reflection, which is usually diffuse in the columnar phase, becomes very sharp and splits into two peaks.[20]

(v) Columnar square (tetragonal) phase (Col_{tet})

The structure of the columnar square phase, which is also known as tetragonal phase (Col_{tet}) is represented in table 1. In this mesophase the columns are upright and they are arranged in a square lattice. This phase also exhibit spontaneous homeotropic alignment of the columns similar to columnar hexagonal phase. This phase is exhibited by sugar molecules, phthalocyanines and supramolecular fluorinated liquid crystals.[37]

(vi) Columnar helical (H) phase

This exceptional mesophase structure with helical order was observed in a triphenylene derivative namely hexahexylthiotriphenylene (HHTT).[38a,b] In this so-called H phase helical columns develop with interdigitate in groups of three columnar stacks. X-ray diffraction experiments have proved that the helical H phase is distinctive to HHTT and certain mixtures of compounds with an average chain length close to 6 carbons.[38c] The H phase found in HHTT is shown in Table 1.

(vii) Columnar lamellar phase (Col_L)

A layered structure with columnar organization is known to exist for mesophases of certain discotic compounds.[39] Such a columnar lamellar mesophase, denoted by the symbol Col_L, is shown in Table 1 where discotic molecules stack to form columns and these columns are arranged in layers, where the columns in layers can slide but the columns in different layers do not possess any positional (translational) correlation. The x-ray profile of this phase in the low angle region displays reflections whose spacings are in the ratio 1:2:3 suggesting the lamellar organization of the columns and there appears a wide angle reflection corresponding to a distance of intracolumnar separation suggesting columnar organization of molecules in the layers. All the classical columnar mesophases included in this section are summarized in Table 1 with related schemes and structural parameters. The number of molecules per unit cell (or cross section) (z) can be estimated according to $z = \rho N_A S h_c / M$**,** where ρ is the density of the liquid crystal phase, N_A is Avogadro's constant, S is the columnar cross-section area, h_o is the height of the columnar slice and M is the molecular weight of the constitutive molecule. S can be calculated from the cell parameters, its expression depends on the geometry of the cell (see Table 1). The number of discoids present in the unit cell (Z_{disc}) is characteristic of the lattice geometry and the proposed model (see Table 1). Consequently, the number of molecules per discoid (N) is easily accessible by dividing the number of molecules in the cross section (z) by the corresponding Z_{disc} value. Therefore, a hypothesis on how mesogen molecules are eventually organized to form the discoidal shape can be formulated.

Table 1. Two-dimensional space groups of columnar liquid crystals with corresponding cross-section area and number of discoids (disc or ellipsoid) Z_{disc} in a cross section.

Type (notation)	**Space group**	**Extinction rules**	**Cross section**			**Three dimensional representation**
			Schema	Area	Discoid number	
Columnar hexagonal (Col_h)	*p*6*mm*	No conditions	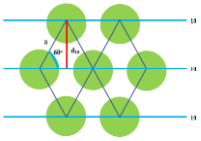	$S = a^2 sin60^o$	$Z_{disc} = 1$	
Columnar tetragonal (Col_{tet})	*p*4*mm*	No conditions	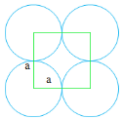	$S = a^2$	$Z_{disc} = 1$	
Columnar rectangular (Col_r)	*p*2*mm*	No conditions	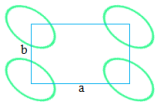	$S = ab$	$Z_{disc} = 1$	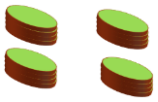
	*c*2*mm*	$hk: h + k = 2n$, $h0: h = 2n$, $0k: k = 2n$	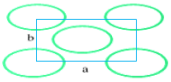		$Z_{disc} = 2$	
	*p*2*gg*	hk: no conditions, $h0: h = 2n$, $0k: k = 2n$	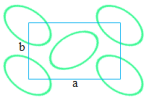		$Z_{disc} = 2$	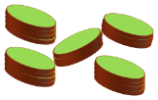
	*p*2*mg*	hk: no conditions, $h0$: no conditions, $0k: k = 2n$	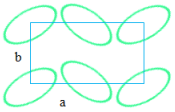		$Z_{disc} = 2$	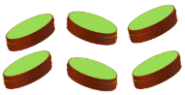
			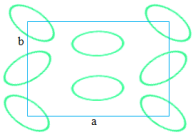		$Z_{disc} = 4$	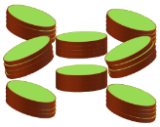
Columnar oblique (Col_o)	*p*1	No conditions	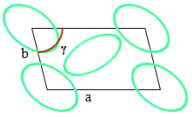	$S = absin\gamma$	$Z_{disc} = 2$	
Columnar plastic(Col_p)						
Columnar helical (H)						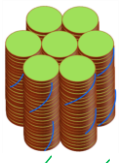
Columnar lamellar (Col_L)						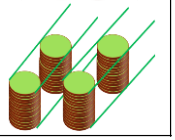

1.12. Identification of thermotropic mesophases

Since the discovery of LC molecules, till date a number of liquid crystalline phases have been observed. Precise characterization of LC phases generally requires the use of different techniques[1] as the structural differences between these phases are quite narrow. The most commonly used device to identify the LC phases is the polarizing optical microscope (POM) that reveals the characteristic optical texture of a mesophase.[1,2a] The identification of mesophases through POM usually involves the magnified view of a thin sample of a mesogenic material sandwiched between a glass microscope slide and a glass coverslip. The textures are usually examined between crossed polarizers, in white light under orthoscopic illumination; the substrates are either chemically treated for homogeneous / homeotropic alignment or used without any pretreatment. Calorimetric study using differential scanning calorimetry (DSC) is a complementary tool to microscopic studies to know the precise phase transition temperature and the enthalpy change associated with the transition. However there are limitations in mesophase characterization by either of these methods as the optical textures of different smectic or columnar phases are difficult to distinguish and the enthalpy values cannot be so characteristic for different phase transitions. Sometimes miscibility studies, in which a well-known liquid crystal phase is physically mixed with an unknown phase to ascertain the nature of the phase, are carried out based on the criterion of complete miscibility of identical phases.[2b] For unambiguous identification of mesophases, structural information such as relative molecular positions, the presence of long-range positional order, the quality of preferred molecular orientation *etc*., can be obtained from diffraction studies. X-ray, electron and neutron radiations are suitable for diffraction studies. X-rays are probably the most convenient and widely used whereas electrons and neutrons have advantages in particular situations. Other experimental techniques such as electro-optic measurements and nuclear magnetic resonance (NMR) spectroscopy are also in use for the characterization of mesophases.

1.13. Application and prospects of liquid crystals

Technologically, LCs have become a part of our daily lives. The established and potential applications of LCs are numerous. First showing up in faces of wrist watches and pocket calculators, but now being used for displays in all sorts of instrumentation, including portable

computers and televisions. Their advantage was first their low power consumption and small size; now LC displays compete with other technologies for attractiveness, ease of viewing, cost and durability.

1.14. Columnar mesophases as a promising media for modern applications

Columnar mesophase offers a one dimensional pathway for the electronic charge migration where the central aromatic core acts as a conducting unit, while the external peripheral chains act as the insulating mantle. This LC phase is of great importance because it allows the possibility to combine different physical properties (optical, conductive) with orientational control of the molecular order, self-healing of structural defects and ease of processability. Organic thin film solar cells having single crystalline organic materials are also promising for flat plate photovoltaic technology. These new organic materials are promising due to their low cost, good processability, large absorption coefficient, good charge carrier mobility whereas the inorganic materials used in this technology is hazardous to the environment. The "edge on" orientation of the Col phases can be translated into field effect transistors (FET) which are the vital components in molecular electronic devices. The high mobility for photo induced charge carriers in the Col phases also make them suitable for their use as active charge transport layer in fast and high resolution xerographic and laser printing applications.[33] Columnar LCs can be used as sensitive sensors for both polar and non-polar molecules.[34] Recently Col phases are gaining importance in the construction of organic light emitting diodes (OLEDs) as they can act as good emitting and conductive materials with proper design. Columnar phase with a combination of hole/electron transport and luminescence properties is an ideal material for the fabrication of OLEDs.[35]

1.15. Introduction to gels

Gels have pervaded our everyday life in a variety of forms. The wet soft solids that we encounter in the form of commercial products such as gel pens, soap, shampoo, toothpaste, hair gels, cosmetics as well as contact lenses *etc*. are all gels derived from polymeric compounds. Polymer gels have been known for centuries and applications in fields as diverse as food, medicine, materials science, cosmetics, pharmacology, sanitation etc. have been realized for

these systems[40]. In general, gels are viscoelastic solid-like materials comprised of an elastic cross-linked network and a solvent, which is the major component. Thus by weight, the gels are mostly liquid, but they behave like solids due to a three dimensional cross-linked network within the liquid. It is the cross-linking within the fluid that gives a gel its structure *i.e.* the hardness and its adhesive property. In other words, the gels are a dispersion of molecules of a liquid within a solid in which the solid is the continuous phase and the liquid is the discontinuous phase. Gel is a solid jelly-like material that can have properties ranging from soft and weak to hard and tough. Gels are defined as a substantially dilute cross-linked system, which exhibits no flow when in the steady-state. The three-dimensional cross-linked network within the liquid may result from physical bonds (physical gels) or chemical bonds (chemical gels) (Fig. 1.16), as well as crystallites or other junctions that remain unbroken within the extending fluid. The word *gel* was coined by 19th-century Scottish chemist Thomas Graham[41]. Any fluid can be used as an extender including water (hydrogels), oil, and air (aerogel). As mentioned earlier, both by weight and volume, gels are mostly fluid in composition and thus exhibit densities similar to those of their constituent liquids. Gelation relies on a balance between solvent–gelator and gelator–gelator interactions.[41c, 42b-g].

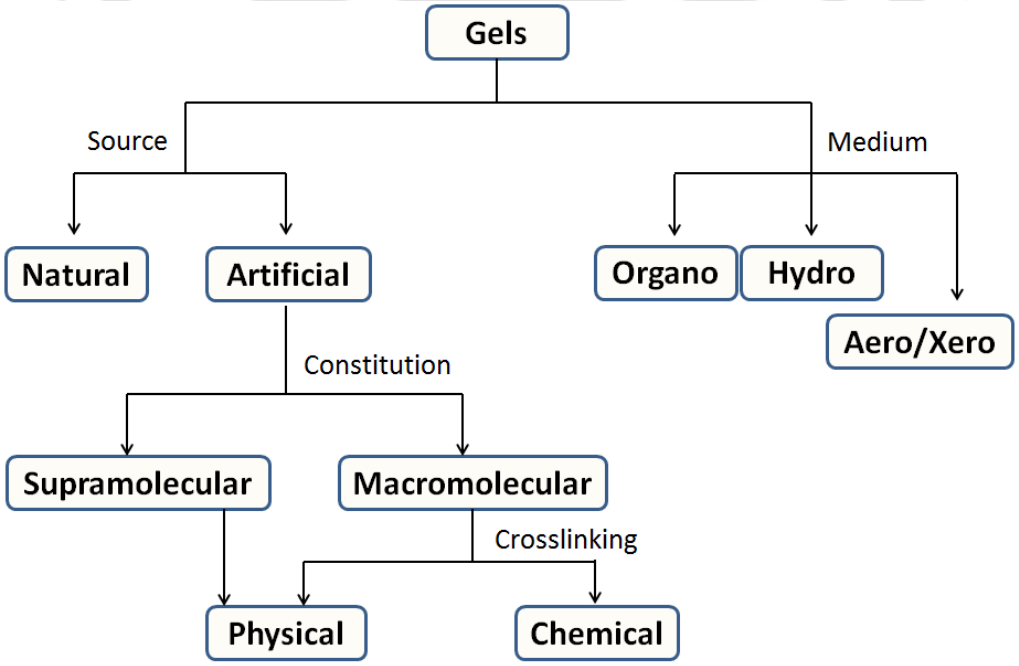

Figure 1.16. Classification of gels.

Edible jelly is a common example of a hydrogel and has approximately the density of water. Gels derived from low molecular mass compounds (‘‘physical gels’’, or ‘‘supramolecular gels’’), although known for a long time, have started to be actively investigated only during the past fifteen years[40] and applications as diverse as those realized for their polymeric counterparts have been envisaged for these systems. Most of the naturally occurring gelators are macromolecular and they form gels by physical cross-linking (usually H-bonding[42]). Such macromolecules include gelatin, collagen, agar, starch etc. Gels derived from synthetic compounds can be subdivided on the basis of their constitution into macromolecular (polymer) and molecular. The formation of gels from macromolecular compounds can either result from chemical cross-linking or physical interactions. When the gels are formed by strong chemical bonds, they cannot be redissolved and are thermally irreversible (e.g., polyester, polyamide, poly(vinyl alcohol), polyethylene) whereas gels formed by weak noncovalent interactions (physical entanglements) are reversible (e.g. polyacrylate, polymethacrylate).

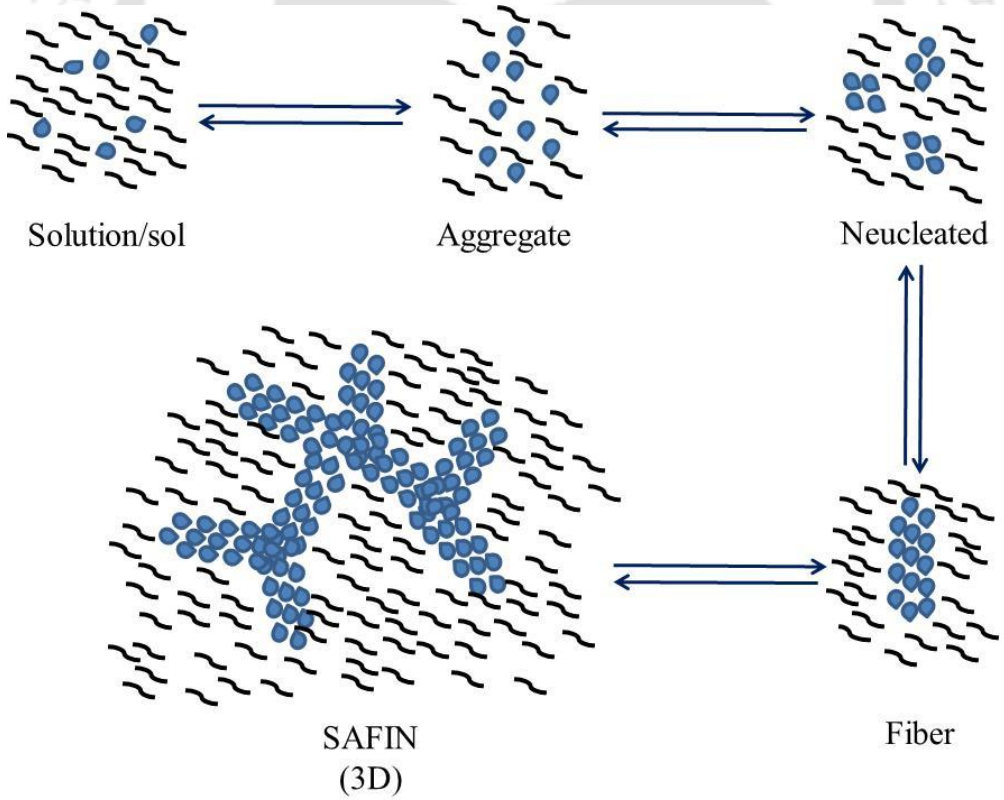

Figure 1.17. Representation of the steps in the evolution of low-molecular-mass organic gelators (LMOGs) (0D objects; tear drops) to fibers (1D objects) and, in some cases, to SAFiNs (3D objects) in liquids (wavy lines).

Gels derived from low molecular mass compounds are supramolecular, in that they are formed through self-aggregation of the small gelator molecules to form entangled 3-dimensional (3D) networks consisting of fibers. These 3D networks are formed by the entanglement of one-dimensional (1D) fibers that interact to form temporary and permanent junction zones; leading to self-assembled fibrillar networks (SAFiN) (Fig. 1.17). This is assisted by the crystallographic mismatches that lead to the branching of the main fiber into daughter fibers. The non-covalent interactions responsible for the 1D growth of fibers are mainly the H-bonding, π–π stacking, donor–acceptor [41] interactions, metal coordination, solvophobic forces (hydrophobic forces for gels in water) and van der Waals interactions. The SAFiN[41b] entraps solvent molecules on a microscopic level, via noncovalent interactions, and on a macroscopic level, *via* capillary forces and surface tension giving rise to solid-like rheological properties. Since these networks involve weak interactions, they can be readily transformed to a fluid (sol) by heating and are generally thermally reversible. Till the late 20th century low molecular mass gelators were largely neglected though it was discovered in the early nineteenth century. In the recent past, molecules of a great structural diversity, for instance from the simplest alkanes to the complex phthalocyanines, have been discovered to be the gelators. With the knowledge gained on the aggregation of gelator molecules during the past decade, attempts are being made to 'design' gelators through the incorporation of structural features (for instance, H-bonding motifs such as amides, ureas and saccharides) that are known to promote one-dimensional aggregation. Gels of a low molecular mass compound are usually prepared by heating the gelator in an appropriate solvent and cooling the resulting isotropic supersaturated solution to room temperature. When the hot solution is cooled, the molecules start to condense and three situations are possible (1) a highly ordered aggregation giving rise to crystals (2) a random aggregation resulting in an amorphous precipitate or (3) an aggregation process intermediate between these two, yielding a gel. The process of gelation involves self-association of the gelator molecules to form long, polymer-like fibrous aggregates, which get entangled during the aggregation process forming a matrix that traps the solvent mainly by surface tension. This process prevents the flow of solvent under gravity and the mass appears like a solid. Scientists have tried to describe the diversity of the molecular structures of gelators and have attempted to shed light on the structure and properties of their supramolecular aggregates.[43] At the microscopic level, the structures and morphologies of supramolecular gels have been investigated by conventional imaging techniques

such as scanning electron microscope (SEM), transmission electron microscopy (TEM), and atomic force microscopy (AFM) while thermal and mechanical studies are used to understand the interactions between these structures. However, at the nanoscale, X-ray diffraction, small angle neutron scattering (SANS) and small angle X-ray scattering (SAXS) are required to elucidate the structures of supramolecular gels. Depending on the dispersion medium or the sol, gel can be classified as hydrogels, organogels and aerogels (Fig. 1.16)

(i) Hydrogel

A hydrogel is a network of polymer chains that are hydrophilic, sometimes found as a colloidal gel in which water is the dispersion medium. Hydrogels consist of more than 90 percent of water and are superabsorbent natural or synthetic polymeric networks. Due to their significant water content, hydrogels have a degree of flexibility similar to natural tissue; they are often used as scaffolds in tissue engineering [44] and may contain human cells in order to repair tissue. The practical uses of hydrogels include breast implants, granules for holding soil moisture in arid areas and dressings for burns and hard-to-heal wounds, vehicles for controlled drug release,[45-46] and pollutant capture and removal.[47]

(ii) Organogels

Organogels or organic gelalators are noncrystalline, nonglassy, thermoplastic solid materials composed of a liquid organic phase entrapped in a three-dimensionally, cross-linked network. The liquid can be, for example, an organic solvent, mineral oil, or vegetable oil. The solubility and particle dimensions of the structures are important characteristics for the elastic properties and firmness of the organogel. Organogels are frequently found in food processing, pharmaceuticals and cosmetics.

(iii) Xerogels

Xerogels are solids formed from gels that do not suffer from shrinkage in the process. If the liquid system is almost entirely or wholly removed from the gel, then it will be called as a xerogel. Xerogels generally retain a high degree of porosity. Rubber and gelatin are examples of xerogels.

(iv) Aerogels

Aerogels are low-density materials created when the liquid component of a gel has been replaced by nitrogen or air. This results in very low density solids and low thermal conductivity that are highly effective as thermal insulators. Aerogels are used as chemical adsorber for cleaning up spills, in imaging devices, optics, and light guides etc.[48]

Since this thesis deals with organogels, our discussion is restricted to this topic only. An efficient methodology to elucidate the nature of an organogel is to begin with a characterization of its rheological and thermodynamic properties. Rheology is the study of the flow of matter, primarily in a liquid state, but also as 'soft solids' or solids under conditions in which they respond with plastic flow rather than deforming elastically in response to an applied force. Rheology offers a convenient method to measure the flow properties of gel like materials and facilitates the classification between "strong" and "weak" gel types.[49] Their flow properties depend upon gelator concentration and angular frequency (ω) of the applied stress. Mechanical parameters indicate the natures of the aggregate networks which, in turn, suggest the nature of the interactions responsible for their cohesion. Procedures such as steady shear, oscillation, stress relaxation, and creep experiments can probe the mechanical properties of the soft viscoelastic materials. The elastic and viscous components, mixed in such non-Newtonian materials, are measured in oscillatory experiments in which a small periodic strain/stress is applied within the appropriate amplitude range defining the linear regime. Dynamic rheological measurements are done to establish the elastic nature of the gel samples that involved strain sweep, angular frequency sweep, and step-strain measurements and it is characterized by $G^*(\omega) = G'(\omega) + iG''(\omega)$, where G' is the storage modulus, G'' is the loss modulus and ω is the angular frequency. Determination of the sol-to-gel phase transition temperature (TSG or T_{gel}) is necessary.[50] It is generally determined by a 'dropping-ball method where a small ball will be placed on top of the gel in a test tube and slowly heated in an oil bath at a fixed heating rate. Tg is defined as the temperature, when the ball had reached the bottom of the test tube.[51] Another important factor is critical gelation concentration (CGC) which means the minimum concentration is required to form a stable gel at room temperature[51b] and it is well known in literature that when the CGC is below or equal to 1 weight% it is called a supergelator.[56]

1.16. Applications

Gels have numerous industrial applications due to the great diversity of the structures that they display on microscopic and mesoscopic scales. Their thermoreversibility, chemical sensitivity, and diversity of nanostructures are intrinsic characteristics of organogels which make them excellent candidates for future industrial developments. Reverse micellar systems (microemulsions) involving gels find numerous applications in biocatalysis, biomembrane mimetics, extraction processes (universal solvents), and preparation of microparticles. Gels find important application in areas such as sensing, hydrometallurgy, cosmetics, food processing, and lubrication. Recovery of spilled crude oil or disposal of used cooking oil frequently involves gels or complex microemulsions. Application of organogels in drug delivery can be illustrated with the example of active enzymes and bacteria entrapped in apolar gels of gelatin. Highly concentrated oil-in-water (O/W) emulsions and various gels have been used as aviation fuels and in cosmetics while highly concentrated water-in-oil (W/O) emulsions are used in some explosives technologies.[52] Various complex mixtures of surface-active components (such as cetyl alcohol and polymers)[53-54] in water and oil are utilized for ointments and creams. Many aqueous gels[55] are employed for macromolecular separations, protein crystallization, etc.

1.17. References

1. (a) S. Chandrasekhar, in *Liquid Crystals*, 2nd ed.; Cambridge University Press: New York, 1994; (b) J. W. Goodby, P. J. Collings, T. Kato, C. Tschierske, H. Gleeson and P. Raynes, Eds. *Handbook of Liquid Crystals: Fundamentals*, Wiley-VCH: Weinheim, Germany, 2014; *Vol.* **1**; (c) T. Geelhaar, K. Griesar and B. Reckmann, *Angew. Chem. Int. Ed.* 2013, **52**, 8798-8809; (d) C. Tschierske, *Angew. Chem. Int. Ed.* 2013, **52**, 8828-8878; (e) Collings, P. J., and Hird, M., *Introduction to Liquid Crystals Chemistry and Physics.*, Taylor and Francis Ltd. London, 1997; (f) Bahadur, B., *Liquid Crystals: Application and Uses.*, *Vol.1-3*, World Scientific, Singapore, 1990; (g) Gray, G. W., *Molecular structure and the properties of liquid crystals.*, Academic press, London and New York, 1962; (h) Demus, D. and Richter, L., *Textures of liquid crystals*, 2nd Ed. Deutscher Verlag f. Grundstoffindustrie Leipzig, 1978; (i) Gray, G. W., in *Handbook of liquid crystals*, *Vol-1*, Eds: Demus, D., Goodby, J. W., Gray, G. W., Spiess, H. -W., and Vill, V., Wiley-VCH, Germany, 1998; (j) Gray, G. W., and Goodby, J. W., *Smectic Liquid crystalline Textures and Structures.*, Leonard Hill, Philadelphia, 1984; (k) de Gennes, P. G., and Prost, J., *The Physics of Liquid Crystals*, Oxford Science Publication, Oxford, 1993; (l) Kumar, S., *Liquid Crystals: Experimental Study of Physical Properties and Phase Transitions*; Cambridge University Press, 1st Ed. 2001; (m) Laschat, S., Baro, A., Steinke, N.,

Giesselmann, F., Hagele, C., Scalia, G., Judele, R., Kapatsina, E., Sauer, S., Schreivogel, A., and Tosoni, M., *Angew. Chem. Int. Ed.* 2007, **46**, 4832.

2. (a) I. Dierking, *Textures of Liquid Crystals*, Wiley-VCH, Weinheim, 2003; (b) H. Sackmann, and D. Demus, *Mol. Cryst. Liq. Cryst*. 1973, **21**, 239; (c) T. Kato, N. Mizoshita, K. Kishimoto, Angew. Chem. 2006, 118, 44; (d) T. Kato, N. Mizoshita and K. Kishimoto, *Angew. Chem. Int. Ed.* 2006, **45**, 38: (e) H. Kawamoto, *Proceedings of the IEEE*, Vol. 90, No. 4, April 2002.
3. (a) F. Reinitzer, Wiener Monatsh. Chem. 1888, **9**, 421; (b) F. Reinitzer, *Liq. Cryst*. 1989, **5**, 7.
4. O. Lehmann, *Z. Phys. Chem.* 1889, **4**, 462.
5. (a) S. Chandrasekhar, B. K. Sadashiva and K. A. Suresh, *Pramana* 1977**, 9**, 471; (b) H. K. Bisoyi, and S. Kumar, *Chem. Soc. Rev*. 2010, **39**, 264–285; (c) K. Praefcke, In *Physical Properties of Liquid Crystals: Nematics*, Dunmur, D. A., Fukuda, A., and Luckhurst, G. R. (eds.), INSPEC, London, U.K., pp. 17–35, 2001; (d) M. Langner, K. Praefcke, D. Kruerke, and G. Heppke, *J. Mater. Chem*. 1995, **5**, 693–699; (e) H. Ringsdorf, R. Wustefeld, E. Zerta, M. Ebert and J. H. Wendorff, *Angew. Chem. Int. Ed*. 1989, **28**, 914–918; (f) A. Grafe, D. Janietz, T. Frese and J. H. Wendorff, *Chem. Mater*. 2005, **17**, 4979–4984; (g) P. H. J. Kouwer, W. F. Jager, W. J. Mijs and S. J. Picken, *Macromolecules*, 2000, **33**, 4336–4342; (h) A. Stracke, J. H. Wendorff, D. Janietz and S. Mahlstedt, *Adv. Mater*. 1999, **11**, 667–670; (i) S. Mahlstedt, D. Janietz, A. Stracke and J. H. Wendorff, *Chem. Commun*. 2000, 15–16; (j) P. H. J. Kouwer, W. F. Jager, W. J. Mijs and S. J. Picken, *Macromolecules*, 2001, **34**, 7582–7584; (k) P. H. J. Kouwer, W. F. Jager, W. J. Mijs and S. J. Picken, *Macromolecules* 2002, **35**, 4322–4329; (l) P. H. J. Kouwer, O. van den Berg, W. F. Jager, W. J. Mijs, and S. J. Picken, *Macromolecules* 2002, **35**, 2576–2582; (m) T. Wohrle, I. Wurzbach, J. Kirres, A. Kostidou, N. Kapernaum, J. Litterscheidt, J. C. Haenle, P. Staffeld, Angelika Baro, F. Giesselmann, S. Laschat, *Chemical Reviews*, 2016, **116**, 1139−1241.
6. O. H. Schönherr, J. H. Wendorff, H. Ringsdorf, Peter Tschirner, *Makromol. Chem. Rap. Commun.* 1986, **7**, 791.
7. (a) P. G. de Gennes and J. Prost, *The physics of Liquid Crystals, 2nd ed.* (Oxford: Clarendon Press), 1993; (b) Y. Hendrikx, J. Charvolin, M. Rawiso and M. C. Holmes, *J. Phys. Chem.*, 87, 3991, 1993; (c) C. Tschierske, C. Curr. Opin. *Colloid Interface Sci*. 2002, **7**, 355-370.
8. (a) D. Demus, *Liq. Cryst.* 1989, **5**, 75-110; (b) C. Tschierske, *J. Mater. Chem*. 1998, **8**, 1485-1508; (c) C. Tschierske, *J. Mater. Chem*. 2001, **11**, 2647-2671; (d) C. Tschierske, *Annu. Rep. Prog. Chem. Sect. C*, 2001, **97**, 191-267; (e) C. Tschierske, *Curr. Opin. Colloid Interface Sci*. 2002, **7**, 69-80.
9. (a) H. Kelker and B. Scheurle, *Angew. Chem.* 1969, **81**, 903; (b) C. T. Imrie and G. R. Luckhurst, in *Handbook of liquid crystals*, *Vol-2B*, Eds.: D. Demus, J. W. Goodby, G. W. Gray and H. -W. Spiess, V. Vill, Wiley-VCH, Germany, 1998, part – III, p.799; (c) C. T. Imrie and P. A. Henderson, *Curr. Opin. Colloid Interface Sci*. 2002, **7**, 298-311; (d) C. T. Imrie in *Structure and Bonding - Liquid crystals, II*, Ed: D. M. P. Mingos, Springer-Verlag, 1999, p.149; (e) N. Tamaoki, *Adv. Mater*. 2001, **13**, 1135-1147; (f) C. V. Yelamaggad, G. Shanker, U. S. Hiremath, and S. K. Prasad, *J. Mater. Chem.* 2008, **18**, 2927-2949; (g) A. S. Achalkumar, U. S. Hiremath, D. S. Shankar Rao and C. V. Yelamaggad, *Liq. Cryst.* 2011, **38**, 1563-1589; (h) V. Borshch, Y. K. Kim, J. Xiang, M.

Gao, A. Jakli, V. P. Panov, J. K. Vij, C. T. Imrie, M. G. Tamba, G. H. Mehl and O. D. Lavrentovich, *Nature Communications*, 2013, **4**, 1-8; (i) E. Allard, F. Oswald, B. Donnio, D. Guillon, J.U. Delgado, F. Langa and R. Deschenaux, *Org. Lett*. 2005, **7**, 383; (j) C. V. Yelamaggad, S. A. Nagamani, U. S. Hiremath, D. S. S. Rao and S. K. Prasad *Liq. Cryst*. 2002, **29**, 231; (k) C. T. Imrie, F. E. Karasz and G. S. Attard, *Macromolecules* 1993, **26**, 545; (l) C. T. Imrie, P. A. Henderson and J. M. Seddon, *J. Mater. Chem.* 2004, **14**, 2486; (m) H. K. Bisoyi, S. Kumar, *Phase transitions*, 2006, **79**, 285-292.

10. (a) J. Tang, R. Huang, H. Gao, X. Cheng, M. Prehm, and C. Tschierske, *RSC Adv.* 2012, **2**, 2842-2847; (b) X. Yang, H. Dai, Q. He, J. Tang, X. Cheng, M. Prehm, and C. Tschierske, *Liq. Cryst.* 2013, **40**, 8, 1028-1034; (c) J. Malthete, A. M. Levulut and N. H. Tinh, *J. Phys. Lett.* 1985, **46**, 875-880; (d) J. Malthete, H. T. Nguyen and C. Destrade, *Liq. Cryst.* 1993, **13**, 171-187; (e) H.-T. Nguyen, C. Destrade and J. Malthete, *Adv. Mater*. 1997, **9**, 375–388; (f) K. E. Rowe and D. W. Bruce, *J. Mater. Chem.* 1998, **8**, 331-341; (g) B. P. Hoag and D. L. Gin, *Adv. Mater.* 1998, **10**, 1546-1551; (h) T. Yasuda, K. Kishimoto and T. Kato, *Chem. Commun.*, 2006, 3399-3401; (i) J. Seo, S. Kim, S. H. Gihm, C. R. Park and S. Y. Park, *J. Mater. Chem.* 2007, **17**, 5052-5057; (j) S.-J. Yoon, J. H. Kim, K. S. Kim, J. W. Chung, B. Heinrich, F. Mathevet, P. Kim, B. Donnio, A.-J. Attias, D. Kim and S. Y. Park, *Adv. Funct. Mater.* 2012, **22**, 61-69; (k) V. N. Kozhevnikov, B. Donnio and D. W. Bruce, *Angew. Chem. Int. Ed.* 2008, **47**, 6286-6289; (l) C. Alstermark, M. Eriksson, M. Nilsson, C. Destrade and H. T. Nguyen, *Liq Cryst.* 1990, **8**, 75-80; (m) D. Fazio, C. Mongin, B. Donnio, Y. Galerne D. Guillon and D.W. Bruce. *J. Mater. Chem.* 2001, **11**, 2852-2863; (n) D. M. Huck, H. L. Nguyen, P. N. Horton, M. B. Hursthouse, D. Guillon, B. Donnio and D. W. Bruce, *Polyhedron*. 2006, **25**, 307-324; (o) A. I. Smirnova and D. W. Bruce, *J. Mater. Chem*. 2006, **16**, 4299-4306; (p) E. Gorecka, D. Pociecha, J. Mieczkowski, J. Matraszek, B. Donnio and D. Guillon, *J. Am. Chem. Soc.* 2004, **126**, 15946-15947; (q) C. Tschierske, *Angew. Chem. Int. Ed.* 2000, **39**, 2454-2458; (r) E. Gorecka, D. Pociecha, J. Matraszek, J. Mieczkowski, Y. Shimbo, Y. Takanishi and H. Takezoe, *Phys. Rev. E.* 2006, **73**, 31704-31708; (s) J. Barbera, E. Cavero, M. Lehmann, J. L. Serrano, T. Sierra and J. T. Vazquez, *J. Am. Chem. Soc.* 2003, **125**, 4527-4533; (t) D. Pucci, *Liq Cryst.* 2011, **38**, 1451-1465; (u) K. Han and B.-K. Cho, *Soft Matter*, 2014, **10**, 7588-7594. (v) X. Yang, H. Dai, Q. He, J. Tang, X. Cheng, M. Prehm, *Liquid crystals*, 2013, **40**, 1028-1034.

11. (a) T. Niori, T. Sekine, J. Watanabe, T. Furukawa and H. Takezoe, *J. Mater. Chem*. 1996, **6**, 1231-1233; (b) R. A. Reddy and C. Tschierske, *J. Mater. Chem*. 2006, **16**, 907-961; (c) H. Takezoe and Y. Takanishi, *Jpn. J. of App. Phys*. 2006, **45**, No. 2A, 597-625; (d) G. Pelzi, S. Diele and W. Weissflog, *Adv. Mater.* 1999, **11**, 707; (e) M. B. Ros, J. L. Serrano, M. R. de la Fuente, C. L. Folcia, *J. Mater. Chem*. 2005, **15**, 5093; (f) C. Tsschierske and G. Dantlgraber, *Pramana* 2003, **61**, 455; (g) J. Etxebarria and M. B. Ros, *J. Mater. Chem*. 2008, **18**, 2919; (h) M. Lehmann, J. Seltmann, A. A. Auer, E. Prochnow and U. Benedikt, *J. Mater. Chem.* 2009, **19**, 1978-1988; (i) M. Lehmann and J. Seltmann, *Beilstein J. Org. Chem*. 2009, **5**, 73 (1-9); (j) T. Niori, T. Sekine, J. Watanabe, T. Furukawa and H. Takezoe, *Mol. Cryst. Liq. Cryst.* 1997, **301**, 337; (k) T. Sekine, Y. Takanishi, T. Niori, J. Watanabe and T. Takezoe, *J. Mater. Chem*. 1997, **7**, 1307; (l) Y. Matsunaga and S. Miyamoto, *Mol. Cryst. Liq. Cryst.* 1993, **237**, 311; (m) R. Cai and E. Samulski, *Liq. Cryst.* 1991, **9**, 617; (n) W. Weissflog, C. H. Lischka and H. Kruth, *Proceeding of the European Conference on Liquid Crystals, Science and technology*,

Zakopane, Poland, December 1997, **10-11, 3-8**, 126. (o) H. T. Nguyen, J. P. Bedel, J. C. Rouillon, J. P. Marcerou, M. F. Achard, *Pramana* 2003, **61**, 395-404; (p) S. Kumar, A. N. Gowda, *Liquid crystal reviews*, 2015, 99-145. (q) S. Lee, H. Kim, E. Tsai, J. M. Richardson, E. Korblova, D. M. Walba, N. A. Clark, S. B. Lee, D. K. Yoon, *Langmuir*, 2015, **31**, 8156-8161.

12. (a) C. Tschierske, *J. Mater. Chem*. 2001, **11**, 2647-2671; (b) C. Tschierske, *Annu. Rep. Prog. Chem. Sect. C*, 2001, **97**, 191-267; (c) C. Tschierske, *Curr. Opin. Colloid Interface Sci*. 2002, **7**, 69-80; (d) K. Borisch, S. Diele, P. Goring, H. Muller and C. Tschierske, *Liq. Cryst.* 1997, **22**, 427-443; (e) K. Borisch, S. Diele, P. Goring, H. Kresse and C. Tschierske, *J. Mater. Chem*. 1998, **8**, 529-543; (c) F. Liu, R. Kieffer, X. Zeng, K. Pelz, M. Prehm, G. Ungar and C. Tschierske, *Nature Communications*, 2012, **3**, 1104-1107; (f) C. Tschierske, *Isr. J. Chem.* 2012, **52**, 935-959; (g) K. Borisch, C. Tschierske, P. Goring, S. Diele, *Chem Commun*, 1998, 2711-2712.
13. (a) H. Zeng and T. M. Swager, *J. Am. Chem. Soc*. 1994, **116**, 761-762; (b) T. M. Swager and H. Zeng, *Mol. Cryst. Liq. Cryst.* 1995, **260**, 301-306.
14. (a) A. Pegenau, P. and Tschierske, *Chem. Commun.* 1996, 2563-2564; (b) M. Lehmann, R. I. Gearba, M. H. J. Koch, and D. A. Ivanov, *Chem. Mater.* 2004, **16**, 374-376; (c) M. Lehmann and M. Jahr, *Chem. Mater.* 2008, **20**, 5453-5456; (d) H. Detert, M. Lehmann and H. Meier, *Materials*, 2010, **3**, 3218–3330; (e) M. Lehmann, *Chem. Eur. J.* 2009, **15**, 3638–3651; (f) D. D. Prabhu, N. S. S. Kumar, A. P. Sivadas, S. Varghese, S. Das, *J. Phys. Chem. B*, 2012, **116**, 13071-13080.
15. M. Lee, D. -W. Lee and B. -K. Cho, *J. Am. Chem. Soc*. 1998, **120**, 13258-13259.
16. (a) J. H. Cameron, A. Facher, G. Lattermann and S. Diele, *Adv. Mater*. 1997, **9**, 398-403; (b) A. Pegenau, T. Hegmann, C. Tschierske and S. Diele, *Chem. Eur. J.* 1999, **5**, 1643-1660; (c) S. I. Stupp, M. Keser and G. N. Tew, *Polymer*, 1998, **39**, 4505-4508; (d) H. Meier, M. Lehmann, and U. Kolb, *Chem. Eur. J.* 2000, **6**, 2462-2469; (e) V. Percec, A. E. Dulcey, V. S. K. Balagurusamy, Y. Miura, J. Smidrkal, M. Peterca, S. Nummelin, U. Edlund, S. D. Hudson, P. A. Heiney, H. Duan, S. N. Magonov, and S. A. Vinogradov, *Nature*, 2004, **430**, 764-768; (f) M. Lehmann, C. Köhn, H. Meier, S. Renker and A. Oehlhof, *J. Mater. Chem.* 2006, **16**, 441-451; (g) B. M. Rosen, C. J. Wilson, D. A. Wilson, M. Peterca, M. R. Imam, and V. Percec, *Chem Rev.* 2009, **109**, 6275-6540; (h) B. Donnio, *Inorganica Chimica Acta*, 2014, **409**, 53-67. (h) V. Percec, M. Glodde, T. K. Bera, Y. Miura, I. Shiyanovskaya, K. D. Singer, V. S. K. Balagurusamy, P. A. Heiney, I. chnell, A. Rapp, H.-W. Spiess, S. D. Hudsonk , H. Duank, *Nature*, 2002, **419**, 384-387; (i) B. Donnio, S. Buathong, I. Bury, D. Guillon, *Chem. Soc. Rev*., 2007, **36**, 1495-1513.
17. a) C. Tschierske, J. Mater. Chem. 2001, **11**, 2647 – 2671; (b) C. Tschierske, J. Mater. Chem. 1998, **8**, 1485 –1508; (c) D. Guillon, Struct. Bonding (Berlin) 1999, **95**, 41 –82. (d) A. Skoulios, D. Guillon, *Mol. Cryst. Liq. Cryst*. 1988, **165**, 317 –332; (e) D. J. Pesak, J. S. Moore, *Angew. Chem. Int. Ed.Engl*., 1997, **36**, 1636-1639.
18. (a) A. M. Levelut, *J. Chem. Phys*. 1983, **80**, 149; (b)F. C. Frank, S. Chandrasekhar, *J. Phys*. 1980, **41**, 1285; (c) C. Destrade, P. Foucher, H. Gesparoux, H. T. Nguyen, A. M. Levelut, J. Malthete, *Mol. Cryst. Liq. Cryst*. 1984, **106**, 121,.
19. (a) F. Morale, R. W. Date, D. Guillon, D. W. Bruce, R. L. Finn, C. Wilson, A. J. Black, M. Schroder and B. Donnio,*Chem. Eur. J.* 2003**, 9**, 2484; (b) C. Destrade, , P. Foucher, H. Gasparoux, H. T. Nguyen, A. M. Levelut, and Malthete, J. *Mol. Cryst. Liq.Cryst*. 1984, **106**, 121–146; (c) B. Donnio, B. Heinrich, H. Allouchi, J. Kain, S. Diele, D.

Guillon, and D. W. Bruce, *J. Am. Chem. Soc*. 2004, **126**, 15258–15268; (d) C. Destwde, N. H. Tinh, L. Mamlok, and Malthete, J. *Mol. Cryst. Liq. Cryst*. 1984, **114**, 139–150.

20. B. Glusen, W. Heitz, A. Kettner, J. H. Wendorff, *Liq. Cryst*. 1996, **20**, 627.
21. (a) K. Ohta, H. Muroki, A. Takagi, K. I. Hatada, H. Ema, I. Yamamoto, K. Matsuzaki, *Mol. Cryst. Liq. Cryst*. 1986, **140**, 131; (b) H. Sakashita, A. Nishitani, Y. Sumiya, H. Terauchi, K. Ohta, I. Yamamoto, *Mol. Cryst. Liq. Cryst*. 1988, **163**, 211.
22. a) Collier_s Encyclopedia, Vol. 12 (Eds.: W. D. Halsey, B. Johnston), Macmilllan, New York 1988; b) W. Burkert, Greek Religion, Harvard University Press, Cambridge, 1985, p. 171.
23. a) G. H. Mehl, A. J. Thornton, J. W. Goodby, *Mol. Cryst. Liq. Cryst*. 1999, **332**, 455 – 461; b) P.Gçring, G. Pelzl, S. Diele, P. Delavier, K. Siemensmeyer, K. H. Etzbach, *Liq. Cryst*. 1995, **19**, 629 –635; c) S. Kumar, M. Manickman *Liq. Cryst*. 1999, **26**, 939 – 941; d) L. Wilson, *Liq. Cryst*. 1994, **18**, 1005 – 1014; e) S. H. Chen, H. Shi, B. M. Conger, J. C. Mastrangelo, T. Tsutsui, *Adv. Mater*. 1996, **8**, 998 –1001.
24. a) J. Barber_, L. Puig, J.-L. Serrano, T. Sierra, *Chem. Mater*. 2004, **16**, 3308 – 3317; b) D. Goldmann, D. Janietz, C. Schmidt, J. H. Wendorff, *Liq. Cryst*. 1998, **25**, 711 – 719; c) K. P. Van den Hout,. R. Mart n-Rapffln, J. A. J. M. Vekemans, E. W. Meijer, *Chem. Eur. J.* 2007, **13**, 8111 – 8123; d) J. J. van Gorp, J. A. J. M. Vekemans, E. W. Meijer, Mol. Cryst. Liq. Cryst. 2003, **397**, 191 –205; e) J. J. van Gorp, J. A. J. M. Vekemans, E. W. Meijer, *J. Am. Chem. Soc*. 2002, **124**, 14759 – 14769; f) J. H. Lee, S. H. Hwang, I. Jang, S. J. Lee, S. H. Yoo, J. Y. Jho, S.-Y. Park, Tetrahedron Lett. 2005, **46**, 7143 –7146; (g) M. Katoh, S. Uehara, S. Kohmoto, K. Kishikawa, *Chem. Lett*. 2006, **35**, 322 –323.
25. a) R. Christiano, D. M. Pereira de Oliveira Santos, H. Gallardo, *Liq. Cryst*. 2005, **32**, 7–14; b) C.-H. Lee, T. Yamamoto, *Mol. Cryst. Liq. Cryst*. 2002, **378**, 13–21; (c) B. G. Kim, S. Kim, S. Y. Park, *Tetrahedron Lett*. 2001, **42**, 2697 –2699; (d) J. C. Chang, J. R. Yeon, Y. S. Chin, M. J. Han, S.-K. Hong, *Chem. Mater*. 2000, **12**, 1076 –1082; (e) J. C. Chang, J. H. Baik, C. B. Lee, M. J. Han, S.-K. Hong, *J. Am. Chem. Soc*. 1997, **119**, 3197 –3198; (f) D. J. Pesak, J. S. Moore, *Angew. Chem*. 1997, **109**, 1709 –1712; (g) S. A. Ponomarenko, S. Kirchmeyer, A. Elschner, B.-H. Huisman, A. Karbach, D. Drechsler, *Adv. Funct. Mater*. 2003, **13**, 591 –596.
26. (a) A. Kohlmeier, D. Janietz, *Liq. Cryst*. 2007, **34**, 289 –294; b) D. Janietz, *J. Mater. Chem*. 1998, **8**, 265 – 274; c) D. Goldmann, D. Janietz, C. Schmidt, J. H. Wendorff, *Angew. Chem*. 2000, **112**, 1922 – 1925; (d) D. Goldmann, D. Janietz, C. Schmidt, J. H. Wendorff, *J. Mater. Chem*. 2004, **14**, 1521 – 1525; (e) D. Goldmann, D. Janietz, C. Schmidt, J. H. Wendorff, *Liq. Cryst*. 1998, **25**, 711 –719; f) J. Barber_, L. Puig, J.-L. Serrano, T. Sierra, *Chem. Mater*. 2004, **16**, 3308 – 3317; g) D. Goldmann, D. Janietz, C. Schmidt, J. H. Wendorff, *Liq. Cryst*. 1998, **25**, 711 – 719.
27. (a) J. W. Goodby, P. J. Collings, T. Kato, C. Tschierske, H. Gleeson, P. Raynes, *Wiley-VCH, Weinheim, Germany* 2014, *1. Handbook of Liquid Crystals: Fundamentals*, ed. (b) C. Tschierske, *Angew. Chem. Int. Ed*. 2013, **52**, 8828 – 8878.
28. J. H. Porada and D. Blunk, *J. Mater. Chem.* 2010, **20**, 2956- 2958.
29. (a) K. Mullen and G. Wegner, *Electronic Materials: The Oligomer Approach*; Wiley-VCH: Weinheim, 1998; (b) R. E. Martin and F. Diederich, *Angew. Chem. Int. Ed.* 1999, **38**, 1350-1377; (c) F. S. Precup-Blaga, J. C. Garcia-Martinez, A. P. H. J. Schenning and E. W. Meijer, *J. Am. Chem. Soc.* 2003, **125**, 12953-12960; (d) F. Lincker, P. Bourgun, P. Masson, P. Didier, L. Guidoni, J.-Y. Bigot, J.-F. Nicoud, B. Donnio, and D. Guillon, *Org.*

Lett. 2005, **7**, 1505-1508; (e) M. O'Neill and S.M. Kelly. *Adv Mater.* 2003, **15**, 1135-1146; (f) A. Contoret, A. Eastwood, S. Farrar, S. M. Kelly, E Nicholls, M. O'Neill, G. Richards and C. Wu, *Mol. Cryst. Liq. Cryst.* 2001, **368**, 271-278; (g) N. H. Sultana, S.M. Kelly, B. Mansoor and M. O'Neill, *Liq Cryst*. 2007, **34**, 1307-1316; (h) C. Gadermaier, G. Lanzani, G. Cerullo, M. Zavelani-Rossi, U. Theissel, B. Hoag, G. Leising, S. De Selvestri and D. L. Gin. *Synth Met.* 2001, **121**, 1323-1324; (i) A. P. Sivadas, N. S. S. Kumar, D. D. Prabhu, S. Varghese, S. K. Prasad, D. S. S. Rao, and S. Das, *J. Am. Chem. Soc.* 2014, **136**, 5416-5423.

30. B. P. Hoag and D. L. Gin, *Adv. Mater.* 1998, **10**, 1546-1551; (f) T. Yasuda, K. Kishimoto and T. Kato, *Chem. Commun.*, 2006, 3399-3401.
31. C. V. Yelamaggad, G. Shanker, R. V. R. Rao, D. S. S. Rao, S. K. Prasad, and V. V. S. Babu, *Chem. Eur. J.* 2008, **14**, 10462-10471.
32. N. G. Nagaveni, M. Gupta, A. Roy, and V. Prasad, *J. Mater. Chem.* 2010, **20**, 9089-9099;
33. (a) C.D. Simpson, J. Wu, M.D. Watsonand, K. Mullen, *J.Mater. Chem*., 2004, **14**, 494-504; (b) S. Laschet, A. Baro, *Angew. Chem.. Int. Ed*. 2007, **46**, 4832- 4887.
34. N. Boden, R. Bissel, J. Clements, and B. Movaghar, *Current science* 1996, **71**, 599-601.
35. T. Christ, B. Glusen, A. Greiner, A. Kettner, R. Sander, V. Stumpflen, and J.H. Wenderff, *Adv. Mater*. 1997, **9**, 48-52.
36. S. K. Prasad, D. S. S. Rao, S. Chandrasekhar and S. Kumar *Mol. Cryst. Liq. Cryst*. 2003, **396**, 121.
37. (a) T. Vlad-Bubulak, J. Buchs, A. Kohlmeier, M. Bruma, and D. Janietz, *Chem. Mater.* 2007**, 19**, 4460; (b) K. Ohta, T. Watanabe, H. Hasebe, Y. Morizumi, T. Fujimoto and I. Yamamoto, *Mol. Cryst. Liq. Cryst*. 1991, **196**, 13; (c) K. Hatsusaka, K. Ohta, I. Yamamoto and H. Shirai, *J. Mater. Chem*. 2001, **11**, 423; (d) M. Ichihara, A. Suzuki, K. Hatsusaka and K. Ohta, *Liq. Cryst*. 2007, **34**, 555; (e) K. Praefcke, P. Marquard, B. Kohne, W. Stephan, A. -M. Levelut and E. Watchtel, *Mol. Cryst. Liq. Cryst*. 1991, **203**, 149; (f) Md. A. Alam, J. Motoyanagi, Y. Yamamoto, T. Fukushima, J. Kim, K. Kato, M. Takata, A. Saeki, S. Seki, S. Tagawa, T. Aida, *J. Am. Chem. Soc.* 2009, **131**, 17722.
38. (a) E. Fontes, P. A. Heiney, W. H. De Jeu, *Phys. Rev. Lett*. 1988, **61**, 1202; (b) P. A. Heiney, E. Fontes, W. H. De Jeu, A. Riera, P. Carroll and A. B. Smith III, *J. Phys. France* 1989, **50**, 461; (c) S. H. J. Idziak, P. A. Heiney, J. P. McCauley, Jr. P. Carroll and A. B. Smith III, *Mol. Cryst. Liq. Cryst*. 1993, **237**, 271.
39. (a) S. Mery, D. Haristoy, J. F. Nicoud, D. Guillon, S. Diele, H. Monobe, and Y. Shimizu, *J. Mater. Chem*. 2002, **12**, 37–41; (b) P. Davidson, A. M. Levelut, H. Strzelecka, and V. Gionis, *J. Phys. Lett*. 1983, **44**, 823–828; (c) R. Ziessel, L. Douce, A. El-Ghayoury, A. Harriman, and A. Skoulios, *Angew. Chem. Int. Ed*. 2000, **39**, 1489–1493; (d) D. Haristoy, S. Mery, B. Heinrich, L. Mager, J. F. Nicoud, and D. Guillon, *Liq. Cryst*. 2000, **27**, 321–328; (e) N. Steinke, W. Frey, A. Baro, S. Laschat, C. Drees, M. Nimtz, C. Hagele, and F. Giesselmann, *Chem. Eur. J*. 2006, **12**, 1026–1035.
40. N. M. Sangeetha, U. Maitra, *Chem. Soc. Rev.*, 2005, **34**, 821–836.
41. (a) P. Terech, R. G. Weiss, *Chem. Rev.* 1997**, 97**, 3133-3159; (b) X. Y. Liu, J.-L. Li, *Soft Fibrillar Materials: Fabrication and Applications*, First Edition. 2013 by Wiley-VCH Verlag GmbH & Co. KGaA; (c) Y. Lan, M. A. Rogers, *CrystEngComm*, 2015, **17**, 8031-8038. (d) N. Yan, Z. Xu, K. K. Diehn, S. R. Raghavan, Y. Fang and R. G. Weiss, *J. Am. Chem. Soc*, 2013, **135**, 8989–8999; (e) X. Y. Liu and P. D. Sawant, *Adv. Mater.*, 2002,

14, 421–426; (f) R.-Y. Wang, P. Wang, J.-L. Li, B. Yuan, Y. Liu, L. Li and X.-Y.Liu, *Phys. Chem. Chem. Phys*., 2013, **15**, 3313–3319; D. Farbi, J. Guan and A. Cesaro, *Thermochim. Acta*, 1998, **321**, 3–16.

42. (a) S. Mukhopadhyay, U. Maitra, *Curr. Sci.*, 2004, **87**, 1666-1683. (b) Y. Wu, S. Wu, G. Zou and Q. Zhang, *Soft Matter*, 2011, **7**, 9177–9183; (c) M. A. Rogers and A. G. Marangoni, *Langmuir*, 2009, **25**, 8556–8566; (d) A. R. Hirst, I. A. Coates, T. R. Boucheteau, J. F. Miravet, B. Escuder, V. Castelletto, I. W. Hamley and D. K. Smith, *J. Am.Chem. Soc*., 2008, **130**, 9113–9121; (e) J. Gao, S. Wu, T. J. Emge and M. A. Rogers, *CrystEngComm*, 2013, **15**, 4507; (f) S. Wu, J. Gao, T. J. Emge and M. A. Rogers, *Soft Matter*, 2013, **9**, 5942; (g) Y. Lan, M. G. Corradini, X. Liu, T. E. May, F. Borondics, R. G. Weiss and M. A. Rogers, *Langmuir*, 2014, **30**, 14128–14142; (h) Y. Lan, M. G. Corradini and M. A. Rogers, *Cryst. Growth Des*., 2014, **14**, 4811–4818.
43. L. A. Estroff, A. D. Hamilton, *Chem. Rev.*, 2004, **104**, 1201-1217.
44. K. Y. Lee, D. J. Mooney, *Chem. Rev.* 2001, **101**, 1869-1879.
45. B. Xing, C-W. Yu, K-H. Chow, P-L. Ho, D. Fu, B. Xu, *J. Am. Chem. Soc.* 2002, **124**, 14846-14847.
46. J. C. Tiller, *Angew. Chem., Int. Ed. Engl.* 2003, **42**, 3072-3075.
47. S. Kiyonaka, K. Sugiyasu, S. Shinkai, I. Hamachi, *J. Am. Chem. Soc.* 2002, **124**, 10954-10955.
48. K. Almdal, J. D. S. Hvidt, O. Kramer, *Polymer Gels and Networks*. 1993, **1**, 5-17.
49. P. Terech, R. G. Weiss, *Chem. Rev.*, 1997, **97**, 3133-3159.
50. J. E. Eldridge, J. D. Ferry, *J. Phys. Chem.* 1954, **58**, 992-995.
51. (a) Z. Qi, N. L. Traulsen, P. M. de Molina, C. Schlaich, M. Gradzielski, C. A. Schalley, *Org. Biomol. Chem.*, 2014, **12**, 503–510; (b) R. G. Weiss, *J. Am. Chem. Soc*, 2014, **136**,7519-7530.; (c) A. R. Hirst, I. A. Coates, T. R. Boucheteau, J. F. Miravet, B. Escuder, V. Castelleto, I. W. Hamley, D. K. Smith, *J. Am. Chem. Soc*. 2008, **130**, 9113−9121.
52. G. Haering, P. L. Luisi, *J. Phys. Chem.* 1986, **90**, 5892-5895.
53. T. de Vringer, J. G. H. Joosten, H. E. Junginger, *Colloid and polymer sci*, 1987, **265**,167-179;
54. H. K. Patel, R. C. Rowe, J. McMahon, R. F. Stewart, *Int. J.of pharma*, 1985, **25**, 13-25.
55. R. J. Phillips, W. M. Deen, J. F. Brady, *J.colloid and inter.sc*, 1990,**139**, 363-373.
56. (a) S. K. Pathak, B. Pradhan, R. K. Gupta, M. Gupta, S. K. Pal, A. S. Achalkumar, *J. Mater. Chem. C*, 2016, **4**, 6546-6561; (b) T. Yamamoto, M. Yoshida, *Langmuir*, 2012, **28**, 8463; (c) M. Zhang, D. Xu, X. Yan,J. Chen, S. Dong, B. Zheng, F. Huang, *Angew. Chem.,Int. Ed.*, 2012, **51**, 7011; (d) R. Yoshida, *Adv. Mater.*, 2010, **22**, 3463.

Chapter II

1,3,4-Oxadiazole / thiadiazole based tris(*N*-salicylideneaniline)s (TSANs)

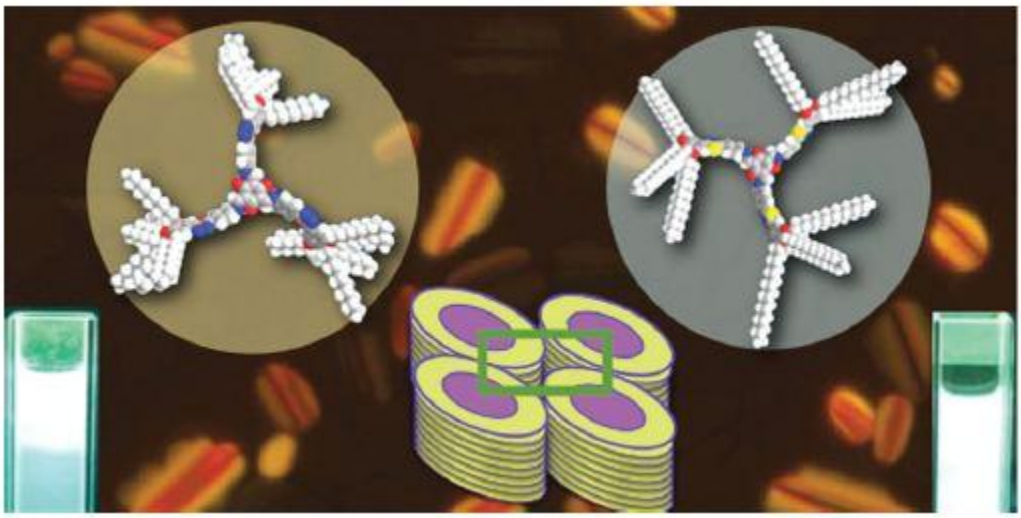

Results have been published in *New J. Chem.,* 2017, **41**, 4680-4688.

2.1. Introduction

Rational molecular design and the synthesis of functional molecules, which stabilize the ordered self-assembly is of great technological relevance. Liquid crystals, which have already realized several commercial applications, are one of the most fruitful areas of supramolecular self-assembly. In this area of study, ideas get translated into devices, which have huge potential in the fields of energy, health care and security.[1] The formation of highly anisotropic ordered self-assemblies and their extreme sensitivity to the external perturbations without losing the ordered structures, self-healing ability make them ideal materials for the device applications.[2] Liquid crystal material design is often aimed at developing a room temperature mesophase, due to the fact that they help in reducing the external energy input and simplify the device fabrication. Recently, Columnar liquid crystals (Col LCs) formed by the one-dimensional stacking of disc-like molecules, polycatenars and star-shaped molecules have been receiving increasing attention. [1] This is because they are the potential alternative to conductive polymers or organic single crystals for application in organic electronic devices like field effect transistors, light emitting diodes, solar cells and photoconductors. They are inexpensive, processable, self-healable and easy to handle in comparison to single crystals and they also possess higher conductivity and supramolecular order in comparison to amorphous polymers.[2] The central aromatic core of such molecules play a major role in imparting the desired material property, whereas their peripheral tails ensure the liquid crystalline self-assembly. Introduction of five membered heterocycles in the molecular architecture provides an unsymmetric distribution of electron density and hence a lateral and/or longitudinal dipole moments in the molecules. The bent structure of the heterocycles can be tuned based on the type and position of the hetero atoms and leading to a variation in the resultant optical and self-assembly behavior.[3] Considering the large number of hydrocarbon based Col LCs which are typically electron rich (*p*-type materials), electron deficient (*n*-type materials) Col LCs are very rare.[4] Organic *n*-type semiconductors and Col LCs are less in number due to the synthetic difficulty and their inherent instability in air. One easy approach to impart the *n*-type nature is by the introduction of heteroatoms in the molecular architecture, in which the electronegative nature of the heteroatoms render the aromatic structure electron deficient. Thus several heterocycle-based molecules are finding application as electron transport/hole blocking and electroluminescent materials. Additionally, several heterocycle

containing mesogens have been reported in recent years, due to the wide variety of luminescent colors they offer as a function of structure and unsymmetric electron distribution and due to the induction of dipole moments and variation in the bent angle of these molecules, a wide variety of mesophases have been stabilized.[5] Mesogens based on 1,3,4-oxadiazoles are widely reported in literature of liquid crystals and organic light emitting diodes, due to their high hydrolytic and thermal stability, blue light emission and *n*-type behavior.[6] Their sulphur containing analogues, *i.e.*1,3,4-thiadiazole based materials are also known for their application in spatial light modulators, optical signal processers, information storage devices, thin film transistors, fast switching ferroelectric materials and fluorescent sensors, as well as in medicinal and agromedicinal chemistry.[7] They also possess comparable thermal and hydrolytic stability, good luminescence properties, higher dipole moment and efficient packing behaviour. However reports on their derivatives showing liquid crystalline self-assembly are few in number in comparison to their oxadiazole counterparts. A few reports appeared recently on rod-like mesogens,[8] banana shaped mesogens,[9] hydrogen bonded LCs,[10] polymeric LCs,[11] polycatenars[12] and star-shaped LCs[13] based on 1,3,4-thiadiazole derivatives. In general, the synthesis and tunability of DLCs to incorporate the functionality is not a straightforward task. In this respect 'star-shaped' molecules or 'hekates' provide an easier alternative to tailor the molecular structure and introduce functional properties.[14] In these molecules, three arms decorated with peripheral tails are symmetrically connected to a central core, which leads to an effective nanoseggregation of incompatible molecular subunits and thus stabilizes the columnar self-assembly. Several central cores for example, 1,3,5-substituted benzene,[15] triazine,[16] triazolotriazines[17] and tris(*N*-salicylideneaniline)s (TSANs)[18] have been utilized with the three arms connected symmetrically. TSANs are relatively a new class of molecules, which assist in stabilizing several functional supramolecular self-assemblies such as liquid crystals,[18,19] H-bonded capsules, molecular clefts,[20] and covalent organic frameworks,[21] and can be easily tailored to introduce features like luminescence, self-organizing ability, molecular recognition and sensing.[22] As part of our ongoing research on the synthesis of luminescent Col LCs and heterocyclic mesogens we envisaged to prepare new star-shaped mesogens based on TSANs. In our earlier paper, we have reported star-shaped mesogens with TSANs as central cores to which three substituted 1,3,4-oxadiazoles are connected. These compounds showed high transition temperature and exhibited Col_h phase. They exhibited blue light emission in solution, which was red shifted in solid state.

Our recent encouraging results on 1,3,4-thiadiazole based star shaped and polycatenar mesogens, which exhibit a broad mesophase width and good luminescence behavior, motivated us to connect unsymmetrically substituted 1,3,4-thiadiazole arms to a central TSANs core. Further we were also interested to study the effect of branching in the peripheral tails of both oxadiazole and thiadiazole based TSANs. Thus the branched tail containing 16 carbon atoms, *i.e.* three 2-hexyldecyloxyl chains were introduced at the periphery in comparison to normal hexyldecyloxyl chain. Their thermal and photophysical behavior were thoroughly investigated to understand the structure property relationship.

2.2. Results and discussion

2.2a. Synthesis and Characterization

The synthetic route for the preparation of target molecules and their precursors is depicted in scheme 2.1. 4-nitrobenzohydrazide was heated with 3,4,5-trimethoxybenzoyl chloride in presence of pyridine as a base and solvent to obtain compound **2**. This on heating in presence of phosphorous oxychloride ($POCl_3$) yielded oxadiazole derivative **3a**. The same intermediate on heating in presence of phosphorous pentasulfide (P_2S_5) provided thiadiazole derivative **3b**. These trimethoxy derivatives were subjected to BBr_3 mediated demethylation[18b] to yield trihydroxy derivatives **4** and **5,** respectively, which upon *O*-alkylation with alkyl bromides yielded corresponding nitro compounds **6a-c**. Compound **6a** was reduced by catalytic hydrogenation to yield corresponding amine **7a**. Compounds **6b-c** were reduced by treating them with zinc powder in presence of ammonium formate to yield compounds **7b-c**. These anilines on treating with 1,3,5-triformylphloroglucinol afforded oxadiazole based TSANs **O-b16**, thiadiazole based TSANs **T-16** and **T-b16**. (Scheme 2.1). 1,3,5-Triformylphloroglucinol was prepared as reported earlier.[18] These compounds existed as an inseparable mixture of regioisomers of C_{3h} and C_s symmetry, which was quantified by ^{1}H NMR by integrating the ratio of the protons corresponding to each isomer (Table.1). The structures of all the intermediates and target molecules were confirmed using ^{1}H NMR, ^{13}C NMR, IR spectroscopy as well as with ESI-HRMS or MALDI-TOF analysis.

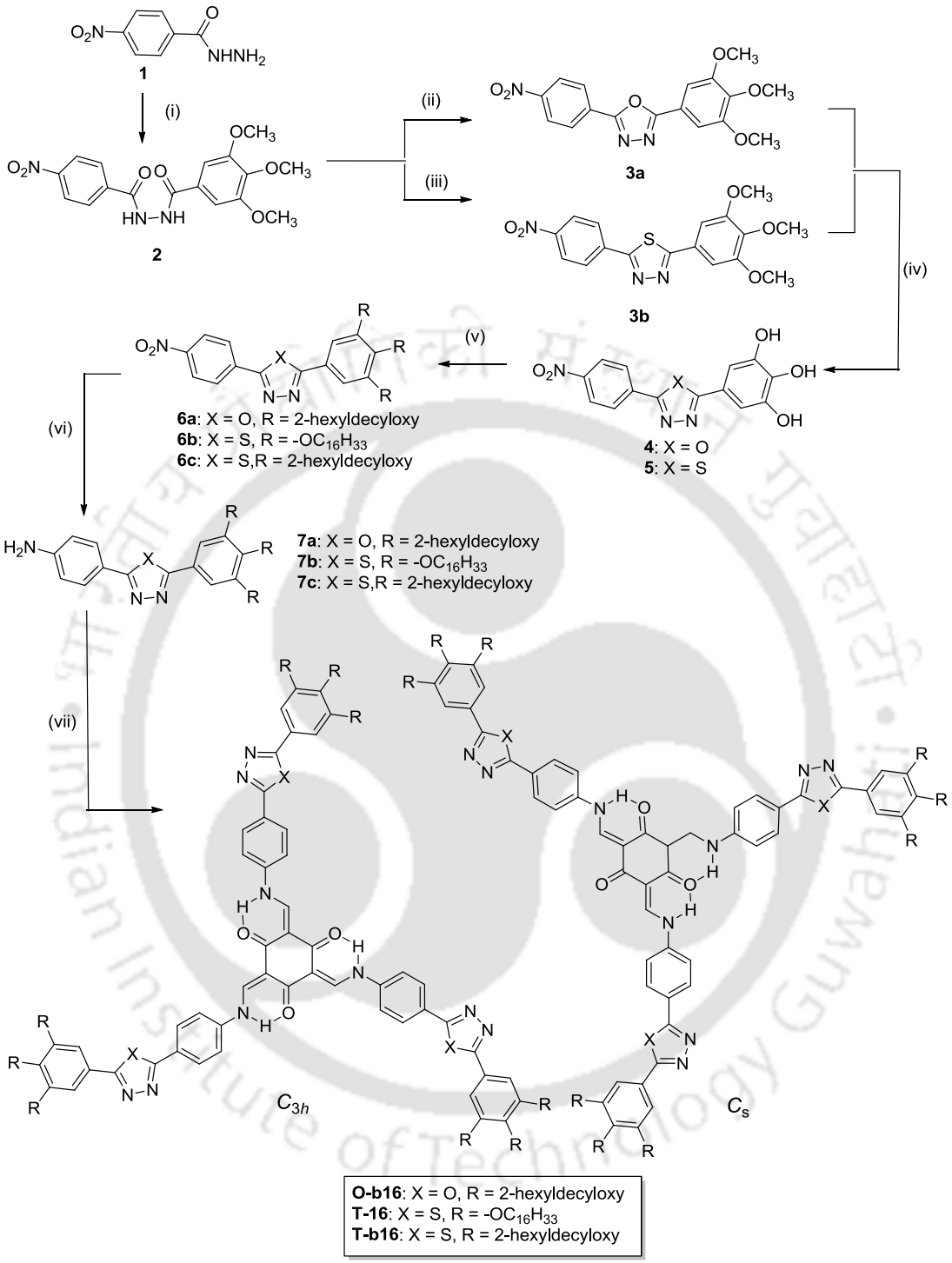

Scheme 2.1. Reagents and conditions: (i) 3,4,5-Trimethoxybenzoyl chloride, pyridine, 60 ^{o}C, 12 h (75%); (ii) $POCl_3$, 100 ^{o}C, 5 h (70%); (iii) P_2S_5, dry THF, 60 ^{o}C, 24 h (60%); (iv) BBr_3, CH_2Cl_2, -78 ^{o}C to rt, 17 h (65-70%); (v) *n*-bromohexadecane or 2-hexylbromodecane, anhydrous K_2CO_3, DMF, 80 ^{o}C, 17 h (60-70%); (vi) 10% Pd-C, H_2 (balloon, 1 atm) THF, rt, 12 h (72%) or Zn powder, $HCOONH_4$, CH_3OH + THF (1:1), rt, 1 h (60-65%); (vi) 1,3,5-Triformylphloroglucinol, Ethanol, Ar, reflux, 6 h (65-80%).

As representative cases from each series, ^{1}H NMR spectra of the 1,3,4-oxadiazole based O-b16 and 1,3,4-thiadiazole based **T-b16** are presented in Figure 2.1.

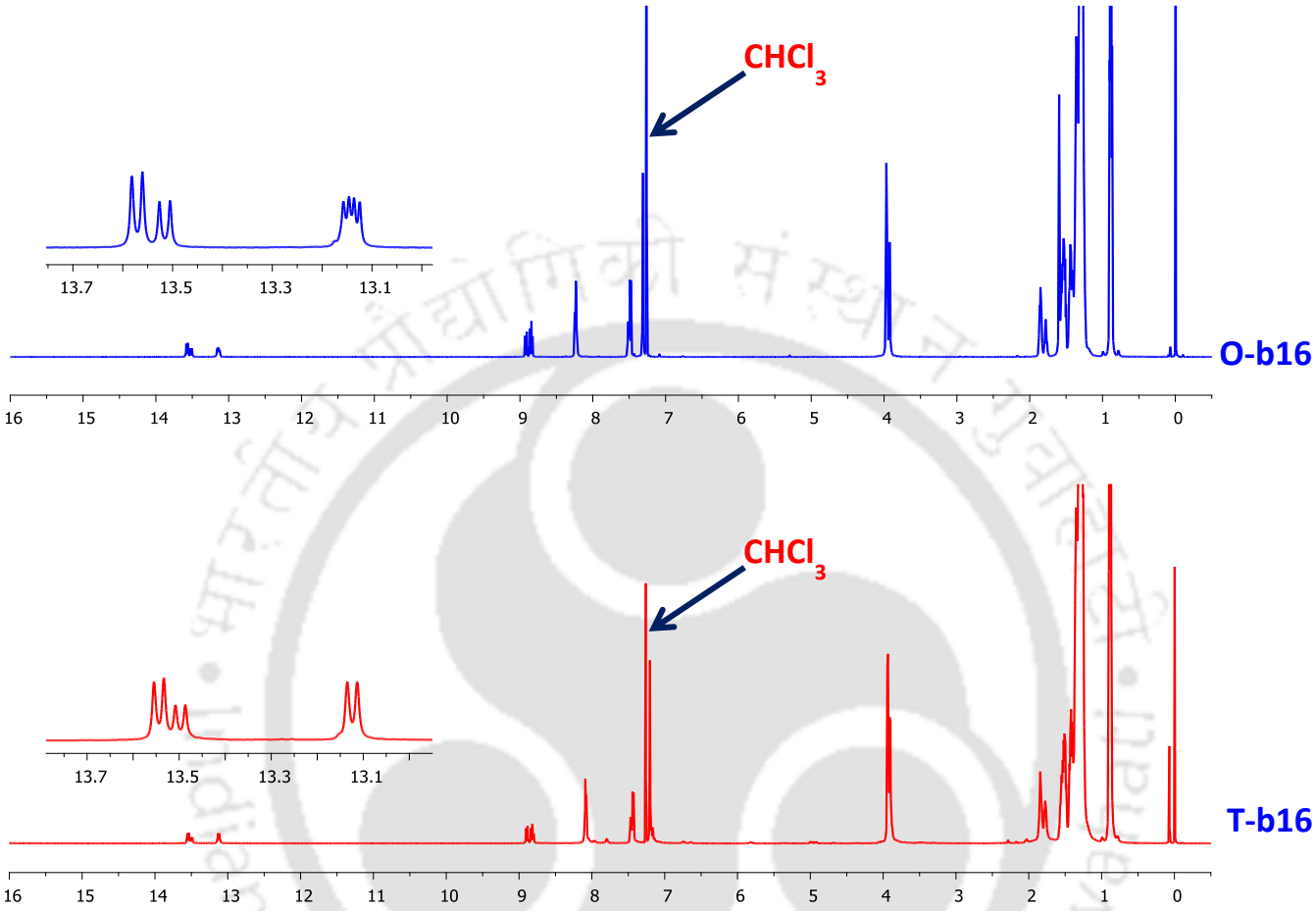

Figure 2.1. ^{1}H NMR (600 MHz) spectra of **O-b16** and **T-b16** in $CDCl_3$.

2.2b. Thermal behavior

The mesogenic behavior of these star shaped molecules was studied with the help of polarizing optical microscopy (POM), differential scanning calorimetry (DSC) and powder X-ray diffraction (XRD) studies. The phase transitions and the accompanying enthalpy changes are summarized in Table 2.1 and graphically represented in Figure 2.2. The data obtained from XRD studies are tabulated in Table 2.2. The thermal behavior of compound **O-16** was reported earlier[18b] and for the sake of comparison with the other oxadiazole derivative **O-b16** and thiadiazole derivatives (**T-16** and **T-b16**), it is included in Table 2.1 and Figure 2.2.

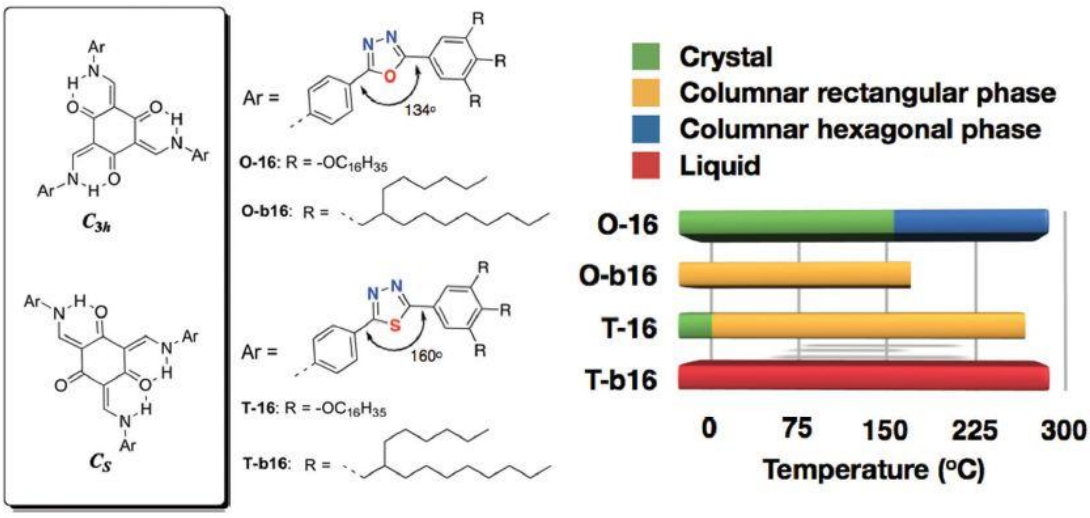

Figure 2.2. Molecular structures of the oxadiazole based TSANs (**O-16**[18b] and **O-b16**), and thiadiazole based TSANs **(T-16** and **T-b16)** and their thermal behavior (based on the heating scans from DSC**)**

Table 2.1. Phase transition temperatures[a] (°C) and corresponding enthalpies (kJ/mol) of regioisomeric TSANs

Entry (C_{3h}: C_s)[b]	Heating	Cooling
O-16[c] (1:2.6)	Cr_1 63.4 (131.6) Cr_2 157.3 (29.4) Col_h 269.2 (5.6) I	I 265.7 (4.9) Col_h 24.6 (51.5) Cr
O-b16 (1.6:1)	Col_r 170 (3.8) I	I 160.1 (3) Col_r[d]
T-16 (1.9:1)	Cr 25.3 (239) Col_{r2} 224.2 (18.2) Col_{r1} 252.1 (0.9) I	I 251.4 (7.1) Col_{r1} 209.4 (16.3) Col_{r2} 23.5 (159) Cr
T-b16 (1.8:1)	Viscous liquid	

[a]Peak temperatures in the DSC thermograms obtained during the second heating and first cooling cycles at 5 °C/min.; Col_h = Columnar hexagonal phase, Col_r = Columnar rectangular phase.[b] Ratio obtained from ^{1}H NMR, [c]Reported in reference 18b. [d]Crystallization was not observed till -10 °C.

The TSANs with three substituted 1,3,4-oxadiazole arms with branched chains, *i.e.* **O-b16** was a viscous sticky compound, which was shearable and birefringent, when we examined with POM. This compound entered isotropic phase at 160 °C and on cooling showed a birefringent texture (Fig. 2.3) that remained as such till room temperature. The DSC scans in the cooling cycle did not show the signs of crystallization even upto -10 °C (Fig. 2.3b). Further the XRD studies carried out at high temperature (140 °C) and at room temperature showed the similar pattern (Fig. 2.3c). The XRD profiles depicting the intensity against the 2θ obtained at 140 °C show one strong reflection at low angle region along with a diffused reflection. In the wide angle a diffused peak was observed that corresponds to the packing of flexible alkyl tails of the star shaped molecules in the columnar phase. The two reflections at the low angle with the *d*-spacings

corresponding to 41.5 and 19.29 Å can be indexed to (01) and (10) reflections of a Col_r phase (*p2mm*) respectively. The sides of the rectangular lattice '*a*' and '*b*' were calculated and found to be 19.29 and 41.5 Å respectively with the lattice area (*S*) of 800.5 $Å^2$.

Considering the reflection corresponding to 5.2 Å as the height of the columnar slice (h_a), we have calculated the lattice volume (*V*) and number of molecules in the unit rectangular cell (*Z*) to be 4138.8 $Å^3$ and 0.8 respectively. The XRD pattern obtained at room temperature was almost similar and confirmed the Col_r phase (Fig. 2.3c and Table 2.2). It is interesting to note that the introduction of branching in the peripheral tails not only helped in reducing the melting point and clearing point of the mesophase, but also changed the type of the Col phase from hexagonal to rectangular. This is in contrary to the disc like molecules where the branching in the peripheral tails does not change the type of the mesophase but only reduce the transition temperatures.[19b,c,23] This difference may be due to the altered shape of the overall molecular structure from disc to star.

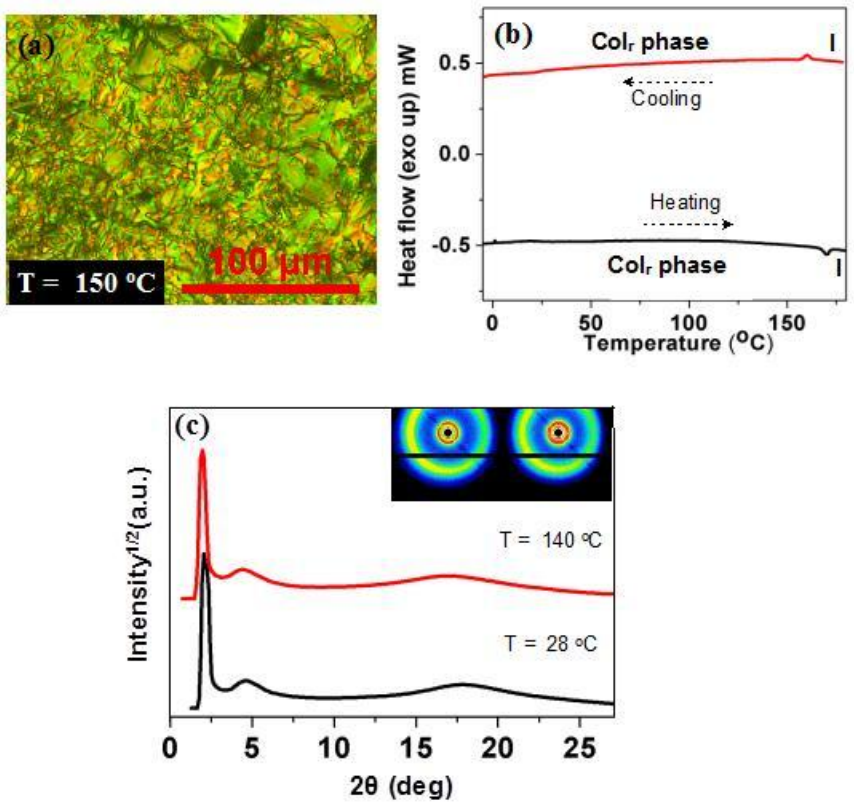

Figure 2.3. POM image of compound O-b16 in Col_r phase at 150 °C (a); DSC scans of compound O-b16 obtained for second heating (heating: black trace) and first cooling (cooling: red trace) (b); XRD profiles depicting the intensity against the 2θ obtained for the Col_r phase of compound O-b16 at 140 °C and at 28 °C (inset provides the image patterns obtained) (c).

TSANs with three substituted 1,3,4-thiadiazole arms with straight chain, *i.e.* **T-16** was a low melting solid at RT, but converted to a birefringent fluid on heating above RT. This exhibited a wide mesophase range of 225 ^{o}C in heating cycle with an isotropic temperature of 252 ^{o}C. Cooling the isotropic liquid at a rate of 2 ^{o}C/min, led to the growth of high birefringent defects intermixed with the homeotropic domains (Fig. 2.4a). At a temperature of ≈ 209 ^{o}C, these defects changed the color as seen in Fig.2.4b and this transition was detected in DSC with an enthalpy change of 16.3 kJ/mol. This phase existed till RT, before crystallizing at 23.5 ^{o}C (ΔH = 159 kJ/mol) (Fig. 2.4c). The XRD profiles depicting the intensity against the 2θ obtained at 230 ^{o}C show one strong reflection at low angle along with a reflection of weak intensity. A diffused peak was observed in the wide angle region, which corresponds to the packing of flexible alkyl tails of the individual molecules stacked in the columnar phase (Fig. 2.4d).

Table 2.2. Results of the (*hkl*) indexation of the XRD profiles of the compounds at a given temperature (T) of the mesophases.[a]

Compounds (D/Å)	Phase (T/^{o}C) Symmetry	d_{obs} (Å)	d_{cal} (Å)	Miller indices (*hk)*	Lattice parameters (Å)
O-b16 (46.3)	Col_r (140) *p2mm*	41.5 19.29 5.17 (h_a)	41.5 19.29	01 10	a = 19.29; b = 41.5; S = 800.5; V = 4138.8; Z = 0.8.
	Col_r (28) *p2mm*	41.44 19.26 4.98 (h_a)	41.44 19.26	01 10	a = 19.26; b = 41.44; S = 798.13; V = 3974.7; Z = 0.8.
T-16 (62.9)	Col_{r1} (230) *p2mm*	45.49 24.22 5.26 (h_a)	45.49 24.22	01 10	a = 24.22, b = 45.49; S = 1101.8; V = 5795.3; Z = 1.2.
	Col_{r2} (140) *p2mm*	43.41 31.86 24.22 12.39 5.08 (h_a)	43.41 31.86 25.68 12.84	01 10 11 22	a = 31.86, b = 43.41; S = 1383.04; V = 7025.9; Z =1.4.
	Col_{r2} (28) *p2mm*	43.55 25.05 13.91 4.90 (h_a)	43.55 25.05 14.44	01 11 21	a = 30.62, b = 43.55; S = 1333.5; V = 6534.2; Z = 1.3.

The diameter (D) of the disk (estimated from Chem 3D Pro 8.0 molecular model software from Cambridge Soft). d_{obs}: spacing observed; d_{cal}: spacing calculated (deduced from the lattice parameters; a for Col_h phase). The spacings marked h_a and h_c correspond to diffuse reflections in the wide-angle region arising from correlations between the alkyl chains and core regions, respectively. Z indicates the number of molecules per columnar slice of thickness h_c, estimated from the lattice area S and the volume V. [b] In the absence of core-core peak, the spacing of the alkyl chain stacking (h_a) is taken for these calculations.

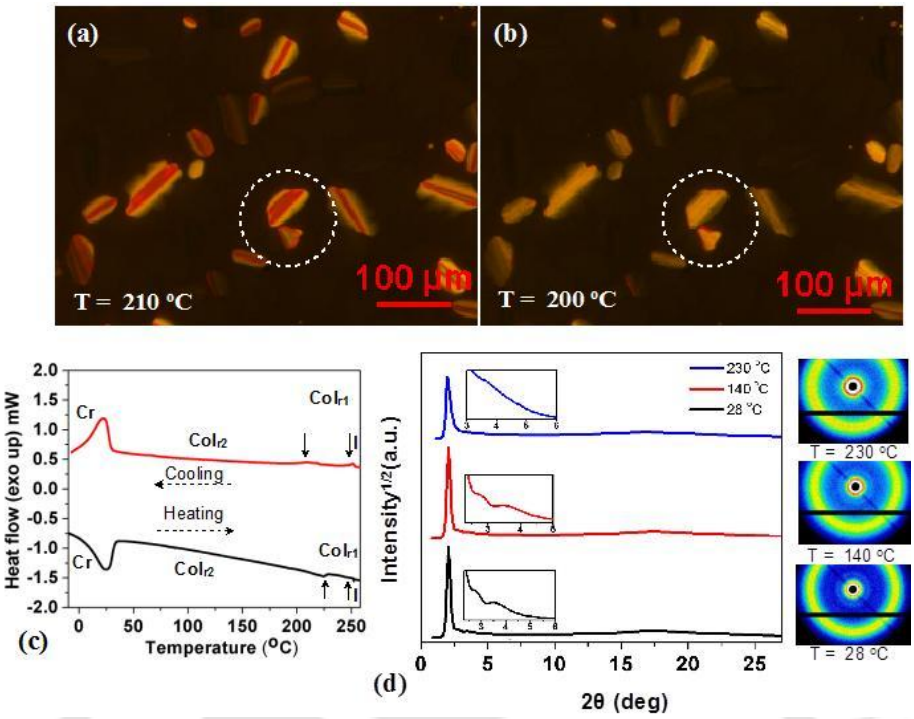

Figure 2.4. POM image of compound **T-16** in Col_{r1} phase at 210 °C (a) and in Col_{r2} phase at 200 °C (b); DSC scans of compound **T-16** obtained for second heating (heating: black trace) and first cooling (cooling: red trace) (c); XRD profiles depicting the intensity against the 2θ obtained for the Col_r phase of compound **T-16** at 230 °C, 140 °C and at 28 °C (inset provides the expanded regions at the low angle; image patterns obtained are provided on the right side) (d).

The two reflections at the low angle region with the *d*-spacings corresponding to 45.49 and 24.22 Å can be indexed to (01) and (10) reflections of a Col_r phase (*p2mm*). The sides of the rectangular lattice '*a*' and '*b*' were calculated and found to be 24.22 and 41.5 Å respectively with the lattice area (*S*) of 1102 $Å^2$. Considering the reflection corresponding to 5.26 Å as the height of the columnar slice (h_a), we have calculated the lattice volume (*V*) and number of molecules in the unit rectangular cell (*Z*) to be 5795 $Å^3$ and 1.2 respectively. Considering the transition observed in DSC and textural difference observed under POM, we were interested to investigate the nature of the mesophase at temperatures below 209 °C. The XRD profile obtained at 140 °C shown several reflections of lower intensity along with a strong reflection at low angle. These four *d*-spacings corresponding to 43.41, 31.86, 25.68 and 12.39 Å which could be assigned to (01), (10), (11) and (22) reflections of a rectangular lattice. Further the diffused peak at the wide angle region corresponding to a *d*-spacing of 5.08 Å, which suggests the packing of flexible alkyl tails and hence Col_r phase (*p2mm*). We have denoted this phase as $Col_{r2,}$ whereas the high temperature phase was denoted as Col_{r1}. Powder XRD pattern obtained at RT was similar to the

diffraction pattern obtained at 140 ^{o}C which confirms the existence of Col_{r2} phase. Such transitions between Col_r phases has been reported earlier.[24]

This interesting effect on the type of the mesophase (from Col_h to Col_r phase) and transition temperatures (high temperature Col phase to RT Col phase) is directly a result of the change in the type of heterocycle from substituted 1,3,4-oxadiazole to substituted 1,3,4-thiadiazole (Fig. 2.5). This enhanced intermolecular interaction may be due to the attractive S····S interactions. Further the bigger atomic size of the sulphur may reduce the rotational freedom of the individual molecules within the column. Another reason may be due to the larger bent angle of the thiadiazole ring (160^{o}) in comparison to the corresponding oxadiazole (134^{o}), which may lead to the better overlap of the arms (Fig. 2.2 and Fig. 2.5).[5]

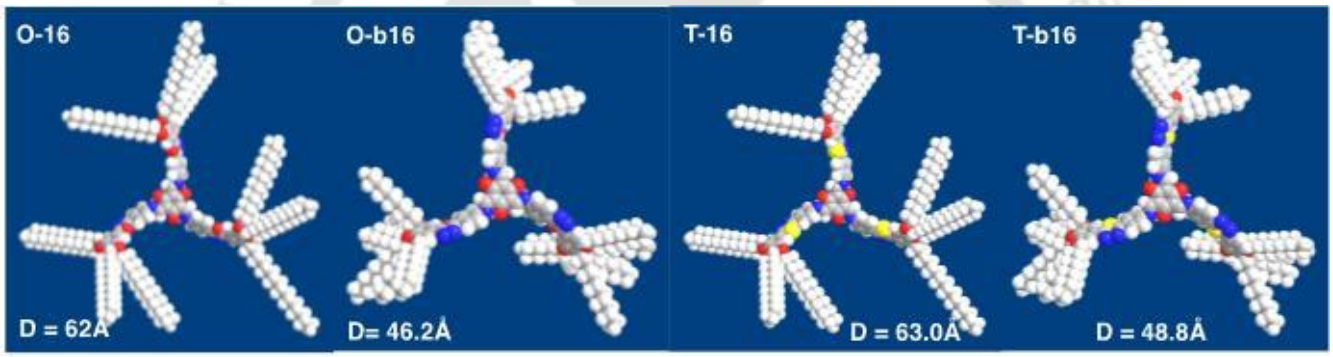

Figure 2.5. Molecular models and diameters (D) obtained for star shaped compounds **O-16**, **O-b16, T-16** and **T-b16** (estimated from Chem 3D Pro 8.0 molecular model software from Cambridge Soft)

The reduced transition temperature and enhanced mesophase width are in accordance with the earlier report on thiadiazole based star shaped molecules.[13b] Again the change in the type of the mesophase on moving from the straight chain oxadiazole derivative (**O-16**) to its branched chain derivative (**O-b16**) is perhaps due to the restriction of rotational freedom for the molecules within the columns, due to the bulkiness of branched chains. The branched chain analogue **T-b16** turned out to be a viscous liquid at room temperature in contrast to the RT Col phase of TSAN **O-b16**. Thus the branched chains are having an impact on the stacking of the central cores of the star-shaped molecules, thus affecting the clearing point (temperature at which the cores unstack from the column) of the compound.

2.3. Photophysical behavior

Photophysical properties of these compounds **O-16**, **O-b16, T-16** and **T-b16** were studied in solution as well as in thin films (Table 3). The absorption spectra of compounds were measured in micromolar THF solutions. Compound **O-16** and **O-b16** exhibited similar absorption spectra with two absorption bands centered at 343 and ≈ 424 nm. They exhibited a single emission maximum centered at 475 nm, with a Stoke's shift of 50-51 nm (Fig. 2.6a). Thiadiazole based TSANs exhibited similar absorption spectra to that of the oxadiazole based TSANs, but with a red shift. The two absorption bands are centered at 350-360 nm and 430 nm. Their emission spectra also display a red shift with an emission maximum at 480 nm (Fig. 2.6b). The light yellow colored solutions in daylight exhibited a cyan to bright green emission under long wavelength UV light (Fig. 2.6c). Relative quantum yields were measured in solution as reported earlier.[25] The thiadiazole based TSANs also showed a slightly higher photoluminescence quantum yield (Table 2.4 and Fig. 2.7). Their optical band gap calculated from the red edge of the absorption onset were found to be in the range of 2.6-2.62 eV.

Table 2.3. Photophysical properties of TSANs

	Solution						Thin film
Entry	Absorption[a] (nm)	Emission [a, b] (nm)	Stoke's shift (cm^{-1})	Quantum yield[f]	ε ($M^{-1}cm^{-1}$)	$\Delta E_{g,opt}$ [c, d]	Emission[e] (nm)
O-16	343, 424	475	51	0.37	54670	2.62	554
O-b16	344, 424	474	50	0.32	52010	2.60	602
T-16	349, 429	480	51	0.38	54290	2.58	608
T-b16	361, 430	481	51	0.44	54810	2.56	572

[a] Micromolar solutions in THF. [b] Excited at the respective absorption maxima. [c]In electron volts (eV). [d]Band gap was determined from the red edge of the longest wave length in the UV-Vis absorption spectra. [e] Emission obtained by exciting the thin films at their respective absorption maxima in solution. [f]Relative quantum yield measured with respect to tetrakis(octyl)-1H-phenanthro[1,10,9,8]carbazole-3,4,9,10--tetracarboxylate in THF solution.

Thin films of these LCs were prepared by annealing the samples in glass slides by annealing them from their isotropic state. Absorption spectra of all the compounds in thin films appeared very broad. The emission spectra of oxadiazole based TSAN **O-16** showed a maximum at 554 nm, while the branched analogue exhibited a red shifted emission maximum at 602 nm. Thiadiazole based TSAN **T-16** exhibited an emission maximum centered at 608 nm, while its

branched analogue **T-b16**, showed a blue shifted emission maximum centered at 572 nm. The red-shifted emission maxima points to the formation of aggregates in the annealed thin films.[25]

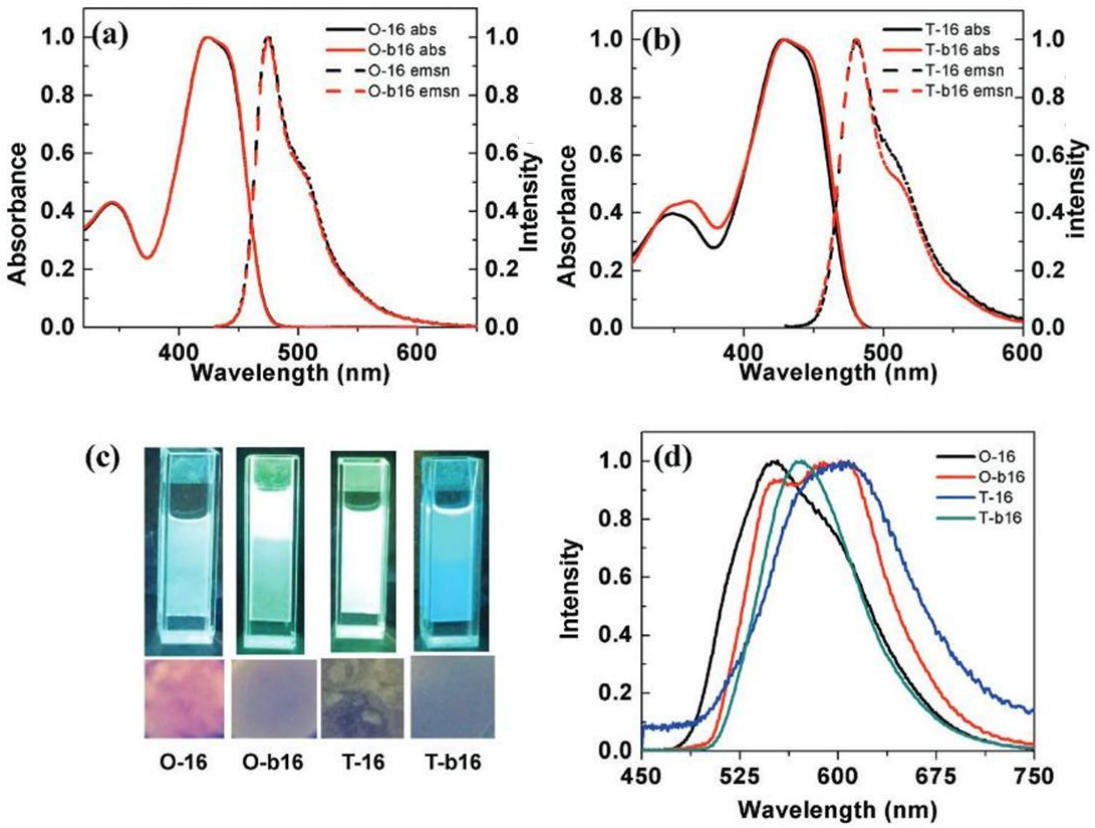

Figure 2.6. Normalized absorption (solid line) and emission spectra (dotted line) in THF solution obtained for compounds **O-16** (black trace) and **O-b16** (red trace) (a); normalized absorption (solid line) and emission spectra (dotted line) in THF solution obtained for compounds **T-16** (black trace) and **T-b16** (red trace) (b); Pictures of micromolar solutions in THF and thin films of compounds as seen with the UV illumination (λ = 365 nm)(c); Normalized emission spectra obtained for the TSANs in the thin film state (d).

Relative Quantum Yield Calculation

Relative quantum yield of compound was measured with respect to tetrakis(octyl)-1H-phenanthro[1,10,9,8]carbazole--3,4,9,10--tetracarboxylate in THF solution as the standard, which is having the relative quantum yield of 1 with respect to fluorescein (Q_f= 0.79) in 0.1M NaOH). Absolute values were calculated according to the following equation:$Q_S = Q_R \times (m_S / m_R) \times (n_S/ n_R)^2$ Where, Q: Quantum yield; m: Slope of the plot of integrated fluorescence intensity *vs* absorbance; n: refractive index (1.407 for THF). The subscript R refers to the reference fluorophore*i.e.* compound carbazole solution in THF and subscript S refers to the sample under investigation. In order to minimize re-absorption effects, absorbance was kept

below 0.15 at the excitation wavelength of 442 nm. Quantum Yield of compound carbazole is 1.01. Simplified equation for the calculation after substituting the appropriate values is given below and values obtained are given in table below.

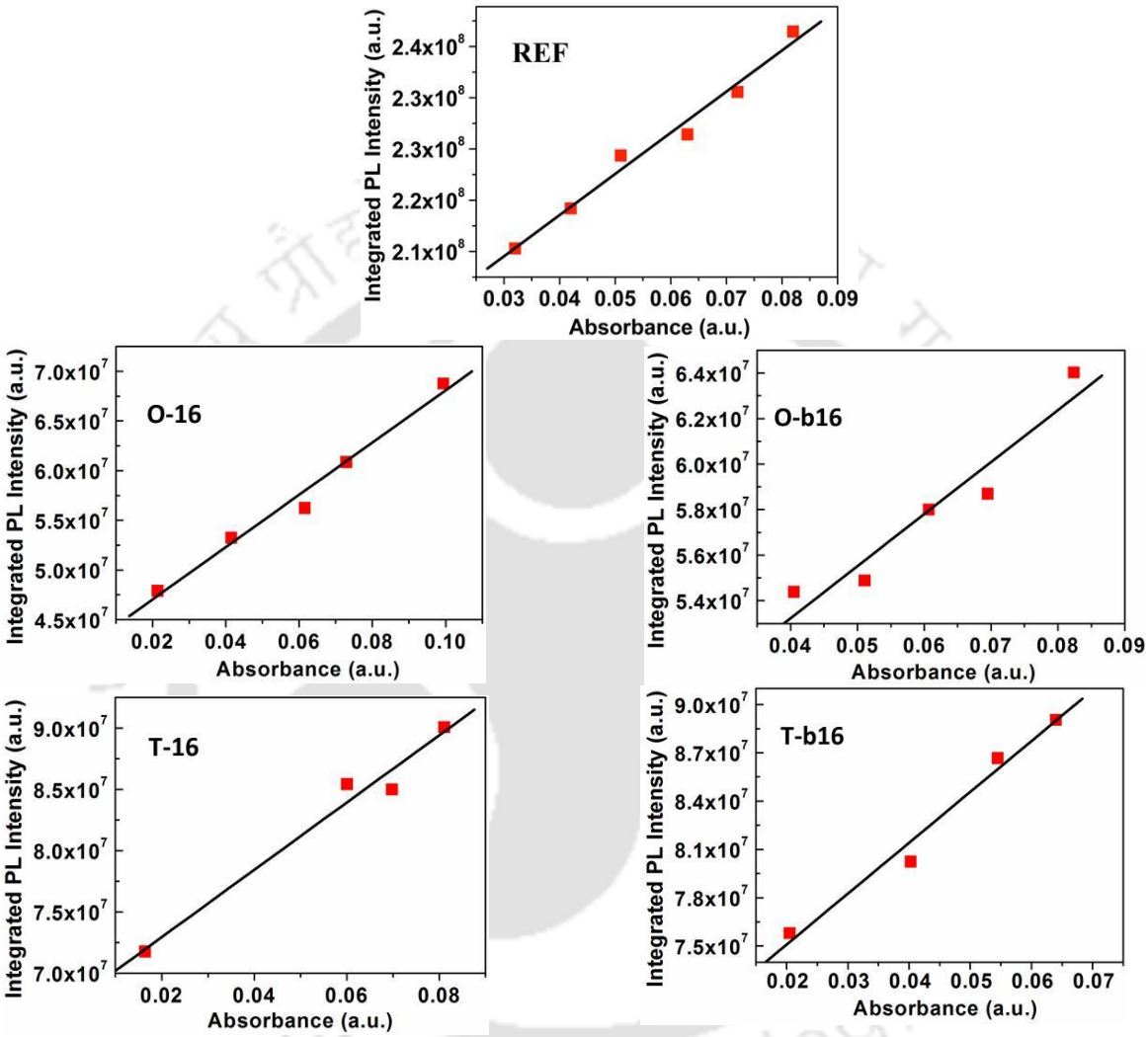

Figure 2.7. Plots of integrated photoluminescence intensity vs absorbance of reference compound and TSANs **O-16, O-b16, T-16** and **T-b16** (micromolar THF solution)

Table 2.4. Relative quantum yields of TSANs

Entry	m_S	m_R	$Q_s^{a,b,c}$
O-16	2.63082×10^{8}	7.2271×10^{8}	0.37
O-b16	2.28589×10^{8}	7.2271×10^{8}	0.32
T-16	2.74607×10^{8}	7.2271×10^{8}	0.38
T-b16	3.15971×10^{8}	7.2271×10^{8}	0.44

[a] Measured in THF; [b]Excited at absorption maxima; [c]Standard carbazole (Q_f = 1.01) in THF solution

2.4. Conclusions

We have prepared two series of TSANs, in which their arms were varied with respect to the central heterocyclic ring and the type of peripheral tails. The central heterocyclic rings were unsymmetrically substituted 1,3,4-oxadiazole and 1,3,4-thiadiazole. The change of an atom in these five membered heterocycles drastically affetcs their self-assembly and photophysical behavior. On moving from oxadiazole to thiadiazoles we noticed an increase in bent angle (due to the bigger size of sulpher), higher longitudinal/lateral dipole moment and attractive S····S interactions in the condensed state. Changing the peripheral tails from straight chain to branched chain also has a major effect on the self-assembly and photophysical behavior in the solic state, which is not usually observed in the case in conventional discotic LCs.

The oxadiazole based TSANs with branched tails exhibited a room temperature Col_r phase, while the straight chain hexadecyloxy analogue exhibited a high temperature Col_h phase. In the case of thiadiazole based TSANs, the compound with hexadecyloxy chains exhibited columnar rectangular phase of wide range from room temperature, while the branched chain analogue turned to be a liquid. Thus in the case of these star-shaped molecules, the type of the peripheral tails not only affects the transition temperature, but also affects the type of self-assembly, which is in contrary to conventional discotic liquid crystals. Introduction of substituted 1,3,4-thiadiazole rings helps in the reduction of melting point and enhances the mesophase width. 1,3,4-Thiadiazole based TSANs exhibit columnar rectangular phase even with the straight peripheral chains in contrast to the oxadiazole based TSANs, because of the attractive intermolecular interactions of the thiadiazole ring. Presence of the bulky branched tails at the

periphery enhances the intermolecular interaction between the cores of 1,3,4-oxadiazole based TSANs, leading to a Col_r phase, while completely destabilize the liquid crystallinity in the case of thiadiazole based TSANs. Thus the present report provides a clear picture of the delicate interplay of the effect of heteroatoms and the branching in the peripheral tails of on the self-assembly and photophysical behavior of star-shaped molecules, which will be of great interest to the scientific community working in the area of supramolecular self-assembly.

2.5. Experimental section

In this section the detailed synthesis procedure and the molecular structural characterization data have been presented for the intermediates and the molecular structural characterization data have been presented for the intermediates and target compounds mentioned in the scheme.

Procedure for the synthesis of 3,4,5-Trimethoxy-N'-(4-nitrobenzoyl)benzohydrazide **(2)**[1]

A mixture of 4-nitrobenzohydrazide (5.5 mmol, 1 equiv.) and dry pyridine (15 ml, 3 vol.) was stirred under nitrogen atmosphere at 0 ^oC. To this, a solution of trimethoxybenzoyl chloride (5.8 mmol, 1.05 equiv.) in dry THF was added drop wise. The reaction mixture was stirred at room temperature for 12 h and then poured into cold water. The whole mass (a mixture of solid and water) was extracted with ethyl acetate (2 × 100 ml). The combined extracts were given water wash, brine wash, dried over anhyd. Na_2SO_4 and concentrated. The solid obtained was recrystallized from hot ethanol.

2: R_f = 0.35 (30% EtOAc-hexane); off white solid; Yield : 75%; IR (KBr pellet): ν_{max} in cm^{-1} 3105, 3002, 1733, 1641, 1528, 1433, 1345, 1277, 1030, 998, 870, 714, 507;^{1}H NMR ($CDCl_3$, 400 MHz): δ 10.21 (s, 1H, CONH), 9.82 (s, 1H, CONH), 8.23 (d, 2H, J = 8Hz, Ar), 8.02 (d, 2H, J = 8Hz, Ar), 7.07 (s, 2H, Ar), 3.89-3.84 (2s, 9H, 3×OCH_3); ^{13}C NMR ($CDCl_3$, 100 MHz): 166.24, 164.54, 153.41, 150.20, 142.16, 136.56, 128.87, 125.68, 123.87, 104.97, 61.105, 56.39. HRMS (ESI+) exact Mass calculated for $C_{17}H_{18}N_3O_7$(M+1): 376.1139, found: 376.1149.

Procedure for the synthesis of 2-(4-Nitrophenyl)-5-(3,4,5-trimethoxyphenyl)-1,3,4-oxadiazole **(3a)**[1]

A mixture of **2** (4.8 mmol, 1 equiv.) and phosphorous oxychloride (72.5 mmol, 5 equiv.) was heated at 100 ^oC for 5 h. The excess $POCl_3$ was distilled off under reduced pressure. Traces of $POCl_3$ in the reaction mixture were quenched firstly with the very slow addition of ice-cold water followed by the addition of sodium bicarbonate solution with cooling. The yellow residue obtained was extracted with chloroform (4×100 ml). The combined extracts was washed with 20 % $NaHCO_3$, water, brine and dried over anhyd. Na_2SO_4. Upon removal of the solvent under

reduced pressure, a yellow solid was obtained that was purified by recrystallization using benzene.

3a: R_f = 0.6 (20% Methanol-Chloroform); Yield: 70%; IR (KBr pellet) : ν_{max} in cm^{-1} 2947, 1596, 1556, 1522, 1497, 1462, 1341, 1323, 1239, 1131, 993, 862 & 727; ^{1}H NMR ($CDCl_3$, 600 MHz): δ 8.38 (d, 2H, *J*=6 Hz, Ar), 8.31 (d, 2H, *J* = 12Hz, Ar), 7.34 (s, 2H, Ar), 3.96 (s, 6H, 2× OCH_3), 3.92 (s, 3H, 1×OCH_3).^{13}C NMR ($CDCl_3$, 150 MHz): 165.65, 162.93, 153.94, 149.63, 141.83, 129.50, 127.94, 124.55, 118.41, 104.55, 61.22, 56.60;HRMS (ESI+) exact Mass calculated for $C_{17}H_{16}N_3O_6$(M+1): 358.1034, found: 358.1032.

Procedure for the synthesis of 2-(4-Nitrophenyl)-5-(3,4,5-trimethoxyphenyl)-1,3,4-thiadiazole **(3b)** [1]

A solution of compound **2** (4.8 mmol, 1 equiv.) in dry THF (30ml) was added to P_2S_5 (17.28mmol, 3.6 equiv.) at 0^{o}C under Ar- atmosphere and reflux for 48hrs. Distilled out the THF and the reaction was poured on to ice water and extracted with $CHCl_3$ (3 × 50ml). The combined organic layer was extracted was with water, brine and dried over anhyd. Na_2SO_4. Evaporation of solvent and recrystallization with ethanol furnished the desired product.

3b: R_f: 0.62 (20% Methanol-Chlroform); Yield: 60%; IR (KBr pellet) : ν_{max} in cm^{-1} 3002, 2975, 2948, 2844, 1596, 1584, 1522, 1452, 1427, 1401, 1337, 1246, 1124, 1090, 998, 850, 747; ^{1}H NMR ($CDCl_3$, 400 MHz): δ 8.37(d, 2H, J= 8Hz, Ar), 8.19 (d, 2H, J = 8Hz, Ar), 7.25 (s, 2H, Ar), 3.97-3.93 (m, 9H, 3 × OCH_3); ^{13}C NMR ($CDCl_3$, 100 MHz): 169.76, 165.44,162.72, 153.88, 149.16, 141.26, 135.83, 128.72, 124.65, 105.44, 61.26, 56.58. HRMS (ESI+) exact Mass calculated for $C_{17}H_{16}N_3O_5S$ (M+1): 374.0805, found: 374.0809.

Procedure for the synthesis of 5-(5-(4-nitrophenyl)-1,3,4-oxadiazol-2-yl)benzene-1,2,3-triol **(4)** [1]

A solution of compound **3a** (1.4 mmol, 1 equiv.) in dry dichloromethane (30 ml) was cooled to -78 ^{o}C and stirred under nitrogen atmosphere. Then, BBr_3 (0.5 ml, 5.04 mmol, 3.6 equiv) was added drop wise to this solution and the reaction mixture was allowed to warm-up to room temperature and continued to stir for 17 h. The reaction mass was poured into ice-water with vigorous stirring to quench the excess BBr_3. The organic layer separated was collected and washed with water (4×100 ml), 5 % $NaHCO_3$ solution (1×50 ml) and dried over anhyd. Na_2SO_4. Evaporation of solvent under reduced pressure yielded a solid compound that was repeatedly washed with methanol.

4: R_f = 0.23 (20% Methanol-$CHCl_3$); yellow solid; yield: 65%; IR (KBr pellet) : ν_{max} in cm^{-1} 3379, 1629, 1604, 1572, 1559, 1529, 1448, 1330, 1211, 1026, 857, 731, 705; ^{1}H NMR (DMSO-d_6, 600 MHz): δ 9.51 (broad s, 3H, 3×OH), 8.42-8.39(m, 2H, Ar), 8.28-8.25(m, 2H, Ar), 7.09 (s, 2H, Ar).^{13}C NMR (DMSO-d_6, 150 MHz): 165.37, 161.96, 148.95, 146.56, 137.79, 129.18, 127.68, 124.64, 112.68, 106.12. HRMS (ESI+) exact Mass calculated for $C_{14}H_{10}N_3O_6$ (M+1): 316.0564, found: 316.0561.

Procedure for the synthesis of 5-(5-(4-nitrophenyl)-1,3,4-thiadiazol-2-yl)benzene-1,2,3-triol **(5)**

A solution of compound **3b** (1.4mmol, 1 equiv.) in dry dichloromethane (30 ml) was cooled to -

78 ^{o}C and stirred under nitrogen atmosphere. Then, BBr_3 (0.5 ml, 5.04 mmol, 3.6 equiv) was added drop wise to this solution and the reaction mixture was allowed to warm-up to room temperature and continued to stir for 17 h. The reaction mass was poured into ice-water with vigorous stirring to quench the excess BBr_3. The organic layer separated was collected and washed with water (4×100 ml), 5 % $NaHCO_3$ solution (1×50 ml) and dried over anhyd. Na_2SO_4. Evaporation of solvent under reduced pressure yielded a solid compound that was repeatedly washed with methanol.

5: R_f = 0.31 (20% Methanol-$CHCl_3$); brownish yellow solid; yield: 70%; IR (KBr pellet) : ν_{max} in cm^{-1} 3487, 2919, 1602, 1516, 1460, 1429, 1332, 1196, 1033, 852, 750; ^{1}H NMR (DMSO-d_6, 400 MHz): δ 8.39 (d, 2H, J=8.8 Hz, Ar), 8.27 (d, 2H, *J*=8.8 Hz, Ar), 7.00 (s, 2H, Ar). ^{13}C NMR (DMSO-d_6, 100 MHz): 169.93, 164.16, 148.58, 146.58, 137.36, 135.41, 128.67, 124.58, 119.27, 106.96. HRMS (ESI+) exact Mass calculated for $C_{14}H_{10}N_3O_5S$ (M+1): 332.0336, found: 332.0342.

Procedure for the synthesis of 2-(4-Nitrophenyl)-5-(3,4,5-tris(alkoxy)phenyl)-1,3,4-oxadiazole **(6a)**

A mixture of compound **4** (0.48 mmol, 1equiv.), 2-hexylbromodecane (1.57 mmol, 3.3 equiv.), anhyd. K_2CO_3 (3.14 mmol, 6.6 equiv.) and DMF (10 ml) was heated at 80 ^{o}C for 17 h under nitrogen atmosphere. Then the reaction mixture was poured on to ice-water and extracted with EtOAc (3 × 50 ml). The combined organic layer was washed with water, brine and dried over anhyd. Na_2SO_4. Evaporation of the solvent and purification of the residue over neutral alumina using hexane followed by ethylacetate-hexane (5%) as eluents furnished the desired product,

6a: R_f = 0.51 (10% EtOAc-hexane); a yellow liquid; yield: 70%; IR (KBr pellet): ν_{max} cm^{-1} 2918, 2849, 1590, 1556, 1523, 1493, 1468, 1436, 1338, 1126, 1022, 861, 729, 703; ^{1}H NMR ($CDCl_3$, 400 MHz): δ 8.39(d, 2H, *J*= 8.8 Hz, Ar), 8.32 (d, 2H, *J*= 8.8 Hz, Ar), 7.29 (s, 2H, Ar), 3.94-3.9 (m, 6H, 3×OCH_2), 1.58-0.84 (m, 94H, 38×CH_2, 6×CH_3); ^{13}C NMR ($CDCl_3$, 100MHz): 166.10, 162.84, 154.10, 149.71,142.24, 129.75, 127.96, 124.58, 117.80, 105.36, 72.08, 39.56, 38.50, 32.13, 31.60, 31.49, 30.45, 30.33, 30.10, 29.98, 29.88, 29.66, 29.59, 27.31, 27.15, 22.91, 14.30. MALDI-TOF exact mass calculated for $C_{62}H_{106}N_3O_6$ (M+1): 988.8082, found: 988.835.

Procedure for the synthesis of 2-(4-Nitrophenyl)-5-(3,4,5-tris(alkoxy)phenyl)-1,3,4-thiadiazole **(6b-c)**

A mixture of compound **5** (0.48 mmol, 1 equiv.), n-bromoalkane (1.57 mmol, 3.3 equiv.), anhyd. K_2CO_3 (3.14 mmol, 6.6 equiv.) and DMF (10 ml) was heated at 80 ^{o}C for 17 h under nitrogen atmosphere. Then the reaction mixture was poured on to ice-water and extracted with EtOAc (3 × 50 ml). The combined organic layer was washed with water, brine and dried over anhyd.Na_2SO_4. Evaporation of the solvent and purification of the residue over neutral alumina using hexanes followed by ethylacetate-hexane (5%) as eluents furnished the desired product, which was further purified by repeated recrystallizations in hexane.

6b: R_f = 0.62 (10% EtOAc-hexane); a yellow solid; yield: 60%; IR (KBr pellet): ν_{max} cm^{-1} 2923, 2846, 1635, 1456, 1273, 1261, 1094, 1019, 801, 762, 749; ^{1}H NMR ($CDCl_3$, 600 MHz): δ

8.37 (d, 2H, *J*= 6 Hz, Ar), 8.19 (d, 2H, *J* = 6 Hz, Ar), 7.22 (s, 2H, Ar), 4.08-4.03 (m, 6H, 3 × OCH_2), 1.87-0.86 (m, 93H, 42 × CH_2, 3 × CH_3); ^{13}C NMR ($CDCl_3$, 100MHz): 170.07, 165.21, 153.86, 149.21, 141.68, 136.08, 128.72, 124.66, 124.52, 106.86, 73.90, 69.66, 32.15, 30.56, 29.94, 29.88, 29.87, 29.80, 29.62, 29.59, 29.54, 26.30, 22.91, 14.32.MALDI-TOF exact mass calculated for $C_{62}H_{106}N_3O_5S$ (M+1): 1004.7853, found: 1004.782.

6c: R_f = 0.53 (10% EtOAc-hexane); a yellow solid; yield: 65%; IR (KBr pellet): ν_{max} cm^{-1} 2917, 2850, 1586, 1523, 1438, 1379, 1344, 1232, 1122, 852, 720; ^{1}H NMR ($CDCl_3$, 400 MHz): δ 8.34(d, 2H, *J*= 8 Hz, Ar), 8.17 (d, 2H, *J*= 8 Hz, Ar), 7.21 (s, 2H, Ar), 3.96-3.90 (m, 6H, 3 × OCH_2), 1.50-0.85 (m, 94H, 38× CH_2, 6 × CH_3); ^{13}C NMR ($CDCl_3$, 100MHz): 171.53, 170.19, 165.10, 153.99, 149.15, 141.60, 136.08, 128.66, 124.62, 124.32, 106.19, 71.96, 67.54, 39.50, 38.41, 37.43, 32.12, 31.55, 29.98, 29.88, 29.59, 27.11, 22.96, 22.91, 22.88, 14.30. MALDI-TOF exact mass calculated for $C_{62}H_{106}N_3O_5S$ (M+1): 1004.7853, found: 1004.735.

Procedure for the synthesis of 4-(5-(3,4,5-Trialkoxyphenyl)-1,3,4-oxadiazol-2-yl)benzenamines **(7a)**

To a solution of nitro compound 5a or $5a_1$ (0.9 mmol, 1 equiv.) in dry THF was added 10 % Pd-C (10 weight % of 6a-b) and stirred under hydrogen atmosphere (balloon) for 12 h (monitored by TLC). The reaction mixture was then filtered through a celite bed. Evaporation of the solvent and purification of residue over neutral alumina followed by ethylacetate-hexane (10 %) as eluents furnished the desired amine.

7a: R_f = 0.25 (30% EtOAc-hexane); a light yellow solid; yield: 72%; IR (KBr pellet): ν_{max} cm^{-1} 2918, 2850, 1614, 1495, 1468, 1390, 1331, 1122, 986, 835, 721; ^{1}H NMR ($CDCl_3$, 400 MHz): δ 7.92 (d, 2H, *J*= 8.8 Hz ,Ar), 7.26 (s, 2H, Ar), 6.80 (d, 2H, *J*= 8.8 Hz, Ar), 3.93-3.88 (m, 6H, 3× OCH_2), 1.51-0.83 (m, 76H, 38×CH_2, 18H, 6×CH_3); ^{13}C NMR ($CDCl_3$, 100MHz): 164.89, 164.30, 153.95, 148.85, 141.39, 128.85, 118.84, 115.47, 114.62, 104.99, 71.98, 39.54, 38.49, 32.12, 31.59, 31.50, 30.46, 30.33, 30.10, 29.98, 29.87, 29.66, 29.59, 28.99, 27.27, 27.14, 26.71, 22.90, 22.59, 14.29; Tof MS ES+ : HRMS (ESI+) exact Mass calculated for $C_{62}H_{108}N_3O_4$ (M+1): 958.8334, found: 958.8403.

Procedure for the synthesis of 4-(5-(3,4,5-Trialkoxyphenyl)-1,3,4-thiadiazol-2-yl)benzenamines **(7b-c)**

To a solution of nitro compound 6a or 6b (0.9 mmol, 1 equiv.) in dry THF was added 10 % Pd-C (10 weight % of 6a-b) and stirred under hydrogen atmosphere (balloon) for 12 h (monitored by TLC). The reaction mixture was then filtered through a celite bed. Evaporation of the solvent and purification of residue over neutral alumina followed by ethylacetate-hexane (10 %) as eluents furnished the desired amine.

7b: R_f = 0.21 (15% EtOAc-hexane); a light yellow viscous liquid; yield: 65%; IR (KBr pellet): ν_{max} in cm^{-1}3456, 2961, 2928, 1634, 1459, 1034, 1016, 687; ^{1}H NMR ($CDCl_3$, 600MHz): δ 7.80 (d, 2H, *J*= 6 Hz, Ar), 7.18 (s, 2H, Ar), 6.73 (d, 2H, *J*= 12 Hz, Ar), 4.06-4.00 (m, 6H, 3 × OCH_2), 1.85-0.86 (m, 93H, 42 × CH_2, 3 × CH_3); ^{13}C NMR ($CDCl_3$, 150MHz):168.34, 166.94, 153.71, 149.44, 140.83, 129.63, 125.52, 120.61, 115.11, 106.57, 73.83, 69.57, 32.15, 30.55, 29.93, 29.88,

29.81, 29.63, 29.58, 26.30, 22.90, 14.33; HRMS (ESI+) exact Mass calculated for $C_{62}H_{108}N_3O_3S$ (M+1): 974.8106, found: 974.8088.

7c: R_f = 0.2 (15% EtOAc-hexane); a light yellow solid; yield: 60%; IR (KBr pellet): ν_{max} cm^{-1} 2918, 2850, 1608, 1585, 1467, 1452, 1425, 1385, 1334, 1122, 832, 653; ^{1}H NMR ($CDCl_3$, 400 MHz): δ 7.80 (d, 2H, *J*= 8.8Hz ,Ar), 7.16 (s, 2H, Ar), 6.73 (d, 2H, *J*= 8.8 Hz, Ar), 3.92-3.87 (m, 6H, 3×OCH_2), 1.59-1.28 (m, 76H, 38×CH_2), 0.87 (t, 18H, 6×CH_3); ^{13}C NMR ($CDCl_3$, 100MHz):168.25, 167.11, 153.88 ,149.35, 140.79, 129.63, 125.35, 120.74, 115.08, 105.96, 76.92, 71.96, 39.52, 38.44, 32.23, 32.20, 32.15, 31.58, 31.50, 30.48, 30.37, 30.13, 30.02, 29.90, 29.70, 29.62, 27.32, 27.27, 27.13, 27.10, 22.98, 22.94, 22.92, 14.34.HRMS (ESI+) exact Mass calculated for $C_{62}H_{108}N_3O_3S$ (M+1): 974.8106, found: 974.8153.

Procedure for the synthesis of Tris(N-salicylideneaniline)s **O-b16**

A mixture of triformylphloroglucinol (0.005 mmol, 1 equiv.) and aniline **7a** (0.19 mmol, 3.4 equiv.) in absolute ethanol (50 ml) was heated to reflux under inert atmosphere for 6 h with vigorous stirring. The dull yellow solid separated upon cooling the reaction mixture was collected by filtration, repeatedly washed with ethanol, and air-dried. The crude product was purified by repeated recrystallizations in a mixture of absolute ethanol-CH_2Cl_2.

O-b16: R_f = 0.64 (40% EtOAc – hexane); an orange solid; Yield 80%; IR (KBr pellet): ν_{max} cm^{-1} 2956, 2925, 2854, 1626, 1598, 1584, 1492, 1456, 1285, 1252, 1179, 1115, 1010, 840, 740, 640; ^{1}H NMR ($CDCl_3$, 600 MHz): δ 13.57 (d, *J*= 12 Hz, =CNH), 13.52 (d, *J*= 12Hz, =CNH), 13.16-13.12 (m, =CNH), 8.93-8.83 (m, 3H, =CHN), 8.25-8.22 (m, 6H, Ar), 7.52 – 7.48 (m, 6H, Ar), 7.32 (s, 6H, Ar), 3.97-3.92 (m, 18H, 9×OCH_2), 1.87-0.87 (m, 280H, 113×CH_2, 18×CH_3). MALDI Tof MS ES+ : m/z for $C_{195}H_{326}N_9O_{15}$ (M+3), Calculated :3034.5007 Found: 3034.868.

Procedure for the synthesis of Tris(*N*-salicylideneaniline)s **T-16** and **T-b16**

A mixture of triformylphloroglucinol (0.005 mmol, 1 equiv.) and aniline **7b** or **7c** (0.19 mmol, 3.4 equiv.) in absolute ethanol (50 ml) was heated to reflux under inert atmosphere for 6 h with vigorous stirring. The dull yellow solid separated upon cooling the reaction mixture was collected by filtration, repeatedly washed with ethanol, and air-dried. The crude product was purified by repeated recrystallizations in a mixture of absolute ethanol-CH_2Cl_2.

T-16: R_f = 0.65 (40% EtOAc-hexane); a brick red solid; yield: 70%; IR (KBr pellet): ν_{max} cm^{-1} 2956, 2925, 2854, 1621, 1595, 1576, 1509, 1448, 1421, 1286, 1252, 1115, 983, 832, 723; ^{1}H NMR ($CDCl_3$, 600 MHz): δ 13.44 (broad s, =CNH), 13.30 (broad s, =CNH), 13.02 (broad s, =CNH), 8.74 (broad s, 3H, =CHN), 8.02 (broad d, 6H, Ar), 7.07 (broad s, 12H, Ar), 4.02 (broad s, 18H, 9 × OCH_2), 1.83-0.88 (m, 279H, 126× CH_2, 9×CH_3). MALDI Tof MS ES+ : m/z for $C_{195}H_{328}N_9O_{12}S_3$ (M+5) Calculated :3084.4467 Found: 3084.177.

T-b16: R_f= 0.62 (40% EtOAc – hexane); a very viscous orange liquid; Yield 65%; IR (KBr pellet): ν_{max} cm^{-1} 2956, 2925, 2854, 1621, 1595, 1575, 1509, 1448, 1421, 1379, 1286, 1253, 1180, 832, 772, 655; ^{1}H NMR ($CDCl_3$, 600 MHz): δ 13.54 (d, *J*= 12Hz, =CNH), 13.50 (d, *J*= 12 Hz, =CNH), 13.12 (d, *J*=12Hz, =CNH), 8.90-8.80 (m, 3H, =CHN), 8.10-8.08 (m, 6H, Ar), 7.47 –

7.43 (m, 6H, Ar), 7.20 (broad s, 6H, Ar), 3.94-3.89 (m, 18H, 9×OCH_2), 1.86-0.87(m, 280H, 113×CH_2, 18×CH_3). MALDI Tof MS ES+ : m/z for $C_{195}H_{327}N_9O_{12}S_3$ (M+4) Calculated :3083.4394 Found: 3083.393.

2.6. References

1. a) C. Tschierske in *Handbook of Liquid Crystals: Fundamentals* (Ed: J. W. Goodby, P. J. Collings, T. Kato, C. Tschierske, H. Gleeson, P. Raynes), Wiley- VCH, Weinheim, Germany 2014; b) C. Tschierske, *Angew. Chem*. 2013, **125**, 8992–9047; *Angew. Chem. Int. Ed.*, 2013, **52**, 8828–8878;
2. a) Q. Li in *Self-organized Organic Semiconductors-From Materials to De- vice Applications* (Ed.: Q. Li), Wiley, Hoboken 2011; b) Q. Li in *Anisotropic Nanomaterials: Preparation, Properties and Applications* (Ed.: Q. Li) Springer 2015.
3. B. Roy, N. De and K. C. Majumdar, *Chem. Eur. J.*, 2012, **18**, 14560–14588.
4. T. W¨ohrle, I. Wurzbach, J. Kirres, A. Kostidou, N. Kapernaum, J. Litterscheidt, J. C. Haenle, P. Staffeld, A. Baro, F. Giesselmann and S. Laschat, *Chem. Rev*., 2016, **116(3)**, 1139–1241.
5. A. Seed, *Chem. Soc. Rev.*, 2007, **36**, 2046-2069.
6. J. Han, *J. Mater. Chem. C*, 2013, **1**, 7779.
7. Y. Hu, C.-Y. Li, X.-M. Wang, Y.-H. Yang and H.-L. Zhu, *Chem. Rev.*, 2014, **114**, 5572–5610.
8. (a) M. Parra, S. Hernandez, J. Alderete and C. Zuniga, *Liq. Cryst*., 2000, **27(8)**, 995–1000; (b) Y. Xu, W. Lu and Z. Tai, *Mol. Cryst. Liq. Cryst. Sci. Technol., Sect. A*, 2000, **350**, 151–159; (c) A. A. Kiryanov, P. Sampson and A. J. Seed, *J. Org. Chem*., 2001, **66**, 7925–7929; (d) M. W. Schroder, S. Diele, G. Pelzl, N. Pancenko and W. Weissflog, *Liq. Cryst*., 2002, **29**, 1039–1046; (e) M. Parra, J. Alderete and C. Zuniga, *Liq. Cryst.*, 2004, **31**, 1531–1537; (f) T. Hegmann, B. Neumann, R. Wolf and C. Tschierske, *J. Mater. Chem*., 2005, **15**, 1025–1034; (g) M. Parra, J. Vergara, P. Hidalgo, J. Barbera and T. Sierra, *Liq. Cryst.*, 2006, **33**, 739–745; (h) B. P. Sybo, A. Bradley, S. Grubb, K. Miller, J. W. Proctor, L. Clowes, M. R. Lawrie, P. Sampson and A. J. Seed, *J. Mater. Chem*., 2007, **17**, 3406–3411; (i) C. F. He, G. J. Richards, S. M. Kelly, A. E. A. Contoret and M. O. Neill, *Liq. Cryst.*, 2007, **34**, 1249–1267; (j) J. Han, X. Y. Chang, L. R. Zhu, Y. M. Wang, J. B. Meng, S. W. Lai and S. S.-Y. Chui, *Liq. Cryst.*, 2008, **35**, 1379–1394; (k) J. H. Tomma, I. H. Rou'il and A. H. Al-Dujaili, *Mol. Cryst. Liq. Cryst.*, 2009, **501**, 3–19; (l) M. C. McCairn, T. Kreouzis and M. L. Turner, *J. Mater. Chem.*, 2010, **20**, 1999–2006; (m) A. K. Prajapati and V. Modi, *Liq. Cryst*., 2011, **38**, 191–199; (n) Q. Song, D. Nonnenmacher, F. Giesselmann and R. P. Lemieux, *J. Mater. Chem. C*, 2012, **1**, 343–350; (o) P. Tuzimoto, D. M. P. O. Santos, T. D. S. Moreira, R. Cristiano, I. H. Bechtold and H. Gallardo, *Liq. Cryst.*, 2014, **41**, 1097–1108; (p) R. C. Tandel and N. K. Patel, *Liq. Cryst.*, 2014, **41**, 495–502.
9. (a) M. Lehmann, J. Seltmann, A. Auer, E. Prochnow and U. Benedikt, *J. Mater. Chem.*, 2009, **19**, 1978–1988; (b) M. Lehmann and J. Seltmann, *Beilstein J. Org. Chem.*, 2009, **5**, 73.
10. M. L. Parra, E. Y. Elgueta, J. A. Ulloa, J. M. Vergara and A. I. Sanchez, *Liq. Cryst*., 2012, **39**, 917–925.
11. (a) M. Sato, *Macromol. Rapid Commun.*, 1999, **20**, 77–80; (b) M. Sato and Y. Uemoto, *Macromol. Rapid Commun*., 2000, **21**, 1220–1225; (c) M. Sato, M. Notsu, S. Nakashima and Y. Uemoto, *Macromol. Rapid Commun.*, 2001, **22(9)**, 681–686; (d) M. Sato, M. Mizoi and Y.

Uemoto, *Macromol. Chem. Phys.*, 2001, **202**, 3634–3641; (e) M. Sato, S. Nakashima and Y. Uemoto, *J. Polym. Sci., Part A: Polym. Chem*., 2003, **41**, 2676–2687; (f) N. S. Al-Muaikel, *Polym. Int.*, 2004, **53**, 301–306; (g) M. Sato, Y. Tada, S. Nakashima, K.-I. Ishikura, M. Handa and K. Kasuga, *J. Polym. Sci., Part A: Polym. Chem.*, 2005, **43**, 1511–1525; (h) M. Sato, Y. Matsuoka and I. Yamaguchi, *Liq. Cryst.*, 2012, **39**, 1071–1081.

12. (a) M. Parra, S. Villouta, V. Vera, J. Belmar, C. Zuniga and H. Z. Zunza, *Z. Naturforsch., B: J. Chem. Sci*., 1997, **52**, 1533–1538; (b) M. Sato, R. Ishii, S. Nakashima, K. Yonetake and J. Kido, *Liq. Cryst.*, 2001, **28**, 1211–1214; (c) C. F. He, G. J. Richards, S. M. Kelly, A. E. A. Contoret and M. O'Neill, *Liq. Cryst.*, 2007, **34**, 1249–1267; (d) S. K. Pathak, S. Nath, R. K. Gupta, D. S. S. Rao, S. K. Prasad and A. S. Achalkumar, *J. Mater. Chem. C*, 2015, **3**, 8166-8182; (e) B. Pradhan, M. Gupta, S. K. Pal and A. S. Achalkumar, *J. Mater. Chem. C*, 2016, **4**, 9669-9673; (f) B. Pradhan, V. M. Vaisakh, G. G. Nair, D. S. S. Rao, S. K. Prasad, and A. S. Achalkumar, *Chem. Eur. J*. 2016, **22**, 17843 – 17856.
13. (a) K.-T. Lin, H.-M. Kuo, H.-S. Sheu and C. K. Lai, *Tetrahedron*, 2013, **69**, 9045–9055; (b) K. S. Mustafa, K. S. Al-Malki, A. S. Hameed and A. H. Al-Dujaili, *Mol. Cryst. Liq. Cryst*., 2014, **593**, 34–42; (c) S. K. Pathak, R. K. Gupta, S. Nath, D. S. S. Rao, S. K. Prasad and A. S. Achalkumar, *J. Mater. Chem. C*, 2015, **3**, 2940-2952.
14. M. Lehmann, *Chem. Eur. J*., 2009, **15**, 3638–3651.
15. (a) Y. D. Zhang, K. G. Jespersen, M. Kempe, J. A. Kornfield, S. Barlow, B. Kippelen, S. R. Marder, *Langmuir*, 2003, **19**, 6534 – 6536. (b) R. Cristiano, D. M. P. D. O. Santos, H. Gallardo, *Liq. Cryst*. 2005, **32**, 7–14. (c) S. Varghese, N. S. S. Kumar, A. Krishna, D. S. S. Rao, S. K. Prasad, S. Das, *Adv. Funct. Mater*., 2009, **19**, 2064 – 2073.
16. (a) C. J. Lee, S. J. Lee, J. Y. Chang, *Tetrahedron Lett*., 2002, **43**, 3863 – 3866; (b) K. C. Majumdar, N. De, B. Roy, A. Bhaumik, *Liq. Cryst*., 2010, **37**, 1459 – 1464; (c) S. Kotha, D. Kashinath, S. Kumar, *Tetrahedron Lett*., 2008, **49**, 5419 – 5423; (d) H. Lee, D. Kim, H.K. Lee, W. Qiu, N.K. Oh, W.C. Zin, K. Kim, *Tetrahedron Lett*., 2004, **45**, 1019 – 1022; (e) H. C. Holst, T. Pakula, H. Meier, *Tetrahedron*, 2004, **60**, 6765 – 6775; (f) U. B. Vasconcelos, E. Dalmolin, A. A. Merlo, *Org. Lett.*, 2005, **7**,1027 – 1030;(g) C. H. Lee, T. Yamamoto, *Tetrahedron Lett*., 2001, **42**, 3993 – 3996; (h) B. Pradhan, S. K. Pathak, R. K. Gupta, M. Gupta, S. K. Pal and A. S. Achalkumar, *J.Mater.Chem.C*, 2016, **4**, 6117-6130.
17. (a) R. Cristiano, H. Gallardo, A. J. Bortoluzzi, I. H. Bechtold, C. E. M. Campos, R. L. Longo, *Chem. Commun*., 2008, 5134 – 5136; (b) R. Cristiano, J. Eccher, I. H. Bechtold, C. N. Tironi, A. A. Vieira, F. Molin and H. Gallardo, *Langmuir*, 2012, **28**, 11590–11598.
18. (a) A. S. Achalkumar , C. V. Yelamaggad, *Tetrahedron Letters*, 2012, **53,** 7108–7112; (b) C. V. Yelamaggad, A. S. Achalkumar, D. S. S. Rao and S. K. Prasad, *J. Org. Chem.*, 2009, **74**, 3168–3171; (c) A. S. Achalkumar, U. S. Hiremath, D. S. S. Rao, S. K. Prasad and C. V. Yelamaggad, *J. Org. Chem.*, 2013, **78**, 527–544; (c) A. S. Achalkumar, B.N. Veerabhadraswamy, U. S. Hiremath, D. S. S. Rao, S. Krishna Prasad, C. V. Yelamaggad, *Dyes and Pigments*, 2016, **132**, 291-305.
19. (a) C. V. Yelamaggad, A. S. Achalkumar, D. S. S. Rao, S. K. Prasad, *J. Am. Chem. Soc*., 2004, **126**, 6506-6507; (b) C. V. Yelamaggad, A. S. Achalkumar, *Tetrahedron Lett*, 2006, **47**, 7071-7075.(c) C. V. Yelamaggad, A. S. Achalkumar, D. S. S. Rao, S. K. Prasad, *J Mater Chem*., 2007, **17**, 4521-4529; (d) C. V. Yelamaggad, A. S. Achalkumar, D. S. S. Rao, S. K. Prasad, *J. Org Chem*., 2007, **72**, 8308-8318.
20. M. Sauer, C. Yeung, J. H. Chong, B. O. Patrick, M. J. MacLachlan, *J. Org. Chem.*, 2006, **71**, 775-788.

21. (a) S. Kandambeth, A. Mallick, B. Lukose, M. V. Mane, T. Heine and R. Banerjee, *J. Am. Chem. Soc.*, 2012, **134**, 19524–19527. (b) S. Chandra, S. Kandambeth, B. P. Biswal, B. Lukose, S. M. Kunjir, M. Chaudhary, R. Babarao, T. Heineand, R. Banerjee, *J. Am. Chem. Soc.*, 2013, ***135***, 17853–17861. (c) C. R. DeBlase, K. E. Silberstein, T.-T. Truong, H. D. Abruña and W. R. Dichtel, *J. Am. Chem. Soc.*, 2013, **135**, 16821–16824. (d) S. Chandra, T. Kundu, S. Kandambeth, R. Babarao, Y. Marathe, S. M. Kunjir and R. Banerjee, *J. Am. Chem. Soc.*, 2014, **136**, 6570–6573.
22. (a) J. A. Riddle, J. C. Bollinger, D. Lee, *Angew. Chem. Int. Ed.*, 2005, **44**, 6689-6693. (b) J. A. Riddle, S. P. Lathrop, J. C. Bollinger, D. Lee, *J. Am. Chem. Soc.*, 2006, **128**, 10986−10987. (c) X. Jiang, J. C. Bollinger, D. Lee, *J. Am. Chem. Soc.*, 2006, **128**, 11732−11733. (d) M. Vieweger, X. Jiang, Y.-K. Lim, J. Jo, D. Lee and B. Dragnea, *J Phys Chem A*, 2011, **115**, 13298–13308. (e) X. Jiang, Y.-K. Lim, B. J. Zhang, E. A. Opsitnick, M.-H. Baik and D. Lee, *J. Am. Chem. Soc.*, 2008, **130**, 16812–16822. (f) Y.-K. Lim, S. Wallace, J. C. Bollinger, X. Chen and D. Lee, *Inorg Chem.*, 2007, **46**, 1694–1703. (g) J. A. Riddle, X. Jiang, J. Huffman and D. Lee, *Angew. Chem. Int. Ed. Engl.*, 2007, **46**, 7019–7022.
23. (a) R. Kleppinger, C.P. Lillyaand, C. Yang, *J. Am. Chem. Soc.*, 1997, **119**, 4097-4102. (b) R. Festag, R. Kleppinger, M. Soliman, J. H. Wendorff, G. Lattermann and G. Staufer, *Liq Cryst*., 1992, **11**, 699-710.(c) D. M. Collard, C. P. Lillya, *J. Am. Chem. Soc.*, 1987, **109**, 7544-7545.
24. C. V. Yelamaggad, A. S. Achalkumar, D. S. Shankar Rao and S. K. Prasad *J. Mater. Chem.*, 2007, **17**, 4521–4529**;** (b) B. Pradhan, S. K. Pathak, R. K. Gupta, M. Gupta, S. K. Pal and A. S. Achalkumar, *J. Mater. Chem. C*, 2016, **4**, 6117.
25. (a) A. Marrocchi, M. Seri, C. Kim, A. Facchetti, A. Taticchi and T. J. Marks, *Chem. Mater*., 2009, **21**, 2592-2594; (b) D. Huang, M. Prehm, H. Gao, X. Cheng,Y. Liu and C. Tschierske, *RSC Adv*., 2016, **6**, 21387–21395.

Chapter III

1,2,4 and 1,3,4-Oxadiazole based tris(*N*-salicylideneaniline)s (TSANs)

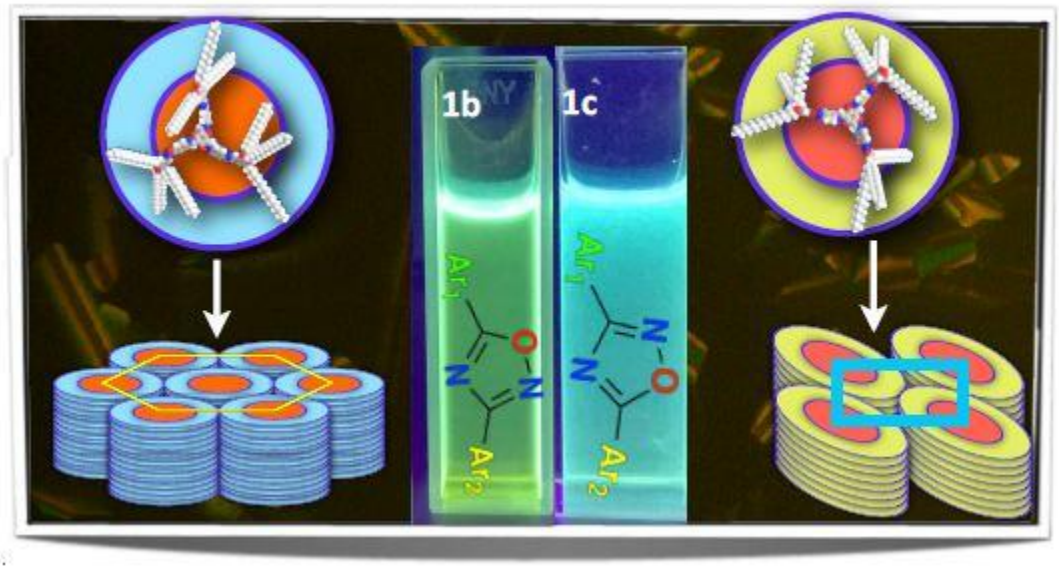

Results have been published in *New J. of Chem*, DOI: 10.1039/C7NJ01766A

3.1. Introduction

Over the years several molecular motifs have been tried to stabilize self-assemblies of π-conjugated molecules, which will enhance the one dimensional (1D) charge migration. This capability garners increased attention nowadays, due to the potential advantages in organic optoelectronics.[1] In this context, high quality single crystals, amorphous polymers and columnar liquid crystals are the major contenders to take over the mantle of next generation semiconductor industries. Each one of them has their own advantages and disadvantages, where one has to make a clever trade off to make a successful choice and tailor them according to the demand. For example, the single crystals vouch for the highest order and consequently the conductivity but obtaining a defect free single crystal (defects act as charge traps) and to handle them in device fabrication is not an easy task.[2] Amorphous polymers have the problem of batch-to-batch reproducibility, difficulty of purification and low conductivity. On the other hand columnar liquid crystals (Col LCs) formed by the disc-like organic molecules are known to have superior order, processability and good anisotropic conductivity. Col LCs are often compared to molecular wires, where the one dimensionally stacked aromatic cores form a central conducting unit, while the peripheral tails function as an insulating sheath, thus leading to a large difference in the charge carrier mobility along the column and across the column.[3] Additionally they have a self-healing ability to overcome the defects, which act as charge traps. Further benefits are the ease of synthesis, tunability of the structure as per the requirement, reproducibility and ease of processability (by solution or by vapor deposition).[4] Though the stabilization of Col LCs was first reported with disc shaped molecules,[5] consequently several novel molecular designs like polycatenars, star shaped molecules, dendrimers and metallomesogens have shown the ability to stabilize this self-assembly.[6] Considering the potential applicability of Col LCs as a bright option in the fabrication of organic photovoltaics (OPVs),[7] organic light emitting diodes (OLEDs)[8] and organic field effect transistors (OFETs)[9], one need to have a flexible platform, where the desired properties can be incorporated by an easy synthetic route, while maintaining Col assembly intact. Star-shaped molecules are relatively a new class of materials that stabilize Col LC phases, with a synthetic flexibility to include various functional properties.[10] These molecules have three covalently linked arms to the central core through flexible or rigid linkers. Though these molecules lack shape anisotropy as in the case of discotics, the nanophase segregation of

incompatible molecular subunits promote the stabilization of Col LC phases. Recently tris(*N*-salicylideneanilines) (TSANs) are receiving great attention from researchers as a useful molecular design to stabilize different self-assemblies.[11] With a careful design this core can provide smart materials, due to its synthetic flexibility, which will help in tuning their material properties. Several research groups utilized this core in the development of molecular switches,[12] sensors,[13] covalent organic frameworks,[14] chiral catalysts.[15] We were able to synthesize several luminescent Col LCs based on TSANs and shown that their self-assembly and luminescence can be tuned by appropriate design of the arms.[16]

Introduction of heterocycles in the liquid crystal design is of immense interest in recent days, because of the sheer number of structural varieties possible and hence the control on their properties.[17] The heterocyclic molecular structure provides a reduced symmetry, strong lateral and/or longitudinal polar induction. Further their incorporation leads to donor–acceptor interactions within the molecules due to unsymmetrical distribution of electron density. All these properties in turn affect the photophysical and self-assembly behavior.[17d] Additionally, it provides an uneven electron density distribution in the molecule and hence a wide range of emission colors are possible. Thus, heterocyclic mesogens are finding a strong footing in the area of OLEDs. Such oriented mesogens exhibit polarized emission.[1] 1,3,4-Oxadiazoles are widely studied heterocycles in liquid crystals and OLEDs, due to their high stability towards hydrolytic, thermal and oxidative deterioration. These materials are known for high luminescence quantum yield and superior electron transporting properties. Thus they are finding application as electron transporting/hole blocking or electroluminescent layers in OLEDs.[17,18] In the recent past TSANs containing unsymmetrically substituted 1,3,4-oxadiazole arms were reported and they exhibited greenish blue emission in solution state and stabilized columnar hexagonal phase.[16e] However, they showed high melting and clearing temperatures. The regioisomeric 1,2,4-oxadiazole is also known for its good emissive nature and high thermal stability, but less studied unlike its 1,3,4-isomer. The unsymmetric ring structure of 1,2,4-oxadiazole moiety provides a strong lateral dipole leading to the stabilization of different mesophases in comparison to the LCs derived from 1,3,4-oxadiazoles.[18–24] Unsymmetrical substitution of 1,2,4-oxadiazole is another effective handle to tune the resultant material properties. 1,2,4-oxadiazole derivatives are known to possess high band gap and high S1 and T1 energies. These properties are favorable for the design

of high triplet energy host materials which are required for the fabrication of efficient phosphorescent OLEDs.[26] Phosphorescent OLEDs are superior in comparison to OLEDs, because they trap both the singlet and triplet excitons, to increase the efficiency. Literature reports suggest that 1,2,4-oxadiazole derivatives have acceptable thermal stability, lower melting points and wider mesophase range in comparison to their 1,3,4-oxadiazole isomers.[18] Further the bending angle of the 1,2,4-oxadiazole core is 140^{o} which is slightly more than the bending angle of the 1,3,4-oxadiazole core (134^{o}).[19] Only few reports are there till now on 1,2,4-oxadiazole containing mesogens exhibiting Col phase.[20-25] Hence we were interested in the introduction of 1,2,4-oxadiazole moieties in TSANs core and study the thermal and photophysical behavior with respect to the earlier reported 1,3,4-oxadiazole based TSANs.

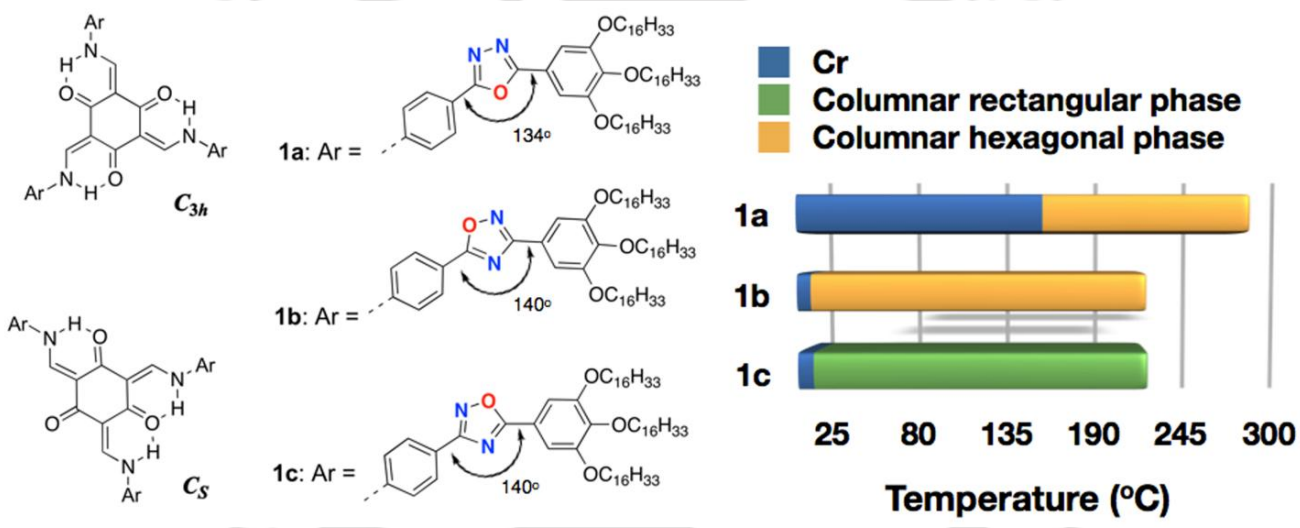

Figure 3.1. Molecular structures of the regioisomeric TSANs **1a** and **1b-c** and their thermal behavior (based on the heating scans from DSC**)**

3.2. Results and discussion

3.2a. Synthesis and Characterization

The synthetic approach for the preparation of the target molecules is presented in Scheme 1 and 2. The 1,3,5-trimethoxybenzaldehyde was converted to corresponding nitrile (**1**) up on treating with hydroxylamine hydrochloride in dimethylsulfoxide (DMSO) at 100 ^{o}C for 3 h. Further reflux of nitrile (**1**) with hydroxylamine hydrochloride in ethanol led to benzamidoxime

intermediate (**2**). Compound **2** on refluxing with 4-nitrobenzoyl chloride in pyridine afforded 5-(4-nitrophenyl)-3-(3,4,5-trimethoxyphenyl)-1,2,4-oxadiazole (**3**) which on demethylation furnished the key precursor, namely, 5-(5-(4-nitrophenyl)-1,2,4-oxadiazol-3-yl) benzene-1,2,3-triol (**4**), in 87% yield. Compound **4** on *O*-alkylation with 1-bromohexadecane yielded the nitro compound **5**, which on catalytic reduction provided the required aniline **6**. Finally, the condensation of aniline **6** with 1,3,5-triformylphloroglucinol (**7**) afforded TSANs **1b** (Scheme 3.1). Similarly, the 4-nitrobenzaldehyde was converted to its respective nitrile (**9)** upon heating

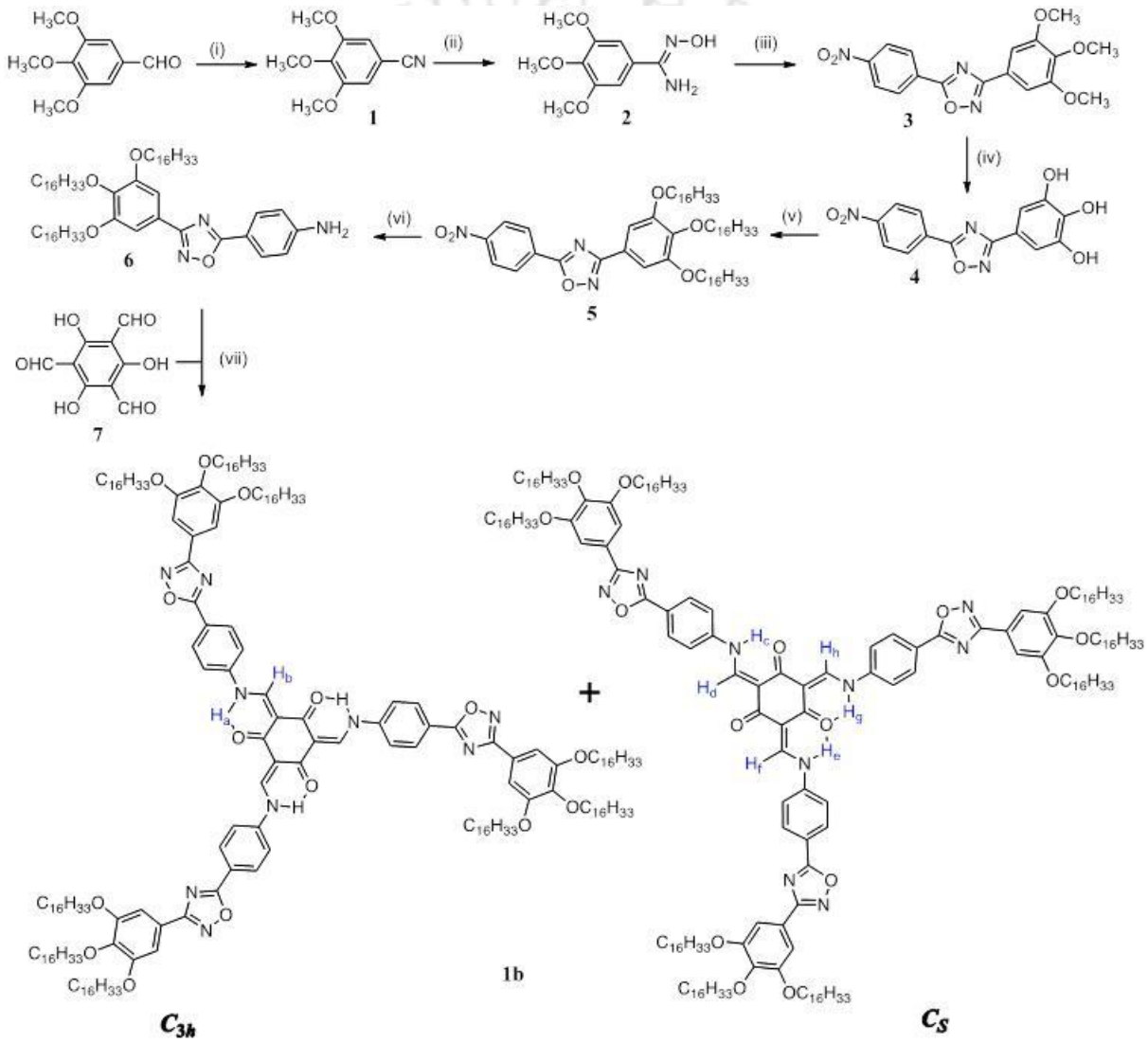

Scheme 3.1. Reagents and Conditions (i) $NH_2OH.HCl$, DMSO, reflux, 3 h (85%); (ii) $NH_2OH.HCl$, triethylamine, CH_3CN, reflux, 24 h (90%); (iii) 4-nitrobenzoyl chloride, pyridiine, reflux, 6 h (80%); (iv) BBr_3, Dry DCM, 0 ^oC-RT, 12 h (87%); (v) 1-Bromohexadecane, anhyd. K_2CO_3, DMF, 80 ^oC, 12 h (64%); (vi) Pd/C, H_2, RT, 6 h (70%); (vii) Ethanol, reflux, 6 h (65%).

with hydroxylamine hydrochloride in DMSO at 100 ^{o}C for 3 h. Further the nitrile (**9**) was converted to benzamidoxime intermediate (**10**) as mentioned earlier, which on further refluxing with 3,4,5-trimethoxybenzoyl chloride in pyridine afforded 3-(4-nitrophenyl)-5-(3,4,5-trimethoxyphenyl)-1,2,4-oxadiazole (**11**). This trimethoxy derivative on demethylation with BBr_3 furnished the key precursor, 5-(5-(4-nitrophenyl)-1,2,4-oxadiazol-3-yl)benzene-1,2,3-triol (**12**) in 57 % yield. The triol **12** on *O*-alkylation with 1-bromohexadecane yielded the nitro compound **13**, which on catalytic reduction provided the corresponding aniline **14**. Finally, the reaction of aniline **14** with 1,3,5-triformylphloroglucinol afforded TSANs **1c** (Scheme 3.2).

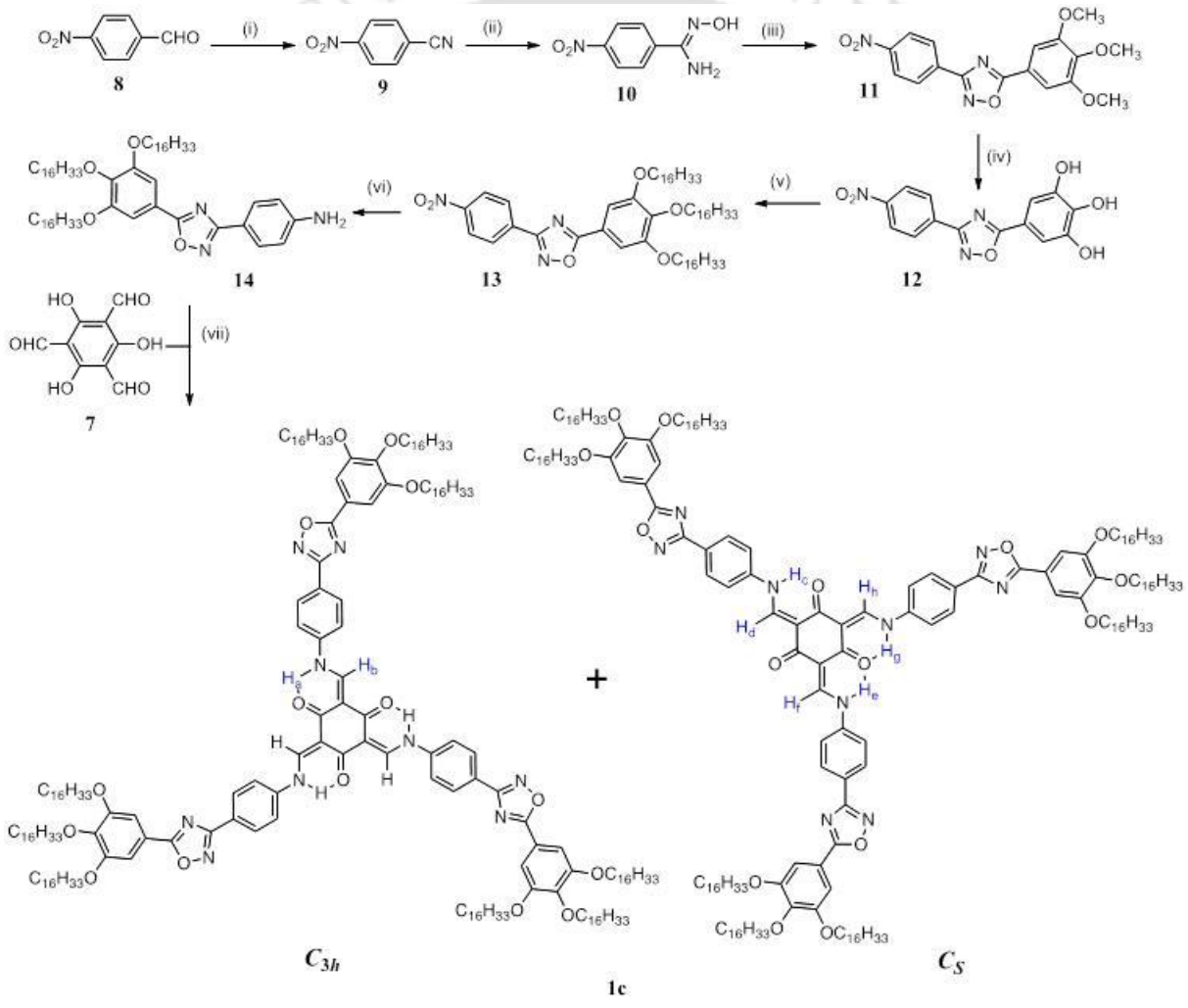

Scheme 3.2. Reagents and Conditions (i) $NH_2OH.HCl$, DMSO, reflux, 3 h (95%); (ii) $NH_2OH.HCl$, triethylamine, CH_3CN, reflux, 24 h (90%); (iii) trimethoxy benzoyl chloride, pyridine, reflux, 6 h (61%); (iv) BBr_3, Dry DCM, 0 ^{o}C-RT, 12 h (57%); (v) 1-Bromohexadecane, anhyd. K_2CO_3, DMF, 80 ^{o}C, 12 h (80%); (vi) Pd/C, H_2, RT, 6 h (41%); (vii) Ethanol, reflux, 6 h (67%).

These compounds existed as an inseparable mixture of isomers of C_{3h} and C_s symmetry, which was quantified by ^{1}H NMR by integrating the ratio of the protons corresponding to each isomer (Scheme 3.1 and 3.2, Table 3.1).

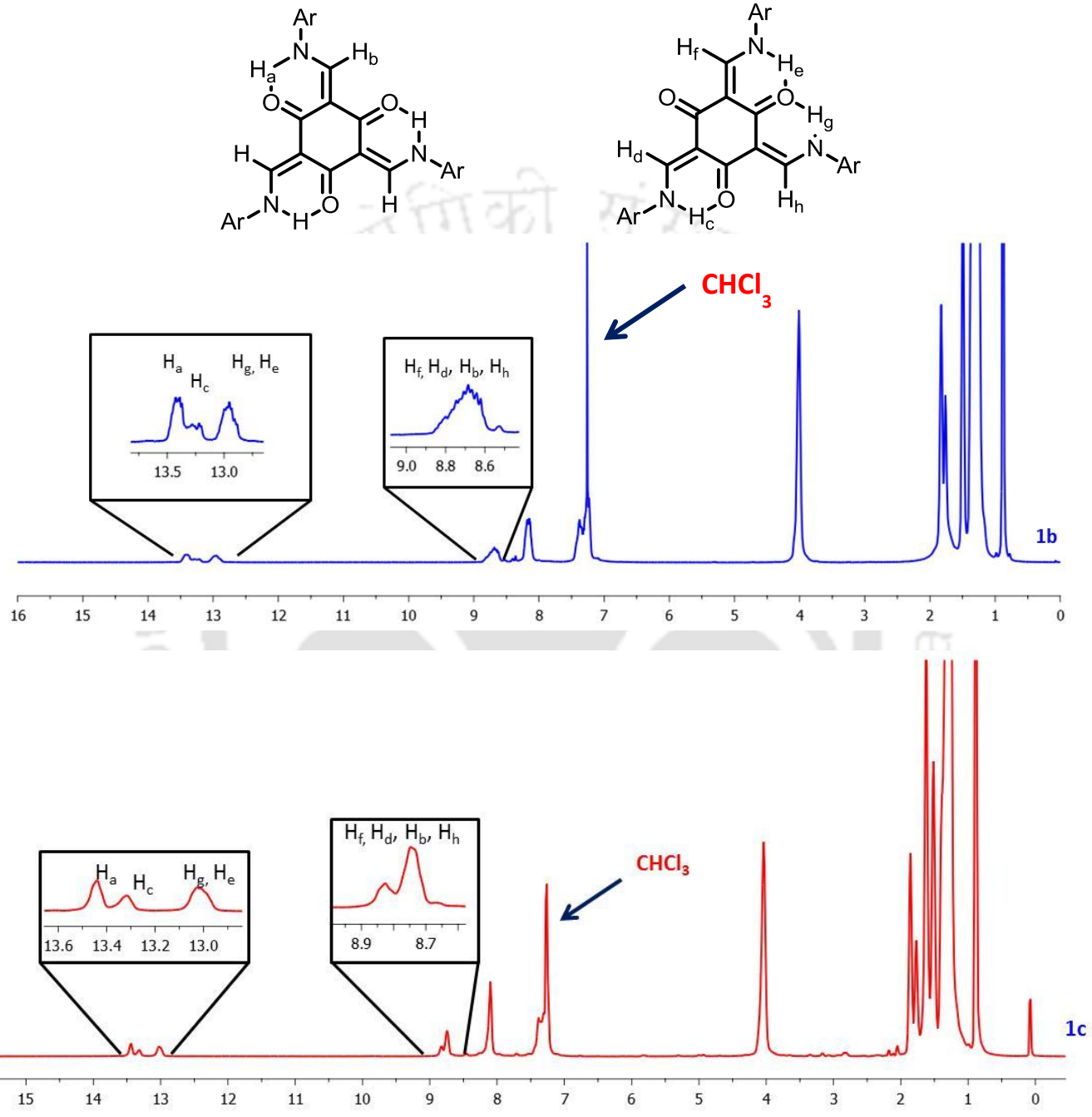

Figure 3.2. ^{1}H NMR (600 MHz) spectra of **1b** and **1c** in $CDCl_3$.

This can be explained as follows. The ^{1}H NMR spectra showed multiple peaks between 8.6-8.9 and 13-13.4 due to coupling between enamine (vinylic:H_b, H_d, H_f, and H_h) and secondary amine (NH: H_a, H_c, H_e, and H_g) protons. The integrated area under the peaks of H_a *vs.* H_c, H_g, and H_e of amine protons or H_b *vs.* H_d, H_f, and H_h can be considered to calculate the ratio of two forms. However, owing to the close proximity of chemical shifts of enamine protons, we have considered the secondary amine protons for estimating the ratio of the two isomers of different rotational symmetry (shown in Table 3.1). The structures of all the intermediates and target molecules were confirmed using routine spectroscopic analysis and ESI-HRMS or MALDI-TOF analysis. To show the characteristic protons peaks, ^{1}H NMR spectra of **1b** and **1c** are presented in Figures 3.2.

3.2b. Thermal behavior

The mesogenic behavior of these star shaped molecules was studied with the help of polarizing optical microscopy (POM), differential scanning calorimetry (DSC) and powder X-ray diffraction (XRD) studies. Thermal gravimetric analyses (TGA) of these compounds showed that they are stable at least upto 250 ^oC (Fig. 3.3). The phase transitions and the accompanying enthalpy changes are summarized in Table 3.1 and graphically represented in Figure 3.1. The data obtained from XRD studies are tabulated in Table 3.2.

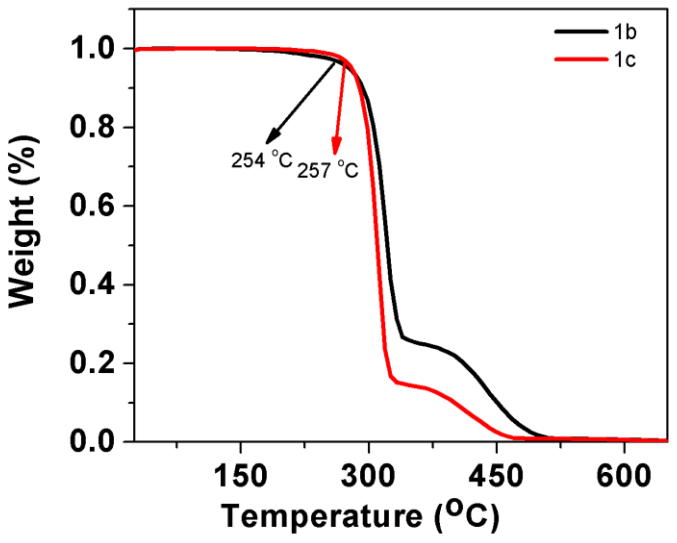

Figure 3.3. TGA curves of TSAN **1b** and **1c**

The thermal behavior of compound **1a** was reported earlier[16e] and for the sake of comparison with the regioisomeric 1,2,4-oxadiazole derivatives, it is provided in Table 3.1.

Table 3.1. Phase transition temperatures [a] (^{o}C) and corresponding enthalpies (kJ/mol) of regioisomeric TSANs

Entry (C_{3h}: C_s)[b]	Heating	Cooling
1a[c] (1:2.6)	Cr_1 63.4 (131.6) Cr_2 157.3 (29.4) Col_h 269.2 (5.6) I	I 265.7 (4.9) Col_h 24.6 (51.5) Cr
1b (2:1)	Cr 32.4 (8.9) Col_h 213.6 (0.1) I	I 203.1 (0.2) Col_h 26 (9.9) Cr
1c (1.8:1)	Cr 33.4 (7.5) Col_r 214.6 (0.2) I	I 204 (0.2) Col_r 25.7 (8.5) Cr

[a]Peak temperatures in the DSC thermograms obtained during the second heating and first cooling cycles at 5 ^{o}C/min.; Col_h = Columnar hexagonal phase, Col_r = Columnar rectangular phase; [b] Ratio obtained from ^{1}H NMR, Fig.3.2; [c]Reported in reference 16e.

Table 3.2. Results of the (*hkl*) indexation of the XRD profiles of the compounds at a given temperature (T) of the mesophases[a].

Compounds (*D*/Å)	Phase (T/^{o}C) Symmetry	d_{obs} (Å)	d_{cal} (Å)	Miller indices (*hk*)	Lattice parameters (Å) Lattice area S (Å^2), Molecular volume V (Å^3)
1b (65)	Col_h (180) *p6mm*	45.48 5.00 (h_a)	45.48	10	a = 52.9; S = 2423.42; V = 12117.12.
	Col_h (100) *p6mm*	47.83 4.98 (h_a)	47.83	10	a = 55.23; S = 2641.61; V = 13155.2.
	Col_h (28) *P6mm*	47.85 4.75 (h_a)	47.85	10	a = 55.3; S = 2648.31; V = 12579.45.
1c (60)	Col_r (140) *p2mm*	45.52 24.27 12.70 5.09 (h_a) 3.72 (h_c)	45.52 24.27 12.87	01 10 13	a = 24.27, b = 45.52; S = 1104.8; V = 4109.74; Z = 0.8.
	Col_r (60) *p2mm*	45.54 24.91 12.69 4.96(h_a) 3.68(h_c)	45.54 24.91 12.46	01 10 13	a = 24.91, b = 45.54; S = 1134.4; V = 4174.6; Z = 0.9.

[a]The diameter (D) of the disk (estimated from Chem 3D Pro 8.0 molecular model software from Cambridge Soft, calculated for the C_{3h} isomer). d_{obs}: spacing observed; d_{cal}: spacing calculated (deduced from the lattice parameters; a for Col_h phase, a, b for Col_r phase). The spacings marked h_a and h_c correspond to diffuse reflections in the wide-angle region arising from correlations between the alkyl chains and core regions, respectively. Z indicates the number of molecules per columnar slice of thickness h_c, estimated from the lattice area S and the volume V.

From the Table 3.1 and Figure 3.1, it is evident that the compound **1a** exhibited columnar hexagonal (Col_h) phase with higher melting and clearing temperatures in comparison to

compound **1b** and **1c**. Compound **1b** melted at 32 ^{o}C with an enthalpy change of 8.9 kJ/mol to form a birefringent fluid. This on further heating cleared to form an isotropic liquid at 214 ^{o}C. The isotropic liquid on cooling at a rate of 5 ^{o}C/min exhibited the formation of rectilinear birefringent defects in the pseudoisotropic texture, which is a characteristic pattern observed for Col phases (Fig. 3.4a). The texture remained as such till room temperature (RT), even though with a concurrent decrease in the fluidity one lowering the temperature. No signs of crystallization were observed at RT, but the DSC scans showed crystallization 26 ^{o}C with an enthalpy change of 9.9 kJ/mol (Fig. 3.4b).

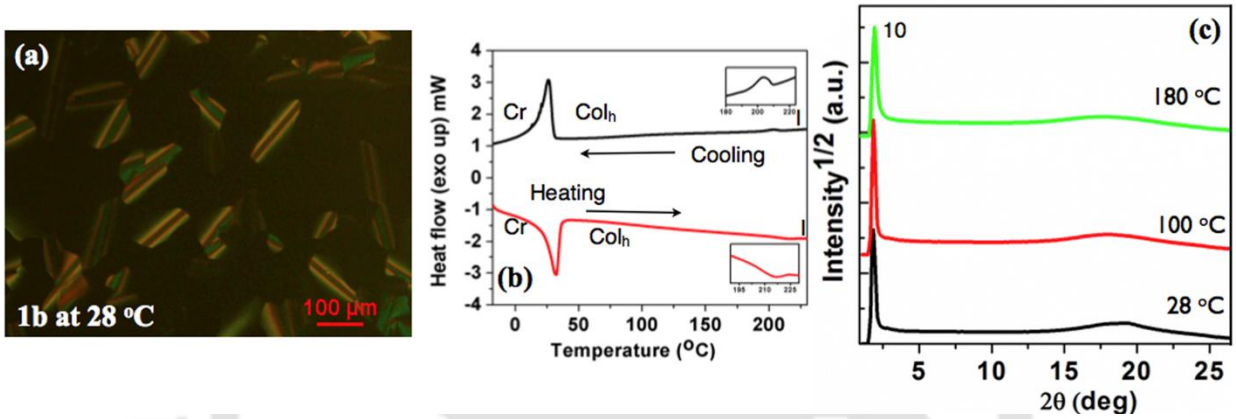

Figure 3.4. POM image of compound **1b** in Col$_h$ phase at room temperature (a); DSC scans of compound **1b** obtained for second heating (heating: red trace) and first cooling (cooling: black trace) (b); XRD profiles depicting the intensity against the 2θ obtained for the Col$_h$ phase of compound **1b** at 180 ^{o}C, 100 ^{o}C and at 28 ^{o}C (c).

The XRD studies were carried out for the sample taken in capillary at different temperature intervals. The XRD diffraction patterns obtained at 180 ^{o}C, 100 ^{o}C and 28 ^{o}C, exhibited a single peak at low angle region along with a diffused peak in the wide angle (Fig. 3.4c, Table 3.2). The single peak at low angle can be assigned to the 100 reflection of a hexagonal lattice (*p6mm*), while the diffused peak at wide angle originates from the packing of flexible alkyl tails. Though the presence of a single peak at the low angle is not sufficient to assign the phase to be Col$_h$, there are several reports in the literature where the single peak at the low angle is attributed to a minimum in the form factor.[27] The XRD pattern of compound **1b** at 28 ^{o}C showed peak with a *d*-spacing of 47.9 Å, from which the hexagonal cell parameter '*a*' was calculated and found to be 55.3 Å (Fig. 3.5). In comparison to the molecular diameter of 65 Å (for C_{3h} isomer, Fig. 3.8), the observed hexagonal lattice constant is 15% less, which indicates the intercalation or folding of the peripheral alkyl tails. Considering the large voids present in the star shaped architecture, it is

possible that these flexible tails may fill this vacant space also. Even though the C_s isomer exists in the Col phase (50% according to the ^{1}H NMR, Table 3.1, Fig. 3.9) formed by compound **1b** the molecular diameter does not vary much in comparison to C_{3h} isomer and it will be averaged out. Basically the C_{3h} and C_s isomers resemble the extensions of shape persistent pseudotriphenylene and benz[*d*]-anthracenylium structures, due to the strong intramolecular hydrogen bonding. However owing to the presence of peripheral flexible alkyl tails the shape is almost disc-like even for the C_s isomer, which is not a circular core.[16d] Further the unit cell area, '*S*' and unit cell volume 'V' were found to be 2423.4 Å^2 and 12117.12 Å^3 respectively. A relatively sharp peak at wide angle corresponding to the stacking of the cores is not observed for **1b** even at RT in comparison to compound **1a**, which exhibited a core-core stacking distance of 3.44 Å.[16e] This means that the core-core interaction is low in compound **1b** in comparison to its 1,3,4-oxadiazole analogue. The self-assembly of compound **1b** is schematically represented in Fig. 3.5.

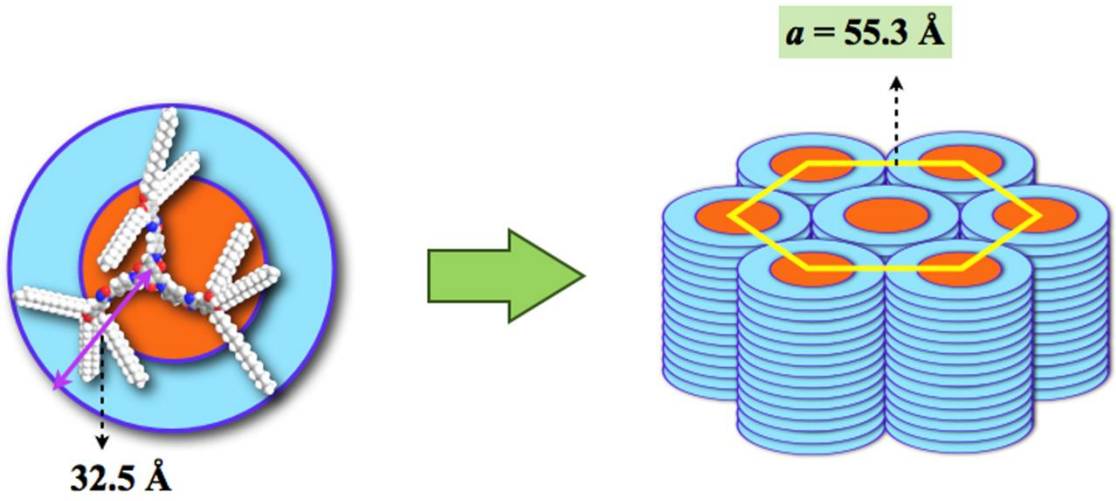

Figure 3.5. Schematic showing the self-assembly of compound **1b** in Col_h phase of *p6mm* symmetry (Derived from the XRD pattern obtained at 28 °C, only C_{3h} isomer shown for the sake of clarity)

Compound **1c**, melted at a temperature of ≈ 33 °C, and had a clearing point of 215 °C, which is similar to that of compound **1b** (Fig. 3.6b). It is understandable that the melting point is related to the melting of alkyl chains, while the clearing point is due to the unstacking of the cores from the columns. Thus the melting and clearing points remain almost same for both the compounds. This shows that the change in the orientation of heterocycle *i.e.* the 3,5-disubstituted-1,2,4-oxadiazole do not have much influence on the melting and clearing points (Fig. 3.1, Table 3.1). On cooling

the isotropic liquid a mosaic texture was appeared with birefringent defects in a homeotropic background (Fig. 3.6a). Often the textural pattern of Col phase is not specific to the symmetry of the Col phase and it has to be cross-checked with the XRD studies. XRD studies of the fluidic phase revealed that, it is a Col phase with a rectangular symmetry. Powder XRD studies were carried out at 140 ^{o}C and 60 ^{o}C. Both the diffraction patterns were similar and showed a strong reflection at the low angle along with two weak reflections. In the wide angle two diffused peaks were observed, where the first one was corresponding to the packing of alkyl tails, while the second one corresponding to the packing of cores. For example the diffraction pattern obtained at 60 ^{o}C showed three reflections at low angle corresponding to 45.54 Å, 24.91 Å and 12.69 Å, which can be indexed to the Miller indices 01, 10 and 13 of a rectangular lattice (*p2mm*) (Fig. 3.6c).

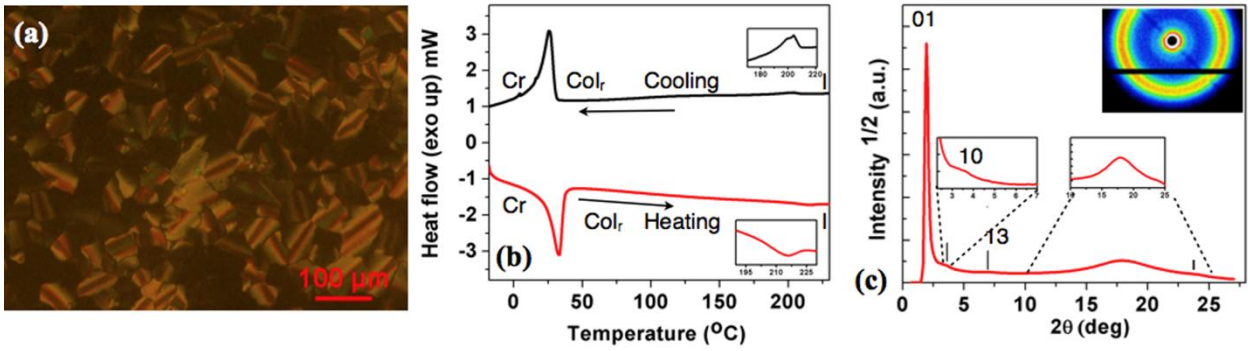

Figure 3.6. POM image of compound **1c** in Col$_r$ phase at 30 ^{o}C (a); DSC scans of compound **1c** obtained for second heating (heating: red trace) and first cooling (cooling: black trace) (b); XRD profiles depicting the intensity against the 2θ obtained for the Col$_r$ phase of compound **1c** at 60 ^{o}C (c).

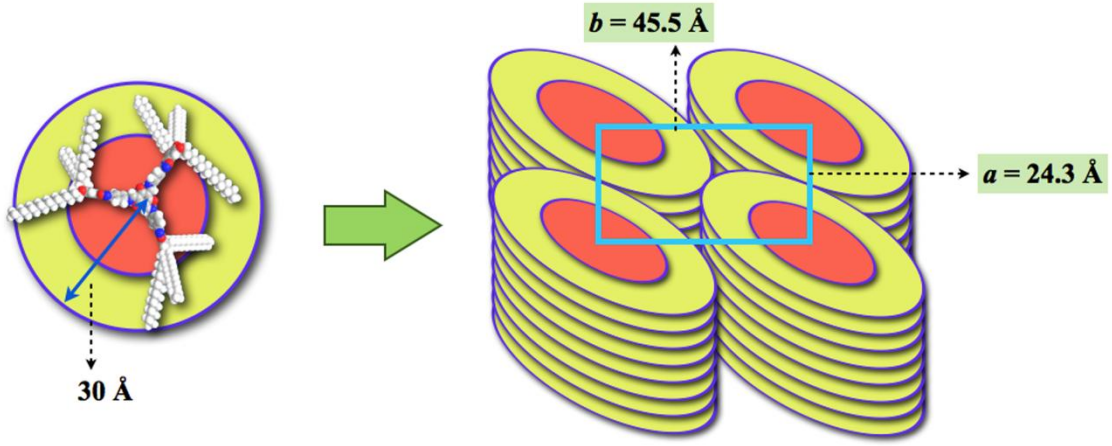

Figure 3.7. Schematic showing the self-assembly of compound 1c in Col$_r$ phase of *p2mm* symmetry (Derived from the XRD pattern obtained at 60 ^{o}C, only C_{3h} isomer shown for the sake of clarity)

The rectangular unit cell has lattice constants a = 24.9 Å and b = 45.5 Å with an area and volume of 1134.4 Å^2 and 4174.6 Å^3 respectively (Fig. 3.7, Table 3.1). The diffused peaks at wide angles centered at 4.96 Å and 3.68 Å, correspond to the packing of alkyl tails and the stacking of cores. The presence of the core-core peak at 3.68 Å signifies the enhanced intermolecular interaction of these star shaped molecules within the columns. Thus the number of molecules (Z) present in

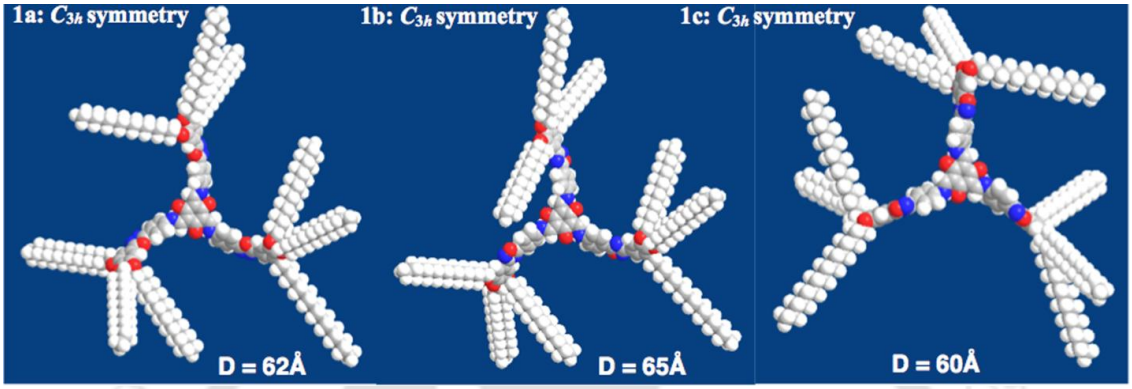

Figure 3.8. Molecular models obtained for star shaped compounds **1a**, **1b** and **1c**; Molecular diameters (D) are given in the inset (estimated from Chem 3D Pro 8.0 molecular model software from Cambridge Soft for C_{3h} isomer).

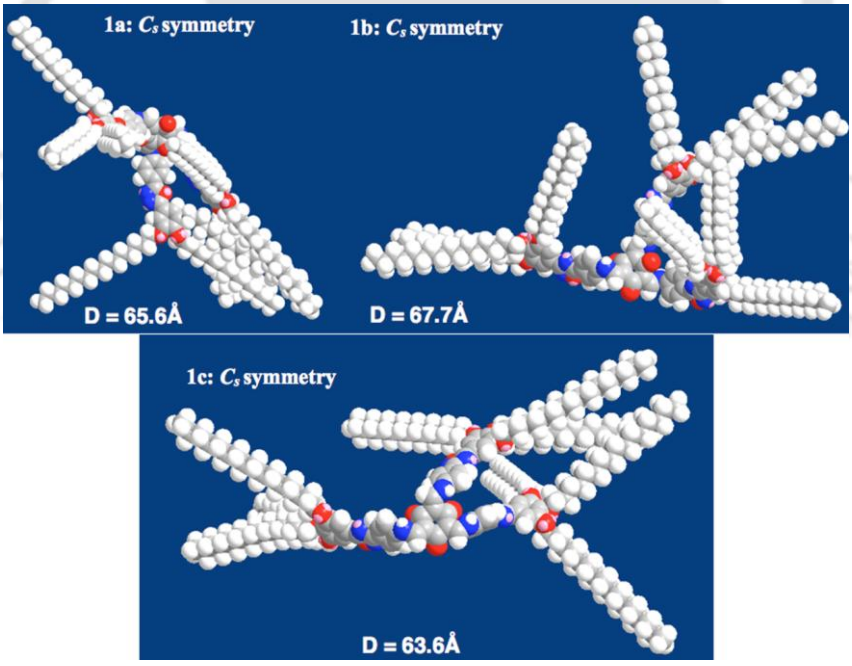

Figure 3.9. Molecular models obtained for star shaped compounds **1a**, **1b** and **1c**; Molecular diameters (D) are given in the inset (estimated from Chem 3D Pro 8.0 molecular model software from Cambridge Soft for C_s isomer).

the unit cell was calculated and found to be approximately equal to 1. This is not observed in the case of compound **1b**. It is to be noted that Col_r phases will be stabilized, only when there are

enhanced intermolecular interactions between the molecules in the column.

Further to understand the different behavior of these regioisomeric compounds we have carried out the molecular modeling studies. The molecular diameters of the star shaped molecules (estimated from Chem 3D Pro 8.0 molecular model software from Cambridge Soft, for C_{3h} isomer) were found to be 62 Å for compound **1a**, 65 Å for compound **1b** and 60 Å for compound **1c**. This means that compound **1a** and **1b** are more stretched (more planar) in comparison to compound **1c** (Fig. 3.8). Compound **1c** attains more of a propeller shape and because of this the molecules are forced to pack in certain order. This result in the increased intermolecular interactions within the column, that leads to the stabilization of Col_r phase as well as the appearance of core-core stacking peak in the XRD pattern. However, earlier reported 1,3,4-oxadiazole based TSANs have shown Col_h phase, and the presence of core-core peak. But in the case of 1,2,4-oxadiazole derivatives, the direction of the net dipole moment is changed in comparison to 1,3,4-oxadiazole derivatives. This difference in the direction and the extent of dipole moment is the result of bending angle provided by the type of heterocycle in the arms of the star shaped molecule. It should be noted that the amount of C_s isomers in both compounds **1b** and **1c** were found to be almost 50% (Table 3.1 and Fig. 3.9), while in the case of compound **1a** it is 2.6 times more than the C_{3h} isomer.[16e] But it has to be noted that, irrespective of the difference in the shape of the isomers, these molecules self-assembled into columnar structure having a 2D lattice of different symmetries. This shows that the difference in the shape of the molecules did not have a major impact on the mesophase stabilization. It is interesting to note that the columnar self-assembly is flexible enough to accommodate this difference in the molecular shape (Fig. 3.8 and 3.9).

3.3. Photophysical behavior

Photophysical properties of these compounds **1a**, **1b** and **1c** were studied in solution as well as in thin films. The absorption spectra of compounds in micromolar THF solutions were taken. Compound **1a** and **1b** exhibited similar absorption spectra with two absorption bands centered at 343 and ≈ 423 nm irrespective of the structural difference. Compound **1c** showed a blue shifted absorption maximum centered at 411 nm. The optical band gap calculated from the red edge of the absorption onset was found to be in the range of 2.62-2.7 eV. The relative quantum yields measured were in the range of 0.27-0.31 (Fig. 3.11). Thin films of these LCs

were prepared by annealing the samples in glass slides by annealing them from their isotropic state. Absorption spectra of all the three compounds in thin film showed a blue shift. Emission spectra of compounds **1a** and **1b** in solution exhibited an emission maximum centered at 473-475 nm with shoulders at 496-499 nm (Stoke's shift of 51 nm). Emission spectrum of compound **1c** was slightly blue shifted with an emission maximum centered at 463 nm with a shoulder band at 491 nm. All the solutions exhibited a bright green fluorescence under the UV light of long wavelength (λ_{ex} = 365 nm). All the thin films showed a broad red shifted emission spectra in the range of 557-620 nm with shoulder bands (Fig. 3.10 and Table 3.3).

Table 3.3. Photophysical properties of TSANs **1a-c**.

	Solution						Thin film	
Entry	Absorption [a] (nm)	Emission [a, b] (nm)	Stoke's shift (cm^{-1})	λ_{onset} (nm)	$\Delta E_{g,opt}$ [c, d]	ε ($M^{-1}cm^{-1}$)	Absorption (nm)	Emission[e] (nm)
1a	343, 424	475, 499	51	474	2.62	73049	366, 420	557, 602
1b	343, 422	473, 496	51	470	2.64	64713	361, 409	614
1c	411	463, 491	52	460	2.70	72808	351, 396	545, 620

[a] Micromolar solutions in THF. [b] Excited at the respective absorption maxima. [c]In electron volts (eV). [d]Band gap was determined from the red edge of the longest wave length in the UV-Vis absorption spectra. [e] Emission obtained by exciting the thin films at their respective absorption maxima.

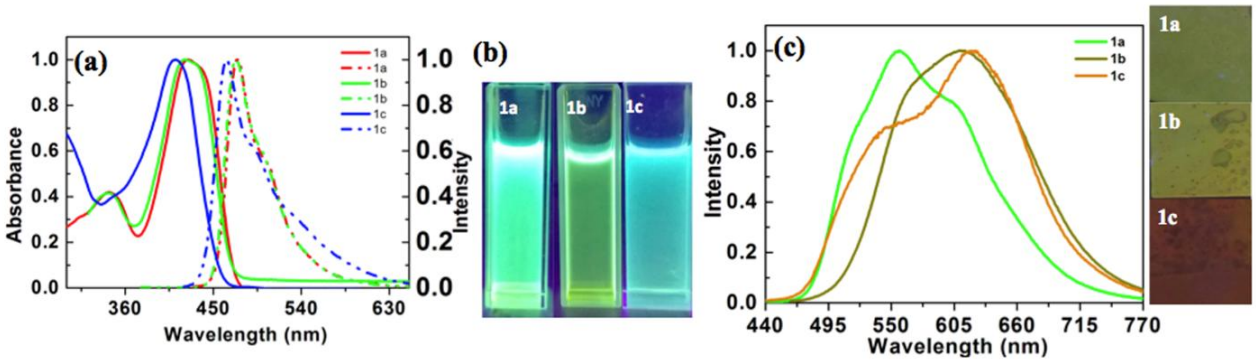

Figure 3.10. Normalized absorption (solid line) and emission spectra (dotted line) in THF solution obtained for **1a-c** (a); Pictures of micromolar solutions of compounds **1a-c** in THF as seen with the UV illumination (λ = 365 nm)(b); Normalized emission spectra obtained for compounds **1a**, **1b** and **1c** in the thin film state (c), right side shows the images of thin films with the UV illumination (λ = 365 nm).

Relative Quantum Yield Calculation

Relative quantum yield of compound was measured with respect to tetrakis(octyl)-1H-phenanthro[1,10,9,8]carbazole-3,4,9,10-tetracarboxylate in THF solution as the standard, which

is having the relative quantum yield of 1 with respect to fluorescein (Q_f = 0.79) in 0.1M NaOH). Absolute values were calculated according to the following equation: $Q_S = Q_R \times (m_S / m_R) \times (n_S / n_R)^2$ Where, Q: Quantum yield; m: Slope of the plot of integrated fluorescence intensity *vs* absorbance; n: refractive index (1.407 for THF).

Table 3.4. Quantum yield of TSANs **1a-c**.

Entry	m_S	m_R	$Q_s^{a,b,c}$
1a	2.63082 ×10^8	7.2271 x 10^8	0.37
1b	2.18814 × 10^8	7.2271 x 10^8	0.31
1c	1.90912 × 10^8	7.2271 x 10^8	0.27
[a] Measured in THF. [b]Excited at absorption maxima . [c]Standard carbazole (Q_f = 1.01) in THF solution			

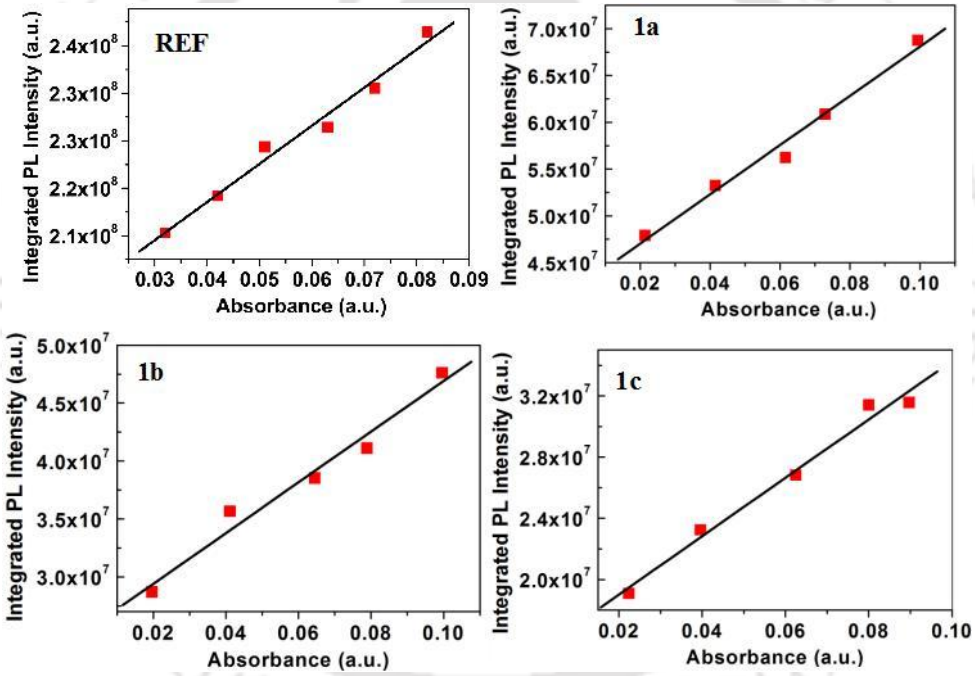

Figure 3.11. Plots of integrated photoluminescence intensity vs absorbance of tetrakis(octyl)-1H-phenanthro[1,10,9,8]carbazole-3,4,9,10-tetracarboxylate (micromolar THF solution) and compounds **1a-c** (micromolar THF solution)

The subscript R refers to the reference fluorophore *i.e.* compound carbazole solution in THF and subscript S refers to the sample under investigation. In order to minimize re-absorption effects, absorbance was kept below 0.15 at the excitation wavelength of 442 nm.

3.4. Conclusions

We have reported two new regioisomeric star-shaped tris(*N*-salicylideneaniline)s, whose arms differ from each other with respect to the substitution at the 3,5-positions of the central 1,2,4-oxadiazole moieties. The effect of this unsymmetrical substitution led to a change in the electron density distribution, which exhibited an effect on the type of the columnar self-assembly. One of these molecules stabilized columnar hexagonal phase, while the other one stabilized columnar rectangular phase. Columnar rectangular phase, which require enhanced intermolecular interactions was observed in the case of star-shaped molecule, where the trialkoxy phenyl group is connected at the 5-position of the heterocycle, whereas columnar hexagonal phase was observed in the case of star-shaped molecule, where the trialkoxy phenyl group is connected at the 3-position of the heterocycle. These compounds showed reduced melting point, clearing point and enhanced mesophase range with respect to the symmetric counterpart (1,3,4-oxadiazole derivative) reported earlier. All the molecules exhibited green light emission in solution, with a comparable quantum yield. 1,2,4-oxadiazole derivatives exhibited much red-shifted emission in comparison to 1,3,4-oxadiazole derivatives in annealed thin film state. This study provides an interesting view on how a simple structural variation, tunes the self-assembly behavior of liquid crystalline molecules. Considering the ability of these molecules to stabilize luminescent Col phases, these molecules have a bright potential for the application in OLEDs.

3.5. Experimental Section

In this section the detailed synthetic procedures and the molecular structural characterization data have been presented for the intermediates and the molecular structural characterization data have been presented for the intermediates and target compounds mentioned in the scheme.

Procedure for the synthesis of 3,4,5-trimethoxybenzonitrile **(1)**

3,4,5-trimethoxybenzaldehyde (10.2 mmol, 1 equiv.) was added to a solution of hydroxylamine hydrochloride (18.9 mmol, 1.85 equiv.) in DMSO (10.2 mL), and the resulting reaction solution was stirred and heated for 3 h at 100 ^{o}C. After cooling to room temperature, water was added to the reaction mixture, which was then extracted with $CHCl_3$ (5×20 mL). The

combined chloroform layers were washed with water (4×20 mL) and dried with Na_2SO_4. Removal of chloroform by rotatory evaporation and high vacuum yielded the desired product which was then recrystallised with ethanol to get the pure product.

R_f = 0.5 (30% EtOAc-hexane); mp: 92-93 ^oC; yield: 85%; IR (KBr pellet): ν_{max} in cm^{-1} 3098.12, 2927, 2845, 2225, 1585, 1506, 1338, 998, 854, 778; ^1H NMR ($CDCl_3$, 600 MHz): δ 6.85 (s, 2H, Ar), 3.89(s, 3H, 1×OCH_3), 3.87(s, 6H, 2×OCH_3) ;^{13}C NMR ($CDCl_3$, 150 MHz): 153.74, 142.50, 119.16, 109.61, 106.89, 61.24, 56.57; HRMS (ESI+) exact mass calculated for $C_{10}H_{11}NO_3$ (M+1): 194.0812, Found: 194.0826.

Procedure for the synthesis of (*Z*)-*N*'-hydroxy-3,4,5-trimethoxybenzimidamide **(2)**

To a stirred solution of 3,4,5-trimethoxybenzonitrile (5.5 mmol, 1 equiv.) in ethanol (6 mL) was added hydroxylamine hydrochloride (12.1 mmol, 2.2 equiv.) and then Et_3N (12.7 mmol, 2.3 equiv.). The solution was stirred under reflux for 18 h. Ethanol was removed under reduced pressure and then diluted with water and the aqueous layer extracted 4 times with DCM. The combined organic phases were dried over Na_2SO_4 and concentrated under reduced pressure. The crude product was purified by recrystallization with ethanol to get the pure product as white solid.

R_f = 0.5 (pure EtOAc); mp: 155-157 ^oC; yield: 90%; IR (KBr pellet): ν_{max} in cm^{-1} 3464, 3333, 3004, 2936, 2834, 1661, 1586, 1304, 854; ^1H NMR ($CDCl_3$, 600 MHz): δ 6.85 (s, 2H, Ar), 4.87(s, 2H, NH_2), 3.88(s, 6H, 2×OCH_3), 3.86(s, 2H, 1×OCH_3); ^{13}C NMR ($CDCl_3$, 150 MHz): 153.53, 153.13, 139.73, 128.23, 103.48, 61.11, 56.43; HRMS (ESI+) exact mass calculated for $C_{10}H_{14}N_2O_4$ (M+1): 227.1026, Found: 227.1033.

Procedure for the synthesis of 5-(4-nitrophenyl)-3-(3,4,5-trimethoxyphenyl)-1,2,4-oxadiazole **(3)**

A mixture of Compound **2** (4.9 mmol, 1 equiv.) and dry pyridine (5 mL) was stirred under Ar-atmosphere at 0 ^oC. To this, solution of 4-nitrobenzoyl chloride (5.3 mmol, 1.1 equiv.) in dry THF was added dropwise. The reaction mixture was refluxed for 12 h and then poured into cold water. The whole mass (a mixture of solid and water) was extracted with $CHCl_3$ (4×30 mL). The combined extract was washed with water, brine and dried over Na_2SO_4 and concentrated under reduced pressure. The crude product was purified by column chromatography on neutral alumina. Elution with 50% DCM-Hexane system to DCM yielded the desired product. Recrystallisation with ethylacetate gives the pure product.

R_f = 0.32 (80% EtOAc-hexane); mp: 208-209 ^oC; yield: 80%; IR (KBr pellet): ν_{max} in cm^{-1} 3121, 2924, 2852, 1596, 1569, 1361, 851, 770, 705, 672; ^1H NMR ($CDCl_3$, 600 MHz): δ 8.42 (s, 4H, Ar), 7.41(s, 2H, Ar), 3.98(s, 6H, 2×OCH_3), 3.93(s, 2H, 1×OCH_3) ;^{13}C NMR ($CDCl_3$, 150 MHz): 173.80, 169.44, 153.86, 150.42, 141.13, 129.69, 129.45, 124.55, 121.64, 104.93, 61.20, 56.55; HRMS (ESI+) exact mass calculated for $C_{17}H_{15}N_3O_6$ (M+1): 358.1034, Found: 358.1047.

Procedure for the synthesis of 5-(5-(4-nitrophenyl)-1,2,4-oxadiazol-3-yl)benzene-1,2,3-triol **(4)**

A solution of Compound **3** (3.6 mmol, 1 equiv) in dry DCM (20 mL) was cooled to -80 ^oC. Then BBr_3 (13.03 mmol, 3.6 equiv.) was added slowly to the cooled solution. The reaction mixture was then allowed to warm to room temperature and stirred for additional 12 h. Subsequently, the

mixture was poured into the ice-water dropwise and precipitate was formed. The precipitate was filtered and washed with water. The crude product was recrystallized from ethanol to get the pure product.

R_f = 0.2 (20% CH_3OH-$CHCl_3$); mp: 256-258 ^oC; yield: 87%; IR (KBr pellet): ν_{max} in cm^{-1} 3633, 3379, 3109, 2924, 2853, 1620, 1506, 1341, 1217, 1109, 858, 769; ^1H NMR (DMSO-d^6, 600 MHz): δ 9.38 (brs, 2H, 2×OH), 8.85(brs, 1H, 1×OH), 8.46(d, 2H, *J* = 6Hz, Ar), 8.39(d, 2H, *J* = 12Hz, Ar), 7.08(s, 2H, Ar) ;^{13}C NMR (DMSO-d^6, 150 MHz): 173.16, 168.74, 149.85, 146.41, 136.88, 129.32, 128.91, 124.60, 115.47, 106.29; HRMS (ESI+) exact mass calculated for $C_{14}H_9N_3O_6$ (M+1): 315.0491, Found: 315.0137.

Procedure for the synthesis of 5-(4-nitrophenyl)-3-(3,4,5-tris(hexadecyloxy)phenyl)-1,2,4-oxadiazole **(5)**

A mixture of compound **4** (1.6 mmol, 1 equiv.), *n*-bromohexadecane (5.23 mmol, 3.3 equiv.), anhyd. K_2CO_3 (10.47 mmol, 6.6 equiv.) and DMF (10mL) was heated at 80 ^oC for 17 h under N_2 atmosphere. Then the reaction mixture poured into ice-water and extracted with EtOAc (3 × 50 mL). The combined organic layer was washed with water, brine and dried over anhyd. Na_2SO_4. Evaporation of the solvent and the purification of crude product over neutral alumina using hexanes followed by 50% CH_2Cl_2-hexane to CH_2Cl_2 as eluents furnished the desired product, which was further purified by recrystallisation with ethylacetate.

R_f = 0.7 (80% CH_2Cl_2-hexane); mp: 86-88 ^oC; yield: 64%; IR (KBr pellet): ν_{max} in cm^{-1} 2919, 2850, 1589, 1565, 1468, 1356, 1231, 1111, 743; ^1H NMR ($CDCl_3$, 600 MHz): δ 8.42 (s, 4H, Ar), 7.37 (s, 2H, Ar), 4.08 (t, 4H, *J* = 6Hz, 2×OCH_2), 4.04 (t, 2H, *J* = 6Hz, 1×OCH_2), 1.25-1.85 (m, 84H, 42×CH_2), 0.86-0.89 (m, 9H, 3×CH_3);^{13}C NMR ($CDCl_3$, 150 MHz): 173.66, 169.65, 160.55, 153.78, 150.40, 141.30, 129.46, 124.55, 121.11, 106.12, 73.80, 69.50, 32.16, 30.58, 29.98, 29.95, 29.89, 29.83, 29.65, 29.59, 26.34, 22.92, 14.34; HRMS (ESI+) exact mass calculated for $C_{62}H_{105}N_3O_6$ (M^+): 987.8003, Found: 987.7330.

Procedure for the synthesis of 4-(3-(3,4,5-tris(hexadecyloxy)phenyl)-1,2,4-oxadiazol-5-yl)aniline **(6)**

To a solution of nitro compound **5** (0.47 mmol, 1 equiv.) in dry THF was added 10% Pd-C (0.046g) (10% wt. of compound **5**) and stirred under hydrogen atmosphere (balloon) for 12 h (monitored by TLC). The reaction mixture was then filtered through a celite bed. Evaporation of the solvent under reduced pressure to get the crude product. The crude product was further purified by neutral alumina using hexanes followed by 10% ethylacetate-hexane as eluents furnished the desired pure amine.

R_f = 0.3 (20% EtOAc-hexane); mp: 85-87 ^oC; yield: 70%; IR (KBr pellet): ν_{max} in cm^{-1} 3327 2919, 2849, 1620, 1501, 1466, 1363, 1237, 1127, 866, 721; ^1H NMR ($CDCl_3$, 600 MHz): δ 8.01 (d, 2H, *J* = 6Hz, Ar), 7.35 (s, 2H, Ar), 6.75 (d, 2H, *J* = 12Hz, Ar), 4.15 (brs, 2H, NH_2), 4.07 (t, 4H. J = 6Hz, 2×OCH_2), 4.02 (t, 2H, *J* = 6Hz, 1×OCH_2) , 1.14-1.86 (m, 84H, 42×CH_2), 0.86-0.89 (m, 9H, , 3×CH_3); ^{13}C NMR ($CDCl_3$, 150 MHz): 176.03, 168.86, 153.60, 150.79, 140.67, 130.28, 122.23, 114.69, 106.01, 100.20, 73.73, 69.40, 32.16, 30.57, 29.98, 29.94, 29.89, 29.84,

29.65, 29.60, 26.33, 22.92, 14.34; HRMS (ESI+) exact mass calculated for $C_{62}H_{107}N_3O_4$ (M+H): 958.8334, Found: 958.9782.

Procedure for the synthesis of TSAN **(1b)**

A mixture of triformylphloroglucinol (0.09 mmol, 1 equiv.) and aniline **6** (0.31 mmol, 3.3 equiv.) in absolute ethanol (20 mL) was heated for reflux under inert atmosphere for 6 h with vigorous stirring. The dull yellow solid separated upon cooling the reaction mixture was collected by filtration, repeatedly washed with ethanol and air-dried. The crude product was purified by repeated recrystallizations with ethylacetate.

R_f = 0.6 (80% CH_3OH-$CHCl_3$); yield: 67%; IR (KBr pellet): ν_{max} in cm^{-1} 2951, 2919, 2851, 1631, 1603, 1509, 1468, 1434, 1289, 1179, 1120, 1016, 846, 761; ^1H NMR ($CDCl_3$, 600 MHz): δ 13.39-13.43 (m, =CNH), 13.27 (s, =CNH), 12.95 (s, =CNH), 8.62-8.75 (m, 3H, =CHN), 8.14-8.18 (m, 6H, Ar), 7.21-7.38 (m, 12H, Ar), 4.01 (broad s, 18H, 9×OCH_2), 1.26-1.83 (m, 252H, 126×CH_2), 0.87-0.89 (m, 27H, 9×CH_3). MALDI-TOF exact mass calculated for $C_{195}H_{323}N_9O_{15}$ (M+2): 3031.4789, Found: 3031.4320.

Procedure for the synthesis of 4-nitrobenzonitrile **(9)**

4-nitrobenzaldehyde (13.23 mmol, 1 equiv.) was added to a solution of hydroxylamine hydrochloride (24.48 mmol, 1.85 equiv.) in DMSO (13 mL), and the resulting reaction solution was stirred and heated for 3 h in an oil bath maintained at 100 ^oC. After cooling to room temperature, water (20 mL) was added to the reaction mixture, which was then extracted with $CHCl_3$ (5×20 mL). The combined organic layers were washed with water and dried over sodium sulphate. The organic layer was concentrated to get the crude product which was recrystallized with ethanol to get the pure product.

R_f = 0.7 (50% EtOAc-hexane); mp:147-149 ^oC; yield: 95%; IR (KBr pellet): ν_{max} in cm^{-1} 2232, 1646, 859, 748; ^1H NMR ($CDCl_3$, 600 MHz): δ 8.36 (d, 2H, *J* = 12Hz, Ar), 7.89(d, 2H, *J* = 12Hz, Ar); ^{13}C NMR ($CDCl_3$, 150 MHz): 150.18, 133.67, 124.47, 118.48, 116.99; HRMS (ESI+) exact mass calculated for $C_{10}H_{11}NO_3$ (M+1): 194.0812, Found: 194.0826.

Procedure for the synthesis of (*Z*)-*N*'-hydroxy-4-nitrobenzimidamide **(10)**

To a stirred solution of 4-nitrobenzonitrile (6.75 mmol, 1 equiv.) in ethanol (10 mL) was added hydroxylamine hydrochloride (14.85 mmol, 2.2 equiv.) and then Et_3N (15.53 mmol, 2.3 equiv.). The solution was stirred under reflux for 18 h. Ethanol was removed under reduced pressure and then diluted with water and the aqueous layer extracted 4 times with DCM. The combined organic phases were dried over Na_2SO_4 and concentrated under reduced pressure. The crude product was further purified by recrystallization with ethanol to get the pure product as yellow solid.

R_f = 0.5 (50% EtOAc-hexane); mp: 155-157 ^oC; yield: 90%; IR (KBr pellet): ν_{max} in cm^{-1} 3463, 3359, 2924, 2853, 2596, 2508, 2459, 1659, 1600, 1340, 862; ^1H NMR (CD_3OD, 400 MHz): δ 8.25 (d, 2H, *J* = 12Hz, Ar), 7.88 (d, 2H, *J* = 12Hz, Ar) ;^{13}C NMR ($CDCl_3$, 150 MHz): 153.98,

150.59, 141.30, 128.98, 125.33; HRMS (ESI+) exact mass calculated for $C_{10}H_{14}N_2O_4$ (M+1): 227.1026, Found: 227.1033.

Procedure for the synthesis of 3-(4-nitrophenyl)-5-(3,4,5-trimethoxyphenyl)-1,2,4-oxadiazole **(11)**

A mixture of Compound **10** (5.5 mmol, 1 equiv.) and dry pyridine (5 mL) was stirred under Ar-atmosphere at 0 ^oC. To this, solution of 3,4,5-trimethoxy benzoyl chloride (6.07 mmol, 1.1 equiv.) in dry THF was added dropwise. The reaction mixture was refluxed for 12h and then poured into cold water. The whole mass (a mixture of solid and water) was extracted with $CHCl_3$ (4 × 40 mL). The combined extract was washed with water, brine and dried over Na_2SO_4 and concentrated under reduced pressure. The crude product was purified by column chromatography on neutral alumina. Elution with 50% DCM-Hexane system to DCM yielded the desired product. Recrystallisation with ethylacetate gives the pure product.

R_f = 0.34 (80% EtOAc-hexane); mp: 205-207 ^oC; yield: 61%; IR (KBr pellet): ν_{max} in cm^{-1} 2924, 2852, 1569, 1361, 851, 770, 705, 672; ^1H NMR ($CDCl_3$, 600 MHz): δ 8.37 (s, 4H, Ar), 7.45(s, 2H, Ar), 3.99(s, 6H, 2×OCH_3), 3.96(s, 2H, 1×OCH_3) ;^{13}C NMR ($CDCl_3$, 150 MHz): 176.52, 167.64, 153.92, 149.68, 142.60, 133.07, 128.73, 124.30, 118.88, 105.66, 61.31, 56.65; HRMS (ESI+) exact mass calculated for $C_{17}H_{15}N_3O_6$ (M+1): 358.1034, Found: 358.1047.

Procedure for the synthesis of 5-(3-(4-nitrophenyl)-1,2,4-oxadiazol-5-yl)benzene-1,2,3-triol **(12)**

A solution of Compound **11** (2.8 mmol, 1 equiv) in dry DCM (40 mL) was cooled to -80 ^oC. Then, BBr_3 (10.08 mmol, 3.6 equiv.) was added slowly to the cooled solution. The reaction mixture was then allowed to warm to room temperature and stirred for additional 12 h. Subsequently, the mixture was poured into the ice cold water dropwise and precipitate was formed. The precipitate was filtered and washed with water. The crude product was recrystallized from ethanol to get the pure product.

R_f = 0.21 (20% CH_3OH-$CHCl_3$); mp: >300 ^oC; yield: 57%; IR (KBr pellet): ν_{max} in cm^{-1} 3637, 3379, 2952, 2924, 2853, 1619, 1506, 1341, 1217, 1109, 1033, 858, 769; ^1H NMR (CD_3OD, 600 MHz): 8.34(d, 2H, *J* = 12Hz, Ar), 8.26(d, 2H, *J* = 12Hz, Ar), 7.15(s, 2H, Ar); ^{13}C NMR (CD_3OD, 150 MHz): 179.12, 169.23, 151.61, 148.22, 140.88, 135.05, 130.20, 125.89, 115.91, 109.39; HRMS (ESI+) exact mass calculated for $C_{14}H_9N_3O_6$ (M+1): 315.0491, Found: 315.0137.

Procedure for the synthesis of 3-(4-nitrophenyl)-5-(3,4,5-tris(hexadecyloxy)phenyl)-1,2,4-oxadiazole **(13)**

A mixture of compound **12** (1.22 mmol, 1 equiv.), *n*-bromohexadecane (4.01 mmol, 3.3 equiv.), anhyd. K_2CO_3 (8.02 mmol, 6.6 equiv.) and DMF (5 mL) was heated at 80 ^oC for 17 h under N_2 atmosphere. Then the reaction moisture poured on to ice-water and extracted with EtOAc (4×50 mL). The combined organic layer was washed with water, brine and dried over anhyd. Na_2SO_4. Evaporation of the solvent and the purification of residue over neutral alumina using hexane followed by 50% CH_2Cl_2-hexane to CH_2Cl_2 as eluents furnished the desired product, which was further purified by recrystallization with ethylacetate.

R_f = 0.69 (80% CH_2Cl_2-hexane); mp: 83-85 ^oC; yield: 42%; IR (KBr pellet): ν_{max} in cm^{-1} 2920, 2851, 1640, 1560, 1526, 1467, 1358, 1243, 1128, 746 ; ^1H NMR ($CDCl_3$, 600 MHz): δ 8.37 (s, 4H, Ar), 7.40 (s, 2H, Ar), 4.06-4.08 (m, 6H, 3×OCH_2), 1.21-1.88 (m, 84H, 42×CH_2), 0.86-0.89 (m, 9H, 3×CH_3); ^{13}C NMR ($CDCl_3$, 150 MHz): 176.80, 167.59, 153.84, 149.67, 142.84, 133.23, 128.73, 124.28, 118.43, 106.81, 73.92, 69.62, 32.16, 30.58, 29.94, 29.90, 29.80, 29.63, 29.60, 29.52, 26.32, 22.29, 22.92, 14.34; HRMS (ESI+) exact mass calculated for $C_{62}H_{105}N_3O_6$ (M+1): 988.8076, Found: 988.8176.

Procedure for the synthesis of 4-(5-(3,4,5-tris(hexadecyloxy)phenyl)-1,2,4-oxadiazol-3-yl)aniline **(14)**

To a solution of nitro compound **13** (0.3 mmol, 1 equiv.) in dry THF was added 10% Pd-C (0.030g) (10% wt. of compound **13**) and stirred under hydrogen atmosphere (balloon) for 12 h (monitored by TLC). The reaction mixture was then filtered through a celite bed. Evaporation of the solvent under reduced pressure to get the crude product. The crude product was further purified by neutral alumina using hexanes followed by ethylacetate-hexane (10%) as eluents furnished the desired pure amine.

R_f = 0.25 (20% EtOAc-hexane); mp: 78-79 ^oC; yield: 41%; IR (KBr pellet): ν_{max} in cm^{-1} 3327, 2919, 2849, 1620, 1501, 1466, 1363, 1236, 1189, 1014, 866, 762, 721; ^1H NMR ($CDCl_3$, 400 MHz): δ 7.87 (d, 2H, *J* = 6Hz, Ar), 7.62 (s, 2H, Ar), 6.72 (d, 2H, *J* = 12Hz, Ar), 4.10 (brs, 2H, NH_2), 4.01-4.09 (m, 6H, 3×OCH_2), 1.19-1.84 (m, 84H, 42×CH_2), 0.86-0.89 (m, 9H, , 3×CH_3); ^{13}C NMR ($CDCl_3$, 100 MHz): 179.83, 166.30, 152.73, 150.79, 141.77, 133.30, 129.45, 124.25, 114.52, 108.30, 73.64, 69.28, 32.15, 30.55, 29.98, 29.95, 29.90, 29.84, 29.62, 29.60, 26.37, 26.31, 22.92, 14.35; HRMS (ESI+) exact mass calculated for $C_{62}H_{107}N_3O_4$ (M+3): 960.8485, Found: 960.8528.

Procedure for the synthesis of TSAN **(1c)**

A mixture of triformylphloroglucinol (0.03 mmol, 1 equiv.) and aniline **14** (0.11 mmol, 3.3 equiv.) in absolute ethanol (20 mL) was heated for reflux under inert atmosphere for 6 h with vigorous stirring. The dull yellow solid separated upon cooling the reaction mixture was collected by filtration, repeatedly washed with ethanol and air dried. The crude product was purified by repeated recrystallizations with ethylacetate.

R_f = 0.61 (80% CH_3OH-$CHCl_3$); yield: 67%; IR (KBr pellet): ν_{max} in cm^{-1}; 2949, 2915, 2855, 1630, 1602, 1506, 1462, 1435, 1289, 1177, 1121, 1019, 848, 762; ^1H NMR ($CDCl_3$, 600 MHz): δ 13.40 (bs, =CNH), 13.32 (bs, =CNH), 12.98(bs, =CNH), 8.70 (m, 3H, =CHN), 8.04 (bs, 6H, Ar), 7.60 (s, 6H, Ar), 7.26-7.34 (m, 6H, Ar), 3.99-4.08 (m, 18H, 9 × OCH_2), 1.24-1.85(m, 352H, 126×CH_2), 0.85 – 0.89 (m, 27H, 9×CH_3); MALDI-TOF exact mass calculated for $C_{195}H_{322}N_9O_{15}$ (M+1): 3030.4705, Found: 3030.4780.

3.6. References

1. A. C. Grimsdale, K. L. Chan, R. E. Martin, P. G. Jokisz, A. B. Holmes, *Chem. Rev*. 2009, **109**, 897−1091.
2. (a) M. Pope, C. Swenberg, *Electronic Processes in Organic Crystals and Polymers*, 2nd ed.; Oxford University Press: London, 1999. (b) H. Klauk, *Organic Electronics: Materials, Manufacturing and Applications*; Wiley-VCH Verlag GmbH: Weinheim, Germany, 2006.
3. S. Laschat, A. Baro, N. Steinke, F. Giesselmann, C. Hagele, G. Scalia, R. Judele, E. Kapatsina, S. Sauer, A. Schreivogel, M. Tosoni, *Angew. Chem. Int. Ed*. 2007, **46**, 4832−4837.
4. (a) Q. Li, *Nanoscience with Liquid Crystals: From Self-Organized Nanostructures to Applications*, ed. Springer, Berlin, 2014; (b) Q. Li, *Self-organized Organic Semiconductors: From Materials to Device Application*, ed. John Wiley & Sons, 2011.
5. S. Chandrasekhar, B. K. Sadashiva, K. A. Suresh, *Pramana* 1977, **9**, 471−480.
6. J. W. Goodby, P. J. Collings, T. Kato, C. Tschierske, H. Gleeson and P. Raynes *Handbook of Liquid Crystals: Fundamentals*, ed., Wiley-VCH, Weinheim, Germany, 2014, vol. 1.
7. (a) L. S. Mende, A. Fechtenkotter, K. Mullen, E. Moons, R. H. Friend and J. D. MacKenzie, *Science*, 2001, **293**, 1119–1122; (b) H. C. Hesse, J. Weickert, M. Al-Hussein, L. Do¨ssel, X. Feng, K. Mullen and L. S. Mende, *Sol. Energy Mater. Sol. Cells*, 2010, **94**, 560–567; (c) Q. Sun, L. Dai, X. Zhou, L. Li and Q. Li, *Appl. Phys. Lett.*, 2007, **91**, 253505.
8. (a) A. Bacher, I. Bleyl, C. H. Erdelen, D. Haarer, W. Paulus and H. W. Schmidt, *Adv. Mater*., 1997, **9**, 1031–1035; (b) A. Bacher, C. H. Erdelen, W. Paulus, H. Ringsdorf, H. W. Schmidt and P. Schuhmacher, *Macromolecules*, 1999, **32**, 4551–4557; (c) I. Seguy, P. Destruel and H. Bock, *Synth. Met*., 2000, **111**, 15–18; (d) T. Hassheider, S. A. Benning, H. S. Kitzerow, M. F. Achard and H. Bock, *Angew. Chem. Int. Ed*., 2001, **40**, 2060–2063; (e) S. Alibert-Fouet, S. Dardel, H. Bock, M. Oukachmih, S. Archambeau, I. Seguy, P. Jolinat and P. Destruel, *ChemPhysChem*, 2003, **4**, 983–985; (f) M. O'Neill and S. M. Kelly, *Adv. Mater.*, 2011, **23**, 566–584; (g) J. Eccher, G. C. Faria, H. Bock, H. von Seggern and I. H. Bechtold, *ACS Appl. Mater. Interfaces*, 2013, **5**, 11935–11943.
9. (a) A. M. van de Craats, N. Stutzmann, O. Bunk, M. M. Nielsen, M. Watson, K. Mullen, H. D. Chanzy, H. Sirringhaus and R. H. Friend, *Adv. Mater*., 2003, **15**, 495–499; (b) S. Cherian, C. Donley, D. Mathine, L. LaRussa, W. Xia and N. Armstrong, *J. Appl. Phys*., 2004, **96**, 5638–5643; (c) B. A. Jones, M. J. Ahrens, M.-H. Yoon, A. Facchetti, T. J. Marks and M. R. Wasielewski, *Angew. Chem., Int. Ed.*, 2004, **43**, 6363–6366; (d) I. O. Shklyarevskiy, P. Jonkheijm, N. Stutzmann, D. Wasserberg, H. J. Wondergem, P. C. M. Christianen, A. P. H. J. Schenning, D. M. de Leeuw, Z. Tomovic, J. Wu, K. Mullen and J. C. Maan, *J. Am. Chem. Soc*., 2005, **127**, 16233–16237; (e) W. Pisula, A. Menon, M. Stepputat, I. Lieberwirth, U. Kolb, A. Tracz, H. Sirringhaus, T. Pakula and K. Mullen, *Adv. Mater.*, 2005, **17**, 684–689; (f) S. Xiao, M. Myers, Q. Miao, S. Sanaur, K. Pang, M. L. Steigerwald and C. Nuckolls, *Angew. Chem. Int. Ed*., 2005, **44**, 7390–7394; (g) J.-Y. Cho, B. Domercq, S. C. Jones, J. Yu, X. Zhang, Z. An, M. Bishop, S. Barlow, S. R. Marder and B. Kippelen, *J. Mater. Chem*., 2007, **17**, 2642–2647; (h) Y. Shimizu, K. Oikawa, K. I. Nakayama and D. Guillon, J. Mater. Chem., 2007, **17**, 4223–4229; (i) H. N. Tsao, H. J. Rader, W. Pisula, A. Rouhanipour and K. Mullen, *Phys. Status Solidi A*, 2008,

205, 421–429; (j) J. P. Bramble, D. J. Tate, D. J. Revill, K. H. Sheikh, J. R. Henderson, F. Liu, X. Zeng, G. Ungar, R. J. Bushby and S. D. Evans, *Adv. Funct. Mater*., 2010, **20**, 914–920.

10. M. Lehmann, *Chem. Eur. J*., 2009, **15**, 3638–3651.
11. (a) J. H. Chong, M. Sauer, B. O. Patrick, M. J. MacLachlan, *Org. Lett*. 2003, **5**, 3823−3826. (b) M. Sauer, C. Yeung, J. H. Chong, B. O. Patrick, M. J. MacLachlan, *J. Org. Chem*. 2006, **71**, 775−788.
12. (a) J. A. Riddle, J. C. Bollinger, D. Lee, *Angew. Chem. Int. Ed*. 2005, **44**, 6689−6693. (b) J. A. Riddle, S. P. Lathrop, J. C. Bollinger, D. Lee, *J. Am. Chem. Soc.* 2006, **128**, 10986−10987. (c) X. Jiang, J. C. Bollinger, D. Lee, *J. Am. Chem. Soc.* 2006, **128**, 11732−11733. (d) M. Vieweger, X. Jiang, Y.-K. Lim, J. Jo, D. Lee and B. Dragnea, *J Phys Chem A*, 2011, **115**, 13298–13308. (e) X. Jiang, Y.-K. Lim, B. J. Zhang, E. A. Opsitnick, M.-H. Baik and D. Lee, *J. Am. Chem. Soc.*, 2008, **130**, 16812–16822. (f) Y.-K. Lim, S. Wallace, J. C. Bollinger, X. Chen and D. Lee, *Inorg Chem*, 2007, **46**, 1694–1703. (g) J. A. Riddle, X. Jiang, J. Huffman and D. Lee, *Angew. Chem. Int. Ed. Engl.*, 2007, **46**, 7019–7022.
13. X. Jiang, M. C. Vieweger, J. C. Bollinger, B. Dragnea and D. Lee, *Org. Lett.*, 2007, **9**, 3579–3582.
14. (a) S. Kandambeth, A. Mallick, B. Lukose, M. V. Mane, T. Heine and R. Banerjee, *J. Am. Chem. Soc.*, 2012, **134**, 19524–19527. (b) S. Chandra, S. Kandambeth, B. P. Biswal, B. Lukose, S. M. Kunjir, M. Chaudhary, R. Babarao, T. Heineand, R. Banerjee, *J. Am. Chem. Soc.*, 2013, ***135***, 17853–17861. (c) C. R. DeBlase, K. E. Silberstein, T.-T. Truong, H. D. Abruña and W. R. Dichtel, *J. Am. Chem. Soc.*, 2013, **135**, 16821–16824. (d) S. Chandra, T. Kundu, S. Kandambeth, R. Babarao, Y. Marathe, S. M. Kunjir and R. Banerjee, *J. Am. Chem. Soc.*, 2014, **136**, 6570–6573.
15. (a) P. Suresh, S. Srimurugan, B. Babu and H. N. Pati, *Tetrahedron-Asymmetry*, 2007, **18**, 2820–2827. (b) C. Mukherjee, A. Stammler, H. Bögge and T. Glaser, *Inorg. Chem*, 2009, **48**, 9476–9484.
16. (a) C. V. Yelamaggad, A. S. Achalkumar, D. S. S. Rao, S. K. Prasad, *J. Am. Chem. Soc*., 2004, **126**, 6506-6507; (b) C. V. Yelamaggad, A. S. Achalkumar, *Tetrahedron Lett*. 2006, **47**, 7071-7075; (c) C. V. Yelamaggad, A. S. Achalkumar, D. S. S. Rao, S. K. Prasad, *J. Mater. Chem.* 2007, **17**, 4521-4529; (d) C. V. Yelamaggad, A. S. Achalkumar, D. S. S. Rao, S. K. Prasad, *J. Org. Chem.*, 2007, **72**, 8308-8318; (e) C. V. Yelamaggad, A. S. Achalkumar, D. S. S. Rao, S. K. Prasad, *J. Org. Chem*. 2009, **74**, 3168-3171; (f) C. V. Yelamaggad, A. S. Achalkumar, *Tetrahedron Lett*. 2012, **53**, 7108-7112; (g) A. S. Achalkumar, U. S. Hiremath, D. S. S. Rao, S. K. Prasad, C. V. Yelamaggad, *J. Org. Chem.* 2013, **78**, 527-544. (h) A. S. Achalkumar, B. N. Veerabhadraswamy, U. S. Hiremath, D. S. S. Rao, S. K. Prasad, C. V. Yelamaggad, *Dyes and Pigments*, 2016, **132**, 291-305. (i) S. K. Pathak, S. Nath, J. De, S. K. Pal, A. S. Achalkumar, *New J. Chem.* 2017, **41**, 4680 – 4688.
17. (a) V. V. Titov and A. I. Pavlyuchenko, *Chem. Heterocycl. Compd*., 1980, **16**, 1–13; (b) M. P. Aldred, P. Vlachos, D. Dong, S. P. Kitney, W. C. Tsoi, M. O. Neill and S. M. Kelly, *Liq. Cryst*., 2005, **32**, 951–965; (c) A. Seed, *Chem. Soc. Rev.*, 2007, **36**, 2046–2069; (d) B. Roy, N. De and K. C. Majumdar, *Chem. – Eur. J*., 2012, **18**, 14560–14588; (e) J. Han, *J. Mater. Chem. C*, 2013, **1**, 7779–7797.

18. (a) C. S. Wang, G. Y. Jung, Y. L. Hua, C. Pearson, M. R. Bryce, M. C. Petty, A. S. Batsanov, A. E. Goeta and J. A. K. Howard, *Chem. Mater*., 2001, **13**, 1167–1173; (b) A. P. Kulkarni, C. J. Tonzola, A. Babel and S. A. Jenekhe, *Chem. Mater*., 2004, **16**, 4556–4573.
19. (a) G. S. Shanker, M. Nagaraj, A. Kocot, J. K. Vij, M. Prehmand, C. Tschierske, *Adv. Funct. Mater*., 2012, **22**, 1671; (b) G. S. Shanker, M. Prehm, M. Nagaraj, J. K. Vij, M. Weyland, A. Eremin and C. Tschierske, *ChemPhysChem*, 2014, **15**, 1323.
20. (a) H. Gallardo, M. Ferreira, A. A. Vieira, E. Westphal, F. Molin, J. Eccher and I. H. Bechtold, *Tetrahedron*, 2011, **67**, 9491; (b) T. E. Frizon, D. S. Rampon, H. Gallardo, A. A. Merlo, P. H. Schneider, O. E. D. Rodrigues and A. L. Braga, *Liq. Cryst.*, 2012, **39**, 769.
21. H. Gallardo, G. Conte, P. A. Tuzimoto, B. Behramand, F. Molin, J. Eccher and I. H. Bechtold, *Liq. Cryst.*, 2012, **39**, 1099.
22. (a) S. V. Subrahmanyam, P. V. Chalapathi, S. Mahabaleswara, M. Srinivasulu and D. M. Potukuchi, *Liq. Cryst*., 2014, **41**, 1130; (b) H. Gallardo, R. Cristiano, A. A. Vieira, R. A. W. N. Filho, R. M. Srivastav and I. H. Bechtold, *Liq. Cryst.*, 2008, **35**, 857; (c) M. Parra, P. Hidalgo, E. Carrasco, J. Barber´a and L. Silvino, *Liq. Cryst.*, 2006, **33**, 875.
23. (a) M. Parra, P. Hidalgo and J. Alderete, *Liq. Cryst.*, 2005, **32**,449; (b) M.A.Parra, P.Hidalgo, J. N. Barber´a and J. Alderete, *Liq. Cryst.*, 2005, **32**, 573.
24. (a) M. L. Parra, P. I. Hidalgo and E. Y. Elgueta, *Liq. Cryst.*, 2008, **35**, 823; (b) M. L. Parra, P. I. Hidalgo, E. A. Soto- Bustamante, J. Barber´a, E. Y. Elgueta and V. H. Trujillo- Rojo, *Liq. Cryst.*, 2008, **35**, 1251.
25. (a) S. K. Pathak, B. Pradhan, R. K. Gupta, M. Gupta, S. K. Pal and A. S. Achalkumar, *J. Mater. Chem. C*, 2016, **4**, 6546—6561; (b) S. K. Pathak, M. Gupta, S. K. Pal, and A. S. Achalkumar, *Chemistry Select*, 2016, **1**, 5107 – 5120.
26. (a) Q. Li, L. S. Cui, C. Zhong, X. D. Yuan, S. C. Dong, Z. Q. Jiang and L. S. Liao, *Dyes Pigm.*, 2014, **101**, 142; (b) Q. Li, L. S. Cui, C. Zhong, Z. Q. Jiang and L. S. Liao, *Org. Lett.*, 2014, **16**, 1622.
27. (a) C. Carfagna, A. Roviello, A. Sirigu, *Mol. Cryst. Liq. Cryst.* 1985, **122**, 151; (b) E. F. Gramsbergen, H. J. Hoving, W. H. de Jeu, K. Praefcke, B. Kohne, *Liq. Cryst.* 1986, **1**, 397; (c) H. Metersdorf, H. Ringsdorf, *Liq. Cryst.* 1989, **5**, 1757; (d) H. Zeng, P. J. Carroll, T. M. Swager, *Liq. Cryst.* 1993, **14**, 1421; (e) J. Barbera, R. Gimenez, J. L. Serrano, *Chem. Mater.* 2000, **12**, 481; (f) Artal, M. C.; Toyne, K. J.; Goodby, J. W.; Barbera, J.; Photinos, D. J. *J. Mater. Chem.* 2001, **11**, 2801–2807; (g) S. Ito, M. Ando, A. Nomura, N. Morita, C. Kabuto, H. Mukai, K. Ohta, J. Kawakami, A. Yoshizawa and A. Tajiri, *J. Org. Chem*., 2005, **70**, 3939; (h) L. Alvarez, J. Barbera, L. Puig, P. Romero, J. L. Serrano, T. Sierrra, *J. Mater. Chem.* 2006, **16**, 3768–3773; (i) A. Hayer, V. D. Halleux, A. Kohler, A. El-Garoughy, E. W. Meijer, J. Barbera, J. Tant, J. Levin, M. Lehmann, J. Gierschner, J. Cornil and Y. H. Geerts, *J. Phys. Chem. B*, 2006, **110**, 7653; (j) C. V. Yelamaggad, A. S. Achalkumar, D. S. S. Rao, M. Nobusawa, H. Akutsu, J. Yamada and S. Nakatsuji, *J. Mater. Chem.*, 2008, **18**, 3433; (k) R. K. Gupta, S. K. Pathak, B. Pradhan, M. Gupta, S. K. Pal and A. S. Achalkumar, *ChemPhysChem*, 2016, **17**, 859.

Chapter IV

Oxadiazole / thiadiazole based stars and polycatenars

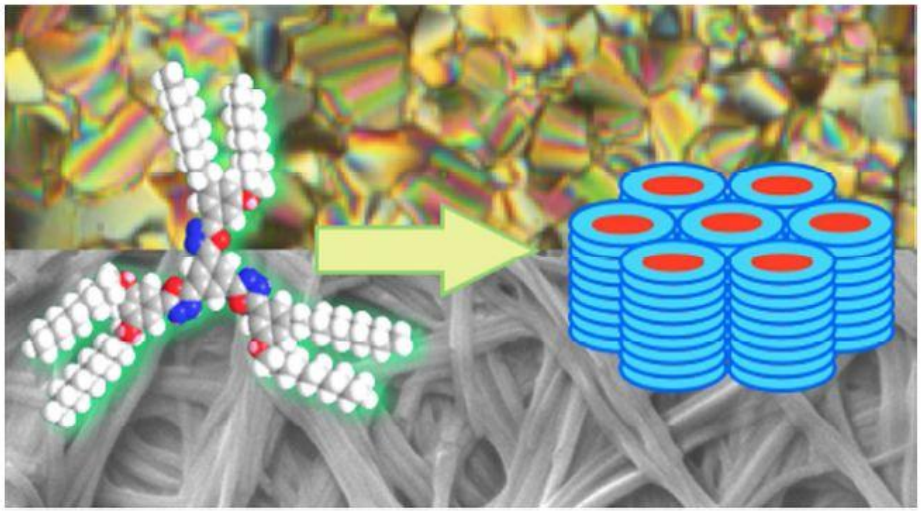

Results have been published in *Molecular system design and engineering*, DOI: 10.1039/C7ME00040E

4.1. Introduction

Highly conjugated aromatic structures are of great interest in the area of organic electronics. The anticipation of novel applications related to solar cells, flexible solid-state display, and low cost printed circuits propelled this ever expanding and exciting area of research.[1] Many efforts to obtain the self-assembled structures of such molecules through different supramolecular approaches are pursued with an ultimate aim of practical applications.[2] Over the years, supramolecular chemistry has grown into a matured field benefitting the biological and material sciences.[3] π-Organogelators are one class of organic molecules with a highly conjugated structure that stabilize the formation of a nonflowing soft material in presence of a solvent. Their structure possesses the inherent properties like fluorescence, charge carrier mobility and electronic conduction.[4] In addition; meticulous molecular engineering enables one to tune and tailor these properties. From the application point of view, how these molecules self-assemble on the substrates during the device fabrication matters a lot. With a careful molecular design one can control the self-assembly of the molecules in their aggregates. Here 'supramolecular chemistry', that is the chemistry beyond the molecule plays a major role, where several weak interactions like π-π interactions, H-bonding and van-der-Waals forces come into picture.[5] Though the solvent is a major component in organogels, the organogels are rather sensitive to the structure of the gelator too. There is a delicate interplay of gelator-gelator and gelator solvent interaction.[6] In other words, it is a tight ropewalk between precipitation and solubility of the gelator in a particular solvent. Since hydrocarbon solvents are mostly used in the case of π-organogelators, the substitution pattern of the flexible alkyl chains on the aromatic core also influences the organogel self-assembly. In literature reports, we often see 3,4,5-trialkoxy and 3,5-dialkoxy substituted benzenes to provide van der Waals interactions.[4]

Liquid crystals (LCs) are another class of supramolecular materials, which have realized many commercial applications, due to their extreme sensitivity to external perturbations like pressure, temperature, electric and magnetic fields.[7] The main difference between organogels and thermotropic LCs is the presence or absence of solvents. The interesting properties of LCs are arising from the macroscopic self-assembly of mesogens, which involve several factors like shape anisotropy, π-π

interactions, H-bonding, van-der-Waals forces and nanophase segregation (segregation of incompatible molecular subunits). The shape anisotropic structures of the mesogens are a combination of hard aromatic part and flexible alkyl chains. During the molecular design these two factors are customized to tune the self-assembly. Especially in the case of columnar (Col) LCs, the central aromatic part helps in providing an ordered one-dimensional (1D) stacking through π-π interactions, while the flexible chains provide the required fluidity in addition to van-der-Waals interactions. Further, their processability by solution coating to get homogeneous, highly ordered thin films is another advantage in comparison to amorphous polymers and organic single crystals.[8] They also provide anisotropic charge carrier mobility along the column direction. Liquid crystalline physical gels – an amalgamation of liquid crystals and gelators are a novel class of stimuli responsive materials. This combination of two components resulted in special electro-optical, photochemical and electronic properties.[6] Usually, the gelators containing hydrogen bonding are used in the preparation of such materials. This is due to the high strength of H-bonding which ranges from 4 to 120 kJ/mol.[9] There are fewer reports on Col LCs that stabilize organogelation mainly through π-π interactions. It is understandable, considering the low strength of π-interactions (0 to 50 kJ/mol). Our recent findings on Col LCs, which stabilize gelation at very low concentration in hydrocarbon solvents (less than 1 wt% or supergelators),[10] motivated us to delve more into the molecular structure-property correlations that govern these intimate interactions in deciding the LC and organogel self-assembly. For this purpose, we decided to synthesize star-shaped molecules and tetracatenars, which are known to stabilize Col phases, when appropriately substituted. These compounds are based on the unsymmetrically substituted 1,3,4-oxadiazole and thiadiazole derivatives.[11] Star-shaped oxadiazole and thiadiazole derivatives with peripheral 3,4-dialkoxy substitutions are already reported to exhibit columnar hexagonal phases.[11a] Thus we have compared the mesomorphic and gelation behavior of these molecules along with the newly synthesized star-shaped molecules, with peripheral 3,5-dialkoxy substitution. Corresponding *p*-substituted and *m*-substituted tetracatenars were also synthesized and investigated for their mesomorphic and gelation behavior in comparison to the star-shaped molecules.

4.2. Results and discussion

4.2a. Synthesis and Characterization

The synthetic route for the preparation of the target molecules is illustrated in scheme 1. Ethyl 3,5-dihydroxybenzoate (**1**) was subjected to *O*-alkylation under Williamson's ether synthesis protocol to get the ethyl 3,5-didecyloxy benzoate (**2**). This ester was converted to the corresponding hydrazide **3** on treatment with hydrazine hydrate in ethanol. Hydrazide **3** was then refluxed with 1,3,5-benzene tricarbonyl trichloride in THF in presence of an organic base yielded tri-*N*-benzoylbenzohydrazides, which was subjected to $POCl_3$ mediated dehydrocyclization to obtain trioxadiazole **4a**. Similar process repeated by treating the hydrazide **3** with 1,4-benzene dicarboxyl chloride and 1,3-benzene dicarboxyl chloride compounds to obtain respective dihydrazides. These compounds were on subjecting to dehydrocyclization with $POCl_3$ yielded the polycatenars **5a** and **6a**.

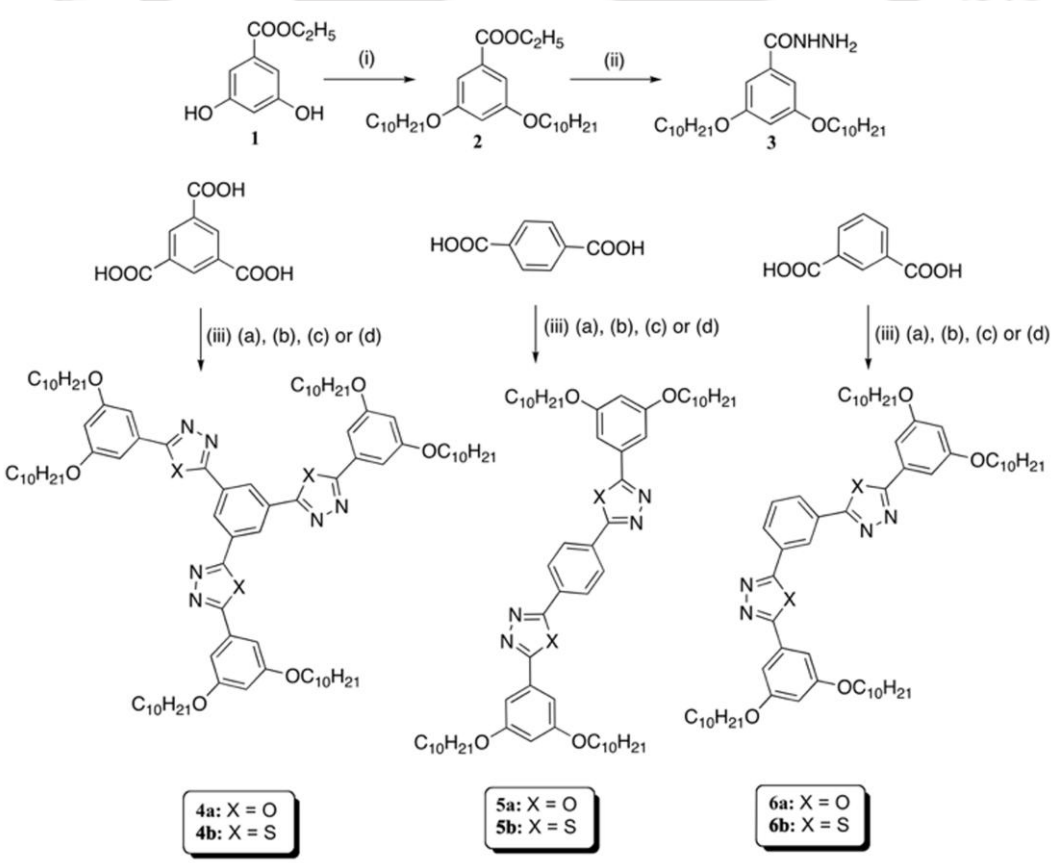

Scheme 4.1. Reagents and Conditions (i) *n*-bromodecane, anhyd. K_2CO_3, DMF, 80 ^oC, 24 h (75 %); (ii) ethanol, $N_2H_4.H_2O$, reflux, 48 h (67 %); (iii) (a) $SOCl_2$, DMF, reflux, 4 h; (b) **3**, THF, TEA, reflux, 12 h; (c) $POCl_3$, 100 ^oC, 24 h (50-60%) for compounds **4a**, **5a** and **6a**; (d) Lawesson's reagent, dry toluene, reflux, 12 h (50-55%) for compounds **4b**, **5b** and **6b**.

Corresponding thiadiazole derivatives (**4b**, **5b** and **6b**) were prepared by refluxing the hydrazides with Lawesson's reagent in anhydrous toluene. The structures of all the intermediates and target molecules were completely characterized through ^{1}H NMR, ^{13}C NMR, IR spectroscopy and ESI-HRMS or MALDI-TOF analysis.

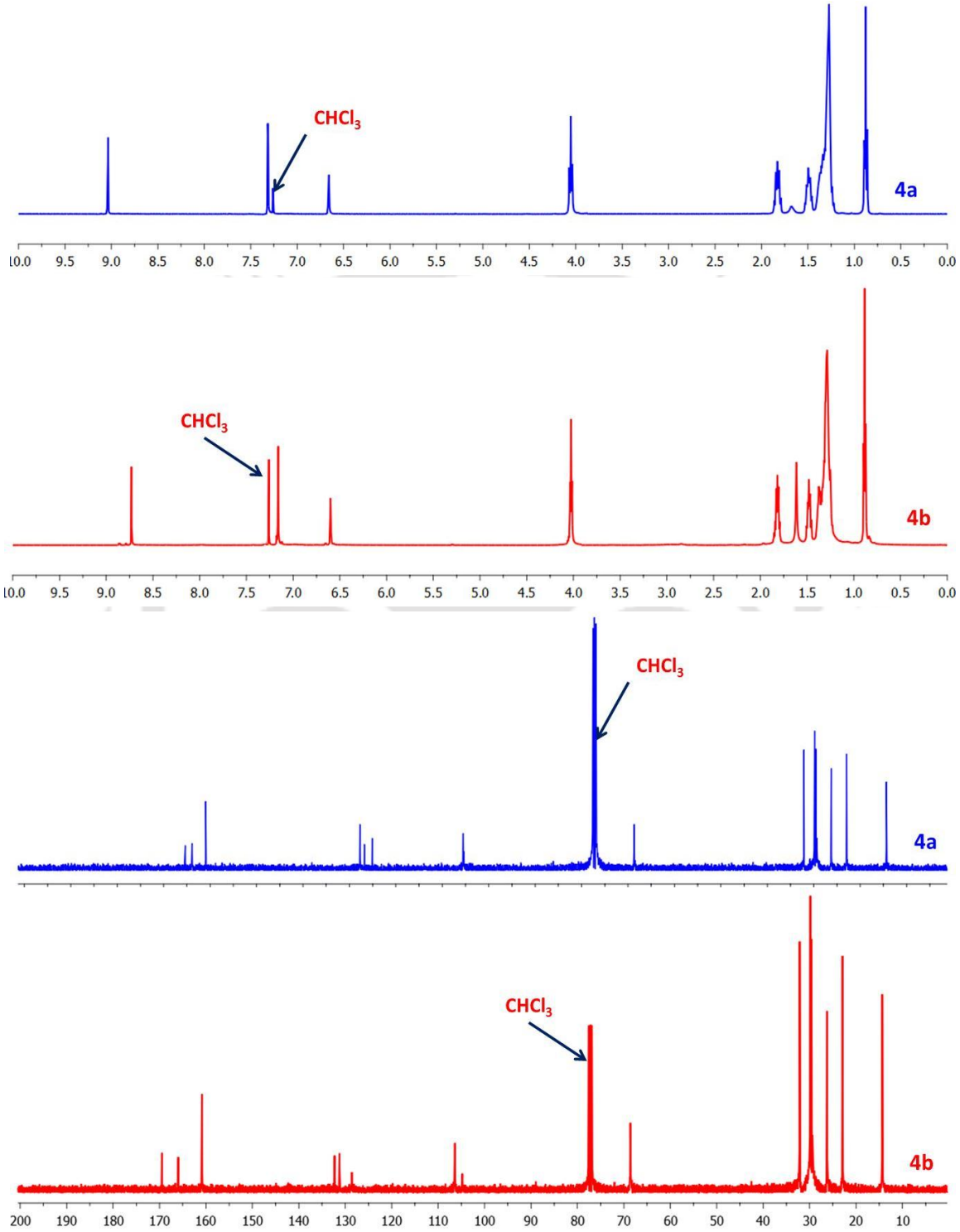

Figure 4.1. ^{1}H NMR (400 MHz) and ^{13}C NMR (100 MHz) spectra of compound **4a** and ^{1}H NMR (600 MHz) and ^{13}C NMR (100 MHz) spectra of compound **4b** in $CDCl_3$.

As representative cases, only the ^{1}H NMR and ^{13}C NMR spectra of **4a** and **4b** are presented in Figure 4.1.

4.2b. Thermal behavior

The mesogenic behavior of these star shaped molecules and polycatenars was studied with the help of polarizing optical microscopy (POM), differential scanning calorimetry (DSC) and powder X-ray diffraction (XRD) studies (wherever required). The phase transitions and the corresponding changes in enthalpy are briefed in Table 4.1. Similarly the data obtained from XRD studies are presented in Table 4.2. The thermal stability of these molecules was investigated through thermogravimetric analysis (TGA). The oxadiazole-based compounds, especially star shaped and *p*-substituted tetracatenars exhibited higher thermal stability (>300 ^{o}C). All the other compounds exhibited a thermal stability at least upto 200-280 ^{o}C (Figure 4.2). Oxadiazole based star-shaped molecule **4a** placed between an untreated glass slide and coverslip, on heating showed a transition to the fluidic birefringent phase at ≈ 79 ^{o}C (ΔH = 11.2 kJ/mol). This phase persisted upto 95 ^{o}C, before converting into an isotropic liquid (Fig. 4.3b). Cooling the isotropic liquid at a rate of 2 ^{o}C/min, led to the growth of colorful mosaic patterns, which stayed upto room temperature (Fig. 4.3a). Cooling scans obtained from the DSC showed that the mesophase crystallized at 11 ^{o}C (ΔH = 4.2 kJ/mol). We have carried out XRD studies at different temperature intervals (Fig. 4.3c). XRD profile obtained at 80 ^{o}C showed a single sharp reflection centered at low angle corresponding to a *d*-spacing of 28.86 Å, along with diffused

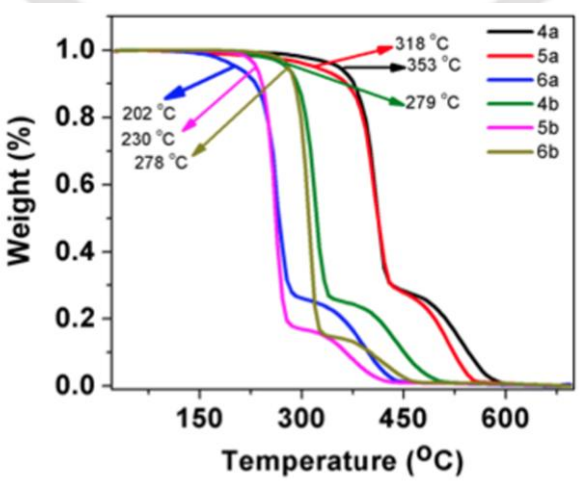

Figure 4.2. TGA plots of the target molecules (heating rate of 10 °C/min, Nitrogen atmosphere).

spacings at wide angle corresponding to 5 Å and 3.77 Å. The first diffused spacing at 5 Å is corresponding to the packing of flexible alkyl tails, while the second diffused spacing at 3.77 Å can be attributed to the packing of cores. The hexagonal lattice parameter '*a*' was found to be 33.3 Å, which is lesser than the calculated molecular diameter (41 Å). The area of the unit cell was 966.6 $Å^2$ and the volume was found to be 3621.3 $Å^3$. The number of molecules forming unit hexagonal cell (Z) was found to be 1.5. This may be due to the intercalation of the arms of the star-shaped molecule. This is supported by the lower value of '*a*' in comparison to the molecular diameter (Table 4.2, Fig. 4.4).

Table 4.1. Phase transition temperatures [a] (°C) and corresponding enthalpies (kJ/mol) of compounds 4a, 4b, 5a, 5b, 6a and 6b.

Entry	Heating	Cooling
4a	Cr_1 15.6 (7.1) 68.4 (28.5) Cr_2 79.4 (11.2) Col_h 94.8 (1.6) I	I 90.5 (1.6) Col_h 11.4 (4.2) Cr
4b	Cr 51 (2.6) I	I 36.1 (1.3) Cr
5a	Cr_1 80.3 (6.1) Cr_2 124.9 (57.1) I	I 101.9 (58) Cr_1 75.2 (10.5) Cr_2
5b	Cr 96.1 (53.9) I	I 75 Cr[b]
6a	Cr 82.7 (51.5) I	I 17.5 (28) Cr
6b	Cr 76.3 (32.4) I.	I 27.3 (3.3) Cr

[a]Peak temperatures in the DSC thermograms obtained during the second heating and first cooling cycles at 5 °C/min.; Cr = Crystal phase, Col_h = Columnar hexagonal phase, [b]Crystallization was observed only under POM, but not detected in DSC.

Table 4.2. Results of the (*hk*) indexation of the XRD profiles of the compounds at a given temperature (T) of the mesophases.[a]

Compounds (*D*/Å)	Phase (T/°C) Symmetry	d_{obs} (Å)	d_{cal} (Å)	Miller indices (*hk*)	Lattice parameters (Å) Lattice area S ($Å^2$), Molecular volume V ($Å^3$)
4a (41.1)	Col_h (80) *p6mm*	28.86 5.0 (h_a) 3.77 (h_c)	28.86	10	a = 33.32; S = 966.6; V = 3621.3; Z = 1.5.
	Col_h (60) *p6mm*	29.72 4.96 (h_a) 3.82 (h_c)	29.72	10	a = 34.32; S = 1018.8; V = 3892; Z = 1.6.
	Col_h (25) *p6mm*	29.74 4.90 (h_a) 3.81 (h_c)	29.74	10	a = 34.34; S = 1020; V = 3845.5; Z = 1.6.

[a]The diameter (*D*) of the disk (estimated from Chem 3D Pro 8.0 molecular model software from Cambridge Soft). d_{obs}: spacing observed; d_{cal}: spacing calculated (deduced from the lattice parameters; a for Col_h phase). The spacings marked h_a and h_c correspond to diffuse reflections in the wide-angle region arising from correlations between the alkyl chains and core regions, respectively. *Z* indicates the number of molecules per columnar slice of thickness h_c, estimated from the lattice area *S* and the volume *V*.

Thiadiazole based star-shaped molecule **4b** turned to be crystalline. Regioisomeric oxadiazole and thiadiazole based star shaped molecules with peripheral alkoxy tails connected to the benzene ring at 3 and 4 positions (**7a** and **7b)**, however exhibited a wide range Col_h phase (Fig. 4.5).[11a] This shows that how a small structural variation like peripheral chain substitution perturbs the self-assembly of star-shaped molecules. *p*-Substituted tetracatenars **5a-b** and *m*-substituted tetracatenars **6a-b** turned out to be crystalline. This means that substitution at 3 and 5 positions of the terminal ring is not conducive to stabilize liquid crystallinity. Star-shaped molecules lack the shape anisotropy of disc-like molecules, where nanophase segregation of incompatible molecular subunits plays a vital role in stabilizing the columnar self-assembly. Thus for the compounds with peripheral 3,5-substitutions, the one with lower bent angles (compound **4a**, with the oxadiazole ring with the bent angle of 134^o) will have higher mesophase stability due to the better space filling in comparison to compound **4b** (thiadiazole ring with the bent angle 160^o).

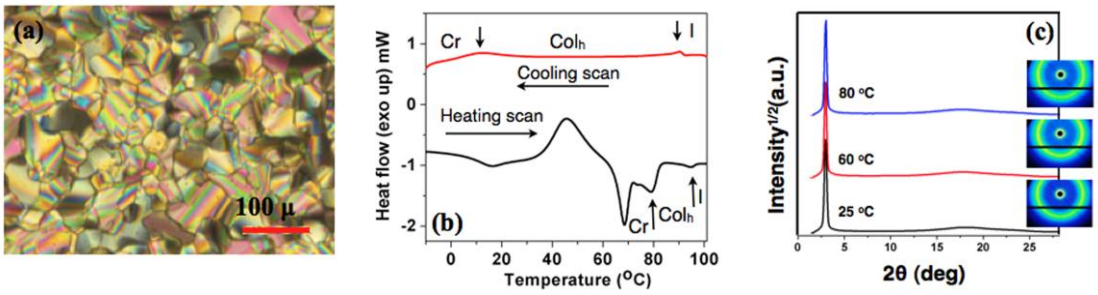

Figure 4.3. POM images obtained for compound **4a** at room temperature (a); DSC thermogram of compound **4a** in the second heating (black trace) and first cooling (red trace) at a scan rate of 5 ^{o}C/min (b); Intensity *vs* 2θ profiles obtained from the XRD patterns obtained for compound **4a** at 80 ^{o}C, 60 ^{o}C and at 25 ^{o}C (c) for Col_h phase (insets show the image patterns).

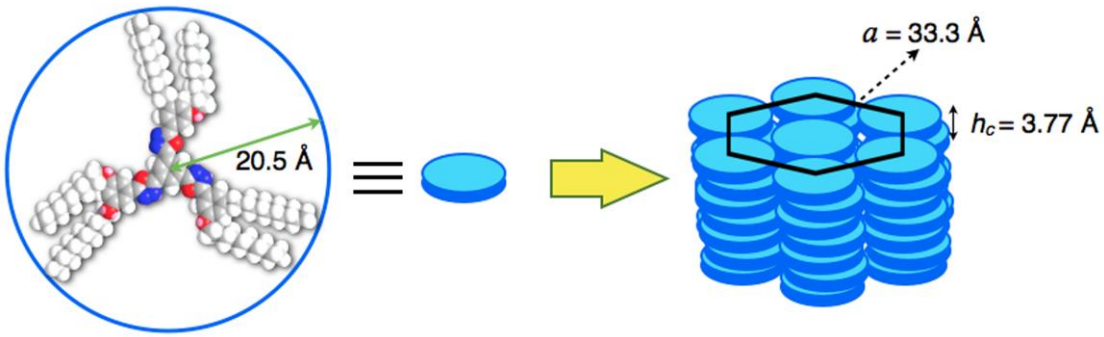

Figure 4.4. Schematic showing the self-assembly of star-shaped oxadiazole derivative **4a** to Col_h phase.

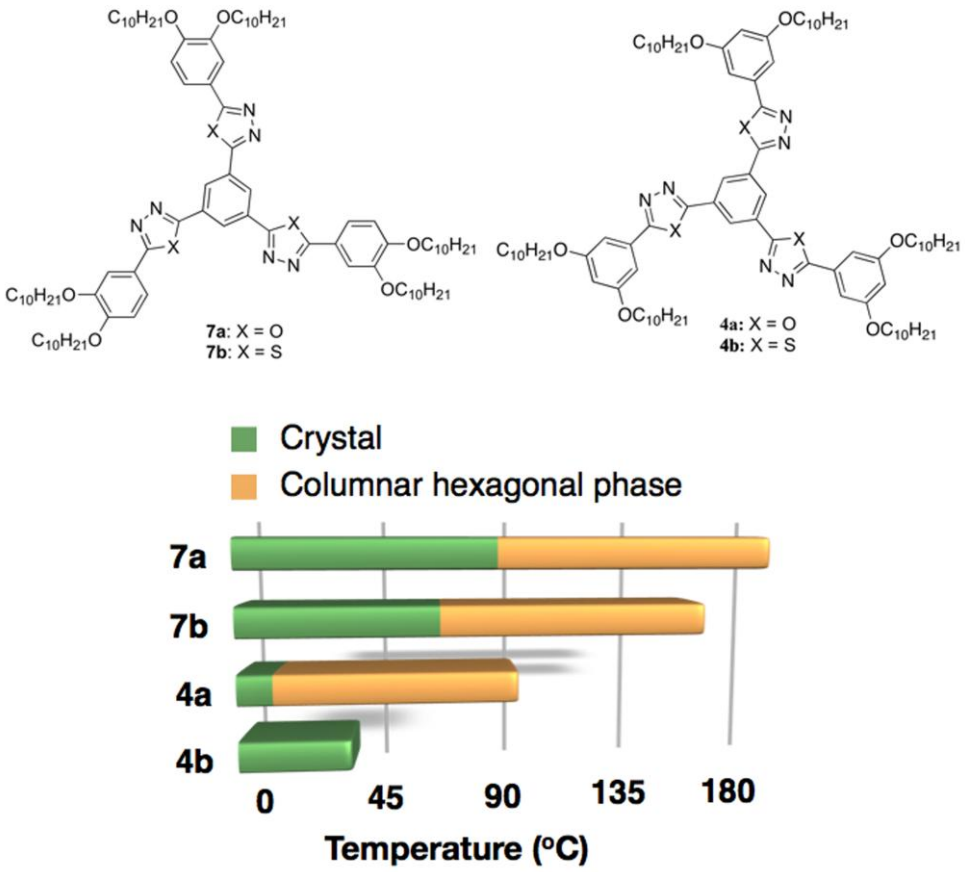

Figure 4.5. Structures of the regioisomeric star-shaped oxadiazole and thiadiazole derivatives reported earlier (**7a-b**)[11a] and of the present study (**4a-b**) and the bargraph showing their thermal behavior (Based on the first cooling in the DSC scan).

4.3. Photophysical behavior

Photophysical properties of the star-shaped compounds (**4a-b**), *p*-substituted polycatenars (**5a-b**) and *m*-substituted polycatenars (**6a-b**) are represented in table 4.3. From the absorption spectra taken in micromolar solutions in THF, it can be seen that the thiadiazole based compounds **4b**, **5b** and **6b** exhibited a red shifted absorption maximum in comparison to oxadiazole based compounds **4a, 5a** and **6a**. In line with the absorption spectra, oxadiazole based compounds exhibited higher optical band gap, in comparison to thiadiazole based compounds. Similar red shift was observed in the emission spectra of thiadiazole derivatives in comparison to oxadiazole derivatives. The observed red shift in absorption and emission of thiadiazole derivatives can be accounted to the higher polarizability and basic nature of sulphur.

Star-shaped molecules and *m*-substituted polycatenars showed lower absorption maxima in comparison to *p*-substituted polycatenars, which is due to the difference in the conjugation.[11b] This is reflected in the values of their optical band gaps, where the *p*-substituted polycatenars showed a lower band gap in comparison to *m*-substituted polycatenars and star shaped molecules. The values of molar absorption coefficients were higher in the case of star-shaped molecules, which were followed by *m*- and *p*-substituted polycatenars. The single absorption band observed for 1,3,4-oxadiazole and thiadiazole based systems is ascribed to the spin allowed π-π* transition of the conjugated system.[11] Stoke's Shift was found to be higher for the star-shaped molecules in comparison to tetracatenars.

The emission spectra were not in line with this observation, where the star-shaped molecules exhibited red shifted emission in comparison to the *p*- and *m*-substituted tetracatenars. The thin films of these compounds prepared by annealing the sandwiched samples from the isotropic state, exhibited visually perceivable blue color, under the irradiation of UV light of long wavelength (λ_{max} = 365 nm). Thus blue emission was observed for both the solutions and thin films. This is promising because there is a scarcity of blue light emitting materials and they are known to have wide band gaps. Synthetically it is difficult to design such conjugated systems and blue light emitters provide flexibility in fine-tuning the emission wavelength on combining with another dopant emitter. This is why, they form vital components in the construction of white OLEDs.[12] Oxadiazole based compounds **4a-c** showed higher quantum yields (0.21-0.68) (Fig. 4.7) than the corresponding thiadiazole derivatives **5a-c** (0.15-0.41), which is in line with the general trend.[11]

Table 4.3. Photophysical properties of compounds

	Solution						Thin film
Entry	Absorption[a] (nm)	Emission[a,b] (nm)	Stokes shift (cm^{-1})	$\Delta E_{g,\,opt}$[c]	Quantum Yield[d]	ε ($M^{-1}cm^{-1}$)	Emission[e] (nm)
4a	298	402	8681.4	3.64	0.21	22728	396
5a	327	383	4471.4	3.47	0.68	13819	420
6a	287	374	8105.2	3.75	0.25	15480	380
4b	321	434	8111.2	3.36	0.18	20594	446
5b	345	367	1737.6	3.17	0.41	15976	457
6b	319	408	6838.2	3.42	0.15	18480	436

[a]Micromolar solutions in THF. [b]Excited at the respective absorption maxima. [c]Band gap was determined from the red edge of the longest wave length in the UV-Vis absorption spectra. [d]Relative quantum yield measured with respect Quinine sulphate solution (0.1 M in con. H_2SO_4). [e]Emission obtained by exciting the thin films at their absorption maxima in solution.

Among all the molecules *p*-substituted polycatenars exhibited higher quantum yields in comparison to star-shaped molecules and *m*-substituted polycatenars.

Thin film of the compound **4a** showed a blue shifted emission in comparison to its solution, while the thin films of other compounds exhibited a red shifted emission maximum. This suggests the formation of aggregates in the thin film state. It is interesting to compare the photophysical properties of regioisomeric star shaped molecules reported earlier, where the peripheral tails are connected to the 3,4-positions of the peripheral benzene ring. Compounds **4a** and **4b** exhibited a blue-shifted absorption and emission maxima in comparison to the isomers (**7a** and **7b,** Fig. 4.6) with peripheral tails connected to the 3,4-positions of the benzene ring in solution.[11a]

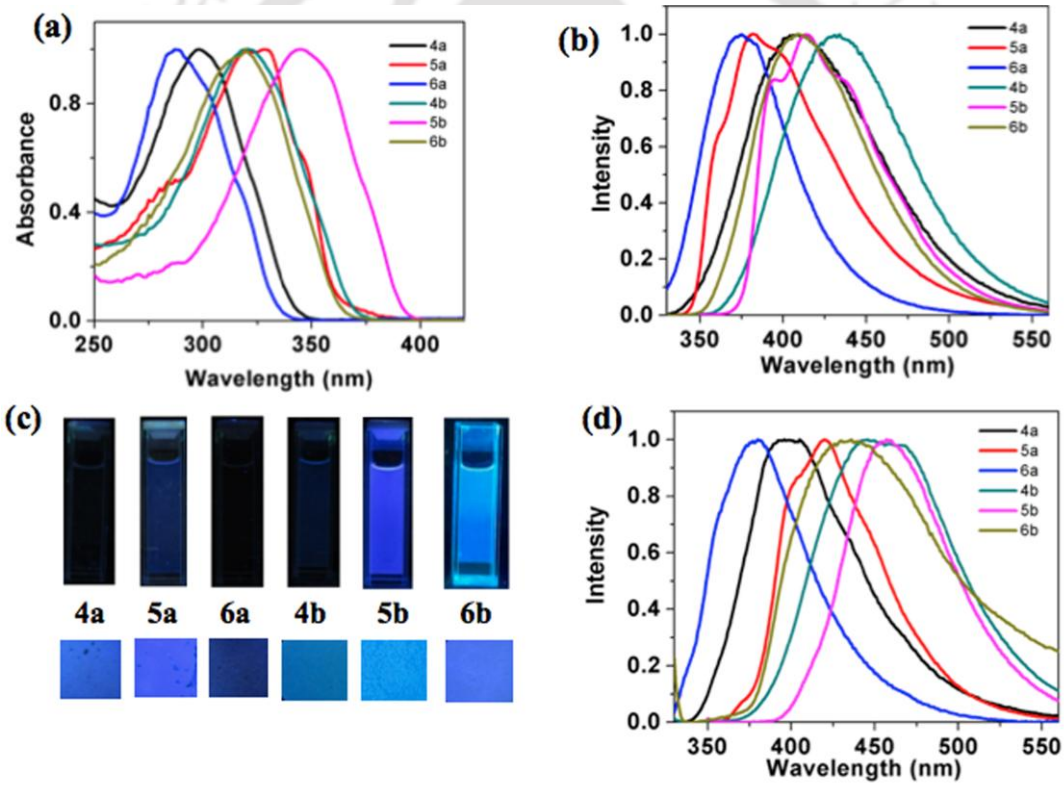

Figure 4.6. Normalized absorption (a) and emission spectra (b) in 20μM THF solution obtained for compounds; Pictures of micromolar solutions in THF and thin films of compounds as seen with the UV illumination (λ_{ex} = 365 nm) (c); normalized emission spectra obtained for compounds in the thin film state (d).

Quantum yield measurement

Quantum yield was measured according to established procedure by using quinine sulfate in 0.1 M H_2SO_4 solution as the standard. Absolute values were calculated according to the following equation: $Q_S = Q_R \times (m_S / m_R) \times (n_S / n_R)^2$,

where, Q: Quantum yield, m: Slope of the plot of integrated fluorescence intensity *vs* absorbance, n: refractive index (1.407 for THF and 1.33 for distilled water). The subscript R refers to the reference fluorophore *i.e.* quinine sulphate solution in 0.1 M H_2SO_4 and subscript S refers to the sample under investigation. In order to minimize re-absorption effects, absorbance was kept below 0.15 at the excitation wavelength of 347 nm. Quantum Yield of quinine sulphate is 0.54. The values of quantum yields obtained are given in table 4.3.

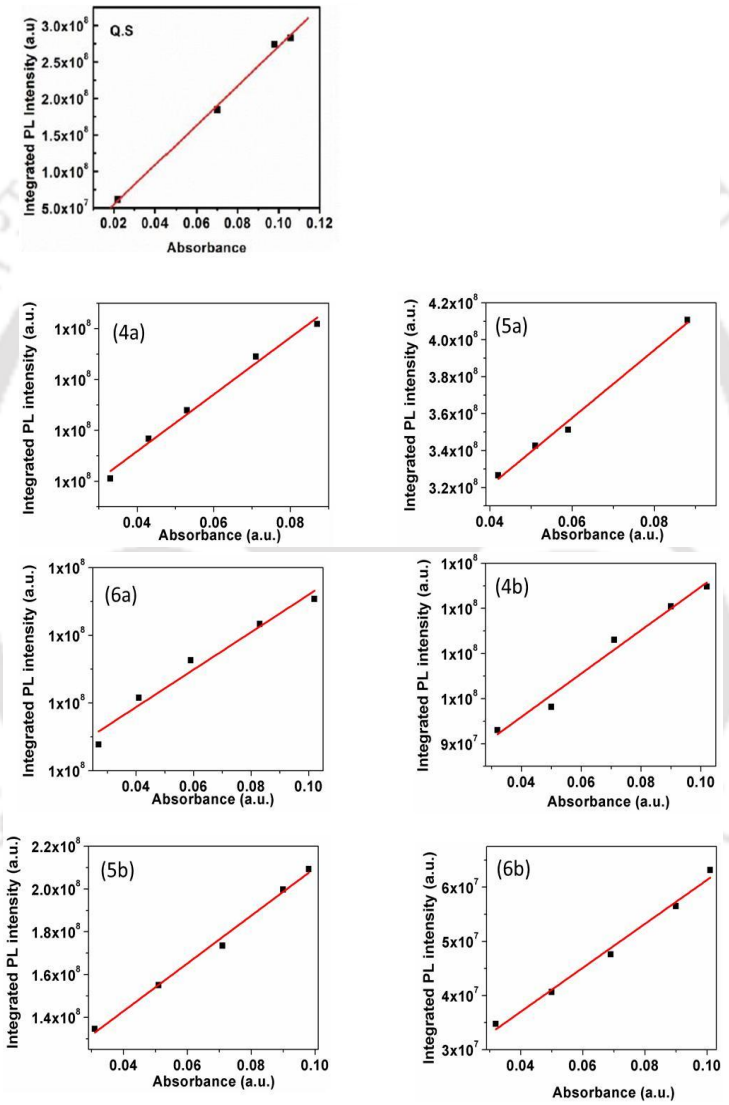

Figure 4.7. Plots of integrated photoluminescence intensity *vs* absorbance of Quinine sulphate (0.1M H_2SO_4 solution) and compounds **4a, 4b, 5a, 5b, 6a and 6c** (micromolar THF solution).

4.4. Gelation studies

All the compounds were tested for their gelation behavior in hydrocarbon based

solvents like hexane, decane and dodecane. Table 4.4 provides the CGC (in wt. %), *i.e.* is the minimum concentration necessary for gelation, and T_{gel} (^{o}C) *i.e.* is the thermal stability of the gels determined by 'dropping ball' method[13] for all the compounds. Only star-shaped oxadiazole derivative (**4a**) formed an opaque gel with a critical gelation concentration (CGC) of 0.9 wt.% in dodecane. Such gelators which form stable gels at less than 1 wt% concentration are termed as 'supergelators'.[14,16] Usually this kind of stable gelation requires strong intermolecular interactions like H-bonding.[15] Supergelators which stabilize gelation mainly through π-π interactions are less in number.[16] As an example, compound **4a** was dissolved in dodecane by heating and left to attain the ambient temperature. The process of gelation was followed with respect to time by fluorescence spectrometry. In solution state the intensity of emission was less, which gradually increased with the decrease in temperature. It has shown a sudden increase at around 80 minutes and further showed small increase with the time (Fig. 4.8a,c). The emission was blue-shifted in comparison to the solution state (Fig. 4.8b). Thus the compound exhibits an enhancement in the emission intensity on gelation (approximately 2.2 times), which can be termed as 'aggregation induced enhanced emission' (AIEE).[17] The gel formation was reversible over many heating and cooling cycles as evidenced with the monitoring of the emission intensity (Fig. 4.8d). It took 80 minutes for the compound to gelate from the point of dissolution as evidenced from the fluorescence studies.

Table 4.4. Gelation behavior and CGCs of compounds **4a-b**, **5a-b** and **7a-b**.

Compound	Hexane	Decane	Dodecane	T_{gel} (^{o}C)
4a	I	P	G(O) (0.9)[a]	-
4b	Soluble	P	S	45
5a	I	P	I	-
5b	P	P	P	-
6a	Soluble	P	S	-
6b	Soluble	Soluble	Soluble	-
7a	P	PG	G(O) (0.6)[a]	50
7b	PG	PG	G(T) (0.5)[a]	52

G = stable gel; I = insoluble; O = opaque; T = transparent; P = precipitate; PG = partial gel; S = soluble; [a]The critical gelation concentration (in wt.%) is the minimum concentration necessary for gelation. T_{gel} is the thermal stability of the gels.

We have also carried out the gelation experiment by suddenly cooling the solution in ice-water bath. In this case gelation occurred within 5 minutes. Here also we observed AIEE effect. The blue shifted emission in the gel state points to the formation aggregates. The corresponding thiadiazole derivative **4b** was clearly soluble and was unable to gelate even on cooling. We were also interested to know the behavior of corresponding regioisomers **7a** and **7b** (Fig. 4.5, Table 4.4). The regioisomeric star-shaped compound **7a** exhibited gelation in *n*-dodecane with a lesser CGC of 0.6 wt.%.

In comparison to compound **4a**, which took a longer gelation time and higher CGC, compound **7a** gelated very fast, within 3-4 minutes at a lower CGC. The gelation was followed by fluorescence spectrometry with a regular time interval. Upon gelation, we noticed a decrease in the emission intensity with a red shift, which is due to the 'aggregation caused quenching' (ACQ) (Fig. 4.9a-c).[18] Regioisomeric thiadiazole derivative **7b** also showed gelation behavior in dodecane at a lower CGC (0.5 wt%) within 4 minutes. Gelation of the compound followed with the help of fluorescence spectroscopy. Interestingly this compound exhibited an AIEE phenomenon with a red shifted emission (Fig. 4.10).

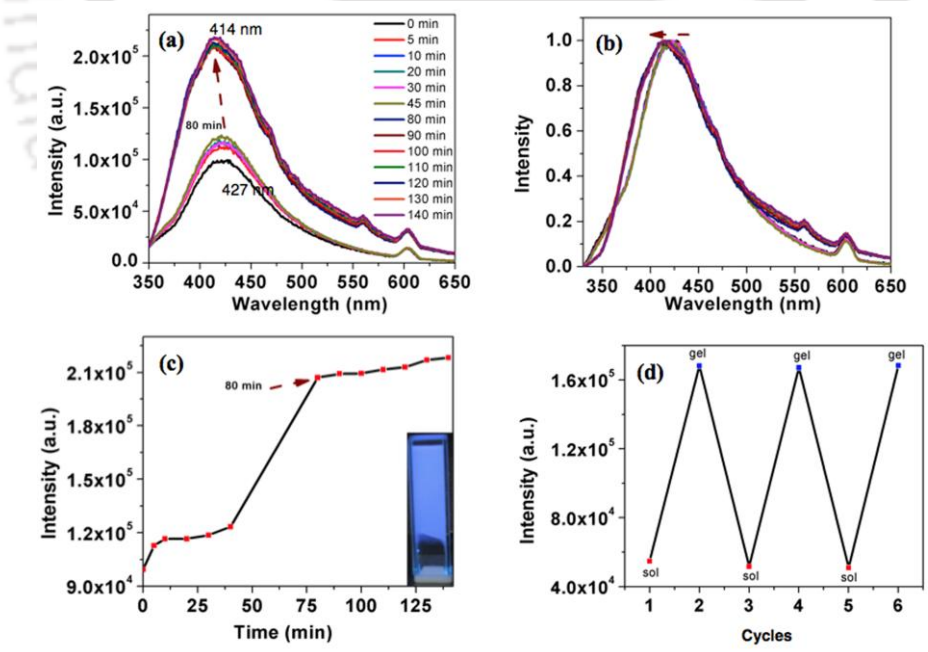

Figure 4.8. Emission spectra showing an increase in the emission intensity with the increase in time from solution to gel state for compound **4a** (a); Normalized emission spectra showing a blue shift on gelation of compound **4a** (b); Emission spectra showing an increase in the emission intensity with the time during transformation of solution to gel (c); Reversible change in the emission intensity on repeated sol–gel transitions (d) (Concentration: 6.7 mM, dodecane, λ_{ex} = 300 nm).

Compound **5a** was insoluble in dodecane even after heating, while compound **5b** was soluble in dodecane. On cooling the solution in ice bath a weak gel was formed, which collapsed immediately within few seconds. It was then heated to get a clear solution and left for some time in room temperature, but then the compound precipitated.

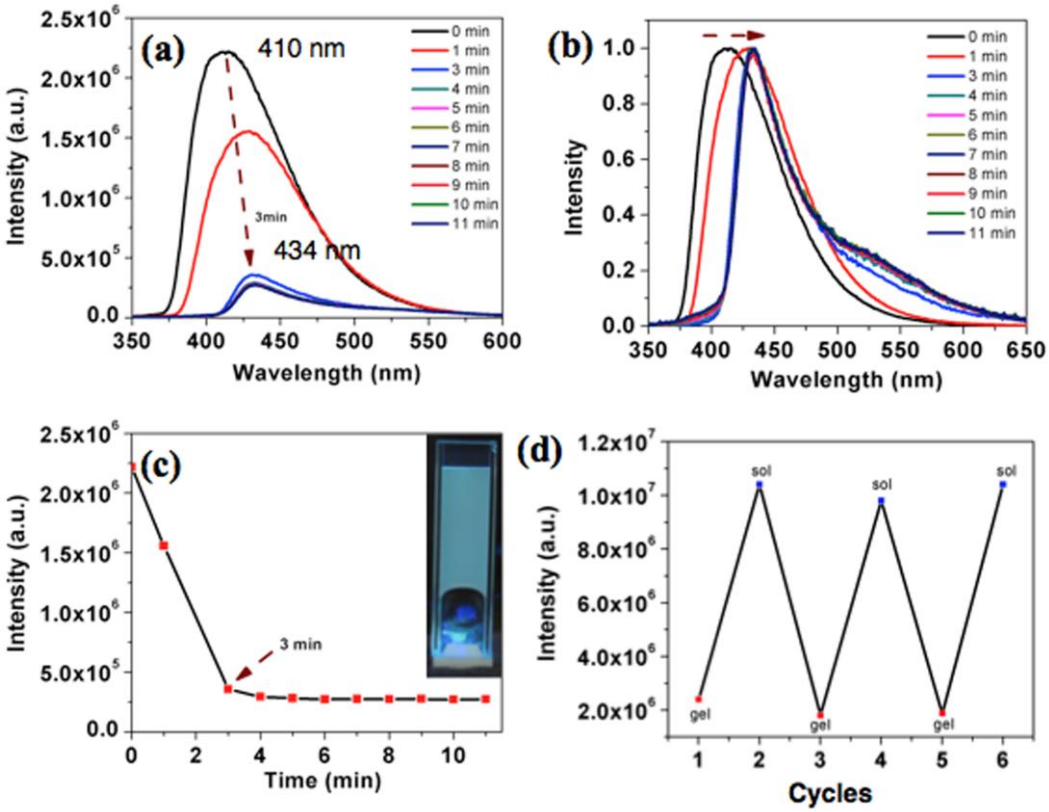

Figure 4.9. Emission spectra showing a decrease in the emission intensity with the increase in time from solution to gel state for compound **7a** (a); Normalized emission spectra showing a red shift on gelation of compound **7a** (b); Emission spectra showing a decrease in the emission intensity with the time during transformation of solution to gel (c); Reversible change in the emission intensity on repeated sol–gel transitions (d) (Concentration: 5.2 mM, dodecane, λ_{ex} = 318 nm)

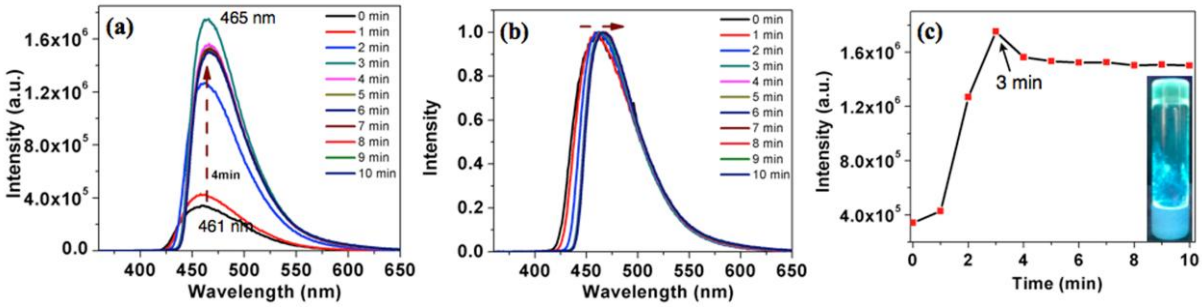

Figure 4.10. Emission spectra showing an increase in the emission intensity with the increase in time from solution to gel state for compound **7b** (a); Normalized emission spectra showing a red shift on gelation of compound **7b** (b); Plot showing the change in the emission intensity at emission maximum with respect to time (c) (Concentration: 5 mM, dodecane, λ_{ex} = 350 nm) Inset shows the image of the gel under the UV light of long wavelength (λ_{ex} = 365 nm).

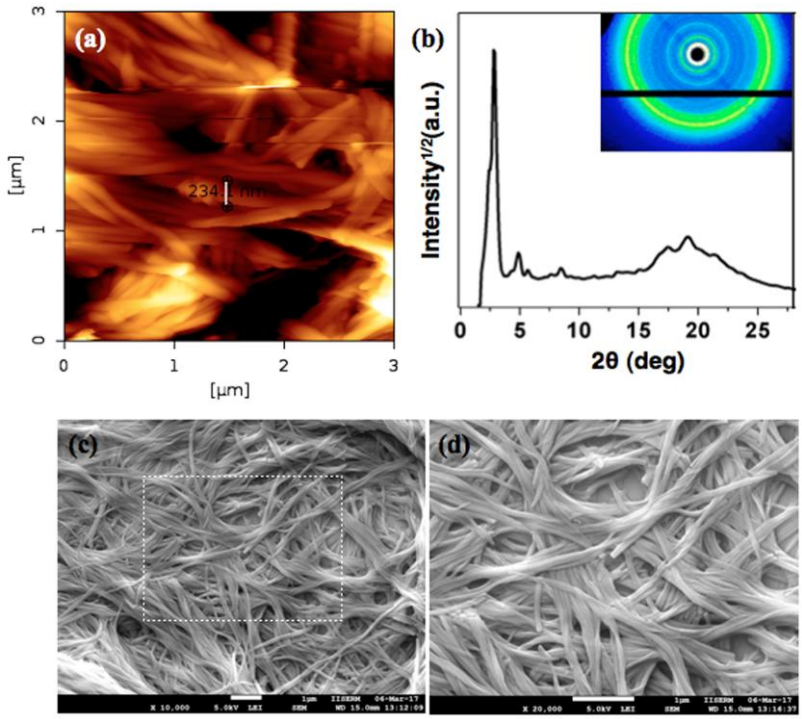

Figure 4.11. AFM image obtained for the xerogel of compound **4a** (a); XRD profile depicting the intensity against the 2θ obtained for the crystalline phase of compound **4a** in xerogel state (inset shows the XRD image pattern obtained) (b); SEM images obtained for compound **4a** (c); an expanded region of the image 9c (scale bar is 1µm) (d).

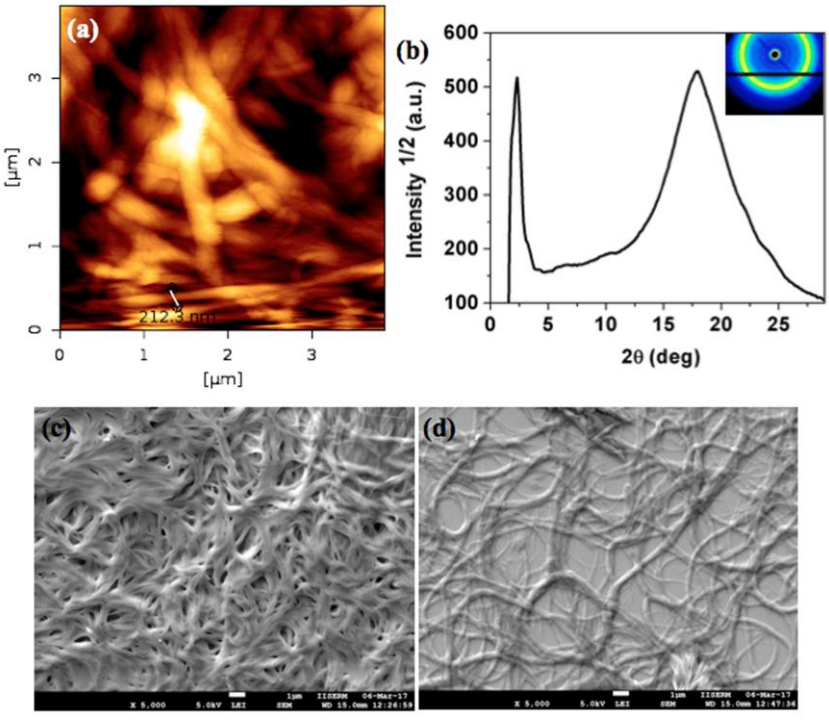

Figure 4.12. AFM image obtained for the xerogel of compound **7a** (a); XRD profile depicting the intensity against the 2θ obtained for the Col_r phase of compound **7a** in xerogel state (inset shows the XRD image pattern obtained) (b); SEM images obtained for compound **7a** (c); SEM image obtained from the another region of the sample (scale bar is 1µm) (d).

Compound **6a** was soluble in dodecane and did not gelate even after keeping for a long time in ice-water bath. The compound **6b** was soluble in dodecane, but precipitated in ice-water bath. The microstructures of xerogels of compounds **4a**, **7a** and **7b** were examined with the help of atomic force microscopy (AFM) and scanning electron microscopy (SEM). The compounds are made soluble in dodecane at their CGC and a very small drop is put in glass slide and kept to form a very thin layer of stable gel. Then these gel films were vacuum dried keeping the structure intact. After complete evaporation of the solvent they were characterized by different scanning probe microscopy techniques like AFM and SEM. These images confirmed the highly entangled network formed by the fibers of several micrometer length (Fig. 4.11a,c,d 4.12a,c,d and 4.13a,c,d). Further the structure of the xerogel was investigated with the help of powder X-ray diffraction studies (Table 4.5). The powder XRD studies of the xerogel of compound **4a**, showed the crystallization of the sample on moving to xerogel state. XRD plot depicting the intensity against the 2θ showed several peaks at low angle and wide-angle region (Fig. 4.11b).

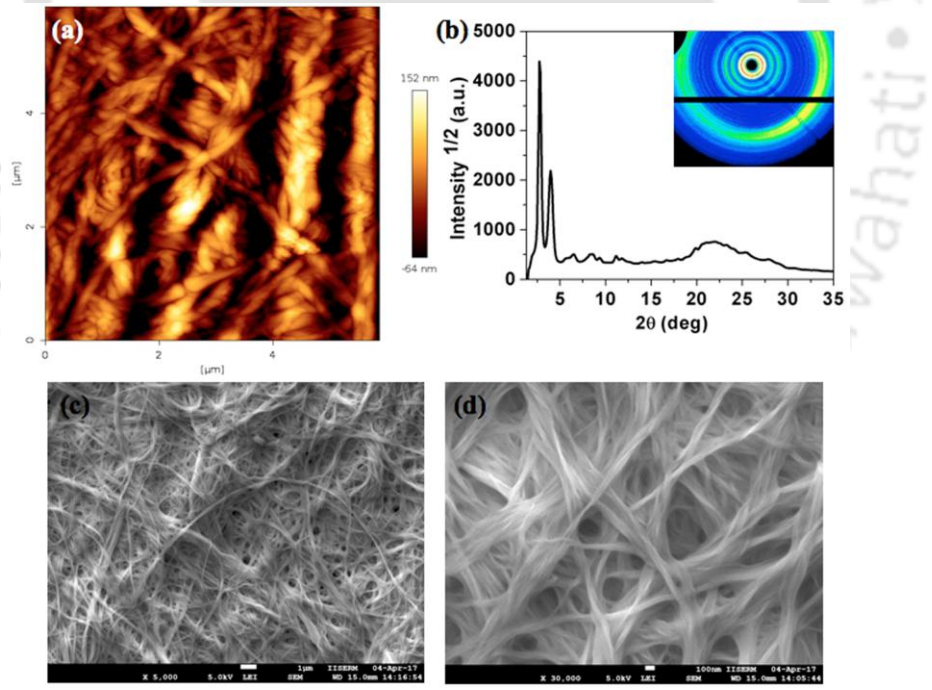

Figure 4.13. AFM image obtained for the xerogel of compound **7b** (a); XRD profile depicting the intensity against the 2θ obtained for the crystalline phase of compound **7b** in xerogel state (inset shows the XRD image pattern obtained) (b); SEM images obtained for compound **7b** (c); An expanded portion of the SEM image (scale bar is 1 μm) (d).

Interestingly the XRD pattern of the xerogel of compound **7a** revealed several peaks ranging from the low angle to mid angle region corresponding to the *d*-spacings of

38.27 Å, 13.58 Å, 8.61 Å and 4.95 Å. In addition there were diffused peaks at wide-

Table 4.5. Results of the (*hk*) indexation of the XRD profiles of the xerogels at room temperature.[a]

Compounds (*D*/Å)	Phase	d_{obs} (Å)	d_{cal} (Å)	Miller indices (*hk)*	Lattice parameters (Å)
4a (41.1)	Cr	31.74 15.74 12.47 11.53 10.49 9.50 7.88 7.27 6.70 6.30 5.91 5.08 4.65 4.17 3.88 3.76 3.34 3.23			
7a (47.7)	Col_r *p2mm*	38.27 13.58 8.61 4.95 4.02(h_a) 3.68 (h_c)	38.27 13.58 7.99 4.84	01 11 14 30	a = 14.55; b = 38.27.
7b (48.4)	Cr	31.83 22.33 15.68 13.67 10.50 9.45 7.96 7.52 6.34 5.78 5.32 4.96 4.47 4.04 3.83 3.52 3.20 2.94 2.72			

[a]The diameter (*D*) of the disk (estimated from Chem 3D Pro 8.0 molecular model software from Cambridge Soft). d_{obs}: spacing observed; d_{cal}: spacing calculated (deduced from the lattice parameters; a for Col_h phase). The spacings marked h_a and h_c correspond to diffuse reflections in the wide-angle region arising from correlations between the alkyl chains and core regions, respectively.

angle corresponding 4.02 Å and 3.68 Å. The first diffused peak corresponds to the

packing of alkyl tails, while the second one corresponds to the packing of cores (Fig. 4.11b, Table 4.5). The first four *d*-spacings can be indexed into (01), (11), (14) and (30) reflections arising from a rectangular lattice of *p2mm* symmetry. The lattice parameters can be calculated were found to be a = 14.55 Å and b = 38.27 Å. But in contrast, the XRD of the xerogel of compound **7b,** shown that it is crystalline with several peaks in the low and mid angle region (Fig. 4.13b).

4.5. Rheological studies

The elastic nature of the gels can be investigated with the help of rheological measurements involving strain sweep, angular frequency sweep and step strain measurements. To understand the dynamic mechanical properties of the organogels of compounds **4a, 7a** and **7b** in dodecane, we executed dynamic frequency sweep measurements at constant stress by quantifying the rheological response. This is characterized by G* (ω) = G'(ω) + iG" (ω). Here G' denotes the storage modulus, G" denotes the loss modulus and ω represents the angular frequency.[19] These measurements are valuable, as the measurements are carried out without affecting the gel structure due to small stress.

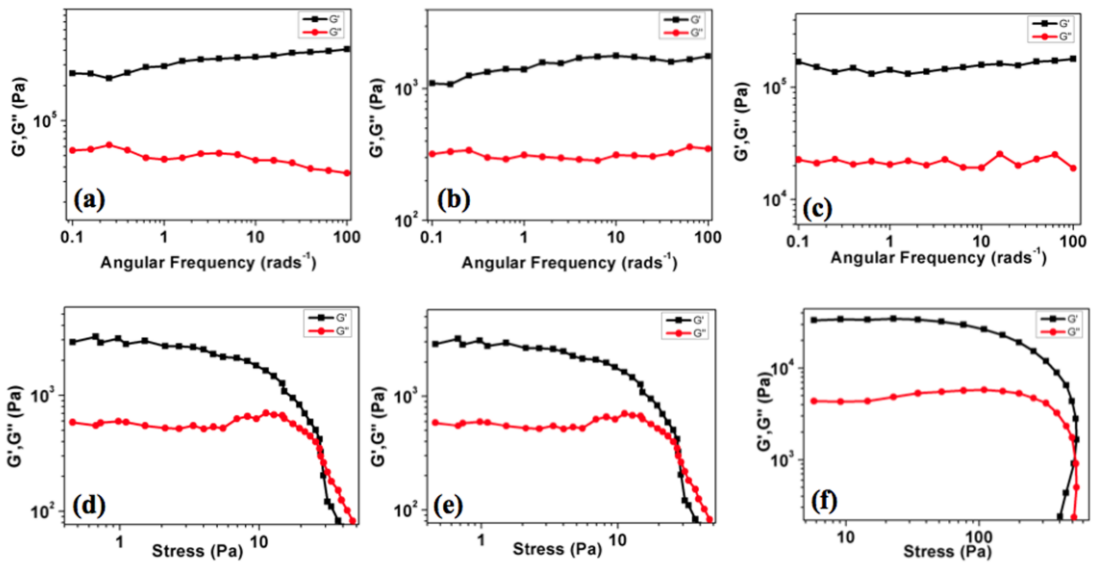

Figure 4.14. Angular frequency (rad s^{-1}) dependence of G' and G" obtained with small stress amplitudes: (a) 0.9 wt% of compound **4a** in dodecane at 25 °C using 0.2 kPa stress; (b) 0.6 wt% of compound **7a** in dodecane at 25 °C using 0.2 kPa stress; (c) 0.5 wt% of compound **7b** in dodecane at 25 °C using 0.2 kPa stress; Stress dependence of G' and G" of the same gels measured at constant frequency (at 25 °C, and frequency at 0.1 Hz) for compound **4a** (d); compound **7a** (e) and compound **7b** (f).

Figure 4.14a, shows measurements of G' and G" for the gels (at CGC, solvent: dodecane) as a function of ω (at 25 °C, by applying 0.2 kPa stress). We can notice two important things from Figure 4.14a-c. Firstly, in all cases the value of G' is found to be larger than G" over the complete range of frequency measurements. This indicates that the gel works as a solid-like, viscoelastic material.[20] Secondly, the dependency of G' and G" on the frequency is not very strong. It should be notable that, even at the lowest frequency attained by the instrument, the liquid like behavior of the gel was not seen. This corroborates that these materials are gels with a large structural relaxation.

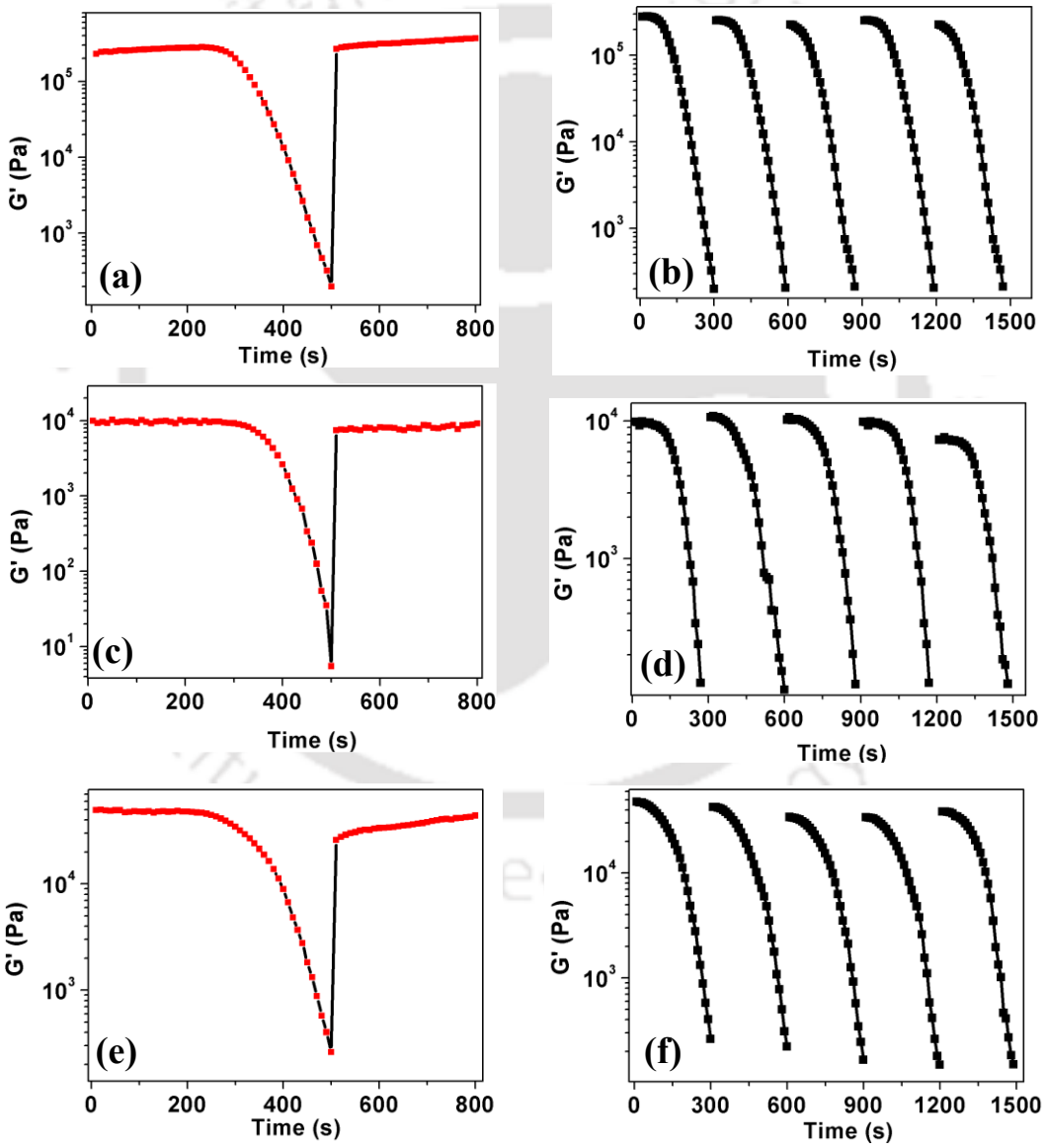

Figure 4.15. Thixotropic nature of organogel at their CGC, for **4a** (a), **7a** (c) and **7b** (e) in *n*-dodecane at 25 °C (Deformation; stress: 0.1 to 100 Pa, time: 300 s, angular frequency: 10 Hz; Recovery; Stress: 1 Pa, time: 300 s; angular frequency: 10 Hz.); Five continuous cycles of measurement for **4a** (b), **7a** (d) and **7b** (f) (at CGC) to prove that gel is thixotropic.

Non-linear rheological measurements were carried out to comprehend the dynamics of sol-gel transitions. Non-linear viscoelastic regime was established by performing the experiments showing stress amplitude dependence of the G' and G". Figure 4.14d-f shows stress-dependent nonlinear measurements of the gel at a fixed frequency of 0.1 Hz. We note two features in these figures. Firstly, at low strain amplitudes G' is almost a constant, corresponding to a linear viscoelastic regime. In this regime, G' is greater than G". This fact corresponds to the solid like behavior of the gel. Secondly, above a critical stress value (2.8 kPa), both G' and G" became strain dependent. This finally results in the viscoelastic liquid-like behaviors at high stress (G">G'). This implies a deformation driven changeover from a viscoelastic solid to viscoelastic liquid. The thixotropic nature of the gel was also confirmed by studying the ability of the gel to recover after the destruction. Experimentally, two continuous processes, *i.e.* deformation and recovery were followed consequently (Fig. 4.15). In the deformation step, a varying stress from 0.2 to 3 kPa (ω of 10 Hz for 300 s) was applied and the values of G' was monitored as a function of time for 300 s. In the recovery step, the storage modulus G' was monitored as a function of same time interval (300 s) for a low shear stress (0.2 kPa; ω:10 Hz). This experiment was repeated at least for five times and the results are presented in Figure 4.14. The results demonstrate the immediate recovery of the gel after the removal of the applied stress, and thus emphasize the mechanical robustness of the materials.[10d]

4.6. Electrochemical studies

Energy levels of HOMO and LUMO levels and the band gaps of all the target molecules were obtained by cyclic voltammetry (CV). The data obtained are tabulated in Table 4.6. CV scans of the compounds displayed irreversible oxidation and reduction waves (Figure 4.17). The optical band gap ($E_{g,opt}$) was estimated from the absorption onset obtained from the absorption spectra in solution. Energy levels of HOMO and LUMO were determined by using the formulae E_{HOMO} = -(4.8 - $E_{1/2,Fc,Fc+}$ + $E_{ox,\ onset}$) eV and E_{LUMO} = $E_{g,opt}$ - E_{HOMO} eV.

Star shaped molecules **4a** and **4b** exhibited HOMO levels of -5.55 and -6.17 eV. In comparison the *p*- and *m*-substituted tetracatenars exhibited lower values for HOMO.

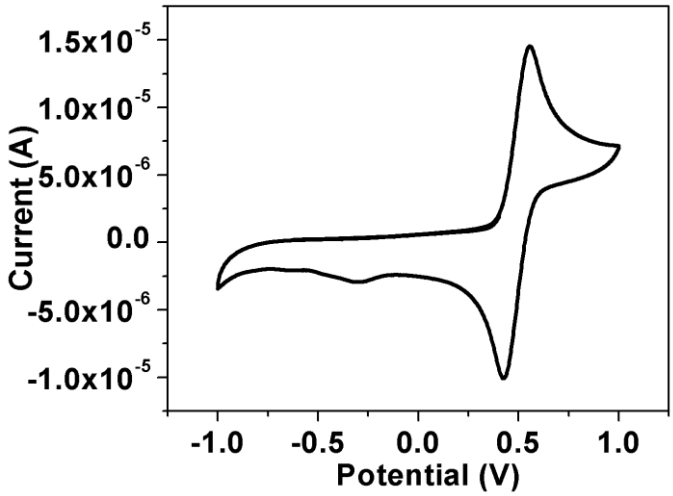

Figure 4.16. Cyclic voltammogram of ferrocene

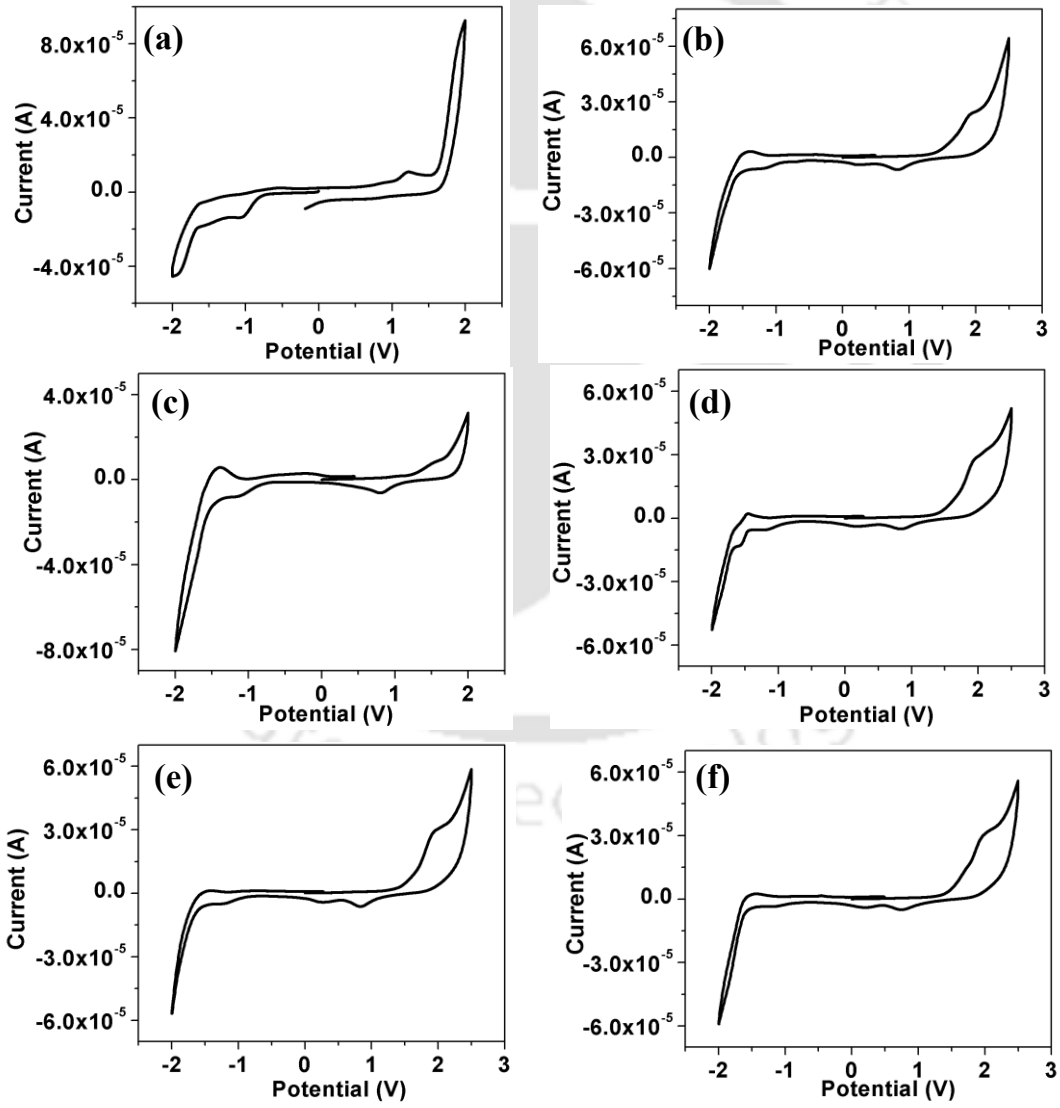

Figure 4.17. Cyclic Voltammograms of compound **4a** (a); **4b** (b); **5a** (c); **5b** (d); **6a** (e); **6b** (f).

The LUMO levels of the star shaped molecules **4a** and **4b** situated at -2.3 and -2.81 eV. In comparison to the star shaped derivatives, the *p*- and *m*-substituted tetracatenars showed lower values of LUMO levels. In comparison to the star shaped thiadiazole derivative **4b**, the *p*- and *m*-substituted tetracatenars (**5b** and **6b**) showed lower values of LUMO levels. In comparison to **4a**, star shaped compound **7a** exhibited lower HOMO and LUMO levels, while the reverse has been observed in the case of thiadiazole derivatives. In comparison to **4b**, the star shaped molecule **7b** showed higher HOMO and LUMO levels. All the thiadiazole based molecules exhibit lower band gap in comparison to oxadiazole based molecules, except compound **4b**.

Table 4.6. Energy levels calculated from cyclic voltammetry[a]

Entry	E_{1oxd}[c]	E_{HOMO}[b,d]	E_{LUMO}[b,e]	$\Delta E_{g,opt}$[b, f]
4a	1.24	-5.55	-2.3	3.05
4b	1.86	-6.17	-2.81	3.36
7a[g]	1.49	-5.76	-2.4	3.36
7b[g]	1.61	-5.88	-2.76	3.12
5a	1.53	-5.84	-2.43	3.41
5b	1.94	-6.25	-3.08	3.17
6a	1.93	-6.24	-2.51	3.73
6b	2.01	-6.32	-2.9	3.42

[a]Micromolar solutions in THF, Experimental conditions: $Ag/AgNO_3$ as the reference electrode, glassy carbon working electrode, platinum rod counter electrode, TBAP (0.1 M) as a supporting electrolyte, room temperature, scanning rate of 0.05 mV s^{-1}; $E_{1/2,Fc,Fc}^{+}$ = 0.49 eV. [b]In electron volts (eV). [c]In volts (V). [d]Estimated from the onset oxidation peak values by using the formula E_{HOMO} = - (4.8 - $E_{1/2,Fc,Fc+}$ + $E_{ox,onset}$) eV. [e]Estimated from the formula E_{LUMO} = ($E_{g,op}$ - E_{HOMO}) eV. [f]Estimated from the formula ΔE_{CV} = E_{LUMO} - E_{HOMO} eV. [f] Band gap determined from the red edge of the longest wave length in the UV-Vis absorption spectra. [g]From reference 11a ($E_{1/2,Fc,Fc}^{+}$ = 0.53)

4.7. Density functional theory (DFT) calculations

We have carried out density functional theory (DFT) calculations using B3LYP hybrid density functional and 6-31G(d,p) basis set for all the calculations and were used to afford the information related to molecular geometry and electronic structure (HOMO-LUMO levels) of all the compounds. For the ease of calculations, we have considered the methoxy analogues of star-shaped molecules (**4a-b, 7a-b**) and tetracatenars (**5a-b, 6a-b**) of all the compounds which are denoted as **4a**^{OMe}, **4b**^{OMe}, **7a**^{OMe}, **7b**^{OMe}, **5a**^{OMe}, **5b**^{OMe}, **6a**^{OMe} and **6b**^{OMe} as the length of the alkyl chains does not affect much on the energy levels.

The energy minimized structures for **4a**^{OMe}, **4b**^{OMe}, **7a**^{OMe} and **7b**^{OMe} are given in Fig. 4.22. The energy minimized structures of tetracatenars **5a**^{OMe}, **5b**^{OMe}, **6a**^{OMe} and **6b**^{OMe} are provided in Fig. 4.23. Pictures of the frontier molecular orbitals (FMOs) and their respective energy levels, provide a knowledge about the length of conjugation and energy band gaps.

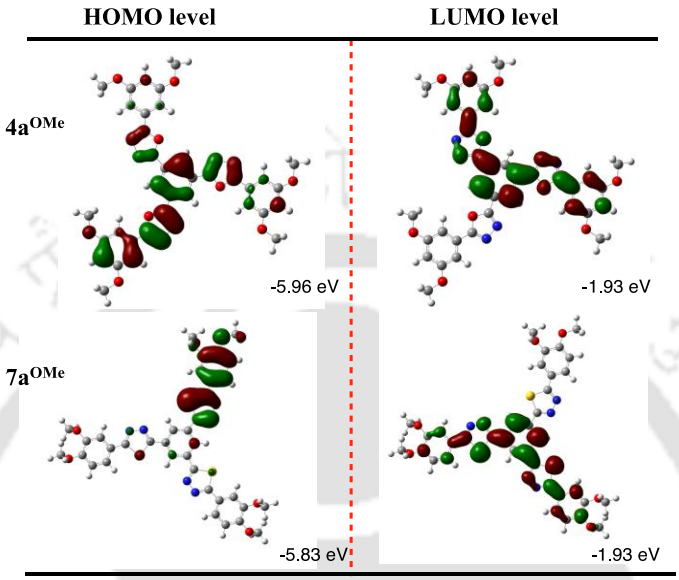

Figure 4.18. HOMO and LUMO frontier molecular orbitals of **4a**^{OMe} and **7a**^{OMe} at the B3LYP/6-31G(d,p) level. HOMO and LUMO denote energies of the highest occupied molecular orbital and the lowest unoccupied molecular orbital, respectively.

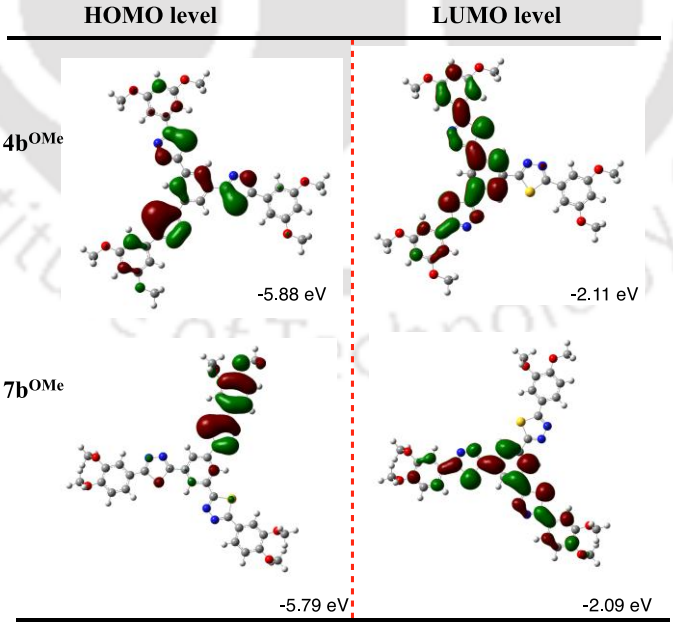

Figure 4.19. HOMO and LUMO frontier molecular orbitals of **4b**^{OMe} and **7b**^{OMe} at the B3LYP/6-31G(d,p) level. HOMO and LUMO denote energies of the highest occupied molecular orbital and the lowest unoccupied molecular orbital, respectively.

The contours of the HOMO and LUMO of star shaped molecules **4a**^{OMe} and **7a**^{OMe} are shown in Fig. 4.18. It is interesting to note that the HOMO levels of 3,5–dimethoxy substituted oxadiazole **4a**^{OMe} shows the distribution of the electron density on one of the arms to the central core along with the adjacent oxadiazole units, while in the case of 3,4–dimethoxy substituted oxadiazole **7a**^{OMe} the electron density is distributed only on one of the arms of the star. Thus the HOMO level of **4a**^{OMe} is situated at a lower level in comparison to that of compound **7a**^{OMe}.

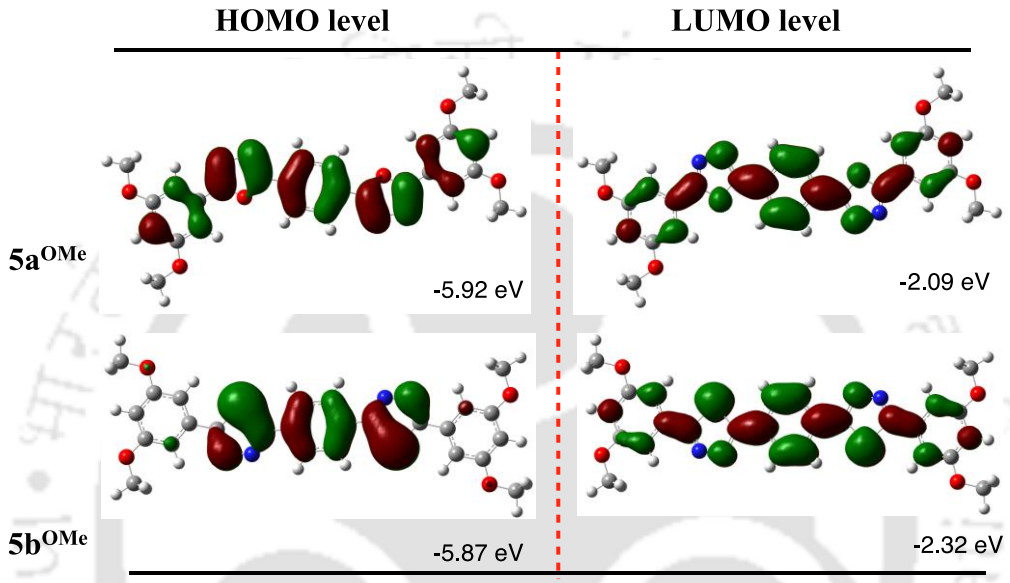

Figure 4.20. HOMO and LUMO frontier molecular orbitals of 5a^{OMe} and 5b^{OMe} at the B3LYP/6-31G(dp) level.

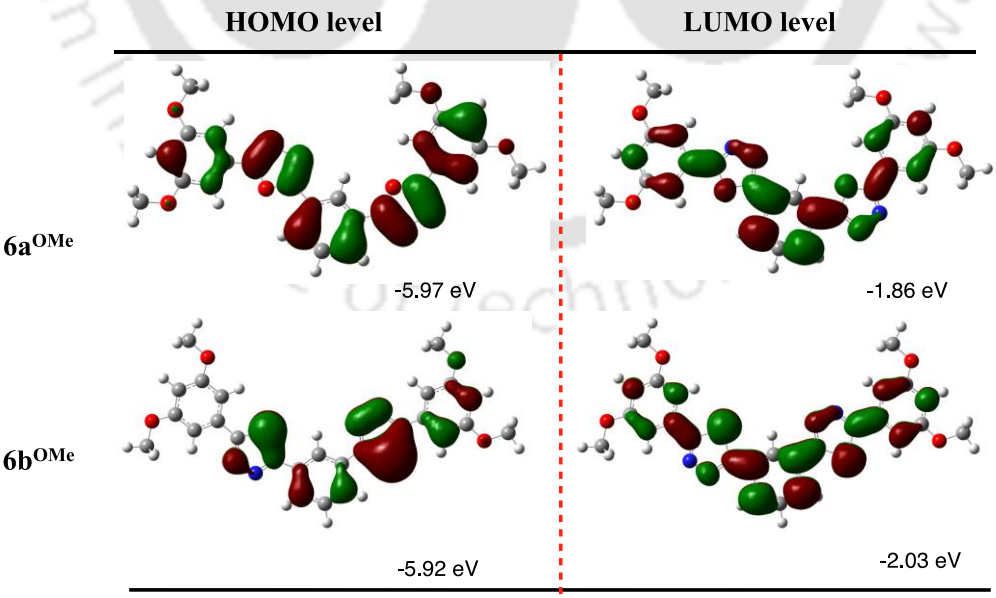

Figure 4.21. HOMO and LUMO frontier molecular orbitals of 5a^{OMe} and 5b^{OMe} at the B3LYP/6-31G(d,p) level.

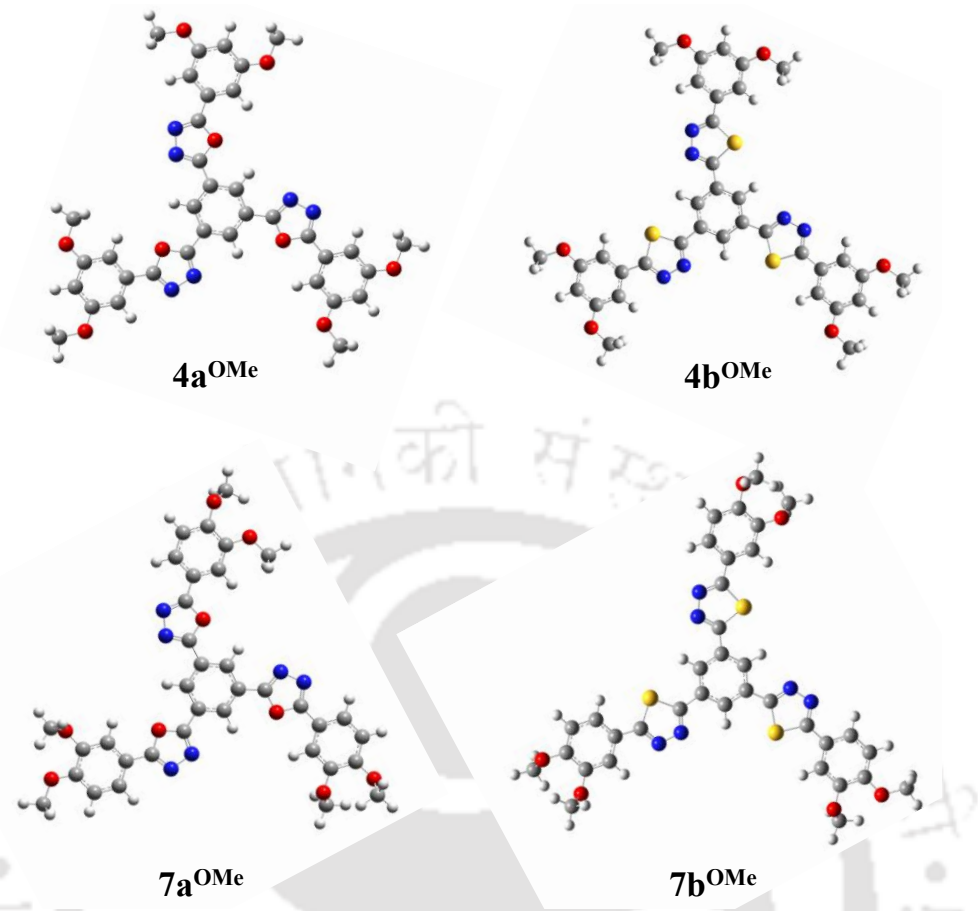

Figure 4.22. Optimized geometry of **4a**^{OMe}, **4b**^{OMe}, **7a**^{OMe} and **7b**^{OMe}

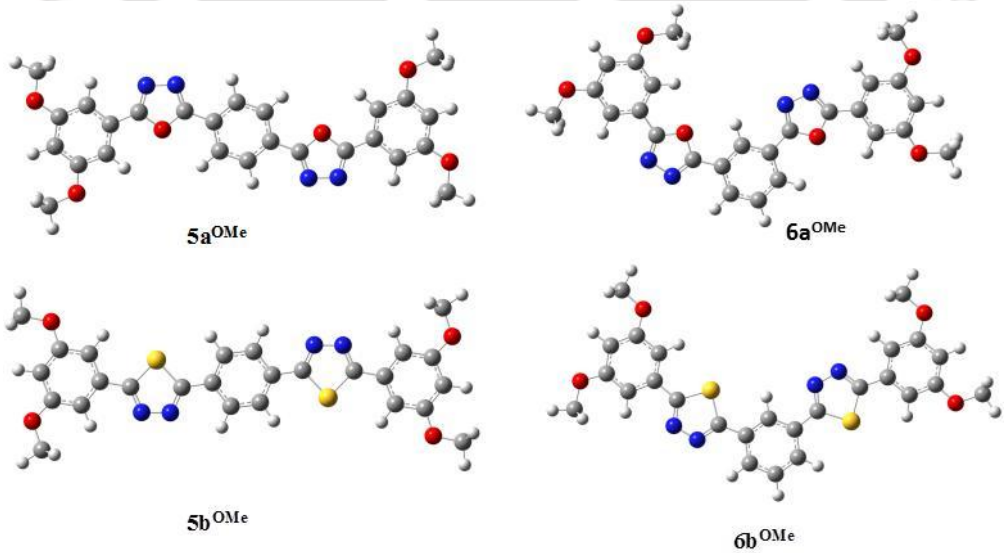

Figure 4.23. Optimized geometry of **5a**^{OMe}, **5b**^{OMe}, **6a**^{OMe} and **6b**^{OMe}

LUMO levels of both the compounds were similar (-1.93 eV), where the electron density is distributed on two arms including the central core. Thus the position of peripheral substitution affects the HOMO level than the LUMO level. We were curious to know the distribution of electron density in corresponding thiadiazole derivatives **4b**^{OMe} and **7b**^{OMe} (Fig. 4.19). Here also the pattern of electron density distribution (*i.e.* the 3,5-substitution *vs* 3,4-substitution) was similar to that of oxadiazole derivatives with respect to substitution. In the case of the HOMO of compound **4b**^{OMe} the electron density distribution was seen on two arms of the star shaped molecule including the central core, while in the case of compound **7b**^{OMe} electron density distribution was seen only on one arm of the molecule. As expected, the HOMO level of **4b**^{OMe} was found to be lower than that of compound **7b**^{OMe}. The electron density of the LUMO levels was found to be distributed on the two arms of the star shaped molecules and there was no much difference in the energy levels. The HOMO levels of the oxadiazole derivatives **4a**^{OMe} and **7a**^{OMe} found to be lower than the corresponding thiadiazole derivatives, while the LUMO levels were found to be higher than the thiadiazole derivatives. Overall the resulting band gap of oxadiazole derivatives was higher (4 eV) in comparison to that of the thiadiazole derivatives (≈ 3.8 eV). This is in line with the earlier studies were oxadiazole based LCs exhibited higher band gaps in comparison to thiadiazole based LCs.[11]

Similarly the energy levels of tetracatenar analogues **5a**^{OMe}, **5b**^{OMe}, **6a**^{OMe} and **6b**^{OMe} were also analyzed. *p*-Substituted tetracatenars **5a**^{OMe}, **5b**^{OMe} (Fig. 4.20) have higher HOMO and lower LUMO levels in comparison to *m*-substituted tetracatenars molecules **6a**^{OMe} and **6b**^{OMe} (Fig. 4.21). The energy gaps of *p*-substituted tetracatenars were also found to be lesser than that of *m*-substituted tetracatenars. Another notable thing was, in the case of oxadiazole based tetracatenars, the electron density distribution was seen across the molecule, while such distribution was not seen in the case of thiadiazole based tetractenars. From these studies it is imperative that the type of hetero cycle and the pattern of peripheral substitution affect the electron density distribution, HOMO-LUMO level and band gap of the conjugated molecules.

4.8. Conclusions

In this report, we have synthesized star-shaped and tetracatenar molecules based on 1,3,4-oxadiazole and thiadiazole derivatives. The peripheral substitution of

alkoxy tails were at 3 and 5 positions of the benzene ring. This substitution has a significant impact on the stabilization of liquid crystalline and gel self-assembly. This was understood by comparing the behavior of newly synthesized star molecules with earlier reported molecules with 3,4-peripheral substitution. The compounds with 3,4 substitution stabilized liquid crystallinity and gelation. In the case of 3,5-substituted star-shaped molecules only oxadiazole derivative stabilized liquid crystallinity and gelation. It is interesting to note that the self-assembly behavior and photophysical properties of these molecules are tremendously sensitive to the type of the heteroatom present in the molecule and the pattern of peripheral substitution. All the tetracatenars were turned out to be crystalline. Considering the gelation is mainly supported by attractive π-π interactions, the role of peripheral alkyl chains and the effect of hetero atom has been analyzed for the first time. The present study also gives a comparison between the molecular requirements for the liquid crystalline self-assembly and organogelation. This class of star shaped molecules is also able to gelate in long chain hydrocarbon solvents at very low concentration. This phenomenon of supergelation even in the absence of attractive H-bonding interactions is exceptional. The effect of peripheral substitution and the type of heteroatom also had a role in the emissive behavior of the compounds in gel state, *i.e.* 3,5-substituted star shaped oxadiazole was AIE active, while the thiadiazole derivative was unable to gelate. In the case of 3,4-substituted star shaped oxadiazole aggregation caused quenching was observed, while in the case of 3,4-substituted star shaped thiadiazole AIE effect was observed. The observation of several fold increase in luminescence intensity upon gelation is important from the viewpoint of emissive solid displays. This report shows that in addition to π-π interactions, nanoseggregation of incompatible molecular subunits like flexible tails also play a major role in stabilizing the organogelation and liquid crystalline self-assembly. The microscopic studies of the xerogels with AFM and SEM showed the entangled network of fibers of several micrometer lengths confirming the long range self-assembly of these molecules. Extensive rheological studies proved the viscoelastic and thixotropic nature of the gels. Electrochemical and DFT studies have shown that, the peripheral substitution significantly affects the HOMO-LUMO levels and the band gaps of the molecules. Finally, this study provides a complete account on the effect of small variations at molecular scale and

its impacts on the nature of supramolecular self-assembly which is of significant relevance in supramolecular chemistry.

4.9. Experimental Section

In this section the detailed synthetic procedures and the molecular structural characterization data have been presented for the intermediates and target compounds mentioned in the scheme.

Ethyl 3,5-dihydroxybenzoate (**1**)

3,5-dihydroxybenzoic acid (5 g, 32.44 mmol.)was dissolved in 20 mL ethanol and catalytic amount of sulphuric acid was added and the reaction mixture was refluxed for 24 h. Nearly 70% of ethanol was distilled off and the reaction mixture was diluted with water and sulphuric acid and unreacted benzoic acid were neutralised with saturated solution of sodium bicarbonate and then extracted with ethyl acetate, washed with water, brine and dried over anhydrous Na_2SO_4, concentrated and finally recrystallized from ethanol.

1: R_f = 0.5 (50% EtOAc-hexane); a brownish solid; mp: 120-125 ^oC; yield: 70-75%; IR (KBr pellet): ν_{max} cm^{-1} 3304, 2997, 1690, 1680, 1607, 1465, 1372, 1338, 1163, 1029, 871, 766; ^1H NMR (CD_3OD, 600 MHz): δ 6.93 (s, 2H, Ar), 6.47 (s, 1H,Ar), 4.89 (s, 2H, 2×OH), 4.31-4.27 (m, 2H, OCH_2), 1.33 (t, 3H, 1×CH_3), ^{13}C NMR (CD_3OD, 150MHz): 168.20, 159.70, 133.32, 108.74, 108.15, 62.03, 14.53; HRMS (ESI+) exact Mass calculated for $C_9H_{11}O_4$ (M+1): 183.0652, found: 183.0658.

Procedure for the synthesis of ethy-l,3,5-bis(decyloxy)benzoate (**2**)[1]

A mixture of ethyl 3,5-dihydroxybenzoate (1equiv.), anhydrous K_2CO_3 (4.4 equiv.), *n*-bromodecane (2.2 equiv.) were taken in dry DMF (20 ml) and heated at 80 ^oC for 17 h under nitrogen atmosphere. Then the reaction mixture was poured into ice-water and extracted with CH_2Cl_2. The combined extract was washed with water and brine, dried over anhydrous Na_2SO_4 and concentrated. The crude product was purified by column chromatography on silica gel. Elution with hexanes followed by 5-10% ethylacetate-hexanes yielded the desired product.

2: R_f = 0.8 (5% EtOAc-hexane); a viscous colorless liquid; yield: 75-80%; IR (KBr pellet): ν_{max} cm^{-1} 2923, 2852, 1722, 1601, 1445, 1468, 1390, 1326, 1232, 1167, 1128, 1055, 858, 762, 720; ^1H NMR ($CDCl_3$, 600 MHz): δ 7.16 (s, 2H, Ar), 6.62 (s, 1H,Ar), 4.37-4.33 (m, 2H, OCH_2), 3.96 (t, 4H, 2×OCH_2), 1.79 -1.27 (m, 35H, 16×CH_2, 1×CH_3), 0.88(t, 6H, 2×CH_3), ^{13}C NMR ($CDCl_3$, 150MHz): 166.75, 160.32, 132.38, 107.81, 106.47, 68.49, 61.27, 32.11, 29.77, 29.58, 29.54, 29.40, 26.22, 22.90, 14.53; HRMS (ESI+) exact Mass calculated for $C_{29}H_{51}O_4$ (M+1): 463.3782, found: 463.3782.

Procedure for the synthesis of 3,5-bis(decyloxy)benzohydrazide (**3**)[2]

A mixture of ethyl 3,5-bis(decyloxy)benzoate (10 mmol, 1equiv.), excess hydrazine hydrate (10 mL), *n*-butanol (20 mL) was refluxed for 40 h. Water (100 mL) was added and resulting precipitate was collected, dried under vacuum, and recrystallized from ethanol to yield pure **3** as a white solid.

3: R_f = 0.3 (20% EtOAc-hexane); a white solid; mp: 72-75 ^oC; yield: 65-70%; IR (KBr pellet): ν_{max} cm^{-1} 3368, 3312, 3129, 2942, 2920, 2851, 1642, 1594, 1517, 1468, 1392, 1358, 1304, 1178, 1077, 1052, 1035, 836, 764, 721, 684; ^1H NMR ($CDCl_3$, 600 MHz): δ 7.48 (broad s, 1H, CONH), 6.83 (s, 2H, Ar) 6.57 (s, 1H, Ar), 3.94 (t, 4H, 2×OCH_2), 3.10 (broad s, 2H, NH_2), 1.78-1.26 (m, 32H, 16×CH_2), 0.89-0.86 (m, 6H, 2×CH_3), ^{13}C NMR ($CDCl_3$, 100MHz): 168.91, 160.64, 134.67, 105.31, 104.98, 68.53, 32.10, 29.78, 29.76, 29.57, 29.52, 29.35, 26.20, 22.89, 14.33; HRMS (ESI+) exact Mass calculated for $C_{27}H_{49}N_2O_3$ (M+1): 449.3738, found: 449.3744.

Procedure for the synthesis of 1,3,5-tris(5-(3,5-bis(decyloxy)phenyl)-1,3,4-oxadiazol-2-yl)benzene **(4a)**[2]

Benzene-1,3,5-tricarboxylic acid (1 equiv.) in 4.5 mL of thionyl chloride and DMF (catalytic amount) was heated under reflux for 4 h. The excess of thionyl chloride was removed by distillation; the crude product (benzene-1,3,5-tricarbonyl trichloride) was dried in vacuo and used for the next reaction without further purification and characterization. The solution of benzene-1,3,5-tricarbonyl trichloride (1equiv.) in THF was added dropwise to a solution of 3,5-bis(decyloxy)benzohydrazide (3.3 equiv.) and triethylamine (3 equiv.) in THF (20 mL). The reaction mixture was stirred at 55 ^oC for 12 h. After cooling, THF was removed through distillation and the residue was extracted with dichloromethane. The extract was washed with water and brine. Dried over anhydrous Na_2SO_4 and concentrated. The resulting crude product was directly used for next reaction where the crude product (1 equiv.) was taken in $POCl_3$ and refluxed for 24 h. The reaction mixture was cooled to room temperature and carefully added to ice-water and extracted with chloroform. After removal of solvent *in vacuo*, the crude product was purified through column chromatography on neutral alumina. Elution with 30-40% ethylacetate-hexane yielded the desired product which was further recrystallized in ethanol.

4a: R_f = 0.85 (50% EtOAc-hexane); a dirty white solid; yield: 55-60%; IR (KBr pellet): ν_{max} cm^{-1} 2921, 2851, 1599, 1551, 1541, 1467, 1441, 1386, 1362, 1290, 1175, 1060, 855, 834, 734, 721, 678; ^1H NMR ($CDCl_3$, 400 MHz): δ 9.04 (s,3H, Ar), 7.32 (d, *J* = 4 Hz, 6H, Ar), 6.66 (s, 3H, Ar), 4.07-4.04 (m, 12H, 6×OCH_2), 1.86-1.22 (m, 96H, 48×CH_2), 0.89-0.86 (m, 18H, 6×CH_3), ^{13}C NMR ($CDCl_3$, 100MHz): 165.89, 163.00, 161.02, 127.56, 126.41, 124.77, 105.79, 105.57, 68.72, 32.12, 29.82, 29.81, 29.64, 29.56, 29.42, 26.27, 22.91, 14.36; MALDI Tof MS ES+ for $C_{90}H_{139}N_6O_9$ (M+1), Calculated :1448.059, Found: 1448.264.

Procedure for the synthesis of 1,4-bis(5-(3,5-bis(decyloxy)phenyl)-1,3,4-oxadiazol-2-yl)benzene (**5a**)[3]

Terephthalic acid (1 eqiv.) in 4.5 mL of thionyl chloride and DMF (catalytic amount) was heated under reflux for 4 h. The excess of thionyl chloride was removed by distillation; the crude product (terephthaloyl dichloride) was dried in vacuo and used for the next reaction without further purification and characterization. The solution of terephthaloyl dichloride (1 equiv.) in THF was added dropwise to a solution of 3,5-bis(decyloxy)benzohydrazide (2.2 equiv.) and triethylamine (2 equiv.) in THF (20 mL). The reaction mixture was stirred at 55 ^{o}C for 12 h. After cooling, THF was removed through distillation and the residue was extracted with dichloromethane. The extract was washed with water and brine, dried over anhydrous Na_2SO_4 and concentrated. The resulting crude product was directly used for next reaction where the crude product (1equiv.) was taken in $POCl_3$ and refluxed for 24 h. The reaction mixture was cooled to room temperature and carefully added to ice-water and extracted with chloroform. After removal of solvent *in vacuo*, the crude product was purified through column chromatography on neutral alumina. Elution with 30-40% ethylacetate-hexane yielded the desired product, which was further recrystallized in ethanol.

5a: R_f = 0.89 (50% EtOAc-hexane); off white solid; yield: 47-52 %; IR (KBr pellet): νmax cm^{-1} 2921, 2851, 1598, 1546, 1493, 1468, 1443, 1356, 1300, 1178, 1049, 838, 853, 731, 680; ^{1}H NMR ($CDCl_3$, 400 MHz): δ 8.30 (s, 4H, Ar), 7.27-7.25 (m, 4H, Ar), 6.63 (s, 2H, Ar), 4.04-4.01 (m, 8H, 4×OCH_2), 1.85-1.27 (m, 64H, 32×CH_2) 0.89-0.86 (m, 12H, 4×CH_3), ^{13}C NMR ($CDCl_3$, 100MHz): 165.35, 163.88, 160.96, 127.72, 126.77, 125.07, 105.48, 105.37, 68.67, 32.12, 29.81, 29.79, 29.61, 29.55, 29.40,26.25, 22.91, 14.36; MALDI Tof MS ES+ for $C_{62}H_{95}N_4O_6$ (M+1), Calculated: 991.724, Found: 991.503.

Procedure for the synthesis of 1,3-bis(5-(3,5-bis(decyloxy)phenyl)-1,3,4-oxadiazol-2-yl)benzene (**6a**)[3]

Isophthalic acid (1 equiv.) in 4.5 mL of thionyl chloride and DMF (catalytic amount) was heated under reflux for 4 h. The excess of thionyl chloride was removed by distillation; the crude product (isophthaloyl dichloride) was dried in vacuo and used for the next reaction without further purification and characterization. The solution of isophthaloyl dichloride (1equiv.) in THF was added dropwise to a solution of 3,5-bis(decyloxy)benzohydrazide (2.2 equiv.) and triethylamine (2 equiv.) in THF (20 mL). The reaction mixture was stirred at 55 ^{o}C for 12 h. After cooling, THF was removed through distillation and the residue was extracted with dichloromethane. The extract was washed with water and brine, dried over anhydrous Na_2SO_4 and concentrated. The resulting crude product was directly used for next reaction where the crude product (0.4 mmol, 1equiv.) was taken in $POCl_3$ and refluxed for 24 h. The reaction mixture was cooled to room temperature and carefully added to ice-water and extracted with chloroform. After removal of solvent *in vacuo*, the crude product was purified through column chromatography on neutral alumina. Elution with 30-40% ethylacetate-hexane yielded the desired product which was further recrystallized in ethanol.

6a: R_f = 0.88 (50% EtOAc-hexane); off white solid; yield: 51-56%; IR (KBr pellet): νmax cm^{-1} 2921, 2851, 1601, 1551, 1467, 1442, 1299, 1174, 1058, 857, 834, 731; ^1H NMR ($CDCl_3$, 600 MHz): δ 8.89 (s, 1H, Ar), 8.33 (d, *J* =4 Hz, 2H, Ar), 7.73 (t, 1H, Ar), 7.29 (s, 4H, Ar), 6.54 (s, 2H, Ar), 4.04 (t, 8H, 4 × OCH_2) 1.83-1.28 (m, 64H, 32 × CH_2) 0.88 (t, 12H, 4 × CH_3), ^{13}C NMR ($CDCl_3$, 150MHz): 165.42, 163.84, 161.00, 130.20, 130.02, 125.33, 125.29, 125.12, 105.52, 68.70, 32.11, 29.79, 29.61, 29.54, 29.42, 26.25, 22.90, 14.34; MALDI Tof MS ES+ for $C_{62}H_{95}N_4O_6$ (M+1), Calculated: 991.724, Found: 991.894.

Procedure for the synthesis of 1,3,5-tris(5-(3,5-bis(decyloxy)phenyl)-1,3,4-thiadiazol-2-yl)benzene **(4b)**[2]

Benzene-1,3,5-tricarboxylic acid (1 equiv.) in 4.5 mL of thionyl chloride and DMF (catalytic amount) was heated under reflux for 4 h. The excess of thionyl chloride was removed by distillation; the crude product (benzene-1,3,5-tricarbonyl trichloride) was dried in vacuo and used for the next reaction as such. The solution of benzene-1,3,5-tricarbonyl trichloride (1equiv.) in THF was added dropwise to a solution of 3,5-bis(decyloxy)benzohydrazide (3.3 equiv.) and triethylamine (3 equiv.) in THF (20 mL). The reaction mixture was stirred at 55 ^oC for 12 h. After cooling, THF was removed through distillation and the residue was extracted with dichloromethane. The extract was washed with water and brine, dried over anhydrous Na_2SO_4 and concentrated. The resulting crude product was directly used for next reaction. The crude product (1equiv.) was taken in dry toluene (8 mL) was added dropwise to a solution of Lawesson's reagent (3.6 equiv.) at room temperature under Argon atmosphere and refluxed for 24 h. Toluene was removed by distillation. After removal of solvent *in vacuo*, the crude product was purified through column chromatography on neutral alumina. Elution with 30-40% ethylacetate-hexanes yielded the desired product which was further recrystallized in ethanol.

4b: R_f = 0.7 (50% EtOAc-hexane); a brown solid; yield: 45-50 %; IR (KBr pellet): νmax cm^{-1} 2924, 2853, 1600, 1458, 1422, 1389, 1345, 1169, 1057, 840, 739, 675; ^1H NMR ($CDCl_3$, 600 MHz): δ 8.73 (s, 3H, Ar), 7.16 (s, 6H, Ar), 6.60 (s, 3H, Ar), 4.04-4.01 (m, 12H, 6 × OCH_2), 1.84-1.24 (m, 96H, 48 × CH_2), 0.88 (t, 18H, 6 × CH_3), ^{13}C NMR ($CDCl_3$, 100MHz): 169.48, 165.97, 160.85, 132.29, 131.25, 128.57, 106.40, 104.78, 68.60, 32.13, 29.84, 29.82, 29.62, 29.57, 29.44, 26.25, 22.91, 14.35. MALDI Tof MS ES+ for $C_{90}H_{139}N_6O_6S_3$ (M+1), calculated: 1495.9913, Found: 1496.623.

Procedure for the synthesis of 1,4-bis(5-(3,5-bis(decyloxy)phenyl)-1,3,4-thiadiazol-2-yl)benzene (**5b**)[3]

Terephthalic acid (1equiv.) in 4.5 mL of thionyl chloride and DMF (catalytic amount) was heated under reflux for 4 h. The excess of thionyl chloride was removed by distillation; the crude product (terephthaloyl dichloride) was dried in vacuo and used for the next reaction as such. The solution of terephthaloyl dichloride (1 equiv.) in THF was added dropwise to a solution of 3,5-bis(decyloxy)benzohydrazide (2.2 equiv.) and triethylamine (2 equiv.) in THF (20 mL). The reaction mixture was stirred at 55 ^oC for 12 h. After cooling, THF was removed through distillation and the residue was extracted with dichloromethane. The extract was washed with water and

brine, dried over anhydrous Na_2SO_4 and concentrated. The resulting crude product was directly used for next reaction. Here the crude product (1 equiv.) was taken in dry toluene (8 mL) to which a solution of Lawesson's reagent (2.4 equiv.) was added dropwise at room temperature under Argon atmosphere and then refluxed for 24 h. Toluene was removed by distillation. After removal of solvent *in vacuo*, the crude product was purified through column chromatography on neutral alumina. Elution with 30-40% ethylacetate-hexane yielded the desired product which was further recrystallized in ethanol.

5b: R_f = 0.7 (50% EtOAc-hexane); off white solid; yield: 47-52%; IR (KBr pellet): νmax cm^{-1} 2920, 2851, 1595, 1463, 1421, 1388, 1345, 1291, 1060, 987, 839, 772, 722, 678; ^{1}H NMR ($CDCl_3$, 600 MHz): δ 8.13 (s, 4H, Ar), 7.15 (s, 4H, Ar), 6.59 (s, 2H, Ar), 4.02 (t, 8H, 4×OCH_2) 1.88-1.28 (m, 64H, 32×CH_2), 0.88 (t, 12H, 4×CH_3), ^{13}C NMR ($CDCl_3$, 100MHz): 168.48, 166.52, 160.34, 132.00, 130.95, 128.16, 105.94, 104.18, 68.06, 31.56, 29.25, 29.23, 29.05, 28.99, 28.84, 25.68, 22.35, 13.79. MALDI Tof MS ES+: m/z for $C_{62}H_{95}N_4O_4S_2$(M+1), Calculated: 1024.6828 Found: 1024.606.

Procedure for the synthesis of 1,3-bis(5-(3,5-bis(decyloxy)phenyl)-1,3,4-thiadiazol-2-yl)benzene (**6b**)[3]

Isophthalic acid (1 equiv.) in 4.5 mL of thionyl chloride and DMF (catalytic amount) was heated under reflux for 4 h. The excess of thionyl chloride was removed by distillation; the crude product (isophthaloyl dichloride) was dried in vacuo and used for the next reaction as such. The solution of isophthaloyl dichloride (1equiv.) in THF was added dropwise to a solution of 3,5-bis(decyloxy)benzohydrazide (2.2 equiv.) and triethylamine (2 equiv.) in THF (20 mL). The reaction mixture was stirred at 55 ^oC for 12 h. After cooling, THF was removed through distillation and the residue was extracted with dichloromethane. The extract was washed with water and brine, dried over anhydrous Na_2SO_4 and concentrated. The resulting crude product was directly used for next reaction. Here the crude product (1 equiv.) was taken in dry toluene (8 mL) to which to a solution of Lawesson's reagent (2.4 equiv.) was added dropwise at room temperature under Argon atmosphere and refluxed for 24 h. Toluene was removed by distillation. After removal of solvent *in vacuo*, the crude product was purified through column chromatography on neutral alumina. Elution with 30-40% ethylacetate-hexane yielded the desired product which was further recrystallized in ethanol.

6b: R_f = 0.69 (50% EtOAc-hexane); dirty white solid; yield: 52-55%; IR (KBr pellet): νmax cm^{-1} 2921, 2852, 1594, 1452, 1432, 1389, 1344, 1056, 836, 721; ^{1}H NMR ($CDCl_3$, 600 MHz): δ 8.58 (s, 1H, Ar), 8.14 (d, *J* =12Hz, 2H, Ar), 7.63 (t, 1H, Ar), 7.15 (s, 4H, Ar), 6.59 (s, 2H, Ar), 4.02 (t, 8H, 4×OCH_2), 1.83-1.28 (m, 64H, 32×CH_2) 0.88 (t, 12H, 4×CH_3), ^{13}C NMR ($CDCl_3$, 100 MHz): 169.02, 167.05, 160.87, 160.81, 131.48, 131.37, 130.20, 127.25, 106.45, 104.58, 68.58, 32.11, 29.80, 29.78, 29.60, 29.54, 29.39, 26.22, 22.89, 14.34. MALDI Tof MS ES+: m/z for $C_{62}H_{95}N_4O_4S_2$(M+1), Calculated: 1024.6828 Found: 1024.606.

4.10. References

1. (a) S. R. Forrest, *Nature*, 2004, **428**, 911-918; (b) A. Facchetti, *Chem. Mater*., 2011, **23**, 733–758.
2. (a) *Self-Organized Organic Semiconductors: From Materials to Device Applications* (Ed.: Q. Li), Wiley, Hoboken, 2011; (b) *Organic Electronics: Materials, Manufacturing and Applications* (Ed.: H. Klauk), Wiley-VCH, Weinheim, 2006; (c) J. Roncali, P. Leriche, A. Cravino, *Adv. Mater*. 2007, **19**, 2045 – 2060; (d) S. R. Forrest, M. E. Thompson, *Chem. Rev.* 2007, **107**, 923-925; (e) E. Menard, M. A. Meitl, Y. Sun, J.-U. Park, D. J.-L. Shir, Y.-S. Nam, S. Jeon, J. A. Rogers, *Chem. Rev*. 2007, **107**, 1117-1160.
3. (a) D. K. Smith, *Supramolecular Chemistry: From Molecules to Nanomaterials* (John Wiley and Sons, Inc., 1999); (b) T. Aida, E. W. Meijer, S. I. Stupp, *Science*, 2012, **335,** 813–817; (c) M. J. Hollamby, M. Karny, P. H. H. Bomans, N. A. J. M. Sommerdijk, A. Saeki, S. Seki, H. Minamikawa, I. Grillo, B. R. Pauw, P. Brown, J. Eastoe, H. Möhwald, T. Nakanishi, *Nat. Chem.*, 2014, **6**, 690–696.
4. (a) S. S. Babu, V. K. Praveen, A. Ajayaghosh, *Chem Rev*, 2014, **114 (4)**, 1973–2129; (b) S. S. Babu, S. Prasanthkumar, A. Ajayaghosh, *Angew. Chem. Int. Ed.*, 2012, **51**, 1766–1776.
5. J. D. Tovar, *Acc. Chem. Res.*, 2013, **46 (7)**, 1527–1537.
6. T. Kato, Y. Hirai, S. Nakaso, M. Moriyama, *Chem Soc Rev*, 2007, **36**, 1857-1867.
7. (a) E.-K. Fleischmann, R. Zentel, *Angew. Chem. Int. Ed.*, 2013, **52**, 8810–8827; (b) M. Bremer, P. Kirsch, M. K. –Memmer, K. Tarumi, *Angew. Chem. Int. Ed.*, 2013, **52**, 8880–8896; (c) M. Funahashi, *J. Mater. Chem. C*, 2014, **2**, 7451-7459.
8. T. Wöhrle, I. Wurzbach, J. Kirres, A. Kostidou, N. Kapernaum, J. Litterscheidt, J. C. Haenle, P. Staffeld, A. Baro, F. Giesselmann, S. Laschat, *Chem Rev*, 2016, **116**, 1139–1241.
9. (a) X. Dou, W. Pisula, J. Wu, G. J. Bodwell and K. Müllen, *Chem. Eur. J.*, 2007, **14**, 240–249. (b) Y. Hirai, H. Monobe, N. Mizoshita, M. Moriyama, K. Hanabusa, Y. Shimizu, T. Kato, *Adv. Funct. Mater.*, 2008, **18**, 1668–1675. (c) Y. F. Bai, K. Q. Zhao, P. Hu, B. Q. Wang and Y. Shimizu, *Molecular Crystals and Liquid Crystals*, 2009, **509**, 60/[802]–76/[818]. (d) B. Bai, C. Zhang, J. Wei, J. Ma, X. Lin, H. Wang, M. Li, *RSC Adv.*, 2013, **3**, 12109-12116. (e) E. Diaz, E. Elgueta, S. A. Sanchez, J. Barbera, J. Vergara, M. Parra, M. Dahrouch, *Soft Matter*, 2017, **13**, 1804–1815. (f) S. K. Pathak, B. Pradhan, M. Gupta, S. K. Pal, A. A. Sudhakar, *Langmuir*, 2016, **32**, 9301−9312.
10. (a) S. K. Pathak, B. Pradhan, R. K. Gupta, M. Gupta, S. K. Pal, A. S. Achalkumar, *J. Mater. Chem. C*, 2016, **4**, 6546-6561; (b) S. K. Pathak, M. Gupta, S. K. Pal, A. S. Achalkumar, *Chemistry Select*, 2016, **1**, 5107 – 5120; (c) B. Pradhan, M. Gupta, S. K. Pal, A. S. Achalkumar, *J.Mater.Chem.C*, 2016, **4**, 9669-9673; (d) B. Pradhan, V. M. Vaisakh, G. G. Nair, D. S. S. Rao, S. K. Prasad, A. A. Sudhakar, *Chem. Eur. J.*, 2016, **22**, 17843 – 17856.
11. (a) S. K. Pathak, R. K. Gupta, S. Nath, D. S. S. Rao, S. K. Prasad, A. S. Achalkumar, *J. Mater. Chem. C*, 2015, **3**, 2940—2952; (b) S. K. Pathak, S. Nath, R. K. Gupta, D. S. S. Rao, S. K. Prasad, A. S. Achalkumar, *J. Mater. Chem. C*, 2015, **3**, 8166—8182.

12. (a) C. Adachi, T. Tsutui, S. Saito, *Appl. Phys. Lett.*, 1990, **56**, 799–801; (b) H. Antoniadis, M. Inbasekaran, E. P. Woo, *Appl. Phys. Lett.*, 1998, **73**, 3055–3057; (c) N.-X. Hu, M. Esteghamatian, S. Xie, Z. Popovic, Ah.-M. Hor, O. Beng, S. Wang, *Adv. Mater.*, 1999, **11**, 1460–1463; (d) S. Tao, Z. Peng, P. Wang, C.-S. Lee, S.-T. Lee, *Adv. Funct. Mater.*, 2005, **15**, 1716–1721.
13. A. Takahashi, M. Sakai, T. Kato, *Polym. J.*, 1980, **12**, 335-341.
14. (a) Z.-X. Liu, Y. Feng, Z.-C. Yan, Y.-M. He, C.-Y. Liu, Q.-H. Fan, *Chem. Mater.*, 2012, **24**, 3751–3757. (b) A. Gopal, R. Varghese, A. Ajayaghosh, *Chem. – Asian J.*, 2012, **7**, 2061–2067; (c) Q. G. Wang, J. L. Mynar, M. Yoshida, E. Lee, M. Lee, K. Okuro, K. Kinbara, T. Aida, *Nature*, 2010, **463**, 339–343; (d) H. M. Wang, C. H. Yang, M. Tan, L. Wang, D. L. Kong, Z. M. Yang, *Soft Matter*, 2011, **7**, 3897-3905.
15. L. E. Buerkle, S. J. Rowan, *Chem. Soc. Rev.*, 2012, **41**, 6089–6102.
16. (a) S. K. Pathak, B. Pradhan, R. K. Gupta, M. Gupta, S. K. Pal and A. S. Achalkumar, *J. Mater. Chem. C*, 2016, **4**, 6546–6561; (b) A. P. Sivadas, N. S. S. Kumar, D. D. S. Varghese, S. K. Prasad, D. S. S. Rao, S. Das, *J. Am. Chem. Soc.*, 2014, **136**, 5416-5423.
17. J. Mei, N. L. C. Leung, R. T. K. Kwok, J. W. Y. Lam, B. Z. Tang, *Chem. Rev.*, 2015, **115**, 11718–11940.
18. J. B. Birks, *Photophysics of Aromatic Molecules*; Ed.; Wiley: London, 1970
19. (a) C. G. Robertson, X. Wang, *Phys. Rev. Lett.* 2005**, 95**, 075703; (b) P. Sollich, F. Lequeux, P. Hebraud, M. E. Cates, *Phys. Rev. Lett.* 1997**, 78**, 2020-2023; (c) H. M. Wyss, K. Miyazaki, J. Mattsson, Z. Hu, D. R. Reichman, D. A. Weitz, *Phys. Rev. Lett.*, 2007**, 98**, 238303; (d) S. K. Pal, A. Agarwal, N. L. Abbott, *Small*, 2009**, 5**, 2589-2596.
20. S. B. Ross-Murphy, *J. Rheol.*, 1995, **39**, 1451-1463.

Chapter V

Tetrazole based supergelator as a sensitive and selective sensor for picric acid

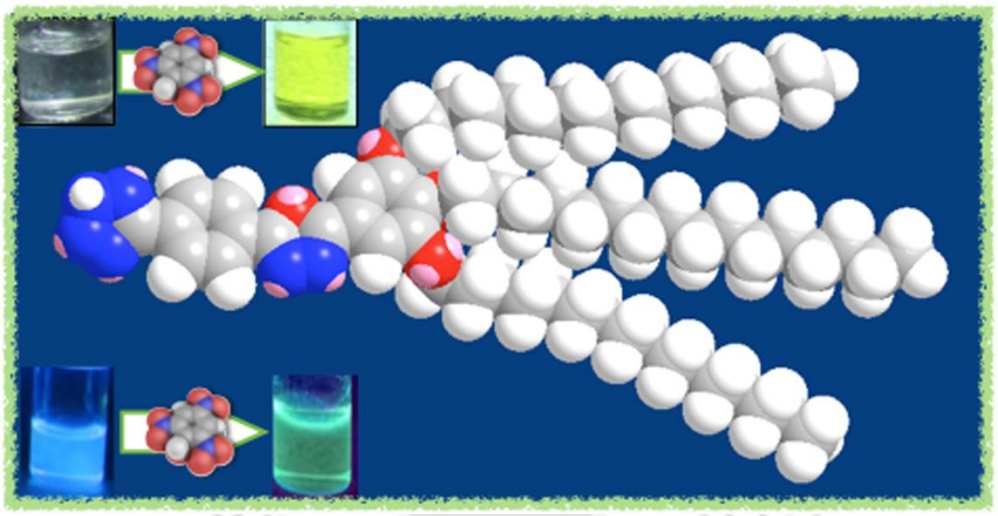

Results have been submitted.

5.1. Introduction

Sensitive and selective detection of explosives is an area of paramount importance in the present era. The increasing number of terror attacks on human civilization is pressing scientists to device an effective way to detect explosives. Apart from this, increasing industrial effluents are causing severe damages to our environment by contaminating the land and water bodies, posing serious health related hazards. Picric acid (PA) is a very powerful explosive, which is even stronger than trinitrotoluene (TNT).[1] Phenols are one of the most common organic water pollutants due to the high solubility and toxicity at very low concentrations. Out of various phenol derivatives, picric acid or 2,4,6-trinitro phenol is a strong organic acid and highly toxic.[1] It seriously affects human eyes, skin and respiratory systems, liver malfunction, and also causes chronic diseases like anemia, cancer, and cyanosis.[2] In spite of that, it's use is inevitable in dye industries, pharmaceuticals, rocket fuel manufacturing, and chemical laboratories.[3] As a result of it's widespread use in several industries and high water solubility, it is contaminating water and soil. Therefore the detection of PA and similar nitro aromatic explosives is of great importance. The specific recognition of PA remains a challenging task for researchers because of the similar electron deficient nature of all the nitro explosives and hence it is an exciting area of research. Various methodologies based on spectroscopic,[4] electrochemical techniques have been utilized for this purpose. [5] Similarly, several small molecule sensors,[6] nanoparticles,[7] nanofibers,[8] gels [9] polymers[10] and metal organic frameworks (MOFs)[11] etc. have been designed for the detection of picric acid. Among these different techniques, especially the fluorescence sensors have high potential and advantages, because of their high sensitivity, cost efficiency, portability, simple instrumentation, easy sample preparation and quick response. This field has caught the attention of researchers and hence several fluorescent sensors for PA have been reported, even though a decade has passed after the first report on a selective PA sensor.[12] Notably, many of these fluorescent sensors show quenching of the fluorescence in response to PA, but the sensors which show a shift in the emission in response to nitroaromatics are rare.[13] Shifting of emission in the visible region produce a change in the emission color, which eases the detection process, thus enabling the naked eye detection with the minimization of errors in the detection. Further, it is

challenging to develop such a sensor, which detects the PA with high selectivity and low detection limit.

Gelators are a class of self-assembled soft matter, which are finding increasing applications in tissue engineering, drug delivery, sensors, light harvesting and photo responsive systems.[14] Tetrazoles form an important class of 5-membered heterocyclic compounds, with a high range of pharmacological and biological activity. The acidic proton of 1-H-tetrazole can form hydrogen bonding (H-bonding) with any electronegative atoms and its application as a fluoride sensor has been reported recently due to its low pKa (3-5) value.[15] In the present work, we report a low molecular weight gelator **1** that consists of a tetrazole unit, a substituted 1,3,4-oxadiazole unit, and long flexible alkyl chains (Fig. 5.1). The oxadiazole unit serves as a fluorophore, the long alkyl chains were selected for their hydrophobic interaction and for stabilizing gelation, while the tetrazole unit acts as a polar unit with an ability to form H-bonding. Tetrazole moiety has been utilized in the molecular design of calamitic[16a-c] and metal containing mesogens.[16d] This has been also utilized in the stabilization of hydrogels[17a-b] and organogels.[17c-d] However reports on tetrazole containing gelators, especially used for the sensing purpose of aromatic explosives, remain rare.[17e-f]

5.2. Results and discussion

5.2a. Synthesis and Characterization

The detailed synthetic route is provided in scheme 1. Ethyl-3,4,5-trihexadecyloxybenzoate (**5**) was obtained from ethyl-3,4,5-trihydroxybenzoate by *O*-alkylation, following the Willimson's ether synthesis protocol. This ester was converted to its benzhydrazide (**4**) by treating with hydrazine hydrate in ethanol. The synthesis of these compounds is reported earlier.[18] The benzhydrazide (**4**) was further treated with 4-cyanobenzoylchloride (**3**) in presence of triethylamine in THF. The compound obtained was subjected to $POCl_3$ mediated dehydrocyclisation to give compound **2**. These compounds were then treated with NaN_3 and NH_4Cl in DMF, to obtain the target tetrazole **1**, through Huisgen 1,3-dipolar cycloaddition reaction. The target molecule obtained was insoluble in common organic solvents and found to be soluble in highly polar solvents like dimethylformamide (DMF) and dimethylsulfoxide (DMSO), on heating. It had a good thermal stability at least up to 279 ^{o}C, as

evidenced from TGA (Fig. 5.2). All the synthesized compounds were characterized by ^{1}H NMR, ^{13}C NMR, IR and Mass spectrometry. We were unable to get ^{13}C NMR of the target compound due to the gelation.

Scheme 5.1

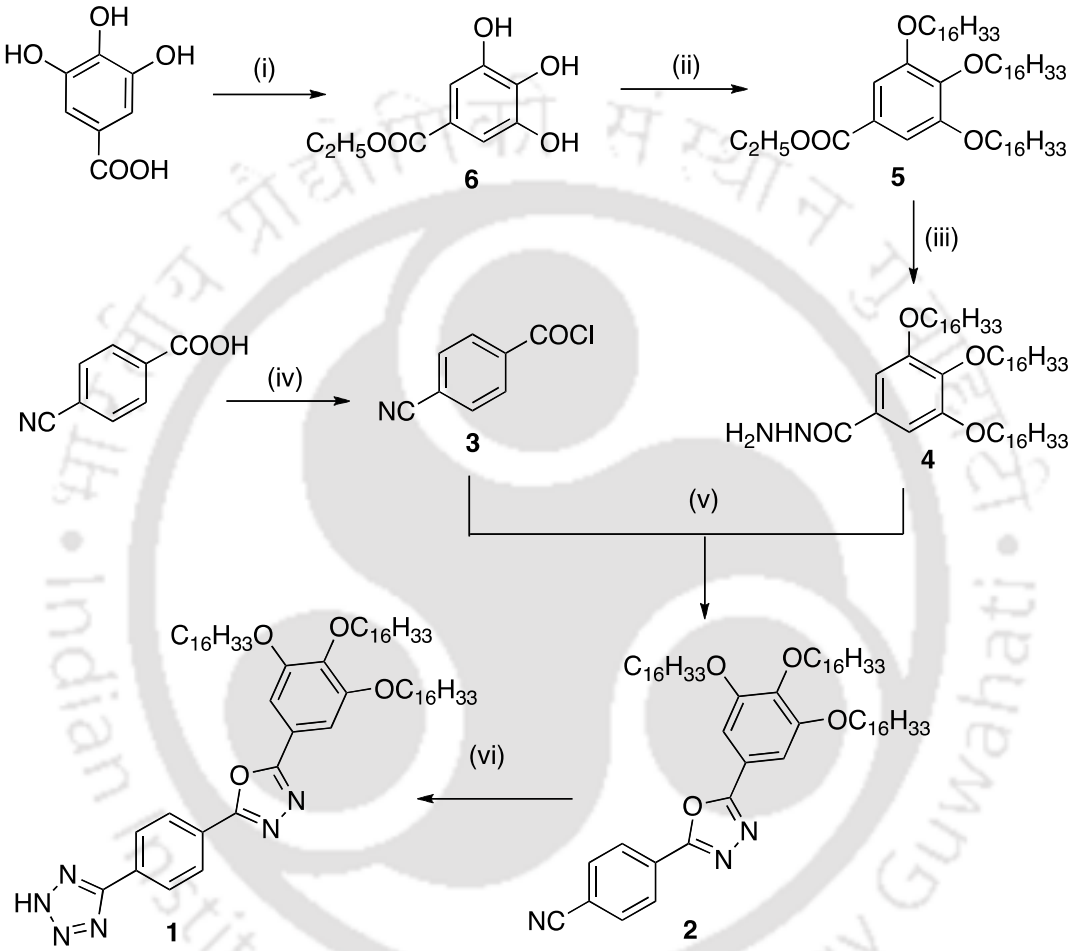

Reagents and conditions: (i) Ethanol, H_2SO_4, reflux, 24 h, 70%; (ii) $C_{16}H_{33}Br$, DMF, 80 ^{o}C, 24 h, 75%; (iii) Ethanol, $N_2H_4.H_2O$, reflux, 48 h, 67% (iv) $SOCl_2$, DMF, reflux, 4 h; (v) (a) THF, TEA, reflux, 12 h; (b) $POCl_3$, reflux, 12 h, 70%; (vi) NaN_3, NH_4Cl, DMF, 120 ^{o}C, 48 h, 56%.

5.3. Gelation studies

Considering the molecular structure containing heterocyclic aromatic ring, which provide ample scope for π–π and dipole-dipole interaction, presence of three long alkyl chains that provide hydrophobic/van der Waals interaction and the presence of a tetrazole ring, which provide H-bonding interaction, we assumed that the molecule **1** would be able to self-assemble to form an organogel (Fig.5.1).

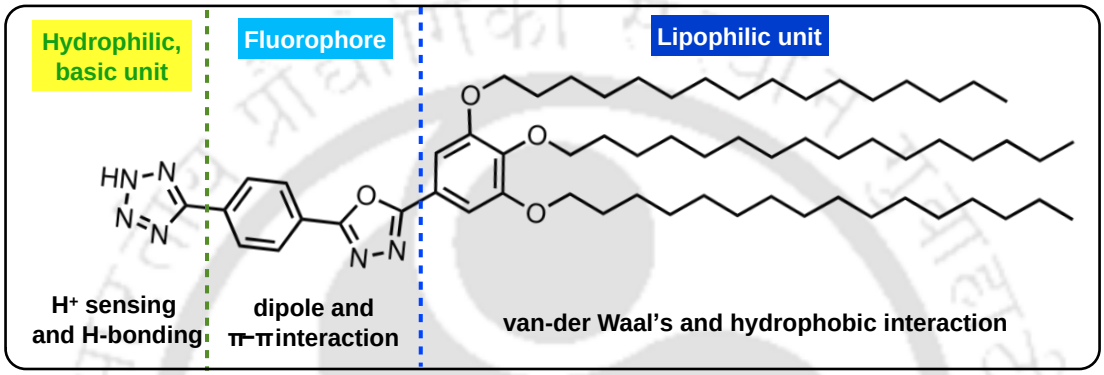

Figure 5.1. Molecular design of organogelator **1.**

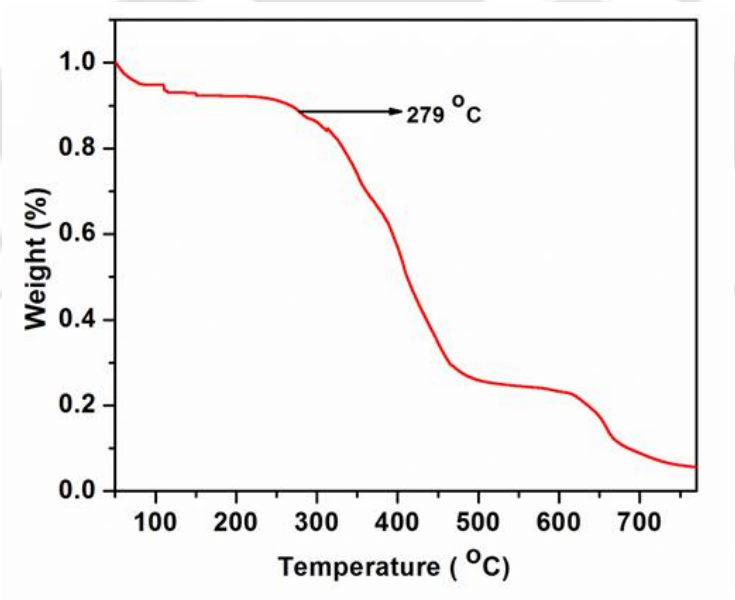

Figure 5.2. TGA graph showing the stability of compound **1** upto 279 °C.

Compound **1** was insoluble in most of the common polar and apolar solvents, aromatic solvents and halogenated solvents. However, it was soluble in dimethylsulfoxide (DMSO) up on heating. Allowing the solution to stand at room temperature for 20 minutes, led to the formation of organogel. This is confirmed by the no flow of the material on inversion of the container (Fig.5.8). The critical gelation concentration (CGC) was also calculated, which was found to be 0.6 wt% in DMSO and the thermal stability (T_{gel}) of the gel was found to be 45 ^{o}C using 'dropping ball method'. This compound comes under the class of 'supergelators' because of the low CGC value.[19] Temperature dependent ^{1}H-NMR spectra of the organogel of compound **1** were recorded in DMSO-d_6 regularly at temperature intervals of every 10 ^{o}C, on heating from room temperature. A clear transformation from gel to sol was observed from the overlay of NMR spectra (Fig.5.3). From the figure 5.3, it is obvious that at lower temperature *i.e.* below T_{gel} the peaks at around 8.1 – 8.25 ppm were broad due to stronger interaction in the gel form. Upon increasing temperature, the peaks became sharper and showed the splitting due to weakening of intermolecular interactions. The gel was stable at least up to a month in closed vial at ambient temperature.

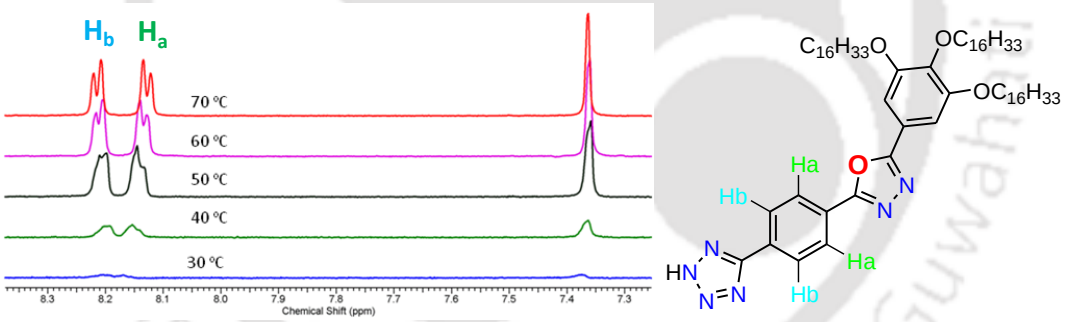

Figure 5.3. Expanded region of the temperature dependent ^{1}H-NMR spectra of compound **1** in DMSO-d_6.

The organogel was further characterized by photophysical studies in DMSO solution. The absorption spectrum of the solution at micromolar concentration showed a band at 318 nm, while the emission spectrum obtained by exciting at the absorption maximum showed an emission maximum at 414 nm with a Stoke's shift of 76370 cm^{-1} (Fig. 5.4). The optical band gap calculated from the onset of absorption was 3.24 eV. The self-assembly could be explored by the concentration dependent UV-Vis spectroscopy, but at higher concentration the absorbance of the

compound exceeded the limits of the instrument and hence we concentrated on the concentration dependent fluorescence.

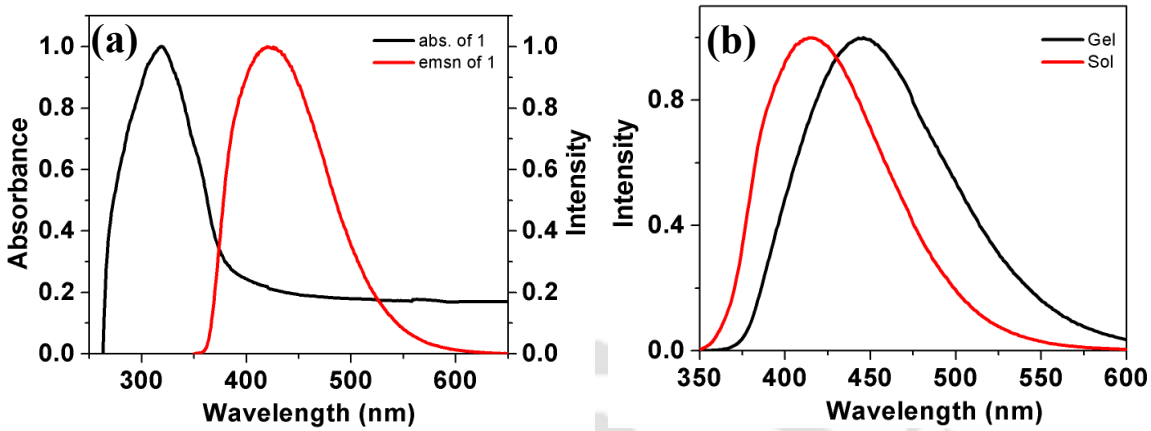

Figure 5.4. Absorption and emission of the compound **1** in micromolar solution of DMSO (a); emission spectra of compound **1** in solution and gel state (concentration: 7.2 mM in DMSO, λ_{exc} = 318 nm)

We measured the fluorescence spectrum as a function of temperature, from the clear solution of the compound at higher temperature to room temperature. On decreasing the temperature, the emission spectrum showed a red shift along with a decrease in the intensity (Fig.5.5a-b). The shift in the emission as well as decrease in the intensity of luminescence is due to the aggregation and associated quenching. The same behavior was noticed with the lapse of time from the point of clear solution (Fig.5.5c-d). The solution, which exhibited a higher luminescence when just dissolved, showed a decrease in the emission intensity with a concurrent red shift with time and gets saturated at 20 min, *i.e.* on complete gelation. The gel formed was reversible for many cycles of heating and cooling, as seen by the change in the emission intensity at its emission maximum (Fig.5.6a). The micromolar solution of compound **1** in DMSO also showed the presence of aggregates as evidenced by the dynamic light scattering (DLS) experiments. The size of the aggregates was found to be approximately 240 nm (Fig.5.6b). Characterization of the morphology of the xerogel film was carried out (after the evaporation of the solvent) using Atomic Force Microscope (AFM) and field emission scanning electron microscope (FE-SEM). These images showed the presence of an entangled network of interwoven fibers of several micrometers in length and an average thickness of 180 nm (Figure 5.7).

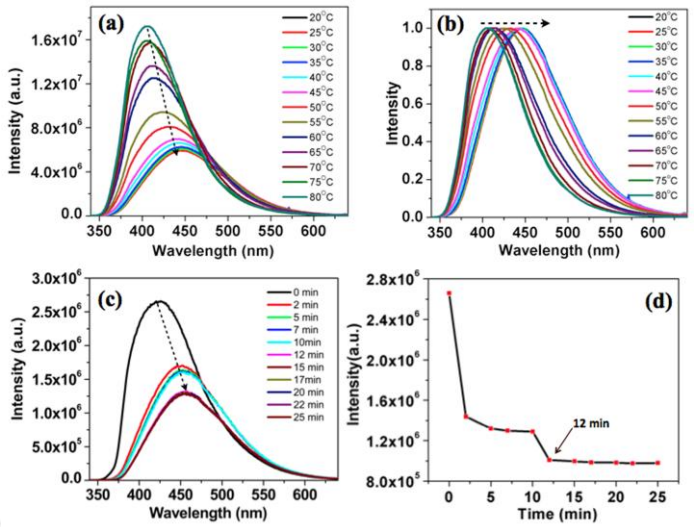

Figure 5.5. (a) Emission spectra as a function of temperature; (b) Normalized emission spectra with respect to temperature; (c) Emission spectra as a function of time; (d) Plot showing the change in emission intensity with respect to time at ambient temperature (concentration: 7.2 mM in DMSO, λ_{exc} = 318 nm).

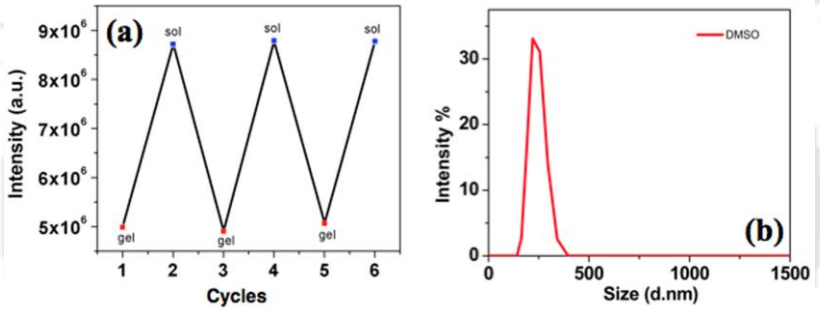

Figure 5.6. (a) Reversible change in the emission intensity at the emission maximum on repeated sol–gel transitions (concentration: 7.2 mM in DMSO, λ_{exc} = 318 nm); (b) DLS profiles of the 20 micromolar solution of compound **1** in DMSO.

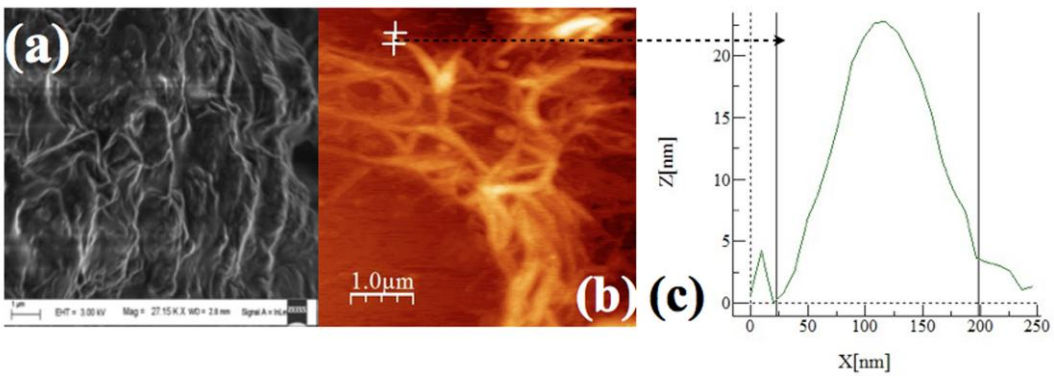

Figure 5.7. FE-SEM image (a); and AFM image (b) of the xerogel films of compound **1** obtained by the slow evaporation of DMSO solution (scale bar: 1µm); Expanded region of a fiber in (b) showing the thickness of an individual fiber (c).

Further, we have tested the sensing ability of the gel of compound **1** towards PA. To the gel formed with a critical gelation concentration (7.2 mM in DMSO), we have added the solution of same concentration containing compound **1** and PA in equimolar amounts. The gel was destabilized and converted into solution. This shows that the addition of PA destabilized the gelation. The destabilization of the gel is explained as below (Fig.5.8b). The organogel is formed by the intermolecular hydrogen bonding between the two tetrazole moieties of molecule **1**. This is further supported by the nanophase segregation of incompatible molecular subunits like flexible chains and hard aromatic cores. The self-assembly of these molecules leads to the formation of long fibers, which entrap a large volume of solvent to form a stable gel. With the addition of PA, the hydrogen bonded self-assembly of compound **1** is broken, and thus dismantling this delicate organization. This was also perceived visually under the irradiation of the UV light of longer wavelength (λ = 365 nm) with a change in the emission color (Fig.5.8a). This observation motivated us to study the response of compound **1** to various nitroaromatic explosives to understand the selectivity and sensitivity.

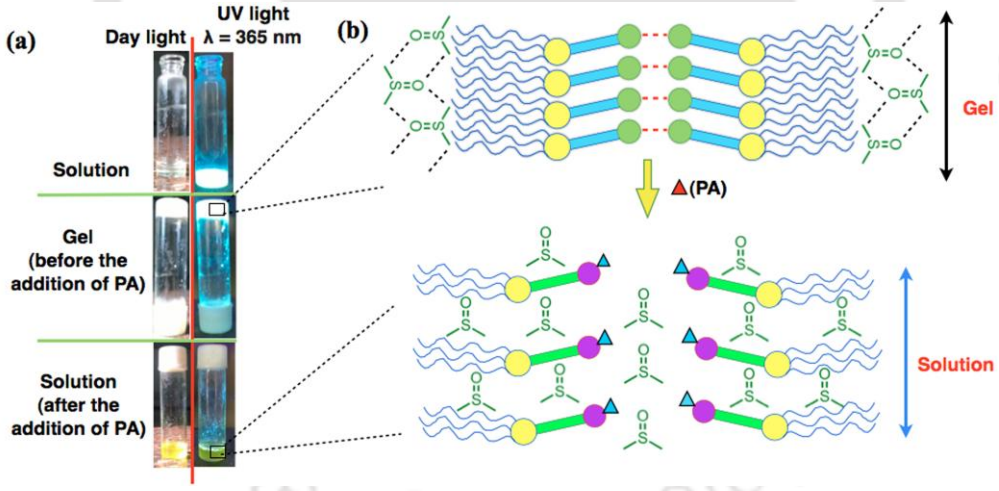

Figure 5.8. Photographs of the images of solution and gel under daylight and UV light of 365 nm, and response of the gel after the addition of PA (a); Schematic showing the destabilization of the gel of compound **1** in DMSO after the addition of PA (b).

Response to nitro aromatic explosives

Considering the ability of the molecule to exhibit emission in solution as well as in gel state along with the presence of a basic azole moieties, we envisaged that this could be a

potential molecule to sense nitrophenol based explosives. Interestingly, the compound showed a very good sensing ability towards PA in the presence of various nitro aromatic explosives (NAEs) in the solution state. The detailed results are presented as below. In order to analyze the sensing behavior of compound **1** toward nitro explosives in solution state and also to explore its selectivity towards PA, fluorometric titration studies were performed in presence of various common NAEs (Fig.5.9). An experimental solution containing compound **1** and any nitro compounds *viz.* 4-nitro toluene (4-NT), 2,4-dinitro toluene (2,4-DNT), 2,6-dinitro toluene (2,6-DNT), benzoic acid (BA), 4-nitrobenzoic acid (4-NBA), 2,4-dinitrobenzoic acid (2,4-DNBA), nitrobenzene (NB), *m*-dinitrobenzoic acid (*m*-DNB), nitromethane (NM), 4-nitrophenol (4-NP), 2,4-dinitrophenol (2,4-DNP) were taken in DMSO (1 mM solution in DMSO) (Fig.5.10a).

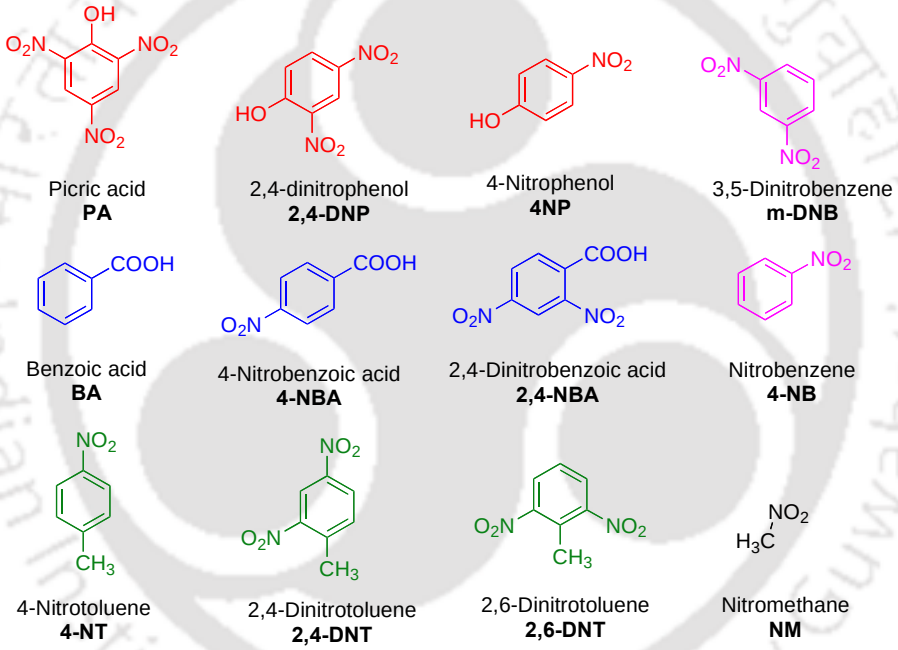

Figure 5.9. Structures of different nitro compounds used in this study

The emission of **1** displayed a significant change upon the addition of PA thus make it as an interesting sensor for the detection of PA (Fig. 5.10a-b). It has been observed that compound **1** showed this selective response even in the presence of other nitro compounds (Fig. 5.10c). An immediate shift in the emission maximum (414 nm) of compound **1** was observed upon adding equimolar solution of PA to compound **1** in DMSO solvent (Fig.5.10). The emission maximum was 414 nm for the neat solution of **1**, but shifted to 486 nm after the addition of PA (Fig.

5.10a,b). The red shift of 72 nm was observed in the emission spectrum after the addition of PA to the compound solution. This leads to disappearance of blue emission of compound **1** along with the appearance of green emission, which could be visualized under UV light of long wavelength (lamp excitation-365 nm) (Fig. 5.11). Interestingly, most of the nitro compounds used in the present study did not produce any significant changes of emission color of compound **1** (Fig.5.10b and 5.11). Though 2,4-DNP and 4-NP shift the emission of compound **1** towards green, the emission was very weak compared to that in presence of PA (Fig.5.10a,b and 5.11). In order to validate the selectivity of compound **1**, its fluorescence shifting by PA was performed in the presence of different nitro compounds. It is important to point out that compound **1** showed remarkable response toward PA even in the presence of various common interfering nitro group containing analytes (Fig. 5.10c). The selective response to PA was also seen unaltered in the presence of common anions (Fig.5.13)

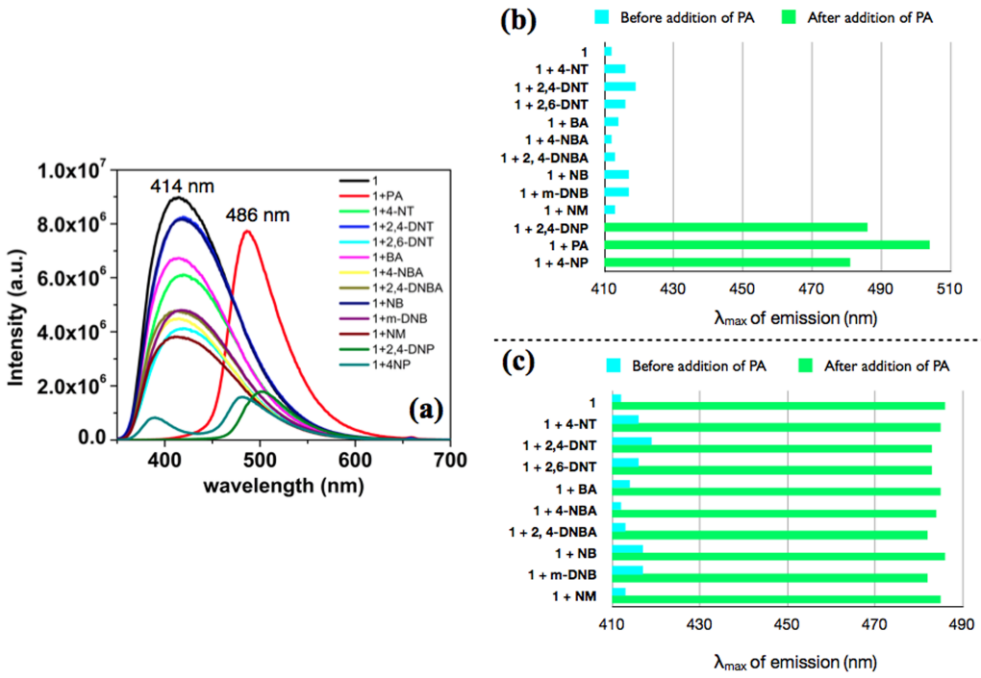

Figure 5.10. Emission spectra of compound **1** and its equimolar solutions with different nitro compounds (Concentration: 1 mM solution in DMSO) (a); Fluorescence response to the different nitro compounds by DMSO solution of **1** (b); Fluorescence response to the PA in presence of different nitro compounds by DMSO solution of **1** (c).

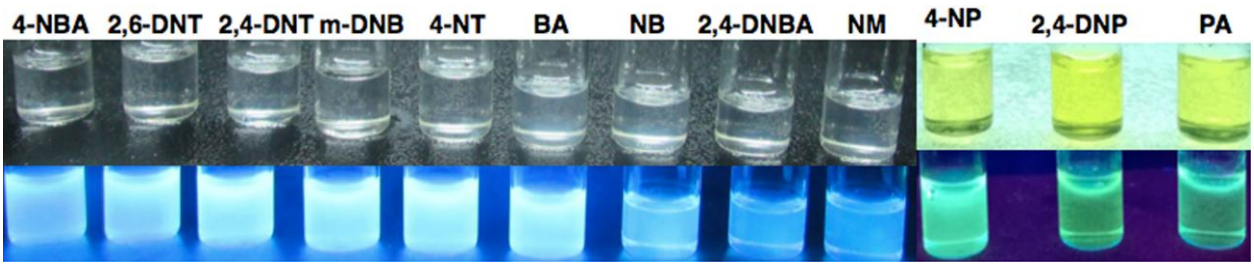

Figure 5.11. Images of equimolar solutions of compound **1** and nitro compounds in daylight (upper row); under UV light of long wavelength (lower row) (Concentration: 1 mM solution in DMSO).

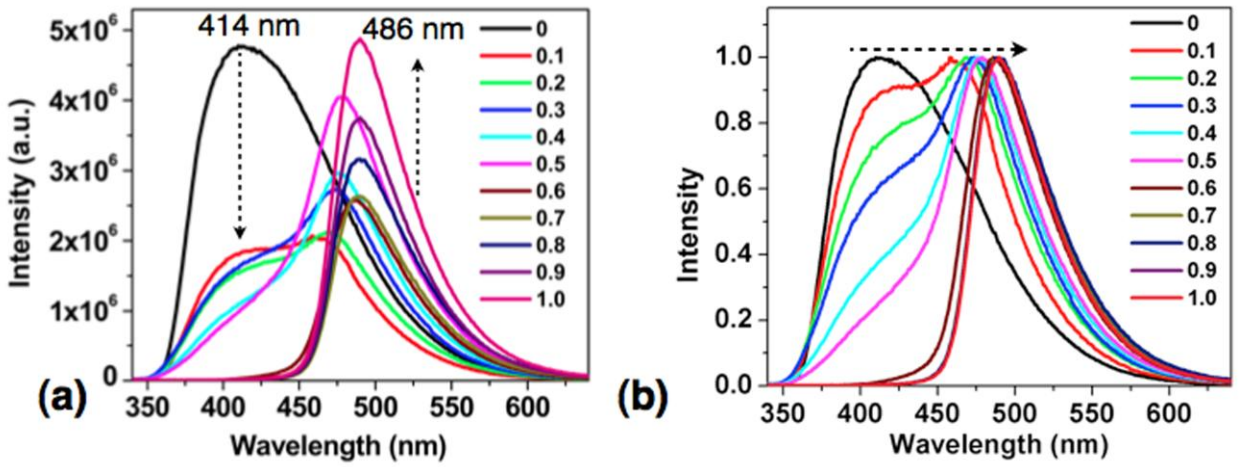

Figure 5.12. Emission spectra of compound **1** on the incremental addition of PA (Equimolar concentration; 1 mM in DMSO; 100 μL addition) (a); normalized emission spectra of compound **1** obtained after the incremental addition of PA (b).

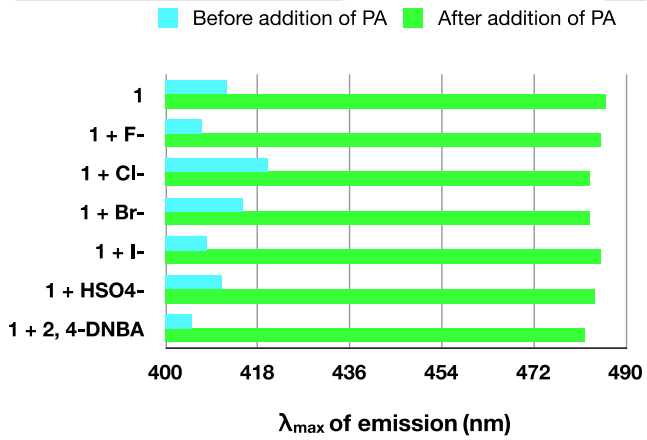

Figure 5.13. Fluorescence response to the PA in presence of different anions by DMSO solution of **1**.

In order to explain the shifting of emission from blue to green, fluorimetric titration of PA to compound **1** was carried out. This was done by an incremental addition of 0.1 mL of PA solution (100 μM) to a 1 mL solution of compound **1** in DMSO (100 μM). It was observed that, firstly there was a decrease in the emission intensity (λ = 414 nm) of compound **1** followed by the formation of a new band at around 459 nm, which indicated the formation of a new species in the mixture. Then, the intensity of this new band showed a steady increase with the concomitant decrease of the band at shorter wavelength (414 nm), which corresponds to the compound **1**. Finally, a red shifted band with an increase in luminescence intensity was observed with an emission maximum of 486 nm (Fig.5.12). The formation of new species was further justified with the help of time resolved photoluminescence spectroscopy where the addition of micromolar solution of PA to a micromolar solution of **1** showed the formation of a new species with longer lifetime (Fig. 5.14). The fluorescence lifetime of the solution of compound **1** in DMSO at a 20 μM concentration was measured by monitoring at its emission maximum (403 nm) showed the presence of two excited species, one with a lower lifetime of [τ_1 = 1.1 ns (34%)] and other with a longer lifetime [τ_2 = 2.5 ns (66%)]. The solution of compound **1** with PA also exhibited two excited species but with longer life times [τ_1 = 2.1 ns (30%)] and [τ_2 = 8.3 ns (70%)] in comparison compound **1** without PA.

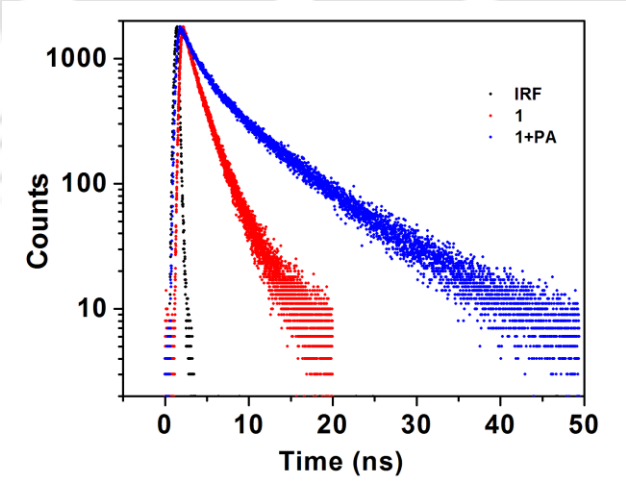

Figure 5.14. The fluorescence decay profiles of compound **1** in DMSO at 10 μM solution (red trace) and after the addition of PA (5 μM solution in DMSO) (blue trace) (black trace is instrument response function: IRF; λ_{exc} = 290 nm)

It is to be noted that when the titration was carried out, by using an equimolar solution of PA in water to the solution of compound in DMSO, there was a red shift in the emission band, but there was a concomitant decrease in the intensity of the new band (Fig.5.15). This emission intensity was reduced to a minimum when the addition of PA completed one equivalent with respect to compound **1**. Thus, it is interesting to note that compound **1** could be able to detect the PA dissolved in water, which acts as a common contaminant. Though we observed a red shifted emission, the emission intensity is reduced in presence of water, which may be due to the quenching of the emission by water.

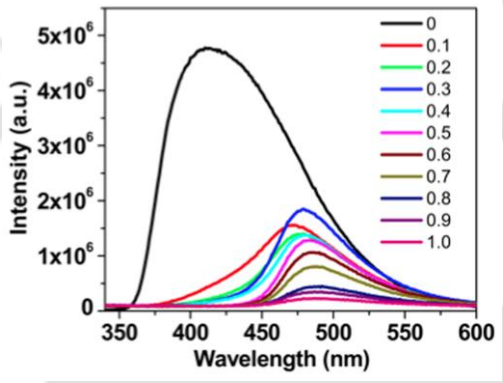

Figure 5.15. Emission spectra of compound **1** on the gradual addition of picric acid in water (Concentration: 1mM of compound 1 in DMSO; 1mM of PA in water, gradual addition of 0.1 mL).

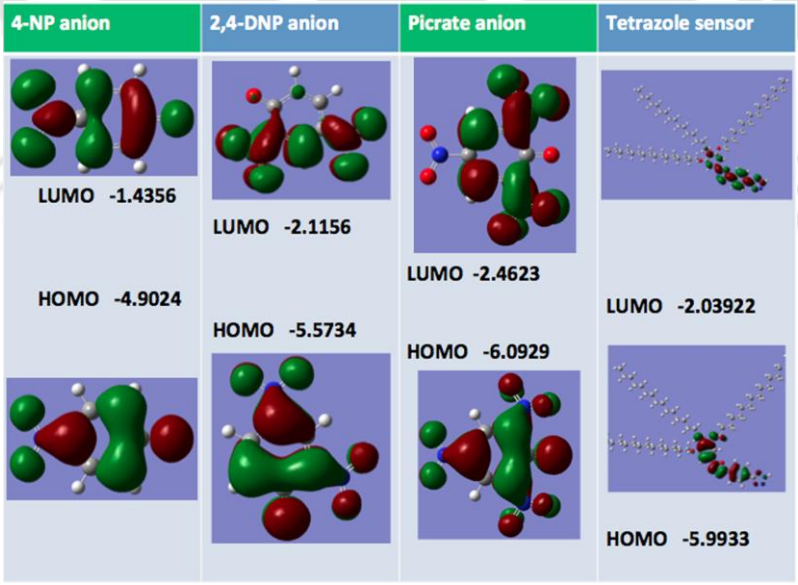

Figure 5.16. HOMO and LUMO orbitals of 4-nitrophenolate anion, 2,4-dinitrophenolate anion, picrate anion and compound **1**.

Most of the fluorescent sensors developed for the detection of picrate ion were based on the quenching of fluorescence. The electron transfer from electron rich picrate anion to the sensor was reported as the mechanism of detection of picrate ion. But in the present case, upon addition of PA a red shift was observed in the emission spectrum of compound **1**. Further to rule out that the electron transfer from picrate anion to compound **1**, we have carried out the Density Functional Theory (DFT) calculations. The DFT studies shown that the energy of the highest occupied molecular orbital (HOMO) of the free compound **1** is –5.99 eV, while that of the lowest occupied molecular orbital (LUMO) is –2.04 eV. In comparison the HOMO and LUMO levels of the picrate anion are found to be –6.09 eV and –2.46 eV respectively. Thus, the energy level of the HOMO of picrate anion is lower than that of LUMO level of compound **1** (Fig.5.16). The actual experimental result describes that shift in emission is observed in response for the picrate anion.

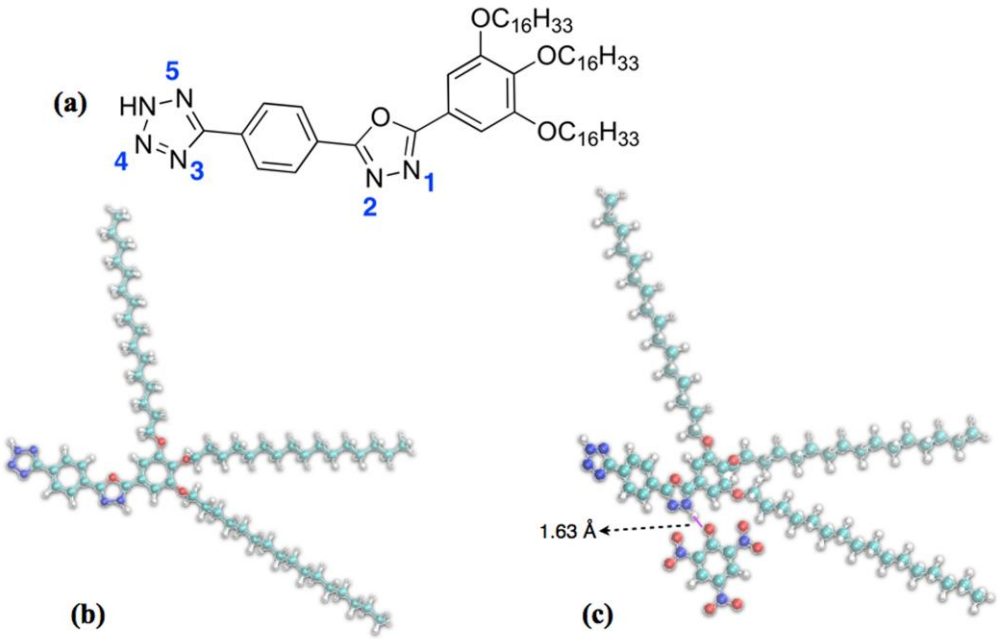

Figure 5.17. Structure of compound **1** showing the possible sites of protonation (a); Energy minimized structure of HA1 (b); Energy minimized structure of the complex formed between HA1 and picrate anion (c).

The other possibility is that, the new species formed by the addition of PA to the solution of compound **1** in DMSO is due to the protonation of compound **1**. Considering the low pKa value

of PA (0.38) and the basicity of the azole rings, this is most probable. There are five basic centers that are available for the protonation two nitrogens on oxadiazole ring and three nitrogens on the tetrazole ring are the possible sites for protonation (Fig. 5.17a). The optimized structures of protonated tetrazole compound can be found in Figure 5.18.

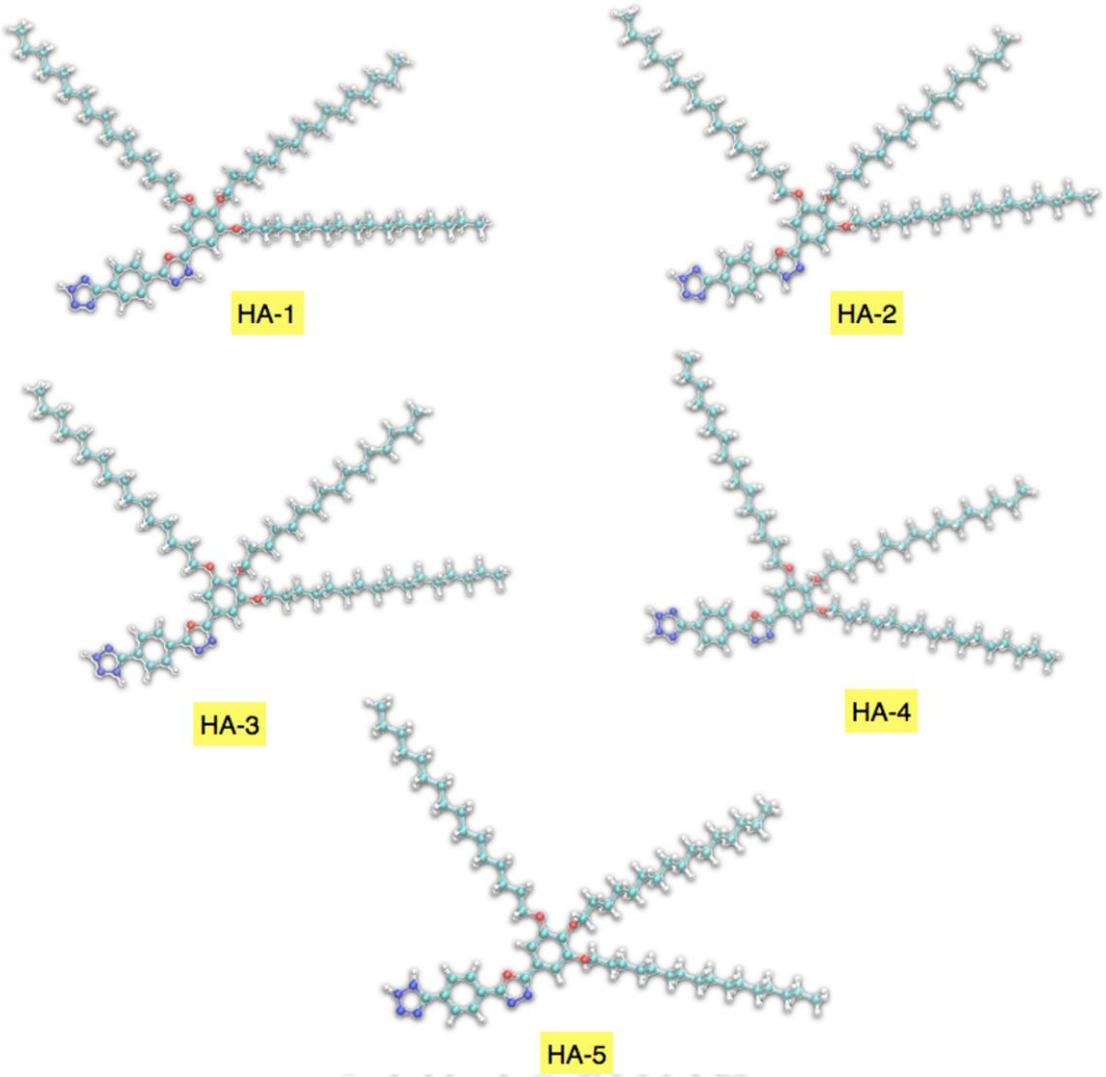

Figure 5.18. Energy minimized structures of possible protonated forms of compound **1**.

Among the 5 possible protonated compounds the DFT calculations suggest that HA1 is the most stable cation (Fig.5.17b, Table 5.1) in the presence of DMSO solvent. To understand further DLS and FESEM studies were carried out in the presence and the absence of PA. The DLS study

showed that the average size of the particle is enhanced in presence PA compared to that in the absence of PA (Fig.5.19). This indicates the formation of large size particle by aggregation (Fig.5.20). However, just the protonation of fluorophore cannot explain the increase in size of the particle. The protonated molecule might form the hydrogen bonded complex with picrate anion and this aggregation could cause the enhancement in particle size. Such hydrogen bonded complex between the protonated sensor and picrate anion was reported.[20] The change in surface morphology in presence of PA further support this (Fig.5.19b). To substantiate the complex formation between the HA1 and picrate anion DFT calculations were performed on HA1, picrate anion and the complex. The stabilization energy thus obtained for complex is 70.6 $kJmol^{-1}$, *i.e.* the energy of this complex is lower than the sum of the energies of HA1 and picrate anion; and HA1 alone.

Table 5.1. Optimized energies of the compounds considered in this study.

Compund name	Energy (kJ/mol)
Protonated tetrazole-5 (HA1)	-8124451.6
Protonated tetrazole-4 (HA2)	-8124447.5
Protonated tetrazole-3 (HA3)	-8124416.7
Protonated tetrazole-2 (HA4)	-8124366.1
Protonated tetrazole-1 (HA5)	-8124374.6
Picrate anion	-2416824.2
Protonated tetrazole (HA1)-picrate complex	-10541346.4

The distance between hydrogen of protonated compound and oxygen of picrate anion is 1.63 Å (Fig.5.17c), while the distance between donor and acceptor of this hydrogen bond is 2.65 Å, suggesting a strong hydrogen bond, which could be mostly electrostatic. No imaginary frequencies were found in all these optimization calculations, suggesting that these structures are minimum points on the potential energy surface. We used B3LYP hybrid density functional and 6-31G(d) basis set for all the calculations. More importantly we performed all these calculations considering the presence of solvent (DMSO) using Polarizable Continuum Model (PCM) as implemented in Gaussian 09.

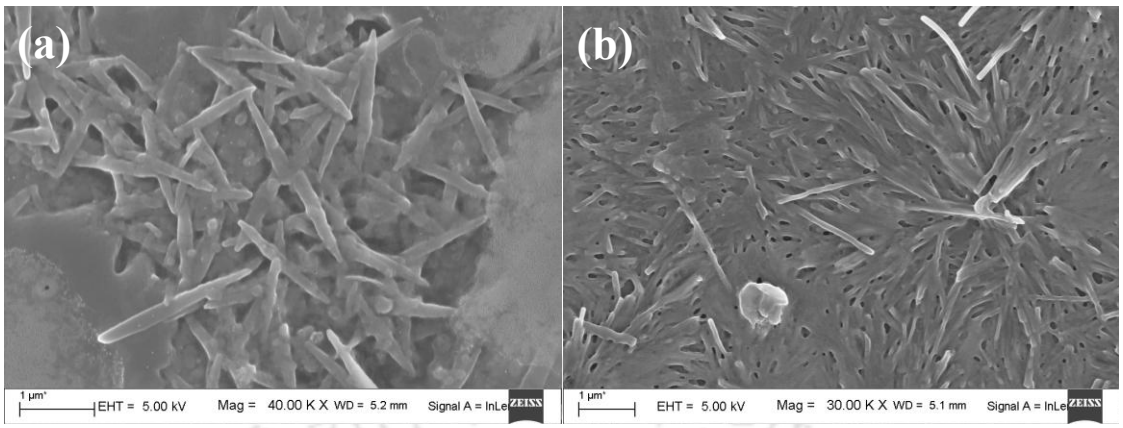

Figure 5.19. SEM image of the film formed by the solution of compound **1** in DMSO (1 mM in DMSO); SEM image of the film formed by the solution of compound **1** in DMSO and PA (1 mM in DMSO) (b).

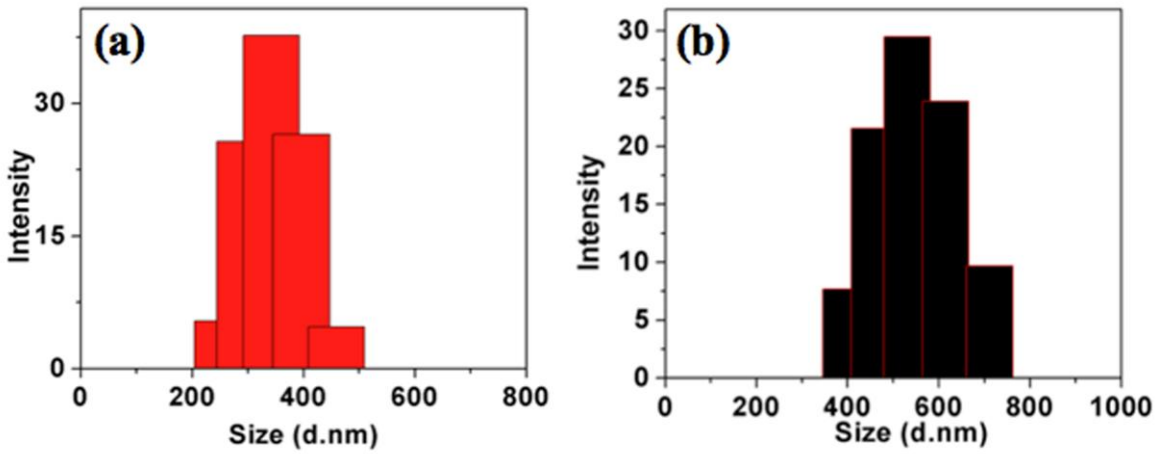

Figure 5.20. DLS profile of the same solution (1 mM in DMSO) (a); DLS profile of the same solution (1 mM in DMSO) (b).

Following facts further supports this hypothesis. PA is reported to deprotonate and form picrate ions in DMSO under normal condition. This is visualized by the red-shifted absorption maximum of PA in DMSO (λ_{max} = 379 nm) in comparison to the absorption maximum in chloroform (λ_{max} = 333 nm) (Fig. 5.21). The red shifted emission is observed from compound **1** only in the presence of nitrophenols, which donate acidic protons. On the other hand, only quenching is observed in other nitro compounds. This confirms that emission is due to the protonated species, which aggregates with picrate anion. The aggregation of protonated compound **1** with picrate anion is expected to reduce the solvent solute interaction, which

reduces the fluorescence lifetime. Thus, the enhancement in the fluorescence lifetime of compound **1** in the presence of PA, further support this hypothesis. This means that the observed spectral changes are due to formation of new complex with picrate. The complex is formed by the interaction of protonated compound **1** with picrate ion and is not due to electron transfer. Further the selectivity of the sensor to PA is due to its lower pK_a value in comparison to 4-NP and 2,4-DNP. Among the nitrophenols, the PA has lower pK_a value. Therefore, the protonation of compound **1** and aggregation of that with counter anion are expected to be more in the presence of PA than with other two nitrophenols. Accordingly, a strong green emission is observed in the presence of PA and the emissions are weak in the presence other nitrophenols (Fig.5.10a,b and 5.11). To visualize the change in compound **1** in response to the incremental addition of PA was attempted with ^1H NMR, but found that the protonated species of compound **1** was not clearly soluble even at a temperature of 65 ^oC. This failed our attempt to detect the changes by NMR spectra. However, the DFT calculations clearly support the complex formation.

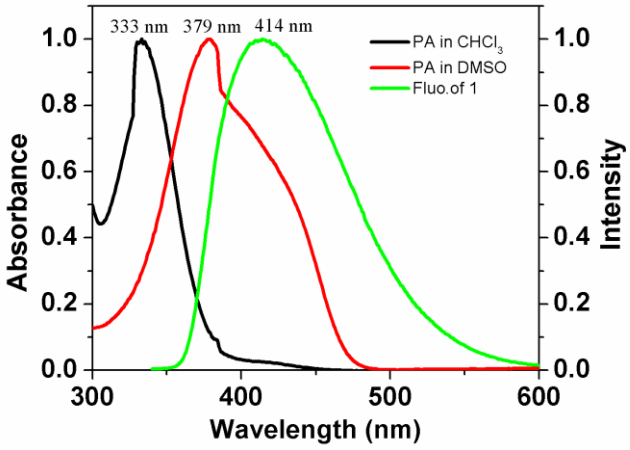

Figure 5.21. Overlay of the normalized absorption spectra of Picric acid in chloroform and DMSO and emission spectrum of compound 1 in DMSO (millimolar concentration)

5.4. Conclusions

In summary a novel organic super gelator was developed, which is only soluble in DMSO and forms a stable gel. The compound has potential application in picric acid sensing in

solution state with a rarely observed shifting of emission maximum in response to the analyte. The compound in its organogel form can also be utilized for the detection of the explosive picric acid as seen by its destabilization of the gel and change in the emission. The mechanism behind this efficient detection could be the formation of complex between the protonation sensor the picrate anion. This produces a visible change emission color. Theoretical and experimental studies revealed that the sensing property is not due to ground state electron transfer. The selectivity to picric acid is due to the ease of deprotonation, which is in turn related to the pKa value of the compound. To the best of our knowledge this is the first example of tetrazole based supergelator which can detect powerful explosive picric acid with a fluorescence switching in the visible region. This compound holds promise for the application in pollution control, border and homeland security, and humanitarian efforts during wars due to its high sensitivity, selectivity and ease of handling.

5.5. Experimental Section

In this section the detailed synthetic procedures and the molecular structural characterization data have been presented for the intermediates and the molecular structural characterization data have been presented for the intermediates and target compounds mentioned in the scheme.

Procedure for the synthesis of ethyl 3,4,5-trihexadecyloxy benzoate (**5**)

A mixture of ethyl gallate (15.1 mmol, 1 equiv.), anhydrous K_2CO_3 (99.9 mmol, 6.6 equiv.), *n*-bromohexadecane (49.83 mmol, 3.3 equiv.) were taken in dry DMF and heated at 80 ^oC for 24 h under nitrogen atmosphere. Then the reaction mixture was poured into water and extracted with ethyl acetate. The combined extract was washed with water and dried over anhydrous Na_2SO_4 and then concentrated. The crude product was purified by column chromatography on silica. Elution with hexanes followed by 2-5% ethyl acetate-hexane yielded the desired product.

R_f = 0.5 (5% EtOAc - hexane); white solid; yield: 75%; IR (KBr pellet): ν_{max} in cm^{-1} 2922, 2850, 1716, 1583, 1468, 1426, 1331, 1218, 1110, 1041; ^1H NMR ($CDCl_3$, 400 MHz): δ 7.25 (s, 2H, H_{Ar}), 4.35 (q, 2H, *J* = 7.2 Hz, $COOCH_2$), 4.01 (t, 6H, 3×OCH_2), 1.25-1.82 (m, 84H, 42×CH_2), 0.87 (m, 12H, 4×CH_3), ^{13}C NMR ($CDCl_3$, 100 MHz): 166.70, 153.04, 142.61, 125.28, 108.29, 73.72, 69.44, 61.17, 33.05, 32.16, 30.56, 29.94, 29.89, 29.87, 29.80, 29.63, 29.60, 29.57, 26.32, 26.29, 22.92, 14.63, 14.33. HRMS (ESI+) exact mass calculated for $C_{57}H_{107}O_5$ (M+1): 871.8119, Found: 871.8031.

Procedure for the synthesis of ethyl 3, 4, 5-tris (hexadecyloxy) benzhydrazide (**4**)

A mixture of ethyl 3,4,5-tri-*n*-hexadecyloxybenzoate (10 mmol, 1 equiv.), excess hydrazine hydrate (20 equiv.), in ethanol was refluxed for 48 h. Excess solvent was removed and water was added to it. Resulting precipitate was collected by filtration, washed with excess water, dried under vacuum, and recrystallization from ethanol gave white solid product.

R_f = 0.52 (20% EtOAc-hexane); white solid, yield: 75%; IR (KBr pellet): ν_{max} in cm^{-1} 3448.94, 3248.41, 2921.55, 2850.68, 1635.32, 1579.85, 1466.26, 1427.84, 1238.90, 1122.06; ^{1}H NMR ($CDCl_3$, 400 MHz): δ 7.22 (br s, 1H, CONH), 6.92 (s, 2H, H_{Ar}), 4.07 (s, 2H, NH_2), 3.99 (m, 6H, 3 × OCH_2), 1.26–1.80 (m, 84H, 42×CH_2), 0.88 (m, 9H, 3×CH_3); ^{13}C NMR ($CDCl_3$, 150 MHz): 168.70, 153.54, 141.92, 127.68, 105.74, 69.60, 30.53, 29.97, 29.95, 29.88, 29.60, 26.30, 22.92, 14.33. HRMS (ESI+) exact mass calculated for $C_{55}H_{105}N_2O_4$ (M+1): 857.8074, Found: 857.8151.

Procedure for the synthesis of 4-(5-(3,4,5-tris(hexadecyloxy)phenyl)-1,3,4-oxadiazol-2-yl)benzonitrile (**2**)

4-cyanobenzoic acid was refluxed with thionyl chloride (excess) in presence of DMF (few drops, as catalyst) for 4 h. Excess thionyl chloride was distilled out and the crude residue **3** was taken in THF and slowly added into the THF solution of compound **4** (3.3 eqv.) and TEA (3 eqv.) under argon atmosphere and then refluxed for 6 h. The reaction mixture was extracted with chloroform, washed with 3 × 50 mL of water. The chloroform extract was dried over Na_2SO_4, evaporated and used as such without any purification. The residue was refluxed with $POCl_3$ for 12 h, and then the reaction mixture was cooled. This was carefully poured into ice-cold water and then extracted with chloroform. The chloroform extract was washed several times with water, dried over anhyd.Na_2SO_4, and concentrated. The compound was further purified by column chromatography over neutral alumina using 10-50% EtOAc:Hexane. Finally the compound was purified by recrystallization in DCM-ethanol mixture.

R_f = 0.5 (60% EtOAc - hexane); white solid; m.p.: 94-96 ^{o}C; yield: 70%; IR (KBr pellet): ν_{max} in cm^{-1} 3448, 2919, 2851, 2230, 1594, 1546, 1492, 1469, 1439, 1122, ; ^{1}H NMR ($CDCl_3$, 600 MHz): δ 8.26 (d, 2H, *J* = 6 Hz, H_{Ar}), 7.84 (d, 2H, *J* = 6 Hz, H_{Ar}) 7.31 (s, 2H, H_{Ar}), 4.08-4.04 (m, 6H, 3×OCH_2), 1.87-1.25 (m, 84H, 42×CH_2), 0.89-0.86 (m, 9H, 3×CH_3), ^{13}C NMR ($CDCl_3$, 100 MHz): 165.74, 163.04,153.87, 141.99, 133.06, 128.03, 127.51, 118.15, 118.04, 115.23, 105.74, 73.88, 69.62, 32.14, 30.55, 29.97, 29.96, 29.94, 29.88, 29.86, 29.79, 29.62, 29.59, 29.52, 26.31, 26.28, 22.91, 14.34. MALDI-TOF exact mass calculated for $C_{63}H_{106}N_3O_4$ (M+H): 968.8183, Found: 968.689.

Procedure for the synthesis of 5-(4-(5-(3,4,5-tris(hexadecyloxy)phenyl)-1,3,4-oxadiazol-2-yl)phenyl)-2H-tetrazole (**1**)

A mixture of compound **2**, NaN_3 (1.5 eqv.) and NH_4Cl (1.3 eqv.) in DMF was heated at 120 ^{o}C for 36 h. DMF was removed in rotavapor and the solid compound was washed several times with water, then with ethanol and chloroform, dried in vacuum to obtain a white solid; yield: 56 %;

m.p.: >300 ^{o}C IR (KBr pellet): ν_{max} in cm^{-1} 3443, 2918, 2850, 1649, 1588, 1556, 1496, 1466, 1379, 1126; ^{1}H NMR (DMSO-D_6, 600 MHz): δ 8.22 (d, 2H, *J* = 6 Hz, H_{Ar}), 8.13 (d, 2H, *J* = 6 Hz, H_{Ar}) 7.37 (s, 2H, H_{Ar}), 4.12 (t, 4H, J = 6Hz, 2 × OCH_2) 4.00 (t, 2H, 1×OCH_2), 1.81-1.19 (m, 85H, 42×CH_2, 1× NH), 0.87-0.84 (m, 9H, 3×CH_3). MALDI-TOF exact mass calculated for $C_{63}H_{107}N_6O_4$ (M+1): 1011.8348, Found: 1012.440.

5.6. References

1. G. V.Perez, A. L. Perez, *J. Chem. Educ*. 2000, **77**, 910-915.
2. M. Nipper, R. S. Carr, J. M. Biedenbach, R. L. Hooten, K. Miller, *Marine Pollution Bulletin*, 2005, **50**, 1205–1217.
3. (a) C. Beyer, U. Bohme, C. Pietzsch, G. Roewer, *J. Organomet. Chem.* 2002, **654**, 187-201.
4. (a) J. M. Sylvia, J. A. Janni, J. D. Klein, K. M. Spencer, *Anal. Chem*. 2000**,** **72**, 5834-5840. (b) K. Hakansson, R. V. Coorey, R. Zubarev, V. L. Talrose, P. Hakansson, *J. Mass Spectrom*., 2000, **35**, 337-346.
5. J.R.C. Junqueira, W.R. de Araujo, M.O. Salles, T.R.L.C. Paixao, *Talanta,* 2013, **104,** 162–168.
6. (a) S. Shanmugaraju, P. S. Mukherjee, *Chem. Eur. J*. 2015, **21**, 6656-6666 (b) M. Alfonso, A. Espinosa, A. Tarraga, P. Molina, *Chemistry Open*, 2014, **3**, 242 – 249. (c) D. S. Kim, V. M. Lynch, K. A. Nielsen, C. Johnsen, J. O. Jeppesen, J. L. Sessler, *Anal. Bioanal. Chem.*, 2009, **395**, 393-400.
7. (a) Y. Jiang, H. Zhao, N. Zhu, Y. Lin, P. Yu, L. Mao, *Angew. Chem., Int. Ed.* 2008, **47**, 8601-8604. (b) Y. Ma, H. Li, S. Peng, L. Wang, *Anal. Chem.* 2012, **84**, 8415-8421. (c) S. S. R. Dasary, A. K. Singh, D. Senapati, H. Yu, P. C. Ray, *J. Am. Chem. Soc*. 2009, **131**, 13806-13812. (d) L. Feng, H. Li, Y. Qu, C. Lu, *Chem. Commun*. 2012, **48**, 4633-4635.
8. (a) Y. Yag, H. Wang, K. Su, Y. Long, Z. Peng, N. Li, L. Feng, *J. Mater. Chem*. 2011, **21**, 11895-11900. (b) Y. Z. Liao, V. Strong, Y. Wang, X. Li, X. Wang, R. B. Kaner, *Adv. Funct. Mater*. 2012, **22**, 726-735.
9. (a) V. Bhalla, A. Gupta, M. Kumar, D. S. S. Rao, S. K. Prasad, *ACS. Appl. Mater. Interfaces.* 2013, **5**, 672-679. (b) N. Dey, S. K. Samanta, S. Bhattacharya, *ACS. Appl. Mater. Interfaces.* 2013, **5**, 8394-8400. (c) A. Sandeep, V. K. Praveen, K. K. Kartha, V. Karunakaran, A. Ajayaghosh, *Chem. Sci.*, 2016, **7**, 4460–4467.
10. (a) S. W. Thomas III, G. D. Joly, T. M. Swager, *Chem. Rev.* 2007**,** **107**, 1339-1386. (b) G. He, H. Peng, T. Liu, M. Yang, Y. Zhang, Y. Fang, *J. Mater. Chem.* 2009, **19**, 7347-7353. (d) Y-J. Hu, S-Z. Tan, G-L. Shen, R-Q. Yu, *Anal. Chim. Acta*, 2006, **570**, 170-175. (e) H. Nie, Y. Zhao, M. Zhang, Y. Ma, M. Baumgarten, K. Mullen, *Chem. Commun.* 2011, **47**, 1234-1236.
11. (a) H. Xu, F. Liu, F. Cui, B. Chen, G. Qian, *Chem. Commun.* 2011, **47**, 3153-3155. (b) B. Gole, A. K. Bar, P. S. Mukherjee, *Chem. Commun.* 2011, **47**, 12137-12139. (c) D. Samanta, P. S. Mukherjee, *Dalton. Trans.* 2013, **42**, 16784-16795. (d) V. Vajpayee, H. Kim, A. Mishra, P. S. Mukherjee, P. J. Stang, M. Lee, H. K. Kim, K. W. Chi, *Dalton Trans.* 2011, **40**, 3112-3115. (e) S. Ghosh, P. S. Mukherjee, *Organometallics*, 2008, **27,**

316-319. (f) S. Shanmugaraju, H. Jadav, P. Y, Patil, P. S. Mukherjee, *Inorg. Chem*. 2012, **51**, 13072-13074. (g) S. Shanmugaraju, S. A. Joshi, P. S. Mukherjee, *Inorg. Chem.* 2011, **50**, 11736-11745. (h) S. S. Nagarkar, B. Joarder, A. K. Chaudhari, S. Mukherjee, S. K. Ghosh, *Angew. Chem., Int. Ed.* 2013, **52**, 2881-2885.

12. R. Ni, R-B. Tong, C-C. Guo, G-L. Shen, R-Q. Yu, *Talanta*, 2004, **63**, 251-257.
13. (a) T. M. Swager, J. H. Wosnick, *MRS Bull*., 2002, **27**, 446– 450; (b) K. Sakakibara, J. P. Hill, K. Ariga, *Small*, 2011, **7**, 1288–1308; (c) A. Rose, Z. Zhu, C. F. Madigan, T. M. Swager, V. Bulović, *Nature*, 2005, **434**, 876–879; (d) V. Bhalla, A. Gupta, M. Kumar, *Org. Lett*. 2012, **14**, 3112-3115. (e) B. Roy, A. K. Bar, B. Gole, P. S. Mukherjee, *J. Org. Chem.* 2013, **78**, 1306-1310, (f) A. Chowdhury, P. S. Mukherjee, *J. Org. Chem.* 2015, **80,** 4064-4075, (g) K. K. Kartha, A. Sandeep, V. K. Praveen, A. Ajayaghosh, *Chem. Rec.*, 2015, **15**, 252–265; (h) N. Venkatramaiah, S. Kumar, S. Patil, *Chem. Commun.*, 2012, **48**, 5007–5009.
14. (a) D. Xuewen, J. Zhou, J. Shi, B. Xu, *Chem. Rev*. 2015, **115**, 13165−13307. (b) S. S. Babu, V. K. Praveen, A. Ajayaghosh, *Chem Rev*, 2014, **114(4)**, 1973-2129.
15. J-Y. Li, X.-Q. Zhou, Y. Zhou, Y. Fang, C. Yao, *Spectrochimica Acta Part A: Molecular and Biomolecular Spectroscopy*, 2013, **102**, 66–70.
16. (a) L. daSilva,; H. Gallardo, R. F. Magnago, I. M. Begnini, *Mol. Cryst. Liq. Cryst.*, 2005, **432**, 1–13, (b) D. R. dos Santos, A. Gabriela, S. de Oliveira, R. L. Coelho, I. M. Begnini, R. F. Magnago, L. da Silva, *Arkivoc*, 2008, **xvii**, 157-166. (c) M. Tariq, S. Hameed, I. H. Bechtold, A. J. Bortoluzzid, A. A. Merlo, *J. Mater. Chem. C*, 2013, **1**, 5583-5593. (d) E. Meyer, C. Zucco, H. Gallardo, *J. Mater. Chem.*, 1998, **8(6)**, 1351–1354.
17. (a) P. C. Andrews, P. C. Junk, M. Massi, M. Silberstein, *Chem. Commun.* 2006, 3317−3319. (b) M. He, J. Li, S. Tan, R. Wang, Y. Zhang, *J. Am. Chem. Soc.*, 2013, **135**, 18718−18721. (c) H. Lee, S. H. Jung, W. S. Han, J. H. Moon, S. Kang, J. Y. Lee, J. H. Jung, S. Shinkai, *Chem. Eur. J.*, 2011, **17**, 2823 – 2827 (d) S. V. Voitekhovich, A. Wolf, C. Guhrenz, A. S. Lyakhov, L. S. Ivashkevich, M. Adam, N. Gaponik, S. Kaskel, *Chem. Eur. J.*, 2016, **22**, 14746 – 14752. (e) Y. Hu, M. Ding, X.-Q. Liu, L.-B. Sun, H.-L. Jiang, *Chem. Commun*., 2016, **52**, 5734-5737. (f) V. Bhalla, A. Gupta, M. Kumar, D. S. S. Rao, S. Krishna Parasad, *ACS Appl. Mater. Interfaces*, 2013, **5**, 672-679.
18. B. Pradhan, S. K. Pathak, R. K. Gupta, M. Gupta, S. K. Pal, A. S. Achalkumar, *J. Mater. Chem. C*, 2016, **4**, 6117-6130.
19. (a) Z.-X. Liu, Y. Feng, Z.-C. Yan, Y.-M. He, C.-Y. Liu, Q.-H. Fan, *Chem. Mater.*, 2012, **24,** 3751–3757. (b) A. Gopal, R. Varghese, A. Ajayaghosh, *Chem. – Asian J.*, 2012, **7**, 2061–2067; (c) Q. Wang, J. L. Mynar, M. Yoshida, E. Lee, M. Lee, K. Okuro, K. Kinbara, T. Aida, *Nature*, 2010, **463**, 339–343; (d) H. Wang, C. Yang, M. Tan, L. Wang, D. Kong, Z. Yang, *Soft Matter*, 2011, **7**, 3897-3905.
20. Y-C. Wu, S-H. Luo, L. Cao, K. Jiang, L-Y. Wang, J-C. Xie, Z-Y. Wang, *Analytica Chimica Acta*, 2017, **976**, 74-83.